

**MODELING AND SIMULATION OF TRANSPORT PHENOMENA
IN PAPER DRYING**

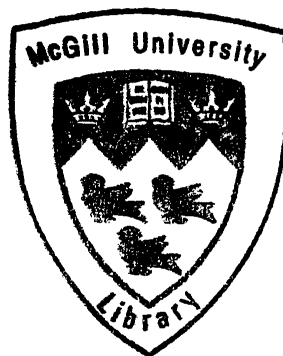
by

Mohsen Sadeghi

A thesis submitted to McGill University in partial fulfillment of the
requirements of the degree of Doctor of Philosophy

Department of Chemical Engineering
McGill University
Montreal

March 2003



© Mohsen Sadeghi
2003

ABSTRACT

A comprehensive microscale model of transport phenomena in paper drying was developed. The model includes five species (free water, sorbed water, air, water vapor, fibers) in three phases: humid air, liquid, solid. All relevant transport mechanisms were treated: capillary transport of free water, diffusion of sorbed water, convective-diffusive transport of water vapor. Effects on drying from the hygroscopic nature of paper were included: the reduced vapor pressure and extra evaporation energy for bound water and the changes in porosity and thickness because of sorbed water removal.

Because of considerable uncertainty associated with the required properties a rigorous sensitivity analysis was performed, using industrial dryer surveys to identify the optimal basis for five key transport properties: air and water relative permeability, water vapor diffusivity, sorbed water diffusivity, paper thermal conductivity.

The model was successfully validated against 32 dryer surveys from a number of paper mills. Dryer surveys utilized include different drying techniques (hot-surface cylinder drying, impingement drying and combinations of cylinder and impingement drying) and the full range of grades from tissue to linerboard. In addition to machine speed the model was proved reliable for sheet temperature prediction, thereby improving the performance from the best previous paper drying model. As measurements within the sheet cannot be made on industrial dryers, moisture and temperature determination inside linerboard dried in a laboratory air impingement dryer provided unique validation of model predictions of internal sheet conditions.

The thickness-direction profiles of moisture content, temperature, pressure and three mass fluxes (water vapor, free water, sorbed water) were analyzed for industrial drying of linerboard, for which differences in local conditions across the sheet are high. Development of a central plateau of high moisture content and two low moisture regions adjacent to the edges was demonstrated. Relative importance of all terms in the heat and mass balance equations was established for two ranges of moisture content: above and below the fiber saturation point. Transport of sorbed water was found to be negligible relative to that for free water and convective transport of water vapor. Evaporation-condensation and conduction were found to be the dominant thermal effects.

RÉSUMÉ

Un modèle détaillé des phénomènes de transport à petite échelle a été développé pour le séchage du papier. Le modèle inclut cinq espèces (eau libre, eau sorbée, air, vapeur d'eau et fibres) et trois phases: air humide, liquide et solide. Tous les mécanismes de transport pertinents du séchage ont été traités: le transport par capillarité de l'eau libre, la diffusion de l'eau sorbée ainsi que le transport de la vapeur d'eau par convection-diffusion. Plusieurs effets sur le séchage de la nature hygroscopique du papier ont été inclus: l'énergie supplémentaire nécessaire à l'évaporation de l'eau liée, la réduction de la pression de vapeur de l'eau liée et les changements de porosité et d'épaisseur provenant de l'enlèvement de l'eau sorbée.

Du fait de l'incertitude considérable associée aux propriétés de transport nécessaires au modèle, une analyse de sensibilité rigoureuse a été menée en utilisant des enquêtes de sécheries industrielles. Cette analyse a permis d'identifier la base optimale pour la détermination de cinq propriétés de transport essentielles: la perméabilité à l'air et à l'eau, la diffusivité de la vapeur d'eau, la diffusivité de l'eau sorbée et la conductivité thermique du papier.

Le modèle a été validé avec succès par des données expérimentales et des données provenant de 32 enquêtes des sécheries d'un grand nombre de papeteries. Les enquêtes de sécherie comprennent différentes techniques de séchage (séchage par contact avec la surface chaude d'un cylindre, séchage par contact direct avec le fluide de séchage ou la combinaison de ces deux techniques) et la gamme complète des qualités de papier, du papier mince au carton à couverture. En plus de la vitesse de la machine, le modèle a prouvé sa fiabilité pour la prédiction de la température de la feuille, améliorant ainsi la performance des modèles de séchage du papier disponibles les plus réputés.

Les profils d'humidité, de température et de pression, et les flux (vapeur d'eau, eau libre et eau sorbée) ont été analysés dans le cadre du séchage du carton plat pour lequel les différences en conditions locales à travers la feuille sont les plus élevées. Le développement d'une zone d'humidité élevée au centre de la feuille avec deux régions de faible humidité près des bords a été démontré. L'importance relative de tous les termes des bilans de chaleur et de masse a été établie pour deux étendues d'humidité au dessus et

au dessous du point de saturation de la fibre. La contribution de l'eau sorbée a été trouvé négligeable relativement à celle du transport de l'eau libre et du transport par convection de la vapeur d'eau. Les effets thermiques associés aux phénomènes d'évaporation, de condensation et de conduction ont été trouvés dominants.

ACKNOWLEDGEMENTS

I would like to express my sincere gratitude to Prof. W.J.M. Douglas, whose endless energy, vision and encouragement were a constant source of inspiration. It was a privilege to be a member of his research group and to learn many valuable lessons, with scope not limited to this thesis.

Thanks to Dr. Jean-François Bond for many interesting discussions and his outstanding work on the McGill first dryer simulator which undoubtedly influenced this thesis.

Thanks to Shaun Sidwall for his work on the dryer surveys that were used in the validation of the present model.

In the course of my study at McGill I had the pleasure of meeting many wonderful people. Special thanks to Françoise Forel, Jean-Phillipe Bernie, Manoj Dixit and Chunxia He.

The financial support of PAPRICAN is gratefully acknowledged.

TABLE OF CONTENTS

ABSTRACT	i
RÉSUMÉ	ii
ACKNOWLEDGEMENTS	iv
TABLE OF CONTENTS	v
LIST OF FIGURES	viii
LIST OF TABLES	x
NOMENCLATURE	xii
1. INTRODUCTION	1
1.1 Research objectives	1
1.2 Papermaking process	3
1.3 Literature review	6
1.4 Thesis structure	21
2. MODEL DEVELOPMENT	22
2.1 Paper structure	22
2.2 States of water in moist paper	28
2.3 Overview of the drying process	30
2.4 Model development	32
2.4.1 Modeling of transport phenomena in porous media	32
2.4.2 Assumptions	34
2.4.3 Conservation of mass	35
2.4.4 Conservation of energy	40
2.5 Mass flux terms	44
2.5.1 Capillary pressure	45
2.5.2 Multiphase flow in porous media	49
2.5.3 Free water transport	52
2.5.4 Water vapor and air transport	54
2.5.5 Sorbed water transport	57
2.6 Structural changes of moist paper	63
2.7 Summary	67
3. TRANSPORT AND THERMODYNAMIC PROPERTIES	68
3.1 Transport properties in moist paper	68
3.1.1 Absolute permeability	68
3.1.2 Relative permeability	74
(a) Simultaneous flow of gas and liquid through porous media	74
(b) Relative permeability of water and air: without furnish dependency	76
(c) Relative permeability of water and air: with furnish dependency	80
(d) Relative permeability of water and air: conclusions	87
3.1.3 Paper thermal conductivity	90

3.1.4	Water vapor diffusivity	96
3.1.5	Sorbed water diffusivity	100
3.1.6	Summary of transport properties in moist paper	101
3.2	Thermodynamic properties of moist paper	104
3.2.1	Capillary pressure in moist paper	104
3.2.2	Sorption characteristics of paper	109
(a)	Vapor pressure reduction	109
(b)	Differential heat of sorption	113
3.3	Fluid thermodynamic and transport properties	116
3.3.1	Gas phase properties	116
(a)	Water vapor properties	117
(b)	Air properties	119
3.3.2	Liquid water properties	119
4.	PARAMETER SELECTION AND MODEL VALIDATION	121
4.1	Testing model performance vs. industrial data	121
4.2	Optimal choice of transport properties	122
4.2.1	Transport properties to be tested	122
4.2.2	Procedure for parameter selection	126
4.2.3	Effect of relative permeability and thermal conductivity	128
(a)	Effect of water relative permeability	129
(b)	Effect of air relative permeability	131
(c)	Effect of thermal conductivity	132
4.2.4	Effect of water vapor diffusivity	133
4.2.5	Effect of sorbed water diffusivity	134
4.2.6	Summary of sensitivity analysis	134
4.3	Model validation	136
4.3.1	Basis for validation	136
4.3.2	Cylinder drying	138
(a)	Newsprint machines	138
(a-1)	Kruger Bromptonville paper machine #1	138
(a-2)	Kruger Bromptonville paper machine #2	142
(a-3)	Kruger Bromptonville paper machine #3	145
(b)	Containerboard machines	148
(b-1)	Trenton corrugated medium machine	148
(b-2)	Mississauga linerboard machine	150
(b-3)	Red Rock linerboard machine #1	151
(b-4)	Red Rock linerboard machine #2	154
(c)	Fine paper machine	155
4.3.3	Air impingement drying	158
(a)	Perkins tissue machine	158
(b)	Scott paper machine	159
(c)	Experimental results	162
4.3.4	Hybrid drying	164
(a)	Canadian International Paper	165
(b)	Tembec Inc.	167

4.4 Summary	169
5. DYNAMICS OF TRANSPORT PHENOMENA DURING DRYING	174
5.1 Methodology	174
5.2 Terminology	175
5.3 Drying dynamics for linerboard	176
5.3.1 Conditions for Norampac PM #1 in Red Rock	176
5.3.2 Cylinder #3	178
5.3.3 Cylinder #15	183
5.3.4 Cylinder #27	189
(a) Moisture content, temperature and pressure at the end of Phase II	189
(b) Mass fluxes of sorbed water, free water and water vapor	190
(c) Water vapor mass flux, n_v	191
(d) Free water mass flux, n_{fw}	192
(e) Sorbed water mass flux, n_s	192
5.3.5 Cylinder #33	197
5.3.6 Cylinder #46	202
5.3.7 Contribution of different mechanisms to drying	204
(a) Mass transfer	204
(b) Heat Transfer	206
(c) Summary	207
6. CONCLUSIONS	209
6.1 Contributions to knowledge	209
6.2 Suggestions for future work	211
REFERENCES	213
APPENDIX	224
A.1 Boundary conditions	224
A.1.1 Base case, cylinder contact side	224
A.1.2 Base case, vapor transport side	225
A.1.3 Multi-cylinder dryer section	225
A.1.4 Air impingement drying	227
A.2 Initial conditions	227
A.3 Numerical solution	228

LIST OF FIGURES

Figure 1-1: Paper machine with a two-tier, multi-cylinder dryer section	4
Figure 1-2: Four phases of cylinder drying, Nissan and Kaye (1955)	9
Figure 2-1: Structural features of a typical chemically pulped softwood fiber	24
Figure 2-2: Effect of beating on pore size distribution of dry unbleached kraft paper	27
Figure 2-3: Typical pore structure of paper	27
Figure 2-4: Moisture content evolution for very slow laboratory hot-surface drying	31
Figure 2-5: Volume fractions in an element of paper	36
Figure 2-6: Equilibrium at a line of contact	46
Figure 2-7: Meniscus in a capillary	47
Figure 2-8: Typical capillary pressure curves for imbibition and drainage	49
Figure 2-9: Typical water sorption isotherm for moist paper	58
Figure 3-1: Correlations for water relative permeability of moist paper	79
Figure 3-2: Correlations for air relative permeability of moist paper	79
Figure 3-3: Effect of moisture content on normalized air permeability of paper	83
Figure 3-4: Water and air relative permeability for LWC paper at 24°C	86
Figure 3-5: Water and air relative permeability for LWC paper at 24°C	86
Figure 3-6: Comparison of different correlations for air and water relative permeability	89
Figure 3-7: Effect of moisture content on thermal conductivity of groundwood handsheets, 340 kg/m ³ (numbers are temperature, °C), Nederveen and Finken (1992)	92
Figure 3-8: Effect of moisture content on thermal conductivity of densified blotting paper, 1030 kg/m ³ (numbers are temperature, °C), Nederveen and Finken (1992)	92
Figure 3-9: Effect of paper type and moisture content on Deff, Karlsson et al. (1992)	99
Figure 3-10: Comparison of correlations for sorbed water diffusivity at 100°C	101
Figure 3-11: Capillary pressure-moisture content relation for various furnishes (24°C) (Asensio, 2000)	107
Figure 3-12: Differential heat of sorption in paper	115
Figure 4-1: Comparison of measured and predicted sheet average temperature, Kruger Bromptonville Machine # 1 (April 1988)	130
Figure 4-2: Sheet average temperature: Kruger paper machine #1 (April 1988)	141
Figure 4-3: Cylinder surface temperature: Kruger paper machine #1 (April 1988)	141
Figure 4-4: Sheet moisture content: Kruger paper machine #2 (August 22, 1995)	145
Figure 4-5: Sheet average temperature: Kruger paper machine #3 (March 1995)	147
Figure 4-6: Cylinder surface temperature: Kruger paper machine #3 (March 1995)	147
Figure 4-7: Evolution of moisture content for laboratory impingement dryer	163
Figure 4-8: Evolution of temperature for laboratory impingement dryer	163
Figure 4-9: Comparison of actual machine speed to model predictions for 32 surveys	171
Figure 5-1: Thickness-direction profiles of moisture content (Red Rock PM#1, 161 g/m ² , Cylinder #3)	180
Figure 5-2: Thickness-direction profiles of temperature (Red Rock PM#1, 161 g/m ² , Cylinder #3)	181
Figure 5-3: Thickness-direction profiles of pressure (Red Rock PM#1, 161 g/m ² , Cylinder #3)	182

Figure 5-4: Thickness-direction profiles of moisture content (Red Rock PM#1, 161 g/m ² , Cylinder #15)	185
Figure 5-5: Thickness-direction profiles of moisture content, Bond and Douglas (Red Rock PM#1, 161 g/m ² , Cylinder #15)	186
Figure 5-6: Thickness-direction profiles of temperature (Red Rock PM#1, 161 g/m ² , Cylinder #15)	187
Figure 5-7: Thickness-direction profiles of pressure (Red Rock PM#1, 161 g/m ² , Cylinder #15)	188
Figure 5-8: Thickness-direction profiles of moisture content and temperature (Red Rock PM#1, 161 g/m ² , Cylinder #27, End of Phase II)	194
Figure 5-9: Thickness-direction profiles of pressure (Red Rock PM#1, 161 g/m ² , Cylinder #27, End of Phase II)	195
Figure 5-10: Thickness-direction profiles of three mass fluxes (Red Rock PM#1, 161 g/m ² , Cylinder #27, End of Phase II)	196
Figure 5-11: Thickness-direction profiles of moisture content (Red Rock PM#1, 161 g/m ² , Cylinder #33)	199
Figure 5-12: Thickness-direction profiles of moisture content, Bond and Douglas (Red Rock PM#1, 161 g/m ² , Cylinder #33)	200
Figure 5-13: Thickness-direction profiles of pressure (Red Rock PM#1, 161 g/m ² , Cylinder #33)	201
Figure 5-14: Thickness-direction profiles of moisture content and temperature (Red Rock PM#1, 161 g/m ² , Cylinder #46)	203
Figure A-1: Felting arrangements	226
Figure A-2: Cylinder pockets	226
Figure A-3: Three phases of drying for a Yankee dryer	227

LIST OF TABLES

Table 1-1: Characteristics of the main paper drying models	8
Table 1-2: Cylinder drying phases of Nissan and Depoy	9
Table 2-1: Chemical composition of wood and different pulps	23
Table 3-1: Experimental values of thickness direction absolute permeability	73
Table 3-2: Grades used for air relative permeability determination (Hashemi, 1996)	81
Table 3-3: Parameters for effective air permeability-moisture content relations for paper (Hashemi, 1996)	82
Table 3-4: Water relative permeability in moist paper (Asensio, 2000)	85
Table 3-5: Humid air relative permeability in moist paper (Asensio, 2000)	85
Table 3-6: Thermal conductivity of dry paper	96
Table 3-7: Correlations for effective air-water vapor diffusivity in paper	97
Table 3-8: Capillary pressure-moisture content relation (Asensio, 2000)	106
Table 4-1: Average error of machine speed prediction for 8 combinations of 3 transport properties, using D_{eff} of Han and D_s of Lin	129
Table 4-2: Comparison of water vapor diffusivity according to correlations of Han and of Ramaswamy	133
Table 4-3: Transport properties chosen for the paper drying model	136
Table 4-4: Design specifications: Kruger paper machine #1 (April 1988)	139
Table 4-5: Operating conditions: Kruger paper machine #1 (April 1988)	139
Table 4-6: Uncalibrated validation: Kruger paper machine #1 (April 1988)	140
Table 4-7: Operating conditions: Kruger paper machine #1 (1994)	142
Table 4-8: Uncalibrated validation: Kruger paper machine #1 (1994)	142
Table 4-9: Design specifications: Kruger paper machine #2	143
Table 4-10: Operating conditions: Kruger paper machine #2	143
Table 4-11: Uncalibrated validation: Kruger paper machine #2	144
Table 4-12: Uncalibrated validation: Kruger paper machine #2 (August 22, 1995)	144
Table 4-13: Design specifications: Kruger paper machine #3	145
Table 4-14: Operating conditions: Kruger paper machine #3	146
Table 4-15: Uncalibrated validation: Kruger paper machine #3	146
Table 4-16: Design specifications: Trenton corrugated medium machine	149
Table 4-17: Operating conditions: Trenton corrugated medium machine	149
Table 4-18: Uncalibrated validation: Trenton corrugated medium machine	149
Table 4-19: Design specifications: Mississauga linerboard machine	150
Table 4-20: Operating conditions: Mississauga linerboard machine	150
Table 4-21: Pocket conditions: Mississauga linerboard machine	151
Table 4-22: Uncalibrated validation: Mississauga linerboard machine	151
Table 4-23: Design specifications: Red Rock linerboard machine #1	151
Table 4-24: Operating conditions: Red Rock linerboard machine #1	152
Table 4-25: Pocket conditions: Red Rock linerboard machine #1	152
Table 4-26: Uncalibrated validation: Red Rock linerboard machine #1	152
Table 4-27: Operating conditions: Red Rock linerboard machine #1, Sack paper	153
Table 4-28: Uncalibrated validation: Red Rock linerboard machine #1, Sack paper	153

Table 4-29: Design specifications: Red Rock linerboard machine #2	154
Table 4-30: Operating conditions: Red Rock linerboard machine #2	154
Table 4-31: Pocket conditions: Red Rock linerboard machine #2	155
Table 4-32: Uncalibrated validation: Red Rock linerboard machine #2	155
Table 4-33: Design specifications: Weyerhaeuser fine paper machine	156
Table 4-34: Operating conditions: Weyerhaeuser fine paper	156
Table 4-35: Uncalibrated validation: Weyerhaeuser fine paper	158
Table 4-36: Design specifications and operating conditions: Perkins tissue machine	159
Table 4-37: Uncalibrated validation: Perkins tissue machine	159
Table 4-38: Design specifications: Scott paper machine	160
Table 4-39: Operating conditions: Scott paper machine	160
Table 4-40: Uncalibrated validation: Scott paper machine	161
Table 4-41: Drying rates: Scott paper machine, 21.1 g/m ²	162
Table 4-42: Design specifications: Laboratory impingement dryer	163
Table 4-43: Experimental conditions: Laboratory impingement dryer	163
Table 4-44: Design specifications and operating conditions: Canadian International	166
Table 4-45: Uncalibrated validation: Canadian International Paper	166
Table 4-46: Design specifications: Tembec Inc.	167
Table 4-47: Operating conditions: Tembec Inc.	168
Table 4-48: Uncalibrated validation: Tembec Inc.	168
Table 4-49: Comparison of measured and predicted values of moisture content, Tembec Inc.	169
Table 4-50: Summary of dryer surveys used in industrial validation	170
Table 5-1: Contribution of different mechanisms to mass transfer	205
Table 5-2: Contribution of different mechanisms to heat transfer	207

NOMENCLATURE

A	cross-sectional area (m^2)
B	basis weight, (g/m^2)
c_p	specific heat (J/kgK)
D_{eff}	effective water vapor diffusivity in paper (m^2/s)
D_s	sorbed water diffusivity (m^2/s)
D_v	normal water vapor diffusivity in air (m^2/s)
g	gravity
h_1, h_2	manometer reading (m), Equation 2-29
H	enthalpy (J/kg)
H_{ds}	differential heat of sorption (J/kg)
j_i	diffusive mass flux of species i ($\text{kg}/\text{m}^2\text{s}$)
k_{eff}	effective thermal conductivity (W/mK)
k_i	effective permeability of species i (m^2)
k_{ri}	relative permeability of species I
K	absolute permeability (m^2)
L	paper thickness (m)
\dot{m}_{fw}	evaporation rate of free water ($\text{kg}/\text{m}^3\text{s}$)
\dot{m}_s	evaporation rate of sorbed water ($\text{kg}/\text{m}^3\text{s}$)
M	molecular weight (kg/kmol)
n_i	mass flux of species i ($\text{kg}/\text{m}^2\text{s}$)
P	pressure (Pa)
\dot{Q}	water flow rate (m^3/s), Equation 2-29
r	pore radius (m)
R	universal gas constant (J/kmolK)
s	solids content (weight of dry solids / weight of dry solids + water)
S	saturation (volume of liquid/volume of voids)
t	time (s)

T	temperature (K)
v_i	velocity of species i (m/s)
X	moisture content (dry basis)
y_i	mole fraction of species i
z	thickness direction

Greek letters

ΔH_{vap}	latent heat of vaporization (J/kg)
ϵ	porosity
θ	contact angle or pore shape factor
μ	dynamic viscosity (kg/ms)
ν	kinematic viscosity (m^2/s)
ρ	density (kg/m^3)
$\bar{\rho}_i$	average mass concentration of species i (kg/m^3)
σ	surface tension (N/m)
σ_0	surface tension at reference temperature (N/m)
ω	moisture content (wet basis)
ω_v	water vapor mass fraction
τ	tortuosity
Λ	weighting factor, Equation 3-23
Θ	vapor pressure reduction factor

Subscripts

0	dry, Equation 3-16
a	air
avg	average
bd	bone-dry
c	capillary
cr	critical

d	dry, Equation 3-24
eff	effective
f	fiber
fw	free water
FSP	fiber saturation point
g	gas
h	hygroscopic region
l	liquid water
max	maximum
nw	nonwetting
par	parallel
ref	reference condition
s	sorbed
ser	serial
v	water vapor
w	wetting

CHAPTER 1

INTRODUCTION

In this chapter the objectives and structure of present study are developed based on industry needs and the current state of knowledge regarding paper drying models and their shortcomings in treatment of transport phenomena within the sheet during drying.

1.1 Research objectives

Pulp and paper is Canada's premier industry by many measures. Forest product exports, including pulp and paper, represent 15% of Canada's total export trade, with nearly two-thirds being exported to the United States. Canada is the world's leading producer of newsprint, accounting for 40% of global output. Almost 75% of Canada's total newsprint production is exported. Remaining competitive in the global economy is a priority for all businesses but those requiring high capital investment, such as the paper industry, are particularly vulnerable. In 1998 in Canada, capital spending by the paper industry amounted to almost 3 billion dollars, for a return on capital of 3.2%. According to Storat (1993), North American paper production in the two decades leading to 1993 increased by over 60% while capital expenditure grew to almost 12% of sales, double that of other manufacturing industries. Paper industry capital investment in developed countries is now concentrated on capacity expansion and rebuilds of existing facilities rather than building new mills.

This industry is also extremely energy intensive, ranking fourth after chemicals, steel and petroleum in energy consumption while leading in energy for drying (Salama et al., 1987). Papermaking is essentially an operation of sheet formation followed by massive water-removal using mechanical, then thermal processes. Water removal by thermal processes in the dryer section of a paper machine accounts for removal of less than 1% of the water originally present in the fiber-water suspension from which the sheet is formed. However the water removal by drying accounts for nearly 1/3 of the total energy consumption in an integrated paper mill (Chiogioji, 1979) and approximately 80% of its steam requirement (Reardon, 1994). Although the paper industry currently meets over 56% of its energy needs internally, primarily through use of low grade wood

material and heat recovery from pulping (Storat, 1993) there is still scope to reduce mill energy requirements within the largest consumer, the paper machine dryer section. Because of the large scale of operation even a small increase in production rate or in the more efficient use of energy can represent substantial economic savings.

Drying is frequently the production bottleneck of papermaking because of substantial improvements in the technologies of forming, dewatering and pressing. Of equal importance, paper properties are developed during drying. Thus increasing the effectiveness of dryer section operation and understanding the evolution of conditions within the sheet which influence product quality constitutes a priority. This is especially so when undertaking the major capital investment of rebuilding a dryer section to achieve increased production or to accommodate changes of grade that increase the dryer load. Another case for the need to predict dryer section performance is in conversion from untreated paper to the higher value grades of sized or coated paper. Essentially all printing and heavier grades are now dried by an assembly of from 40 to 90 steam heated cylinders. One accommodation to increased dryer load, simply addition of cylinders, is costly and not always possible due to space constraints. A very recent trend is to incorporate high intensity drying techniques such as air impingement, infrared and gas-fired conduction drying at some location in the cylinder dryer section, thereby producing what has been termed “multiple technique” drying, Bond et al. (1996), or a “hybrid” dryer section, Hashemi and Douglas (2000a, 2000b). The design and optimization of hybrid dryer sections requires a dryer simulator able to treat the case where the moist paper passes through any number of different drying techniques, in any sequence, as the sheet goes from wet to dry.

Although there are large incentives for developing design alternatives for optimized designs for major rebuilds, such occasions happen infrequently. However there are also routine needs or opportunities to use a dryer simulator to identify small changes in dryer operation. Such cases involve equipment changes that are at most minor, with the objective of increasing production, decreasing operating cost or changing drying related product quality attributes such as curl. Thus the incentive for having a reliable dryer simulator derives from all levels of change, from major rebuilds down to those involving just operating conditions without significant capital cost. Dryer simulators can also be

used in personnel training and troubleshooting. Incompletely developed paper drying technologies in need of mathematical modeling include impingement air drying, gas-heated cylinder drying and impulse and Condebelt drying for printing and heavier grades as well as through air drying for tissue grades.

The most challenging component of an industrial dryer simulator is the treatment of internal transport phenomena, i.e. flow, heat and mass transfer within the sheet during drying. Consequently the focus of this thesis is on constructing a comprehensive model of transport phenomena within a sheet of paper during drying. Only a sophisticated model that includes all the transport processes involved can be the basis of a reliable simulator. A comprehensive model will also take into account the hygroscopic nature of porous moist paper. In addition the model must be able to treat the numerous boundary condition changes necessary to simulate any combination of the cylinder and air impingement drying techniques, the building blocks of the hybrid dryer sections which are the wave of the future.

1.2 Papermaking process

In virtually all papermaking the raw material is wood pulp fibers from trees, eucalyptus and, in tropical areas, bagasse. The fibers used may be either virgin (not recycled) or recycled. The two main categories of furnish for the paper machine are chemical and mechanical pulp. In chemical pulping the logs are cut into chips, then soaked in chemicals under high pressure and temperature to dissolve the lignin. In mechanical pulping the suspension of pulp passes between large rotating serrated disks which separate the consolidated structure of wood into lignocellulosic fibers. There are many variations and combinations of these two basic methods of pulping. For recycled product, used paper is disintegrated in water, generally with deinking, followed by several cleaning steps. Recycled fiber usually is not of as good quality as virgin fiber.

In preparation for papermaking the pulp and any chemical additives used to enhance specific properties arrive at the sheet forming section in a water suspension of solids content about 0.5%. Figure 1-1 shows a typical layout of a paper machine with a multi-cylinder drying section.

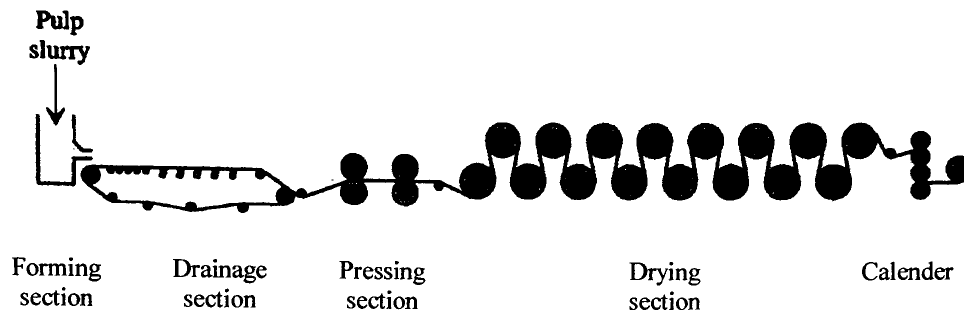


Figure 1-1 Paper machine with a two-tier, multi-cylinder dryer section

The basic components of a paper machine are:

1. *Forming and drainage section:* A pressurized headbox distributes the fiber suspension on an endless moving forming screen. Here the fibers form a wet web and dewatering occurs by gravity and by suction. The sheet exits with a solids content of about 20%, i.e. a moisture content of about 4 kg/kg dry.
2. *Press section:* The sheet passes through a series of presses where water is removed by compression of the sheet during which the paper structure is consolidated. The sheet leaves the press section at a solids content of about 37-50%, moisture content of 1.7 to 1 kg/kg dry.
3. *Dryer section:* Water is evaporated and the properties of the dry sheet are developed through fiber bonding. Printing and heavier grades are generally dried over a series of steam-heated cylinders while tissue and toweling are dried by impingement air drying, sometimes following a through air drying stage. Drying by contact heat transfer to the sheet from the steam heated cylinders is generally supplemented by air convection heat transfer to the sheet in the dryer pocket, the open draw region which occurs between adjacent cylinders. The dryer pockets are typically supplied with warm, dry air to enhance the convective drying. For coated paper it is necessary to start with a non-contact process, IR or air impingement drying, until the coating is consolidated. Paper exits the dryer at about 92-97% solids content, a moisture content of 3% to 8% kg/kg dry, depending on the grade and whether this is the final product or is followed by a sizing or coating operation.

4. *Calender and reel section*: The sheet is compressed between metal rolls to give a smoother surface for better printability. The calendered paper is wound onto a reel.

For an initial dry solids content of 0.5% in the fiber suspension entering the paper machine, for the major grades the dewatering capacities at each stage are approximately:

Forming section: 200 kg water / kg dry

Press section: 2.5 kg water / kg dry

Dryer section: 1.5 kg water / kg dry

Although water removal in the dryer section is very small, most of the energy consumption occurs at this stage of papermaking.

Multi-cylinder drying has been the universally used system for producing printing and heavier grades of uncoated paper. Machines producing lighter grades such as newsprint and fine paper usually contain about 40-50 cylinders, typically of 1.5-1.8 m diameter, heated by condensing steam. Drying heavier grades such as linerboard may require up to about 90 cylinders. Synthetic screens, termed dryer fabrics or felts, support the moist, low strength sheet and press it against the cylinders, thereby enhancing the contact heat transfer coefficient and reducing the frequency of sheet breaks. Normally the steam pressure is gradually increased from the wet to the dry end of the dryer section for reasons of both paper properties and energy efficiency. Typically the dryer is divided into separate sections for each steam pressure level and there may also be sections with different felting and sections of different pocket ventilation. Steam pressures may range from slightly below atmospheric at the wet end up to about 900 kPa at the dry end of a linerboard machine. Dryer sections are enclosed in hoods, thereby providing control of drying conditions to avoid excessive moisture nonuniformity in the cross-machine direction (CD) and to recover heat from the warm, moist exhaust air.

A common configuration has been the two-tier dryer section with upper and lower rows of cylinders, Figure 1-1. Traditionally two felts have been used, one for each tier of cylinders, leaving the sheet unsupported in the open draws between cylinders. As the speed of paper machines increased, excessive sheet flutter in these open draws increased

the frequency of sheet breaks. This problem has been addressed by introduction of the single-felted layout in which a single felt supports the web continuously in the draws as well as around the cylinders. The single-felted design prevents sheet flutter at the edges and substantially reduces shrinkage of the web in the CD direction. However there is either little drying in the lower tier, where the sheet is insulated from the cylinder by the felt, or no drying at all if, as is sometimes practiced, the lower tier consists of small unheated cylinders acting simply as turning cylinders. Since the late 1970s a great increase in machine speed has been achieved, due in part to introduction of the single-felt configuration at the wet end where the sheet has little strength. The fastest newsprint machine in the world runs a 9-meter wide paper web at just over 1900 m/min (115 km/h) and there are numerous machines now running at speeds over 1700 m/min (100 km/h).

Air convection drying occurs as a secondary drying mechanism in the draws between cylinders in multi-cylinder dryer sections, as noted above. Air convection drying is used as the primary drying mechanism to obtain unrestrained drying of kraft sack paper, for non-contact drying of coated paper and for high intensity drying of tissue and toweling. In the latter case the thin web may be completely dried in one pass around a single large steam-heated cylinder, of diameter 3.5-5.5 m, mostly surrounded by an impingement air hood from which the hot drying fluid issues as high velocity jets from an array of round nozzles in the hood. This configuration is termed a Yankee dryer. In order to produce tissue and toweling of minimum density (maximum “bulk”) drying in two stages may be used, with impingement air (Yankee) drying preceded by through air drying in which the hot drying air is blown or sucked through the wet sheet.

1.3 Literature review

Since the 1950s numerous drying models have been proposed. Along with the increase in computer speed and capabilities and an increased recognition of the complexities of the transport phenomena involved in drying, the models grew more complicated. Current models range from those based only on the external transport mechanisms without consideration of gradients of pressure, moisture content or temperature in the thickness direction of sheet, to complex models using microscale

modeling of transport phenomena within the sheet along with the ability to simulate different configurations and different drying techniques.

The first comprehensive literature review, Kirk (1984), covered simulation models to 1980. In their review up to 1992, Wilhelmsson et al. (1993) provided a concise tabular summary which was extended by Sidwall et al. (1999a). This perspective, further updated here as Table 1-1, identifies separately the liquid and vapor phase components of internal mass transfer, an aspect now determined to be centrally important. Great variability is evident in the extent to which simulator models have included aspects external to the sheet involving the steam and condensate system, the cylinder dynamics (shell resistance, condensate layer, spoiler bars) and ventilation of the dryer pocket air.

The central feature of internal transport within the sheet is the most difficult part of paper drying modeling. This aspect has evolved gradually, from evaporation only at the surface, to an evaporating front, towards a fully microscale model encompassing all the controlling transport phenomena. Some current models which focus on external systems, i.e. steam and condensate flows, still employ the evaporating front assumption for the sheet drying model but computer power now enables simulation of all aspects without the major simplifications necessary earlier. Paper drying models which have been notable during this evolution now are discussed.

The landmark contribution to paper drying modeling was the Nissan and Kaye (1955) division of each cylinder - dryer pocket unit into 4 sections, Figure 1-2. This model allowed for contact heat transfer by conduction from the cylinder, for convection and radiation to the paper and for evaporation from the sheet. The original calculations for a dryer section took 120 man-hours with a desk calculator. At first Nissan thought that due to the felt, little water removal took place in phase II. In subsequent versions Nissan et al. (1960,1961) modified this model, first to allow the felt to absorb liquid water, then to allow for vapor diffusion into the felt and condensation there. Although model complexity thereby expanded, calculation time with the digital computer then available decreased to about 40 minutes, after about 70 h preparing the code, of which only 25 h was directly for computer programming. Further experimental work disproved the earlier belief that the felt absorbed liquid water and revealed that felts remove moisture only as water vapor.

Table 1-1 Characteristics of the main paper drying models

Author(s)	Internal Transport			External Systems			Validation	
	Liquid	Vapor	Heat	Steam	Cylinder	P.V.	Lab	Industrial
Nissan et al. (1955-1961)			✓				✓	
Lehtikoski (1970)			✓		✓			
Depoy (1972)			✓		✓			✓
Powell & Strong (1974)			✓					✓
Hartley & Richards (1974)	✓	✓	✓				✓	✓
Knight & Kirk (1975-1980)					✓			✓
Rhodium & Göttching (1979)			✓					✓
Snow (1980)	✓	✓	✓		✓	✓		✓
Lemaitre et al. (1980)				✓	✓	✓	✓	✓
Lee et al. (1981-1983)	✓	✓	✓				✓	✓
Donner & Renk (1982)		✓	✓	✓	✓			✓
Karlsson et al. (1982-1992)				✓		✓		
Lampinen & Toivonen (1984)	✓	✓	✓				✓	
Abbott et al. (1984)				✓	✓	✓		✓
Iida (1985)								✓
Valmet (1985-1988)	✓	✓	✓	✓	✓	✓		✓
Pearson (1986)								
Lehtinen (1990)	✓		✓		✓			
Ramaswamy (1990)	✓	✓	✓					✓
Asensio & Seyed-Yagoobi (1992)	✓	✓	✓					
Deshpande & Pulkowski (1992)					✓			✓
Heikkilä (1992)			✓		✓	✓	✓	
Karlsson and Timofeev (1994)				✓	✓			✓
Reardon (1994)	✓	✓	✓	✓	✓			✓
Wilhelmsson et al. (1996)			✓	✓	✓			✓
Persson & Stenström (1996)				✓	✓			✓
Bond and Douglas (1996), Sidwall et al. (1999a)	✓	✓	✓	✓	✓	✓	✓	✓
Asensio (2000)	✓	✓	✓					

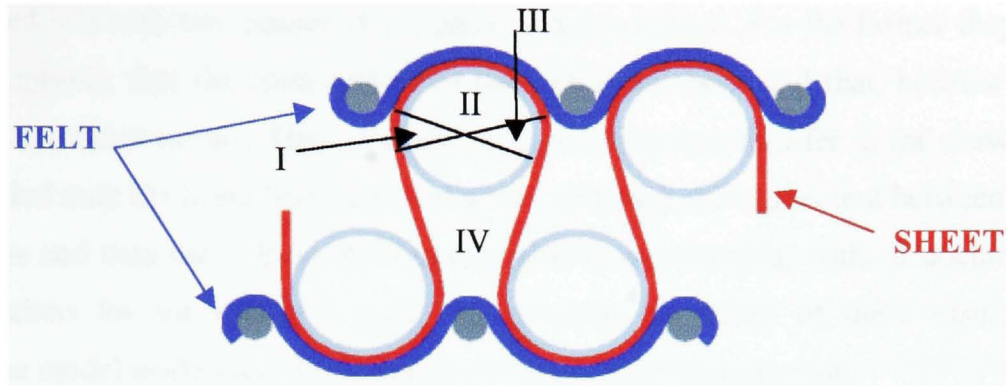


Figure 1-2 Four phases of cylinder drying, Nissan and Kaye (1955)

Lehtikoski (1970) extended Nissan's model by further dividing the dryer section into four zones: pre-heating (increasing rate drying), constant rate drying, falling rate drying and fast-falling rate drying. The heat transfer coefficients for the cylinder-paper and paper-felt contact at the start of each zone were given. Intermediate values were computed through linear interpolation. A unique feature was calculation of the felt temperature and moisture content. The model was not validated experimentally.

Depoy (1972) expanded the Nissan system to five phases, adding felt modeling, Table 1-2. His phase 4 is the cylinder area in contact with air, with phase 5 for the felt when not in contact with the sheet. The mass transfer coefficient was determined by matching actual machine data against the simulation results. Depoy studied the drying rates using both modern synthetic dryer fabrics and older cotton-asbestos felts. Comparisons made of the model and actual paper machines provided acceptable results, although details are lacking concerning how these validations were carried out.

Table 1-2 Cylinder drying phases of Nissan and Depoy

	Cylinder/Paper	Cylinder/ Paper/Felt	Paper In Draw	Cylinder	Felt
Nissan	I & III	II	IV	-	-
Depoy	1	2	3	4	5

Powell and Strong (1974) proposed a simplistic model in which the drying process was divided into only two phases, dryer phase and draw phase. For the former they made two assumptions: that the open surface of the web is adiabatic and that, because of the felt, no evaporation occurs. They assumed no convective heat transfer in the draw phase and included only the latent heat of vaporization. Although fair agreement between model predictions and data taken from Montgomery (1954) was claimed, without documenting the conditions for the industrial data, the excessive simplicity of these assumptions renders the model inadequate for simulation of paper machine operation.

The Hartley and Richards (1974) model considered both liquid and vapor internal diffusion as well as internal heat transfer. The temperature of the contact surface of the web was assumed equal to that of cylinder surface, i.e. zero resistance to contact heat transfer. This assumption left the convective heat and mass transfer coefficients as parameters to be fitted. The effect of the felt on evaporation was stated to be included but was not detailed. Although external systems were excluded, the model was fitted to both laboratory and paper machine data. As will be explained in Chapter 4, a tuned or calibrated validation, as is the case here, provides little credibility for a model.

Knight and Kirk (1975) proposed a model emphasizing the operating conditions, including number and diameter of cylinders, condensate flow rate and thickness, machine speed and steam pressure. Their FORTRAN model assumed the sheet could not support internal gradients of temperature or moisture in the thickness direction, now known to be incorrect. Kirk (1980) used the results to form power series correlations incorporating speed, basis weight, cylinder-paper contact heat transfer coefficient, cylinder diameter, draw length, felt evaporation reduction factor and critical moisture content. With these empirical correlations, evaporation rate and number of cylinders could be predicted but the model used lacks validity.

A simulation model based on experimental data was presented by Rhodius and Göttsching (1979). Internal heat transfer was treated by an effective thermal conductivity but internal mass transfer was ignored. The effect of web shrinkage was included in the model. The presence of the felt was treated by a drying rate reduction factor. In order to obtain the cylinder-paper contact heat transfer coefficient, simulations were run until the calculated paper temperature agreed with measurements. No external systems were

considered, severely limiting the applicability of the model which in any case was not properly validated, i.e. without calibration or tuning.

The model of Snow (1980), reportedly from 1966 work, allowed for internal heat, liquid and vapor transfer. Developed mainly for optimization and dryer design, this model included many operating conditions but made no allowance for the felt. For each furnish one entered a sheet thermal conductivity and heat capacity having no dependence on moisture content or temperature. Snow reported that the 1966 experimental techniques should be improved but that the model, when compared to others of that time, provided good results. Snow's model is notable in that it appears to have been the first to treat internal mass transport.

The Lemaitre et al. (1980) model dealt extensively with the external systems but with heat and mass transfer within the sheet not being treated. Coefficients for transfer of heat (between cylinder and sheet) and mass (between sheet and fabric, fabric and air) were obtained with non-linear parameter estimation from measured cylinder surface temperatures and literature values. The model produced acceptable results for dryer sections similar to those used to obtain the heat and mass transfer coefficients and would be valid only for such limited use. By ignoring internal transport the model lacks generality and predictive ability and would be invalid for heavier grades or for high intensity drying of all grades of paper.

The model of Hinds, Lee and Neogi (1981,1983) was based on a comprehensive experimental study. Their lab techniques enabled determination of the coefficients for heat conduction and for liquid and vapor transport within the sheet, which they found to be specific to each grade used. They then applied this model to industrial dryers, reporting that predictions were within 2% of measured average drying rates. These simulations were done by tuning the simulation to one machine for one grade, then applying the tuned model to several other paper machines with other grades from fine paper to corrugated medium, but without changing any model parameters. The normalized simulation results matched measured average drying rates well but energy consumption predictions deviated by up to 15% with heavier grades. With tuned simulations providing fair predictions for grades from fine paper to corrugated medium, this model demonstrates the importance of considering internal transport phenomena.

Donner and Renk (1982) assumed the liquid transfer by capillary pressure gradient to be negligible. Vapor phase mass transfer, internal heat transfer and cylinder operating conditions were taken into account. They showed the utility of simulations for diagnosing the source of poor performance when troubleshooting dryers, claiming cylinder temperature measurements to be an inferior method. Their model assumed negligible cylinder to sheet contact heat transfer resistance and did not treat felting, oversimplifications leading to excessively high heat transfer rate prediction.

In the Karlsson and Soininen (1982) model the effect of fabric was included through a paper-air heat transfer coefficient reduction factor expressed as a function of fabric porosity, thickness and heat conductivity. The model was reported to include the pocket ventilation as well as steam and condensate systems. The effect on drying of different furnishes, including recycled fibers and deinked pulp, was investigated. A mathematical model for the effect of dryer fabric was presented. Karlsson and Paltakari (1992) of the VTT research centre in Finland and Helsinki University of Technology respectively, resumed the work on the original model and claimed that for the low intensity conditions of cylinder drying, the internal processes must be taken into account for basis weight over 120 g/m^2 . However Bond et al. (1992) report significant internal gradients at much lower basis weight. With a model accounting for variable sheet porosity and thickness, Karlsson and Paltakari made internal temperature and moisture measurements for sheets up to 480 g/m^2 , but no validation was reported.

The Lampinen and Toivonen (1984) cylinder drying model treated mass transfer as water vapor diffusion and liquid moisture capillary flow. Heat transfer was modeled by an apparent heat conductivity, claimed to include the effects of both convection and conduction mechanisms. For the capillary pressure they developed an equation based on a new model for paper structure. They did not however separate bound water from free water, and they applied the capillary transport mechanism to the entire range of moisture content although this mechanism does not apply in the very important hygroscopic region. They claimed excellent agreement when this model was applied for newsprint although the validation was performed only against laboratory measurements, not paper machine performance data.

The Abbott et al. (1984) model, using the GEMS general simulation system, is intricate in its external systems modeling (several modules such as dryer cylinders, thermocompressors, steam coil air heaters, air-air heat exchangers, etc. are included) but uses over-simplified sheet modeling with no internal transport. As GEMS is not specific to drying, let alone paper drying, building cylinder dryer sections from such general simulation systems is difficult and greatly oversimplifies treatment of the complex transport phenomena actually occurring.

Iida (1985) expanded upon Lee and Hinds work, proposing for printing paper to assume no thickness-direction gradients of temperature or moisture content, thereby greatly reducing computation time. Such an approximation, even if not greatly in error for cylinder drying of the lightest weight grades, would make the model inapplicable for cylinder drying of heavier grades of paper or for drying even light-weight grades by any high intensity drying process. The model is unusual in its consideration of CD moisture nonuniformity. A fine paper dryer section was simulated but the discrepancy between actual and predicted performance was not reported.

Eskelinen et al. at Valmet Paper Machinery (1985) gave few details of their addition of external systems to the Lampinen model, but showed several applications for troubleshooting dryer sections. These authors, being from a dryer manufacturer, released few details. The world's major paper dryer builders - Valmet (now Metso), the former Beloit company, Voith-Sulzer and Mitsubishi - all require their own models but these proprietary simulators are neither in the public domain nor are they released to their paper company customers.

Lehtinen (1990) studied the evaporation within the sheet during drying at temperatures above the saturation temperature corresponding to the ambient pressure. Condensate and contact heat transfer coefficients were identified for individual cylinders and a linear temperature profile across the cylinder shell was assumed. No validation against industrial data was reported.

The model of Ramaswamy (1990) for conventional and high intensity drying (defined as high temperature cylinder drying plus high mechanical pressure) assumed an internal pressure build-up while the sheet is on the cylinder, then instant pressure release with expansion of water vapor as the sheet leaves the cylinder. A detailed microscale

model describing the internal sheet dynamics was used. The model did not consider felting or allow for specification of varying cylinder or pocket conditions. As all cylinder and pocket conditions were identical, as recorded in the code, this model has only limited potential. High intensity drying was simulated for the case of high cylinder contact temperature and applied mechanical pressure, both taken as constant over the complete drying time. As this model treats only one type of dryer at a time and is limited to use of only one set of conditions for the entire dryer section, it would not be capable of simulating hybrid drying in which two or more drying processes are used sequentially as the sheet goes from wet to dry. The more common forms of high intensity air drying, i.e. impingement air drying and through air drying widely used for tissue and toweling production, were not included in the model.

The Asensio and Seyed-Yagoobi (1992) model is an improved version of the Han (1970) work. Correlations for estimation of sheet thickness and porosity during drying were included and experimental results were used to develop an empirical correlation for the cylinder-paper contact heat transfer coefficient. They made an arbitrary assumption that the fabric reduces the evaporation rate by 20%. Neither external systems nor heat transfer through the cylinder shell were included. No validation was reported.

Deshpande and Pulkowski (1992) of Beloit Corp. detailed the operating conditions but used the simplest internal model, i.e. no thickness direction gradients. A simulation model of general validity, i.e. to apply for the broad range from cylinder drying of heavier paper to drying any grade by a high intensity process, requires representation of the actual internal transport phenomena. For the contact heat transfer coefficient they used a single value with no dependence on moisture content, an erroneous assumption as shown by the measurements of Rhodius & Göttching (1979) which showed that this contact coefficient decreases by about 40% as the sheet goes from wet to dry. This dependency is detailed in the Appendix. Deshpande and Pulkowski used the condensate heat transfer coefficient as the tuning parameter, but provided no details of the model nor any validation against paper machine data. They simply claimed that the predicted and measured cylinder surface temperatures were close.

Heikkilä (1992) developed a model for drying of pigment coated paper webs. Liquid penetration from the coating layer into the base sheet and redistribution of coating

components as well as convective, infrared and contact drying mechanisms were included. Overall drying rates measured for several pilot coating machines were compared with model prediction and fair agreement was claimed.

Karlsson and Timofeev (1994) proposed yet another model which ignored the thickness-direction gradients of temperature and moisture content, an unacceptable assumption for reasons provided earlier. They used an overall steam-to-paper heat transfer coefficient, expressed as a function of moisture content. The effect of the dryer fabric was included as an experimentally determined reduction factor. The model is notable for its inclusion of vacuum rolls, often found on modern high speed paper machines. When the fabric is in contact with the vacuum roll, a modified mass transfer coefficient which is a function of vacuum pressure and the web moisture content is used.

Reardon (1994) developed a paper drying model in which liquid transport is described by capillary action and gas phase transfer is considered to include convective and diffusive components. However this model ignores the presence of bound water and makes the incorrect assumption that all water, including bound water, is transported by capillary action. Another shortcoming of this model is the lack of a separate mass balance equation for air. Thus although the convective bulk transfer of gas phase is included, in order to calculate the pressure gradient across the sheet a correlation between pressure, temperature and moisture content has been assumed. Using data from Australian Newsprint Mills paper machines the model was validated, without any reported tuning, with good results but the applicability to other grades has not been investigated.

A pamphlet by Kiiskinen and Retulainen (1995) of the VTT Technical Research Centre, Finland, details BALAS (Balance Simulator), a Windows based program with a graphical user interface to calculate mass and energy balances, analyze heat recovery, optimize processes and develop unit operation models. Its use for analysis of the influence of new drying techniques on paper mill energy management is claimed.

Wilhelmsson et al. (1996) applied their simulation to nine machines. The Windows program was in Borland Pascal with a graphical user-interface for entering machine geometry and operating conditions. Elements included single and double tier drying and vacuum rolls. The output is written to three print files and one report file. With machine speed specified for a 40 cylinder dryer, simulation on an IBM 486-66 MHz computer

required 5 minutes for predicting exit moisture content after the calculation coefficients were tuned. Two parameters, the condensate coefficient and cylinder-to-paper contact heat transfer coefficient at zero moisture content, could be tuned simultaneously so the simulation results would perfectly fit the measured machine operating conditions. As their model incorrectly assumes no internal mass transport phenomena, its applicability would be limited to overall dryer performance for light weight sheets only, dried under low intensity drying conditions.

Persson and Stenström (1996) applied the Wilhelmsson et al. simulator to a machine producing 211 g/m² paperboard, proposing its use to predict several operating condition changes for machine speed-up. The simulator may be tuned with its two parameters, specified above, to the measured dryer exit moisture content. However, because this work uses a model without internal gradients, its predictions for changed conditions are not reliable as large gradients are known to exist with the heavy grades they used. They also propose use of an IR dryer to preheat the sheet after the press section, but do so only by increasing the input sheet temperature without including the associated mass transfer in the model.

Niemenmaa et al. (1996) of VTT and Finntech Ltd. introduced the Advanced Paper Mill Simulator (APMS), built on the Advanced PROcess Simulator (APROS). The VTT Internet homepage, NET1/NET2, details these programs. APROS, a general-purpose environment with a graphical user interface and tools for model development, is connected to an object-oriented real-time database. The user chooses graphical components from the model libraries, defining the variables in query forms for each component. Each element represents a component of a sub-process (Hierarchical Structure) defined by pre-programmed differential equations. This program is reported to simulate the high intensity drying techniques of IR and airfoil dryers as well as cylinder dryers. Internal mass transfer differential equations are solved, but an important limitation is the unrealistic assumption of no internal temperature distribution, contrary to the substantial gradients determined at McGill for low intensity drying of heavier papers or high intensity drying of paper of any grammage. Niemenmaa et al. propose the program for use in design, plant analysis and employee training.

The Bond and Douglas microscale model, introduced by Bond et al. (1996) and subsequently refined substantially as reported by Sidwall et al. (1999a), then subjected to extensive validation by Sidwall et al. (1999b), is capable of treating single or multiple technique drying for cylinder and Yankee drying. Table 1-1 shows that of all models previous to the present work, this one is the most comprehensive as it not only includes a complete treatment of internal transport and external systems but also has been validated against experimental and industrial data. This model is therefore discussed in detail below. For this McGill University development Fralic et al. (1997) reported the successful validation and application to three newsprint machines. Sidwall et al. (1999a) detailed the structure of this model, Sidwall et al. (1999b) reported the most extensively documented validation for the greatest variety of paper grades and drying techniques while Sidwall and Douglas (1999) described its use to increase paper machine productivity.

Although the Bond and Douglas description of transport phenomena within the sheet during drying was one of the most sophisticated when it appeared but, like all models of complex systems, it included some simplifications which are unrealistic. Liquid water transport was treated as a diffusive process for the entire moisture content range. This treatment neglects the physical reality of one transport mechanism for interfiber pore water at high moisture content, capillary transport, and a different mechanism for transport of water sorbed in the fibers by diffusion at low moisture content. Moisture transport over the entire range of moisture content is treated through an effective diffusion coefficient highly dependent on moisture content, based on experimental data. For transport in the gas phase, convective transport of water vapor was not included, with transport treated as by diffusion with an empirical diffusivity. Consistent with the mass transfer modeling the energy transfer is modeled with conduction as the only mechanism. Another aspect of that model is a local evaporation term included to account for the phase change of liquid water to vapor within the sheet. To estimate the evaporation term, the characteristic dimension for air flow through moist paper developed by Polat et al. (1989) was used. Inclusion of the local evaporation term adds complexity to the model as three more parameters are needed to evaluate the term (characteristic dimension, effective transport area and mass transfer coefficient), thereby

increasing the uncertainty associated with the physical properties used. Finally there are shortcomings in some of the effective transport properties used: the high effective water vapor diffusivity used offsets the absence of convective gas phase transport in the model, and an effective moisture diffusivity independent of paper density was employed although the Lee and Hinds (1980) correlation used includes a density term.

The above analysis treats only the internal transport within the sheet but does not include the aspects of the boundary conditions on the sheet or the modeling of the external systems. The Bond and Douglas model, as described by Sidwall et al. (1999a), incorporates the latter aspects including the most complete treatment of the external systems (steam, cylinder and dryer pocket ventilation) of any of the dryer models listed in Table 1-1 that are in the public domain. Treatment of external systems, discussed in the Appendix, is much simpler than the analysis of transport phenomena within the sheet, the focus of the present study. Hence the modeling of the external systems by the first McGill University dryer simulator is used unchanged when validating, in Chapter 4, the new model for transport phenomena within the sheet, developed in Chapters 2 and 3.

Despite these deficiencies in the modeling of transport phenomena within the sheet in the Bond and Douglas model, their dryer simulator, without tuning or calibration, provided the remarkably good paper machine speed validation results reported by Sidwall et al. (1999b). They also showed that sheet internal moisture content and temperature predictions were consistent with those measured in the laboratory investigation of Bond et al. (1996). However, as noted by Sidwall et al. (1999b), validations using paper machine dryer surveys showed that sheet and cylinder surface temperature were consistently under-predicted, probably a consequence of the simplified description of internal heat and mass transfer. Therefore their predicted thickness direction gradients of moisture content, temperature and air humidity, important for aspects of paper quality, cannot be taken as reliable. These findings suggest that deficiencies in the Bond and Douglas modeling of transport processes within the sheet are the sources of poor prediction of sheet conditions. While such errors were largely compensating when the model was applied for machine speed prediction the validations of Sidwall et al. indicate that such compensation of errors does not apply to the prediction of conditions within the sheet.

For a study oriented to the convective drying of lumber, Asensio (2000) developed a model distinguished by its thorough description of internal transport phenomena, including the treatment of water vapor transport by diffusion and convection as well as liquid transport by both capillary action and diffusion of sorbed water. As will be seen subsequently, the treatment in the present thesis differs with respect to the mechanism used for sorbed water transport and the description of the porous medium (paper vs. wood). Also, where she assumed that all hygroscopic moisture is bound water, it will be shown in Chapter 2 that none of the hygroscopic moisture exists as bound water until the moisture content of paper has decreased to only about half the value at the onset of the hygroscopic region. Most importantly, because the objective of Asensio's study was convective drying of lumber, her model does not include the boundary conditions and external systems necessary for simulating the operation of a paper machine. Therefore the model, although quoted here because of its importance, has limited relevance to paper drying simulation.

Drying simulators could also be used in conjunction with so called "expert systems". A Paper Drying Expert System (PDES) is described on the Internet, NET1. This one-year project with EDS of Canada Ltd., KanEng Industries Inc. and three paper companies, Abitibi-Price, Stone-Consolidated and Domtar, was to design a prototype expert system to troubleshoot dryer sections and optimize the steam and condensate system. The Windows based program was claimed to be "...a fundamentally sound and useful tool for monitoring and recording the performance of an S & C {Steam and Condensate} system and for helping to diagnose the causes of poor performance." The PDES prototype, an off-line tool, was validated in two paper mills and the results prompted further development towards on-line implementation and commercialization. The PMA (Paper Maker's Advisor) project, detailed in NET2, is the on-line follow-up to PDES. Nault and Maltais (1997) discussed the application of the on-line module in the Windsor mill of Domtar Inc. The system, installed in 1995, was subsequently improved. The base program compares 50 press and dryer section inputs to entered benchmarks. The entered low and high levels of the latter come from actual and limiting operating conditions. When measurements reach either benchmark, machine operators receive an

alarm and suggestions of corrective action based on previous operations. This diagnostic ability based on past experience is the central feature.

NET3 states that “Currently, the main players in the PMA project are KanEng, Abitibi-Consolidated, and NRC (National Research Council). The first two are collaborating under SIMCON (Software for Integrated Manufacturing Consortium, an umbrella organization that facilitates the management of projects done jointly by groups of companies). KanEng will put the system on-line, do the testing, and eventually maintain and market the PMA. Abitibi-Consolidated will provide the test sites, and NRC will focus mainly on research aspects.” No further update is presently available. With no predictive capability an expert system is not a simulator but is simply an analyzer of multi-variable system performance. The full record of operation that must be maintained over time for the use of an expert system is in itself an important aid to good dryer operation. However for any change in paper specifications or operating conditions outside of previous experience, an expert system cannot predict what conditions would be required. An expert system, if used in combination with a dryer simulator, would provide a comprehensive basis for analysis of current operation and for simulation of performance with new operating conditions.

In conclusion, over many years considerable effort has been made to deal with the aspects of internal transport phenomena and external systems required for simulation of paper drying. Models have made a great variety of simplifying assumptions to describe paper drying. Transport phenomena within the sheet, being the most complicated part of the modeling, suffer the most. Some models are developed for a particular paper grade or drying process, restricting their applicability. Validation against actual industrial data for a variety of drying techniques and a wide range of paper grades is as important as model development but most studies have reported only limited, if any, validation. These shortcomings demonstrate the need for a comprehensive model which (1) does not ignore any significant transport mechanism, (2) includes all the external systems required in simulation of an actual dryer section, and (3) is extensively validated.

Thus the objective here is to develop a model encompassing all important transport mechanisms within the sheet and to validate and test this model for a wide range of paper grades produced by hot surface contact drying, impingement air drying or combinations

of cylinder and convection air drying, and finally, to use this model to gain insight into the complex interaction of transport phenomena within sheet during paper drying.

1.4 Thesis structure

Chapter 2 details the development of a comprehensive microscale model of paper drying, including the general heat and mass balance equations, mass flux terms for different species and correlations for sheet thickness and porosity estimation. In Chapter 3 all transport and other physical properties required in the numerical modeling of drying are presented. Chapter 4 completes the selection of transport properties needed by the model and presents the most comprehensive validation of a paper drying model yet reported. Internal dynamics of flow, heat and mass transfer and the resulting thickness gradients of gas pressure, temperature and moisture content are discussed in Chapter 5. The thesis closes with presentation in Chapter 6 of the contributions to knowledge and suggestions for future work.

CHAPTER 2

MODEL DEVELOPMENT

This chapter presents the assumptions made in developing a comprehensive model of paper drying and the resulting mass and energy balances. The main mechanisms of flow, heat and mass transfer within the sheet for all components involved in the drying process are discussed as well as the treatment to incorporate the hygroscopic behavior of paper. A quantitative expression for paper deformation and corresponding changes in thickness and porosity during drying is included.

2.1 Paper structure

Porous media, material having void spaces within a solid particulate matrix, cover a wide range of structures. Materials as diverse as petroleum reservoirs, soil, concrete, grain and other granular materials all have a packed bed structure of particles of spherical, cylindrical, irregular or elongated shape. The porosity, or volume fraction of voids, of consolidated particulate material ranges from about 3% for very elongated or platelet particles, to 40% for material with spherical particles. Paper is a porous material of complex structure composed generally of irregular, elongated wood pulp fibers, although some non-wood fibers such as cotton, bamboo or bagasse are used. Paper porosity may range from about 30% to 90%. The porosity is reduced substantially with the presence, for some grades, of fines coming from either the pulp or from inorganic filler.

The highly complex structure of paper is generated by the pulping process, the blending of fibers of different length, thickness, morphology and orientation, by filler and fiber fines, by chemical additives, by sheet thickness and by the type of sheet former. Consideration of the process by which paper is produced provides insight into its structure. Pulping breaks down the raw material into fibers suspended in water. The pulping process may be entirely mechanical, chemical or combinations of mechanical and chemical action such as semi-chemical or chemi-mechanical pulping. Mechanical pulp is produced either by pressing debarked short logs axially against a revolving grindstone in the presence of water, or with modern technology, by passing wood chips through refiners. The applied mechanical energy raises the wood temperature. When the wet

lignin in the middle lamella reaches a critical softening temperature, about 120-130°C, the fibers separate under the applied shearing force with only limited damage to their structure, i.e. some fiber shortening and fines production (delaminated fiber walls, etc.). These pulps are produced in yields, on a water free basis, of 85-95%. In chemical pulping wood chips are impregnated with delignifying solutions and maintained at 150-170°C in batch or continuous digesters. On discharge the fibers are separated from the solution of residual chemicals and dissolved wood components. The pulping chemicals penetrate the wood structure and react mainly with lignin, rendering it soluble, but the hemicellulose is also modified and cellulose may be slightly degraded. Usually about 90% of the lignin and half the hemicellulose are removed. Thus unbleached chemical pulp has a typical yield of 45-55% and the fiber structure is profoundly changed from that in wood or in mechanical pulp. About 90-95% of the lignin is removed when producing bleachable grade chemical pulps. Bleached chemical pulps are produced by separately treating the washed unbleached pulps with several delignifying and brightening chemicals. The effect of the pulping process on pulp composition is demonstrated in Table 2-1, abridged from Peel (1999). About 1/3 of paper is made primarily from mechanical pulp.

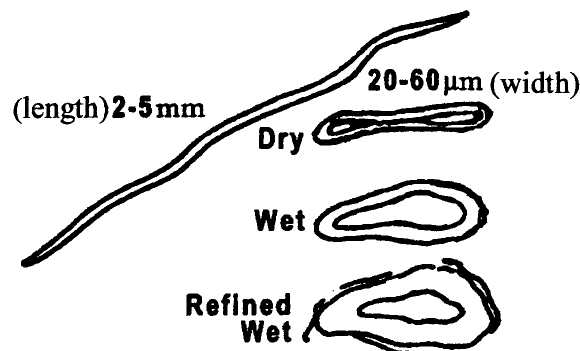
Table 2-1 Chemical composition of wood and different pulps

	Component →	Cellulose (%)	Hemicellulose (%)	Lignin (%)	Soluble material (%)
Raw material	Softwoods	40-45	25-35	26-30	4-12
	Hardwoods	38-48	28-40	16-25	4-8
Component retention	Mechanical pulp	100	~100	~100	~25
	Chemical pulp (unbleached)	~90-95	~32	~9-25	~5
	Chemical pulp (bleached)	~90	~30	< 0.5	~1

Chemical pulp, primarily cellulosic fibers, may be dried for storage and transportation, in which case the pulp is subsequently rewetted to form the aqueous

suspension fed to the paper machine. Chemical pulping considerably alters the physical properties of fibers. Cellulosic fibers from various wood species or non-wood sources differ greatly in physical and chemical properties. For paper made from mechanical pulps the intense physical action during pulping produces lignocellulosic fibers of irregular shape along with fiber fines which add complexity to the sheet structure.

The general characteristics of a typical coniferous (“softwood”) tracheid after chemical pulping are shown in Figure 2-1 (Peel, 1999). These fibers, usually curled and kinked when dry, scarcely change in length during drying. Dry unrefined fibers are usually partly collapsed into a ribbon like shape. When rewetted, fibers can be 20% wider and 60% thicker. Also, never-dried fibers may have 50% greater wet thickness than those which have been dried and re-wetted. Wet fibers are slightly reduced in width on refining but their walls delaminate and thicken (5-30%). On drying, refined fibers revert nearly to their original dimensions but are usually more collapsed and with slightly thinner cell walls.



**Approx. Thickness of
Springwood Cell Wall Layers**

Primary wall	P	0.06 μm
Outer secondary wall	S1	0.1-0.2 μm
Inner secondary wall	S2	1-5 μm
Tertiary wall	S3	0.1 μm

Figure 2-1 Structural features of a typical chemically pulped softwood fiber

The wet web from the paper forming section goes through a succession of water removal stages – drainage, suction dewatering, pressing and drying. During these

operations capillary forces in the wet sheet draw together not only the fibers but also the internally and externally loosened wall material. When sufficient water has been removed during drying, hydrogen bonding begins to affect the transition in structure from an unconsolidated web to a consolidated sheet, at first through water bridges, eventually by direct bonds between water and the hydroxyl groups of the carbohydrate polymers. The capillary forces become stronger as water retreats into cracks and inter-fibrillar spaces where the radius of curvature of the menisci becomes smaller. As drying proceeds the material shrinks, pores close and fiber morphology is affected by the hydrogen bonding between fibers occurring at their intersections. Rigdahl and Hollmark (1986) make the following observations regarding the network of chemical pulp fibers in paper:

1. Fibers often have the form of flat ribbons.
2. Fibers generally lie parallel to the plane of the sheet.
3. In the plane of the sheet, fibers are preferentially oriented in the machine direction.
4. Fibers are often curled.
5. The fiber length distribution depends on the fiber source.
6. The number of bonds per length of fiber varies greatly from only a few bonds per lignocellulosic fiber from mechanical pulping, to the extreme when the entire face of a cellulosic fiber from chemical pulping is bonded to adjacent fibers.

Anisotropy in porous media produces properties of different value in different directions. Paper is intrinsically anisotropic because a thin sheet is formed by deposition of a flocculated fiber suspension on a wire mesh moving at high speed. The mechanisms making paper anisotropic are, in the thickness dimension, fiber alignment parallel to the sheet surfaces and, in the machine direction (MD), the direction of motion of the wire mesh supporting the wet web. The pore structure of paper, likewise anisotropic, affects properties such as porosity, density and permeability, thereby influencing the properties relating to liquid and vapor phase transport of moisture, humidity and heat through moist sheets during drying. Paper permeability depends on pore size and the interconnectivity of pores. The network of fibers creates a network of pores, forming a two-phase system in which the pores between the fibers are a fundamental element of paper structure. The

apparent pore volume in a sheet can be calculated from the density of the solid phase and apparent (bulk) density of the sheet.

Pore size distribution is defined by the relative frequency for pore dimensions over the range up to the maximum pore size. The pore size distribution of dry paper is a function of fiber length and diameter, the extent of development of fibrillation of fibers, the degree of inter-fiber bonding and the amount and type of fiber fines or inorganic fillers added. Although pores in paper are highly irregular and far from cylindrical, attempts to estimate a pore size distribution have usually been based on assuming cylindrical pores with circular openings. With such a model the size distribution of pores may be obtained by the mercury intrusion method. If evacuated dry paper is placed in mercury and the pressure gradually increased, mercury enters the paper, the smaller pores becoming increasingly accessible to mercury as the applied pressure is increased. Bristow and Kolseth (1986) showed that the pore structure of dry paper may be represented by a logarithmic normal distribution. Figure 2-2, which shows some typical pore size distributions, illustrates how increased beating of a chemical pulp, identified through the SR index (derived from Schopper Riegler) gives smaller pores and a narrower pore size distribution. As beating proceeds the pulp drains more slowly in forming a wet web of fibers and is said to be “wetter”, “slower”, or “less free”. The SR index derives from a drainage test used to assess the effect of beating on paper properties. The introduction of finely divided inorganic filler to improve printability leads to smaller pores and a narrower pore size distribution. The pore size and pore size distribution of moist and dry paper is substantially different due to the hygroscopic nature of pulp fibers.

It should be noted that the above discussion concerning pore structure derives from the use of mercury porosimetry and Scanning Electron Microscopy, both of which are limited to dry paper. For the study of paper drying it is the highly variable pore structure of moist paper as a function of moisture content that is relevant. Polat et al. (1989) analyzed the shortcomings of the numerous approaches which have been used to establish the pore structure of moist paper and contributed a new method based on the application of fluid mechanics to flow through moist paper of variable moisture content. The results of their determination of effective pore size for moist paper are summarized in section 2.5.4.

The highly complex pore structure of dry paper is illustrated in Figure 2-3 where two types of pores can be identified. Interfiber pores form a continuous network in the

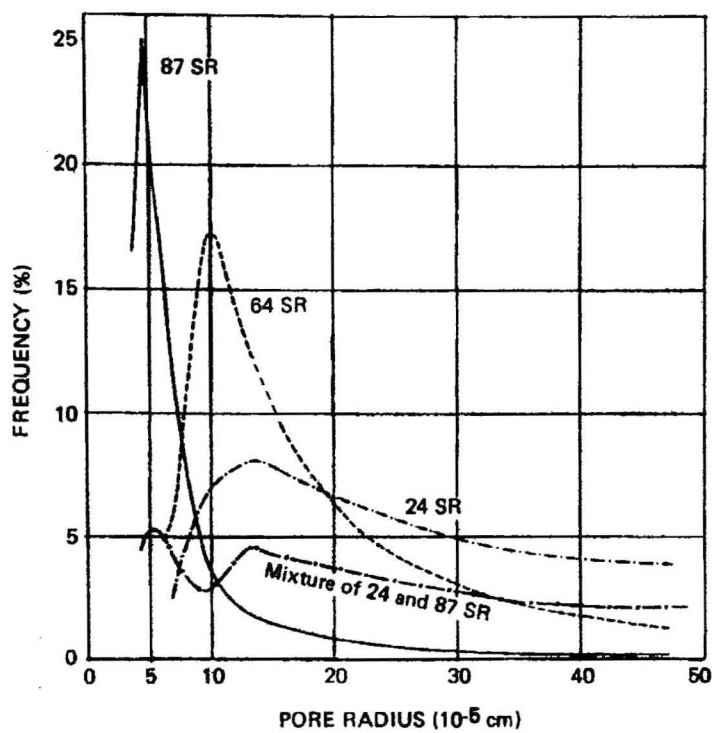


Figure 2-2 Effect of beating on pore size distribution of dry unbleached kraft paper

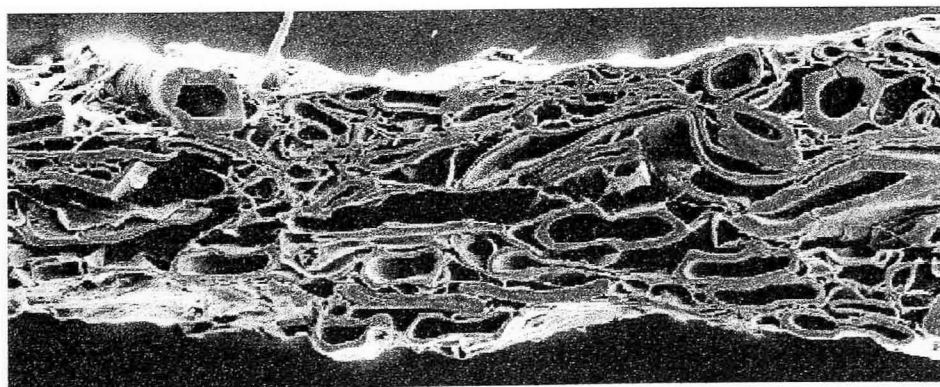


Figure 2-3 Typical pore structure of paper

sheet, providing small channels for diffusive and convective transport of water vapor and air, and when free water is present, to its transport by capillary forces. Intrafiber pores on the other hand exist within the fibers and therefore do not participate in interfiber

capillary transport of free water. During drying, water trapped in intrafiber pores can diffuse slowly from one fiber to another towards the sheet surface or to an interfiber pore surface to evaporate and be transported in the vapor phase through these pores to the sheet surface.

2.2 States of water in moist paper

Fiber-water interactions are fundamental to the drying process. In the low moisture content range, from about 0.4 kg/kg dry down to dryness as will subsequently be shown, water is held inside the moist sheet by the following mechanisms, listed in order of decreasing bond strength (British Paper and Board Industry Federation, 1978):

1. Monolayer adsorption on the cellulose surface by hydrogen bonding.
2. Multilayer adsorption near the cellulose surface by van der Waals bonding.
3. Capillary adsorption in intrafiber pores inside the fiber wall.
4. Capillary adsorption in interfiber pores between the fibers.
5. Capillary adsorption in the lumen.

The amount of water held depends on the type of pulp fibers. Longer fibered pulp holds more moisture than short fiber furnish, and moisture adsorption decreases with beating. The presence of fiber fines and inorganic filler also affects the retention of adsorbed moisture. Clay for example holds less water by adsorption than cellulose. Consequently for the low moisture content range considered here, for which there is no liquid water in the interfiber pores, the equilibrium moisture content in a clay loaded moist paper will be less than that for an unloaded paper.

The above paragraph deals with fiber-water interactions in the moisture content range near the end of drying, i.e. the region from about 0.4 kg /kg dry down to dryness. However for the higher moisture content range during the earlier part of the drying process the sheet consists initially of water saturated fibers with additional water in the interfiber pores. At some later stages in the drying when the moisture content is below that of the fiber saturation point, there is no water in the interfiber pores but the moisture content of the unsaturated fibers is sufficiently high that none of the water is adsorbed by

bonding mechanisms described above but is simply physically absorbed within the fibers. With liquid water passing through several stages, i.e. as interfiber pore water, as water in saturated fibers, as physically absorbed water in unsaturated fibers, as adsorbed water bonded to the polymeric constituents of the fibers, it is necessary to define carefully the terms used to describe these various states of liquid water.

Thermodynamics provides basic definitions for components in different phases. It is subsequently shown in Figures 2-9 and 3-12 that, at moisture contents down to about half that of the fiber saturation point, the liquid water physically sorbed in the fibers continues to exert the full vapor pressure of bulk water and to have the latent heat of vaporization of bulk water. Thus in this moisture content range the water sorbed in unsaturated fibers is indistinguishable thermodynamically from bulk water. At lower moisture contents, Figures 2-9 and 3-12 show that the molecular forces between water and the wood pulp polymers clearly differentiate such adsorbed water from bulk water.

However for the fundamental description of drying the criteria provided by transport phenomena are more relevant than those from the thermodynamics. From this perspective the transport of the water physically sorbed in unsaturated fibers over the moisture content range from the fiber saturation point down to about half that level is very much more constrained than is the interfiber pore water present when the fibers are saturated. Thus although during drying the liquid water can be present in the sheet in three states, i.e. interfiber pore water, physically absorbed water in the fibers and bound adsorbed water in the fibers, transport phenomena criteria justifies the use of just two states for liquid water. Therefore at moisture contents above the fiber saturation point the interfiber pore water will for convenience always be referred to as “free water”. Below the fiber saturation point where the water is first present as physically absorbed in the fibers, then at lower moisture contents as bound water adsorbed to various degrees to the fibers, such water will consistently be referred to as “sorbed water”. The transport of free water through the interfiber pore structure is governed by permeability expressions. The transport of sorbed water inside the fibers is treated by diffusion relations.

At the start of drying, moist paper is a mixture of three phases: solid (fibers, fiber fines, possibly inorganic filler fines), liquid (water), and gas (humid air). Five species must be included in a microscale drying model: solids, free water (located in interfiber

pores), sorbed water, air and water vapor. Total moisture content is the sum of free water, sorbed water and water vapor. Air must be included as the transport of humid air is a basic element of the mechanism of drying. As paper is a hygroscopic porous medium, at sufficiently low moisture content two aspects of the role of adsorbed water in the drying mechanism must be considered: more energy is required to evaporate bound water than bulk water, and bound water exerts a lower vapor pressure than bulk water. The hygroscopic nature of paper further complicates drying in that sorbed water removal results in collapse of the fibers, hence reduction in sheet porosity and thickness, discussed in section 2.5.

2.3 Overview of the drying process

The fundamentally different processes of hot-surface conduction drying and air convection drying of paper are now discussed. In hot-surface conduction drying, paper is heated on one side by contact heat transfer from a hot surface impermeable to mass transfer while the evaporated water is convected away from the other side. In air convection drying, water vapor may leave the sheet from the same surface at which there is a heat flux from a flow of unsaturated air. In the standard process for drying printing and heavier grades, paper moves through a multi-cylinder dryer section of cylinders heated by condensing steam. While the sheet is in contact with a cylinder, heat transfer to the sheet occurs by hot surface contact conduction. However in the open draws between cylinders, convective drying occurs from both sides of the sheet, often enhanced by a flow of relatively warm, dry ventilation air to this region termed the dryer pockets. Heat transfer within the sheet may occur by conduction, by convection due to mass fluxes and by the evaporation-condensation mechanism. Transport of humid air occurs under the driving force of vapor concentration gradients and by pressure-driven bulk flow, thereby creating both heat and mass transfer in the gas phase. Sorbed water, water vapor and air are all present within the sheet, while at high moisture content free water is also present. The mass transfer mechanisms for moisture within the sheet include free water flow by capillary action, water vapor convective and diffusive flow and diffusion of sorbed water. Air within the web moves by diffusion and by pressure gradient driven convection. These transport mechanisms are detailed in sections 2.4 and 2.5.

Hot-surface conduction drying of paper for constant drying conditions at extremely low drying rates is illustrated in Figure 2-4 (McCabe et. al., 1993). Industrial drying is a very much faster operation: to go from the wet to dry in a paper machine typically takes less than a minute for heavy linerboard and only a fraction of a second for tissue and toweling. In addition, as will be elaborated shortly, in the cylinder dryer section of a paper machine the sheet is subjected to repeated changes in drying conditions which change the drying curves substantially from those for the very simple case illustrated in Figure 2-4.

There is initially a warm-up period, from A to B in Figure 2-4, when there is little evaporation while most of the heat supplied by the hot surface is absorbed as sensible heat, raising the temperature of moist sheet. A constant rate period follows, from B to C, in which the moisture content decreases linearly while a constant rate of heat transfer to the sheet controls the drying rate. During the constant rate period the fibers are saturated with water and there is free water in the interfiber pores, which provides constant conditions for contact heat conduction at the sheet-cylinder contact surface, hence the constant drying rate. In the absence of radiation the temperature of the paper during the constant rate period is the wet-bulb temperature of the air on the side from which water vapor leaves the sheet. External mass transfer is governed by the vapor concentration difference between that of the sheet surface and its surroundings.

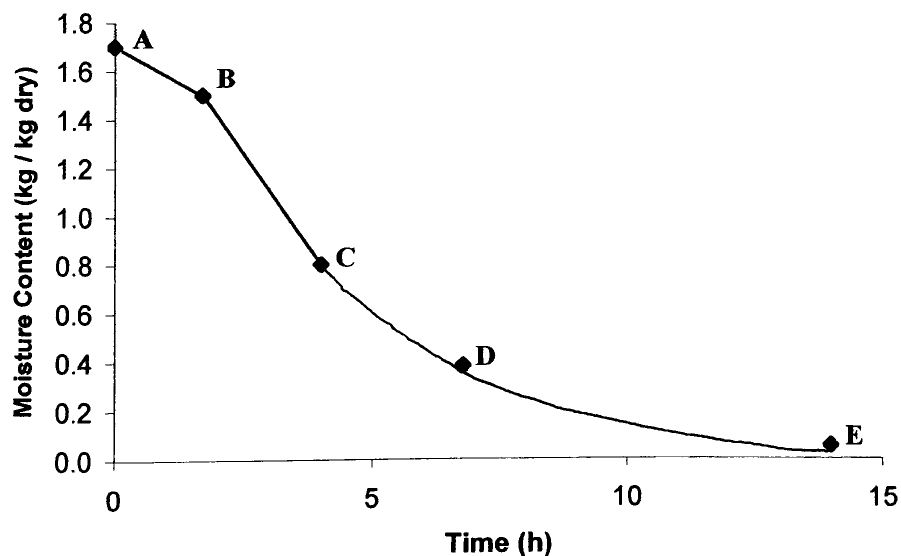


Figure 2-4 Moisture content evolution for very slow laboratory hot-surface drying

At the critical moisture content (point C) corresponding approximately to elimination of the free water from the pores of the sheet in contact with the hot surface, a falling rate period of drying begins. In this period there is no longer a sufficient capillary supply of moisture to maintain a fully wet surface with saturated fibers, so the drying rate becomes controlled by internal heat and mass transfer resistances. A second period of falling-rate drying may begin, point D, where the remaining moisture is as bound water with no free water remaining. With moisture only as bound water the vapor pressure of water and the transport coefficients of the low moisture content paper drop more rapidly.

The dynamics of industrial drying, with much higher drying rates, is more complex than the Figure 2-4 slow-drying case. Under industrial conditions typically there are large moisture gradients across the sheet thickness dimension, so sheet average moisture content, as shown on Figure 2-4, no longer provides a meaningful description. Depending on the sheet moisture content and on the condensing steam pressure, the rate of hot surface cylinder drying is in the range 10 to 70 kg/m²h while air impingement drying rate at the wet end can be as high as 450 kg/m²h. In a paper machine cylinder dryer section there may be no constant rate period due to changing external conditions such as the steam pressure in the cylinders and variation of conditions in the dryer pockets of the open draws between the cylinders. Furthermore, the distinction between two falling rate periods is not observed in industrial paper drying because of the significant moisture gradients which exist across the thickness dimension of the sheet. Development of thickness-direction gradients of moisture content, temperature, pore air humidity and gas phase pressure is a fundamental characteristic of industrial paper drying. Not only do such gradients affect the drying rate but they also influence paper properties. These important characteristics will be discussed in Chapter 5.

2.4 Model development

2.4.1 Modeling of transport phenomena in porous media

Considering the complex, anisotropic structure of moist paper, the modeling of transport phenomena behavior during drying would be formidably difficult if the analysis were conducted at the pore level. Instead, the present study uses a continuum approach. A porous medium is considered a continuum if any bulk behavior can be described by a

local average value definable everywhere. In many theoretical models of drying the governing differential equations are derived, often through a shell balance, in an intuitive manner from the well-known point equations of continuum physics. However a firm scientific basis should be established for applying the continuum treatment to a porous medium. The approach of Whitaker (1997a) for a rigorous theory of drying was by using the method of volume averaging (Whitaker, 1967 and 1969; Slattery, 1972). This method is a spatial-smoothing technique, just as the averaging of turbulent transport processes is a time-smoothing technique (Whitaker, 1977b). Governing “point equations” of mass, momentum and energy balance were developed, then averaged using a Representative Elementary Volume (REV) to obtain macroscopic equations describing the transport of heat and mass in the porous media. As a result the local values of temperature, moisture content, etc. are definable everywhere, regardless of the phase in which the particular point is located. Other techniques, like multiple scale expansion (Bensoussan et al., 1978), have also been developed in order to define an equivalent continuum medium.

Macroscopic equations thus developed could be simplified further by the assumption of homogeneity (Dullien, 1992). A necessary condition of homogeneity is that all macroscopic samples of a scale that is comparable with that of the medium have the same permeability, porosity, etc., i.e. a medium whose properties are independent of its size. By contrast, in a heterogeneous medium properties fluctuate depending on sample size because it does not contain a statistically representative distribution of pores. Certain properties, e.g. permeability, reflect heterogeneous morphology to a much greater extent than others such as porosity. Dullien states that a sufficient condition of homogeneity of the medium is that macroscopic samples taken from the medium display statistically indistinguishable pore morphologies. Such samples contain statistically indistinguishable samples of pore bodies (portions of pore space bounded by solid surfaces) and pore throats (where the hydraulic radius of the pore space is minimum) that are distributed in space uniformly in a state which is either disordered (like molecules in a gas) or ordered (molecules in a crystal). Real porous media never fully meet but may approach this condition of homogeneity.

The model to be developed here applies the macroscopic heat and mass balance equations to paper by assuming it to be a homogenous continuum. To do so according to

the principles of volume averaging, the volumetric effect of different phases should be included. As the transport of sorbed water was not included in Whitaker's original equations, his treatment is expanded here by adding necessary terms to the heat and mass balance equations. Inclusion of sorbed water transport also necessitates the treatment of sheet structural changes which occur when such water is removed. A structural model is included in the present study (section 2.6) to enable estimation of sheet porosity and thickness as a function of sheet moisture content and temperature. While sheet porosity is calculated locally and varies in the thickness direction, sheet thickness is estimated based on the average moisture content and temperature.

2.4.2 Assumptions

The following assumptions i to xii are required for the development of the general heat and mass balance equations, sections 2.4.3 and 2.4.4. Assumption xiii will be used for the free water flux calculation, section 2.5.3:

- i. Solid, liquid and gas phases are concurrently present within a porous media which is treated as a homogenous continuum. The gas phase consists of water vapor and air, assumed to behave as an ideal gas
- ii. Paper web is sufficiently thick that macroscopic equations can be developed, i.e. paper thickness is much greater than that of a single fiber
- iii. Paper is a capillary porous body, allowing capillary-induced moisture migration
- iv. Local thermodynamic equilibrium exists between solid, liquid and gas phases
- v. Evaporation and condensation occur within the pores, thereby contributing to heat transfer within the web
- vi. Negligible inertia, viscous dissipation and reversible work contributions from each phase to the energy equation
- vii. All flow, heat and mass transfer occurs only in the thickness direction through the web
- viii. Negligible shrinkage in a numerical solution time interval
- ix. No internal heat source, $\Omega = 0$
- x. Negligible energy accumulation due to solid deformation

- xi. Change of water vapor mass is negligible relative to that for liquid mass, $\frac{\partial \bar{\rho}_v}{\partial t} = 0$
- xii. Negligible change in ΔH_v in a numerical simulation time step
- xiii. Negligible gravitational transport of free water and gas phase

Assumption (ii) can be justified by comparing the numerical values of paper thickness with fiber thickness for different paper grades. Dry sheet thickness for tissue, newsprint and linerboard grades has typical values of 45, 100 and 270 μm , respectively. Maximum wet sheet thickness could be two to three times the dry thickness. Typical fiber thickness is about 4 μm . Thus the ratio of dry sheet thickness to single fiber thickness is about 45:4 (tissue), 100:4 (newsprint) and 270:4 (linerboard), sufficiently large in all cases to justify assumption (ii). Assumption (iv) considers the temperature of all phases to be equal (Whitaker, 1977b). For paper drying, the one-dimensional spatial analysis of assumption (vii) is reasonable as there is no mechanism to create gradients for heat and mass transfer in the plane of the sheet of the order of magnitude of those in the thickness direction. Cross-machine (CD) variation in moisture content with wet or dry streaks in the plane of the sheet is a common problem. However as the CD dimension is from a few meters to 10 m, CD moisture content gradients and corresponding fluxes are negligible compared to those in the thickness dimension in the order of 100 μm .

2.4.3 Conservation of mass

For an element of paper as shown in Figure 2-5 the macroscopic continuity equations are now developed for the four species involved in drying. The four resulting equations will be reduced to two continuity equations for total moisture and air. With the definition of porosity, fibers and interfiber pores occupy volumes in the ratio of $(1 - \epsilon) : \epsilon$. When there is liquid water in these pores the pore volume is divided between humid air and liquid water in the ratio of $(1-S) : S$ where S is the fractional degree of saturation. This fraction of void volume occupied by liquid water, S , is related to porosity, to X (dry basis moisture content) and to species density ρ_f and ρ_l by the following relation:

$$S = \frac{1 - \varepsilon \rho_f X}{\varepsilon \rho_l} \quad (2-1)$$

Moisture content, saturation and species density terms are all local point values. As explained in section 2.4.1 porosity is also defined locally as a function of moisture content and temperature. This relation is valid for both non-hygroscopic and hygroscopic media. For hygroscopic media, saturation is zero for moisture content at and below the limit which defines that region. Therefore saturation, S , is unity when the pores are entirely filled with water, and zero at the moisture content defining the onset of hygroscopic region to be discussed in section 2.5.5. Equation 2-1 does not apply within the hygroscopic region. For the drying of paper where the initial moisture content may be in the order of $X = 1.5 \text{ kg / kg dry}$ and porosity ε about 60%, the corresponding upper limit of saturation is about $S = 0.75$.

Fiber $(1 - \varepsilon)$	Gas $\varepsilon (1 - S)$	Free Water εS
------------------------------	------------------------------	-------------------------------

Figure 2-5 Volume fractions in an element of paper

Species continuity equations are developed for free water, sorbed water, water vapor and air.

Free water:

$$\frac{\partial \bar{\rho}_{fw}}{\partial t} + \nabla \cdot \mathbf{n}_{fw} = -\dot{m}_{fw} \quad (2-2)$$

Sorbed water:

$$\frac{\partial \bar{\rho}_s}{\partial t} + \nabla \cdot \mathbf{n}_s = -\dot{m}_s \quad (2-3)$$

Water vapor:

$$\frac{\partial \bar{\rho}_v}{\partial t} + \nabla \cdot \mathbf{n}_v = \dot{m}_{fw} + \dot{m}_s \quad (2-4)$$

Equations 2-2 to 2-4 are valid for any given volume of the medium. Each species, however, occupies only a fraction of the sheet volume. Therefore the mass concentration terms in these equations are average values defined over the entire medium, meaning that the volumetric effect of the relevant phase is included. Considering the volume fractions identified previously, these concentrations can be related to species density as follows:

$$\begin{aligned} \bar{\rho}_{fw} &= \varepsilon S \rho_l \\ \bar{\rho}_v &= \varepsilon (1 - S) \rho_v \end{aligned} \quad (2-5)$$

The evaporation terms \dot{m}_{fw} and \dot{m}_s representing the mass of evaporated free water and evaporated sorbed water per unit volume of the medium per unit time, are unknown. A single continuity equation for moisture can be written by adding three species continuity equations, which eliminates the local evaporation terms:

$$\frac{\partial (\bar{\rho}_{fw} + \bar{\rho}_s + \bar{\rho}_v)}{\partial t} + \nabla \cdot (\mathbf{n}_{fw} + \mathbf{n}_s + \mathbf{n}_v) = 0 \quad (2-6)$$

Recalling the definition of dry basis moisture content, X , the resulting continuity equation for total moisture can be rewritten as:

$$(1 - \varepsilon)\rho_f \frac{\partial X}{\partial t} + \nabla \cdot (n_{fw} + n_s + n_v) = 0 \quad (2-7)$$

$(1 - \varepsilon)$ appears in the equation to allow for the solid phase volume fraction.

Dry basis, X , and wet basis, ω , moisture contents are related by:

$$\omega = \frac{X}{1 + X} \quad \text{or} \quad X = \frac{\omega}{1 - \omega} \quad (2-8)$$

where ω is the mass ratio of water to dry solids and water. Another parameter commonly used in the paper industry is the web solids content, s , the ratio of dry solids to dry solids and water:

$$s = 1 - \omega = \frac{1}{1 + X} \quad \text{or} \quad X = \frac{1 - s}{s} \quad (2-9)$$

Solids content from the press section into the dryer section in paper machines ranges from 37% to 50%, i.e. a moisture content X of 1 to 1.7. Paper is dried typically to a solids content of 92 to 97%, i.e. 3 to 8% moisture content. Special cases are that paper is dried to the limit of about 98% solids content, 2% moisture content, before entering the size press used for fine paper or before entering the coater for the case of coated paper. Such low values of moisture content are used to minimize the cross-machine moisture nonuniformity that detracts from coating or sizing effectiveness.

A separate continuity equation is written for air:

$$\frac{\partial \bar{\rho}_a}{\partial t} + \nabla \cdot n_a = 0 \quad (2-10)$$

The volume fraction of gas phase, $\varepsilon(1-S)$, is included to relate the average mass concentration to air density, calculated from the ideal gas law:

$$\bar{\rho}_a = \varepsilon(1 - S)\rho_a \quad (2-11)$$

It is necessary to express the air mass balance in terms of the state variables T , P_g and X . Based on the definition of average mass concentration and the ideal gas law, the first term on the left hand side of Equation 2-10 can be written as:

$$\frac{\partial \bar{\rho}_a}{\partial t} = \varepsilon(1 - S) \frac{\partial}{\partial t} \left(\frac{M_a (P_g - P_v)}{RT} \right) + \rho_a (1 - S) \frac{\partial \varepsilon}{\partial t} - \rho_a \varepsilon \frac{\partial S}{\partial t} \quad (2-12)$$

As a deformable, hygroscopic medium, paper shrinks as sorbed water is removed during drying. Hence porosity, ε , is a function of time, as reflected in Equation 2-12. This porosity derivative term equals zero while the sheet is not shrinking, i.e. until the start of removal of sorbed water. The effect of shrinkage on air concentration is generally considered negligible as assumed by Ramaswamy (1990) and Asensio (2000). Treating this term as negligible does not mean that paper shrinkage is ignored, as will be discussed in section 2.6. Assumption (viii) from section 2.4.2 can now be applied:

viii. Negligible effect of shrinkage on air concentration

With this assumption, Equation 2-12 can be written as:

$$\frac{\partial \bar{\rho}_a}{\partial t} = \varepsilon(1 - S) \frac{M_a}{RT} \left[\frac{\partial P_g}{\partial t} - \frac{\partial P_v}{\partial t} - \frac{P_g - P_v}{T} \frac{\partial T}{\partial t} \right] - \rho_a \varepsilon \frac{\partial S}{\partial t} \quad (2-13)$$

The continuity equations for the four species participating in drying have thereby been reduced to two equations: Equation 2-7 for total moisture and Equation 2-10 for air. The four mass fluxes, n_i ($i = fw, s,v,a$), required to make the equations solvable, are defined in section 2.5 based on the diffusive and/or convective transport mechanisms relevant to each species.

As the enthalpy of bound water is reduced due to adsorption on the fiber walls, the differential enthalpy of bound water equals the free water enthalpy minus the differential heat of sorption, H_{ds} (Stanish et al., 1986; Perre et al., 1988). The dependence of H_{ds} on moisture content and temperature is discussed in Chapter 3. Since the evaporation of bound water requires more energy than for free water, the sum of latent heat of evaporation and differential heat of sorption has been multiplied by the evaporation rate of sorbed water (term (e) in Equation 2-14). The physical meaning of the Equation 2-14 terms is:

- (a) Energy accumulation
- (b) Convection effects due to temperature gradient
- (c) Heat conduction
- (d) Heat effect associated with evaporation of free water
- (e) Heat effect associated with evaporation of sorbed water
- (f) Convective effect from the differential heat of sorption of sorbed water

Local evaporation rates of free and sorbed water are not known but can be replaced using the species continuity equation developed in section 2.4.2. From Equation 2-3:

$$H_{ds} \frac{\partial \bar{\rho}_s}{\partial t} + H_{ds} (\nabla \cdot \mathbf{n}_s) = -H_{ds} \dot{m}_s \quad (2-17)$$

And from Equation 2-4:

$$\Delta H_{vap} \frac{\partial \bar{\rho}_v}{\partial t} + \Delta H_{vap} (\nabla \cdot \mathbf{n}_v) = \Delta H_{vap} (\dot{m}_{fw} + \dot{m}_s) \quad (2-18)$$

Applying the distribution law to the divergence operator in Equation 2-18 leads to:

$$-\Delta H_{vap} \frac{\partial \bar{\rho}_v}{\partial t} - \nabla \cdot (\Delta H_{vap} \mathbf{n}_v) + \nabla (\Delta H_{vap}) \cdot \mathbf{n}_v = -\Delta H_{vap} (\dot{m}_{fw} + \dot{m}_s) \quad (2-19)$$

Energy effects from vaporization of sorbed water occur only within the hygroscopic region. Considering the relationship between sorbed water mass concentration and total moisture density, the first term on the left hand side of Equation 2-17 can be rewritten as:

$$H_{ds} \frac{\partial \bar{\rho}_s}{\partial t} = (-H_{ds}) \nabla \cdot (n_{fw} + n_v + n_s) - H_{ds} \frac{\partial \bar{\rho}_v}{\partial t} - H_{ds} \frac{\partial \bar{\rho}_{fw}}{\partial t} \quad (2-20)$$

The differential heat of sorption is zero at moisture contents above those of the hygroscopic region and, as will be shown subsequently, down to moisture contents quite low within the hygroscopic region. Within the hygroscopic region, however, there is no free water flux. Therefore, Equation 2-20 can be simplified as:

$$H_{ds} \frac{\partial \bar{\rho}_s}{\partial t} = (-H_{ds}) \nabla \cdot (n_v + n_s) - H_{ds} \frac{\partial \bar{\rho}_v}{\partial t} \quad (2-21)$$

Using this approximation and expanding the divergence operator with the distribution law, Equation 2-17 becomes:

$$-\nabla \cdot (H_{ds} n_v) + \nabla H_{ds} \cdot (n_v) - H_{ds} \frac{\partial \bar{\rho}_v}{\partial t} = -H_{ds} \dot{m}_s \quad (2-22)$$

Equations 2-18 and 2-22 can be used to replace the local evaporation terms in the energy balance. Substituting these two equations results in the total energy balance:

$$\begin{aligned} \rho c_p \frac{\partial T}{\partial t} + \left[(n_{fw} + n_s) c_{pl} + n_v c_{pv} + n_a c_{pa} \right] \cdot \nabla T + (\Delta H_{vap} + H_{ds}) \frac{\partial \bar{\rho}_v}{\partial t} \\ (a) \qquad \qquad \qquad (b) \qquad \qquad \qquad (c) \\ = \nabla \cdot \left[k_{eff} \cdot \nabla T - (\Delta H_{vap} + H_{ds}) n_v \right] + \nabla (\Delta H_{vap}) \cdot n_v + \nabla H_{ds} \cdot (n_v + n_s) \\ (d) \qquad \qquad \qquad (e) \qquad \qquad \qquad (f) \qquad \qquad \qquad (g) \end{aligned} \quad (2-23)$$

The meaning of the seven terms of the Equation 2-23 is:

- (a) Energy accumulation
- (b) Convective effects from the temperature gradient
- (c) Vapor accumulation portion of free and sorbed water phase change terms
- (d) Heat conduction
- (e) Evaporation-condensation heat transfer within pores (heat pipe effect)
- (f) Convective effect from the latent of vaporization
- (g) Convective effect from differential heat of sorption in hygroscopic region

Assumption (xi) from section 2.4.2 can be used to simplify the energy balance equation. Many researchers (Bories et al., 1986; Bories, 1988; Couture et al., 1994) have made the reasonable assumption that the change of vapor mass is negligible compared to that for liquid mass:

$$\text{xi.} \quad \frac{\partial \bar{\rho}_v}{\partial t} = 0 \quad (2-24)$$

As a result, term (c) in Equation (2-23) becomes zero.

Another assumption concerns the variation of latent heat of vaporization with moisture content and temperature. The latent heat varies by less than 0.1% per degree Celsius. As a result, variations in heat required for vaporization of free water due to moisture and temperature changes are negligible in the small time interval of the numerical solution (assumption (xii) from section 2.4.2) and the spatial variations of ΔH_v can be evaluated using the moisture and temperature from the previous time step, hence simplifying the numerical solution.

xii. Negligible change in ΔH_v in a numerical solution time step

Some of the remaining terms in Equation 2-23 may be negligible but until such an analysis has been made (Chapter 5) all terms are retained in the energy equation.

The evaporation-condensation term (e) warrants particular attention. Heat transfer through a wet porous medium is enhanced due to an evaporation-condensation mechanism which occurs within the pores (Dreshfield, 1956; Krischer, 1962; Phillip and DeVries, 1957; DeVries, 1958). After water is vaporized at the surface of a wet sheet or in the interior of a sheet which has a dry surface but wet interior, water vapor will be transported by diffusion and/or convection into a cooler region of the web where the local temperature is below the saturation temperature so that some water vapor condenses. This transport through the sheet constitutes an evaporation-condensation cycle. The contribution of the evaporation-condensation mechanism to heat transfer has been investigated both experimentally and numerically. Moyne and coworkers (Degiovanni and Moyne, 1987; Azizi et al., 1988) present techniques for measuring the apparent thermal conductivity of porous materials over a range of temperature. Lampinen (1979) calculated the contribution from vapor diffusion to the overall heat flow in a numerical example and concluded that heat conductivity determinations should be made at low temperature differences to avoid the evaporation-condensation effect. This subject is treated further in Chapter 3.

Lehtinen (1982, 1989, 1990b) investigated additional possible heat transfer mechanisms. In the presence of high temperature gradients, Marangoni convection within the capillary water present in the pores was observed experimentally (Lehtinen, 1982). A mathematical model for Marangoni convection of inter-fiber water in paper was developed and examined for both conventional and high intensity drying conditions. Lehtinen concluded that Marangoni convection generally has a negligible contribution to the overall heat transfer within the web during conventional multi-cylinder paper drying, although marginal effects may be observed when high cylinder temperatures are employed. Marangoni convection has not been considered by other researchers or in the present model.

2.5 Mass flux terms

The four mass flux terms in the general heat and mass balances (Equations 2-7, 2-10 and 2-23) need to be identified based on the mechanisms controlling transport of the four corresponding components which contribute to overall transport of mass and heat in

the drying process. These components, as noted earlier, are free water, sorbed water, water vapor and air. Free water moves through the interfiber pores by capillary action. Intrafiber water within the cell walls is sorbed water, not subject to capillary transport. The convective contribution to the drying process due to bulk fluid motion, for both liquid water and humid air, is characterized by the theory of two-phase flow in porous media, which will be treated after introducing the concept of capillary pressure. Theoretical and empirical methods for the several transport coefficients and physical properties needed in order to calculate the mass fluxes are discussed in Chapter 3.

2.5.1 Capillary pressure

Capillary pressure, a basic parameter affecting the behavior of porous media containing two or more immiscible fluid phases, relates the pressures in the two fluid phases. Capillary systems in porous media involve a solid particulate phase and at least two fluid phases (in paper: liquid water and humid air). Wettability, the ability of liquid to spread over the solid phase, is characterized by the contact angle, defined now before capillary pressure is elaborated.

For a drop of liquid on a smooth, plain solid surface, Figure 2-6, the liquid may remain a drop displaying a finite angle of contact θ between the two boundaries: liquid/gas and solid/liquid. Contact angle θ is defined as the angle subtended by the tangent to the solid/liquid boundary at a point and the tangent to the liquid/gas boundary constructed at the same point on the three-phase line of contact. At equilibrium, the force components parallel to the solid surface are:

$$\sigma_{lg} \cos\theta = \sigma_{sg} - \sigma_{sl} \quad (2-25)$$

where σ_{lg} and σ_{sg} are the surface tension of liquid and solid, respectively, and σ_{sl} is the interfacial tension between liquid and solid. This equation, first given by Young for a liquid drop resting in air on a solid surface, relates the contact angle to the surface tensions of three interfaces.

The value of the contact angle θ ranges between 0° and 180° . The particular value of $\theta = 90^\circ$ requires that $\sigma_{sl} = \sigma_{sg}$. The other special case, $\theta = 0^\circ$, is of great significance

because that is the limit for liquid spreading on the solid. The condition for $\theta = 0^\circ$ is $\sigma_{lg} = \sigma_{sg} - \sigma_{sl}$. As the difference $(\sigma_{sg} - \sigma_{sl})$ increases from 0 to σ_{lg} , the contact angle θ decreases from 90° to 0° .

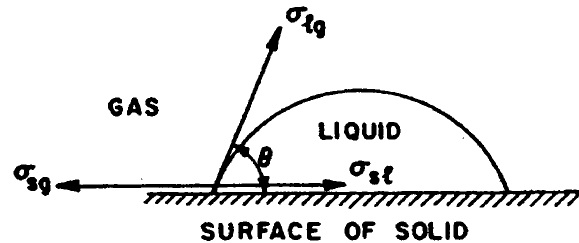


Figure 2-6 Equilibrium at a line of contact

In the case of paper drying the two phases which can be present in the interfiber pores are humid air and liquid water. Water is the wetting fluid and the air-water vapor mixture is the nonwetting fluid because the contact angle at a liquid/gas and liquid/solid interface is between 0° and 90° when measured from the liquid side. While contact angles within porous media cannot be measured, the wettability of the medium can be deduced from its imbibition behavior (Dullien, 1992). Imbibition, the opposite of drainage or desaturation, denotes the process when the wetting phase saturation is increasing.

Unless treated by a sizing solution to increase wetting resistance, paper undergoes spontaneous imbibition in that water as well as most other wetting fluids will displace the nonwetting gas from the sheet by capillary force alone. This indicates a high degree of wettability, i.e. a very small contact angle. Many researchers in fact simply assume a contact angle of zero between cellulose fibers and water (Spolek and Plumb, 1980; Ramaswamy, 1990; Reardon, 1994). For a number of commercial paper products and grades, a variety of wet end sizing or wetting resistance agents are added to the paper to modify the fiber surface energy so as to reduce the wettability.

Figure 2-7 demonstrates the meniscus in a capillary (pore). Capillary pressure is defined as the pressure difference across the interface between the wetting and nonwetting fluids:

$$P_c = P_{nw} - P_w \quad (2-26)$$

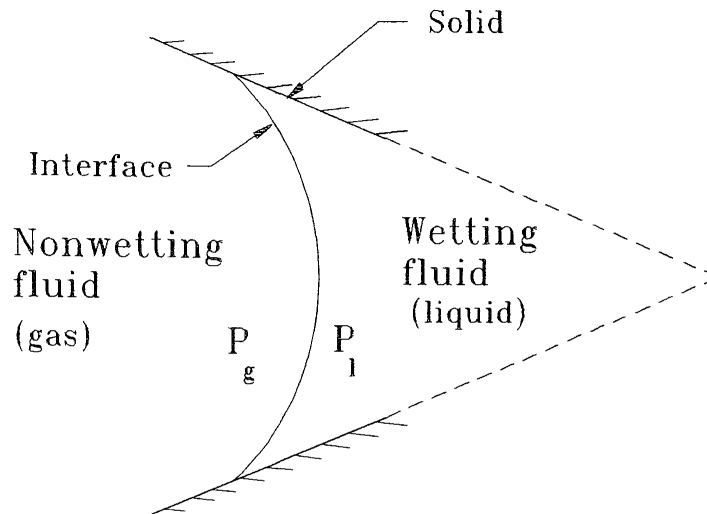


Figure 2-7 Meniscus in a capillary

The Young-Laplace equation (Carey, 1992) relates the capillary pressure across the interface to the interfacial tension (excess free energy per unit of interface area) and the geometry of the interface as specified below:

$$P_{nw} - P_w = \sigma \left(\frac{1}{r_1} + \frac{1}{r_2} \right) \quad (2-27)$$

where σ is the surface tension and r_1 and r_2 are the radii of curvature. In conical pores or cylindrical tubes of small radius, r , the radius of curvature is equal to $r/(\cos \theta)$ where θ is the contact angle measured through the wetting phase. As a result, the Young-Laplace equation becomes:

$$P_c = \frac{2\sigma \cos\theta}{r} \quad (2-28)$$

Hence capillary pressure, defined as the surface tension that maintains a mechanical equilibrium between the two fluids of different pressures, is inversely related to pore radius. For a cylindrical capillary this equation is derived by equating the hydrostatic

pressure difference across the meniscus surface to the surface tension forces acting along the capillary wall surface.

In a porous medium saturated with a wetting fluid, the nonwetting fluid will not imbibe or spontaneously penetrate into the medium and displace the wetting phase unless the pressure in the nonwetting fluid exceeds that of the wetting phase by the amount of the capillary pressure. Considering paper as an assembly of pore bodies and pore throats as discussed in section 2.4.1, the applied pressure must be increased until it exceeds the capillary pressure at the pore throat, where local pore radius is a minimum. Once through the throat, the pore radius expands and therefore the local capillary pressure is less than the applied force, with the result that the wetting fluid is forced out of the pore until the nonwetting fluid encounters a smaller pore throat (Dullien, 1992). The displacement of a wetting phase by a nonwetting phase is typically called drainage.

In a porous medium with pores of a wide size range, capillary migration of the fluid is limited by the size of the pore throats. As drying proceeds and the wetting phase saturation decreases, surface tension draws water preferentially into the smaller pores, for which the capillary pressure is higher. However, hysteresis of contact angle and pore structure effects result in capillary hysteresis (Dullien, 1992). This means that there are a variety of capillary pressure values possible for a given saturation depending on how that saturation level was reached. The limits on capillary pressure hysteresis are the capillary pressure curves obtained from a drainage experiment where the sample was initially 100% saturated with the wetting fluid, and an imbibition experiment where the sample was initially at 0% wetting fluid saturation. The typical shapes of drainage and imbibition capillary pressure curves are illustrated in Figure 2-8 for sandstone (Dullien, 1992). For paper drying analysis, only drainage capillary pressure vs. saturation is relevant and as such has been the subject of experimental measurements. In Chapter 3, section 3.2, drainage curves corresponding to different paper grades are presented.

During drainage of a water-wet porous medium like paper the wetting fluid, water, will initially be displaced from pores of large radius due to surface tension effects. Additional penetration by the nonwetting phase, air, and the resulting drainage of water from smaller pores requires successively higher levels of capillary pressure. The slope of the capillary pressure-saturation curve becomes increasingly steep at lower levels of

saturation. The saturation at which the curve is essentially vertical has been called the “irreducible saturation”. Below this saturation the wetting fluid is trapped, i.e. further increases in capillary pressure will not result in displacement of wetting fluid and reduction of saturation. As noted in section 1.2 of Chapter 1, the range of moisture content for paper entering the dryer section is about 1 to 1.7 kg/kg dry. The exact values of corresponding saturation, S , depend on the particular fiber density and sheet porosity but typically at a moisture content of 1.5 kg/kg dry, pores are up to 80% filled with water while at $X = 1$ pores could be half empty, $S = 0.5$. This subject is further discussed in section 2.5.5.

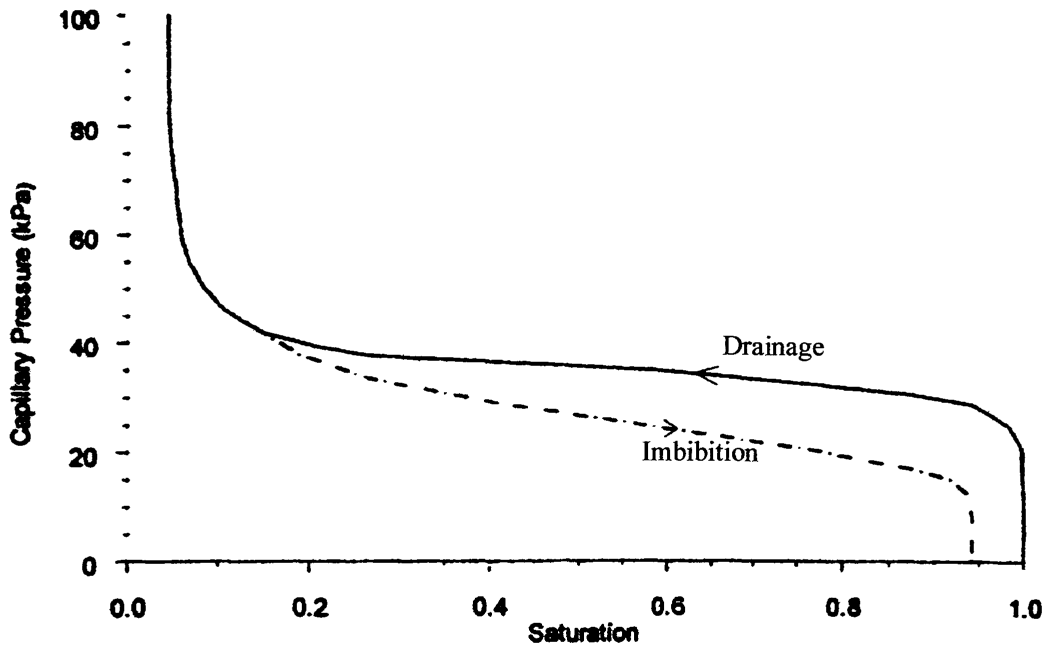


Figure 2-8 Typical capillary pressure curves for imbibition and drainage

2.5.2 Multiphase flow in porous media

In addition to the continuity and energy balance equations developed in section 2.4, a fundamental equation for conservation of momentum for flow through paper is necessary to complete the mathematical description of the drying process. The most common macroscopic momentum equation used to characterize fluid velocities for flow in a porous medium is Darcy’s law. In 1856 Henri Darcy published a 647-page report concerning his efforts to modernize the public water works of Dijon, France (Darcy,

1856; Hubbert, 1956). In an appendix to that report Darcy described his experiments on the determination of flow of water through sand. His apparatus consisted of a vertical iron pipe packed with one of a choice of sand filters through which water flowed at 100% saturation of the sand. Mercury manometers located above and below the sand bed measured the pressure drop across the bed. Darcy observed that the volume of water flow rate per unit cross-sectional area of sand, \dot{Q}/A , was linearly proportional to the pressure drop across the bed:

$$\frac{\dot{Q}}{A} = v = K \frac{h_1 - h_2}{L} = -K \frac{h_2 - h_1}{L} \quad (2-29)$$

where K is a proportionality factor, L the bed thickness, h_1 and h_2 the manometer readings above and below the sand, respectively. Darcy stated that K was a “coefficient dependent on the permeability of the sand”.

Darcy’s original work defined a proportionality factor, K , for a porous medium 100% saturated with water. His law has been extended to other fluids by introducing fluid viscosity. The generalized form of Darcy’s law for single-phase flow in any direction is:

$$\vec{v} = -\frac{K}{\mu} (\nabla P - \rho \vec{g}) \quad (2-30)$$

At low and modest flow rates, Darcy’s law states that the pressure drop for a specific porous medium is directly proportional to flow rate. Equation 2-30 is valid for single phase laminar flow in a saturated homogeneous porous medium where the permeability is independent of position. Thus Darcy’s law is limited to viscous or creeping flow (pore or particle Reynolds number of less than one) for Newtonian fluids having no slip boundaries through an isotropic medium (Dullien, 1992). At higher flow rates, inertial and turbulent flow effects cause deviation from Darcy’s law, for which one method of accommodation is by insertion of a flow correction factor into Equation 2-30.

Darcy’s law can also be derived from the Navier-Stokes equation by local volume-averaging techniques (Hubbert, 1956; Whitaker, 1986; Kaviany, 1991). One approach to

modeling single-phase flow in porous media is to treat it as a flow inside conduits. While the Navier-Stokes equation describes at the microscopic level the motion of fluids in conduits of arbitrary shape, it can only be applied in an average sense to flow through a porous medium which has a complexity of channels available for flow (Bird et al., 1960). Essentially the Navier-Stokes equation describes a balance of forces which relates the pressure gradient to the flow velocity when inertial forces are negligible relative to viscous forces (small Reynolds number flows). Modeling of flow inside conduits as simple, one dimensional, laminar channel flow leads to the Hagen-Poiseuille type of equation. Darcy's law for flow in porous media is analogous to the Hagen-Poiseuille equation for laminar flow in a horizontal pipe:

$$v_{avg} = \frac{D^2 \Delta P}{32 \mu L} \quad (2-31)$$

Alternatively, Equation 2-31 may be considered a special case of Darcy's law rather than vice versa (Hubbert, 1956).

The macroscopic equations for two-phase flow in a porous medium are typically written as a generalization of Darcy's law for single phase laminar flow in a porous medium which apply to both steady and unsteady flow (Bear, 1972; Marle, 1981):

$$\vec{v}_i = -\frac{k_{ri} K}{\mu_i} (\nabla P_i - \rho_i \vec{g}) \quad (2-32)$$

In Equation 2-32 the *effective* or phase permeability, $k_i = k_{ri} K$, of the medium to each fluid, i , is written as a function of the *relative* permeability, k_{ri} , for flow of fluid i and the absolute permeability, K , of the medium. As explained in section 2.5.1, the pressure differential between the nonwetting and wetting fluid at any point in the porous media is defined as the capillary pressure, P_c . Therefore the pressure gradients of the two phases can be related by their capillary pressure gradient:

$$\nabla P_c = \nabla P_{nw} - \nabla P_w \quad (2-33)$$

For the case of air-water flow through paper, liquid water and humid air are, respectively, the wetting and the nonwetting fluid.

Dullien (1992) has discussed the applicability limits of Equation 2-32. This equation is generally valid for strongly water-wetted porous media, i.e. when the contact angle is very small. In this situation, the gas and liquid phases are separated by a stable interface and capillary forces at the liquid-gas interface control the two-phase flow. The nonwetting fluid will preferentially occupy the larger pores and the wetting fluid the smaller pores. However, some wetting fluid will remain in the large pores as a film along the pore wall, thereby forming a continuous network of fluid while the nonwetting fluid flows through the central region of the pores. For this type of water-wetted media the two fluids are hydrodynamically independent and Darcy's law can be applied to each fluid.

In paper drying, free water transport and the convective component of humid air transport are driven by the corresponding pressure gradients. For both flows Darcy's law, Equation 2-32, can be used to express the species velocity, as elaborated in the following sections.

2.5.3 Free water transport

This water transport term in the mass and energy balance equations, Equations 2-7 and 2-23, is related to water average velocity by:

$$\mathbf{n}_{fw} = \rho_{fw} \mathbf{v}_{fw} \quad (2-34)$$

In order to calculate \mathbf{v}_{fw} , the phase average velocity of free water, Darcy's law for multiphase flow, Equation 2-32, is used:

$$\mathbf{v}_{fw} = -\frac{k_r K}{\mu_l} (\nabla P_{fw} - \rho_l \mathbf{g}) \quad (2-35)$$

Therefore the free water mass flux becomes:

$$\rho_{fw} v_{fw} = -\frac{k_r K}{v_l} (\nabla P_{fw} - \rho_l g) \quad (2-36)$$

Recalling the definition of capillary pressure, free water pressure can be expressed as a function of total gas pressure:

$$P_{fw} = P_g - P_c \quad (2-37)$$

so that the liquid mass flux becomes:

$$\rho_{fw} v_{fw} = -\frac{k_r K}{v_l} (\nabla P_g - \nabla P_c - \rho_l g) \quad (2-38)$$

Assumption (xiii) from section 2.4.2, “Negligible gravitational transport of free water and gas phase” will now be used to simplify Equation 2-38. Numerous investigators, Spolek (1981), Plumb et al. (1985), Ramaswamy (1990), Reardon (1994) and Asensio (2000) all consider gravitational transport negligible relative to capillary transport of liquid water. Asensio (2000) estimates that the capillary pressure contribution to fluid flow would be approximately 10 kPa for a moisture gradient of 5% across the sheet thickness (difference of moisture content at the top and the bottom divided by sheet thickness). The corresponding gravimetric pressure contribution to water transport would be an entirely negligible 1-5 Pa. Reardon (1994) obtains similar values and notes that centrifugal pressure generated by the serpentine passage of the web around the cylinders during cylinder dryer section operation will be about 20 Pa and hence also negligible. Thus the mass flux equation takes the following final form:

$$\rho_{fw} v_{fw} = -\frac{k_r K}{v_l} (\nabla P_g - \nabla P_c) \quad (2-39)$$

2.5.4 Water vapor and air transport

The mass fluxes for water vapor, n_v , and air, n_a , are defined relative to a fixed coordinate:

$$n_v = \rho_v v_v \quad (2-40)$$

$$n_a = \rho_a v_a \quad (2-41)$$

The gas phase, a binary air-water vapor mixture, moves relative to the fixed coordinate at the gas bulk velocity of v_g . Due to different molecular weights, the water vapor and air components of the gas phase will inter-diffuse and their respective velocities will be different from that of the gas bulk (Cunningham and Williams, 1980). As a result, the fluxes of water vapor and air with respect to a fixed coordinate can be written as the sum of two components: a convective component due to bulk motion of the gas phase and a diffusive component due to counter-diffusion of water vapor and air. The mass fluxes of water vapor and air are then written as (Bird et al., 1960):

$$n_v = \rho_v v_v = \rho_v v_g + j_v \quad (2-42)$$

$$n_a = \rho_a v_a = \rho_a v_g + j_a \quad (2-43)$$

where

$$j_v = -j_a \quad (2-44)$$

and the $\rho_i v_g$ terms have been introduced for the convective component of species i flux.

As noted in the in previous section, gravitational transport is negligible for free water and, considering the ratio of gas to liquid density, such transport of gas phase is lower yet. Darcy's law for multiphase flow, Equation 2-32, is simplified using the gravitational transport assumption (xiii) from section 2.4.2 to describe the gas phase bulk velocity:

$$v_g = -\frac{k_{rg}K}{\mu_g}(\nabla P_g) \quad (2-45)$$

Whitaker (1977a) presents the diffusive mass flux of each species, j_i , as:

$$j_i = -\rho_g D_{\text{eff}} \nabla \left(\frac{\rho_i}{\rho_g} \right) \quad (2-46)$$

It is possible to express the diffusive flux, written according to Fick's first law of diffusion, in terms of gas phase pressure. First Equation 2-46 is rewritten as:

$$j_v = -\rho_g D_{\text{eff}} \nabla \omega_v \quad (2-47)$$

where $\omega_v = \frac{\rho_v}{\rho_g}$ is the vapor mass fraction. The gradient of mass fraction is related to the gradient of mole fraction by (Bird et al., 1960):

$$\nabla \omega_v = \frac{M_a M_v}{M^2} \nabla y_v \quad (2-48)$$

where M is the molecular weight of the mixture:

$$M = \frac{\rho_v + \rho_a}{\rho_v/M_v + \rho_a/M_a} \quad (2-49)$$

Applying the ideal gas law gives:

$$y_v = \frac{P_v}{P_g} \quad (2-50)$$

Therefore Equation 2-47 can be written as:

$$j_v = -\left(\frac{D_{\text{eff}} M_a M_v}{MRT}\right) P_g \nabla \left(\frac{P_v}{P_g}\right) \quad (2-51)$$

Because of the assumption of local phase equilibrium, water vapor pressure is equal to the saturation pressure while there is liquid water in the pores. In its absence at lower levels of moisture content, vapor pressure can be related to the sorbed water concentration through a sorption isotherm, to be discussed later.

The most comprehensive experimental investigation of the convective flow of humid air through moist paper is that of Polat et al. (1989). This study covered both the low flow rate region where Darcy's law adequately describes the air flow process, and the higher air flow region where Darcy's law must be replaced by the application of the full momentum balance. An important benefit of including both flow rate ranges was that this enabled determination of the characteristic dimension for air flow through moist paper, d_p . This d_p , once determined, applies as the effective pore size dimension over the entire flow rate region from laminar to turbulent flow. Over the moisture content range which occurs from the wet to dry end of a paper dryer Polat et al. found that d_p decreases from the range of 15 to 45 μm for wet paper, down to 5 to 15 μm for dry paper, with this variation of the d_p -moisture content relation being related to basis weight. As Polat et al. also established that air flow through paper should not be treated as flow around particles of the dimension of pulp fibers, but as flow through pores of the size found in paper, the characteristic dimension thereby defined is the appropriate dimension to be used for flow characterization, not the dimension of the fibers as has often been used for this purpose. For the present study, however, as Darcy's law satisfactorily describes the convective flow of gas phase the effective pore size of Polat et al. is not needed.

Fick's law of diffusion applies to ordinary or free molecular diffusion, i.e. diffusion in pores of size much larger than the mean free path of the gas molecules. Knudsen diffusion refers to gas flow occurring in very small capillaries, typically pores smaller than 100 \AA in diameter where the mean free path of the gas molecules is less than the size of the capillary (Dullien, 1992). Knudsen diffusion, which has been included in the

models of Lehtinen (1986) and Perre and Turner (1997), can be modeled using Fick's law and a Knudsen diffusivity coefficient. Lehtinen (1986) estimated that in channels of diameter about 10^{-2} μm , diffusion is totally Knudsen while both normal and Knudsen diffusion occur in channels up to 10 μm . In paper, Knudsen diffusion could be present in the small inter-fiber pores. Perre and Turner (1997) suggested an effective diffusivity by assuming that ordinary and Knudsen diffusion occur in series:

$$D_{\text{eff}} = \frac{1}{\frac{1}{(D_{\text{eff}})_{\text{ordinary}}} + \frac{1}{(D_{\text{eff}})_{\text{Knudsen}}}} \quad (2-52)$$

Knudsen diffusion coefficients are an order of magnitude smaller than ordinary diffusion coefficients and are strongly dependent on pore size. For small pores (0.5 μm) the effective diffusivity relation of Perre and Turner gives values about 40% lower than ordinary diffusion at a pressure of 0.1 atm, only 10% lower at 0.5 atm, while the difference is negligible at $P = 1$ atm. As paper is dried at atmospheric pressure and the gas phase pressure within the sheet can be above atmospheric, only ordinary diffusion need be considered in the modeling of paper drying.

2.5.5 Sorbed water transport

As discussed earlier, water within the sheet may be as free or sorbed water. Sorbed water, also called hygroscopic moisture, includes water in the intrafiber pores and any adsorbed to the walls of pores. The composition of the wood and the nature of the pulping process both affect the amount of sorbed water since lignin and hemicellulose are more hydrophobic than cellulose. For paper made from chemical or chemimechanical pulp, the pulping process and extent of refining also affect the amount of sorbed water.

The extent of adsorption is a measure of the strength of bonding between sorbate and surface. One manifestation of adsorption is the reduction in equilibrium vapor pressure for the sorbate. Figure 2-9 illustrates a typical water sorption isotherm for moist paper (correlation of Bond and Douglas (1996) based on the experimental results of Prahll (1968)). This representation shows the effect of paper moisture content on the vapor

pressure reduction factor (ratio of sorbed water to that for bulk water at the same temperature). Other contributing factors to this vapor pressure reduction for moisture trapped within the fiber walls may be due to dissolved solids and that sorbed water in very small capillaries will exert a lower vapor pressure due to concave curvature of capillary interior surface (Geankoplis, 1993). Sorption isotherms are discussed in more detail in Chapter 3.

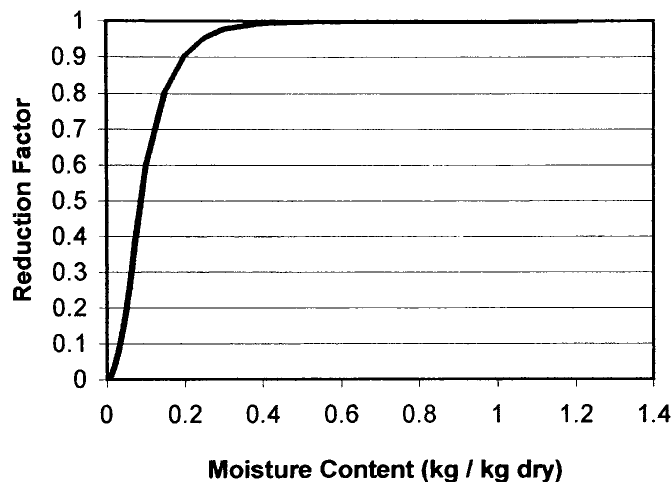


Figure 2-9 Typical water sorption isotherm for moist paper

The hygroscopic nature of paper has a two-fold effect on drying rate. First, at low moisture content the mechanism of drying by vapor transfer is retarded by the reduction in vapor pressure noted above. This effect results in reducing both the vapor density gradient that controls vapor transport by diffusion and the pressure difference that controls vapor transport by convective flow. The second effect is embodied in the differential heat of sorption, the incremental heat of vaporization required to evaporate a unit mass of sorbate (water) from the paper in addition to the free evaporation energy at that temperature. This effect was included in term (e) of the macroscopic energy balance, Equation 2-14. During drying first the free water evaporates, next the water physically absorbed in the fibers, and finally water adsorbed to the lignocellulosic matrix. Adsorbed water is the last to be removed because both the vapor pressure reduction and heat of sorption effects, coming from a common cause, become more significant as drying progresses to low sheet moisture content. Reardon et al. (1999) estimate that with the

approach to zero moisture content, the differential heat of sorption represents 60% of the free water latent heat of vaporization. It is demonstrated in Chapter 3 that the differential heat of sorption becomes significant at dry basis moisture contents below about 0.3 kg/kg dry, consistent with the moisture content at which the vapor pressure drops significantly below that of free water, Figure 2-9.

Before formulating the sorbed water mass flux it is important to identify the onset of the hygroscopic region, i.e. the moisture content at which interfiber pores are completely emptied of liquid water but the fibers remain fully saturated with water. A commonly used identifier of the hygroscopic region is the fiber saturation point (FSP). At the FSP moisture content the fiber cell walls are fully saturated with sorbed water (Spolek and Plumb, 1980; Reardon, 1994). As experimental determination of the FSP (usually done by solute exclusion measurements using polymers of certain molecular size) is not a simple test, correlations have been developed to estimate the fiber saturation point of particular paper grades as a function of temperature (Harrmann and Schulz, 1990).

Another variable which has been used to indicate the hygroscopic region is the water retention value (WRV). The WRV is the moisture content after centrifuging wet pulp for a specified time at a specified g-force, typically 30 minutes at 900 g force. Smook (1990) states that the WRV is a good approximation for the fiber saturation point. In practice, samples of known FSP are normally used to calibrate the centrifuge apparatus for WRV measurement. As the FSP is considered more accurate than the WRV, which is highly dependent on the centrifuge test operation conditions, the FSP is the preferred measurement.

Other indicators of sorbed water have also been suggested. Geankoplis (1993) defines equilibrium moisture content (EMC) as the moisture content of an initially dry material when it comes to equilibrium in an environment of 100% relative humidity. This residual moisture can be identified from isotherm data which relate the equilibrium moisture content in the paper to the relative humidity of the environment for sorption, not desorption. As Prahl (1968) showed, the equilibrium moisture content of paper depends on whether moisture is taken up from a dry state or lost from a wet state, i.e. a significant hysteresis exists between moisture sorption and desorption. As drying is a moisture

reduction process which starts with water in the pores whereas EMC determination starts from dry paper, the EMC value is not relevant to the analysis of drying.

Researchers investigating lumber drying have used the irreducible moisture content, determined for a decreasing moisture content, as the onset of hygroscopic region (Asensio, 2000). This moisture content (explained in section 2.5.1) determined from drainage experiments, corresponds to the moisture at which the capillary pressure curve becomes vertical (Figure 2-8). Below this moisture content increasing the capillary pressure will not cause additional displacement of the wetting phase. Experimental drainage results of Asensio (2000) for linerboard indicate that only sorbed water is present below a moisture content of approximately 56% dry basis (36% wet basis) and that the irreducible moisture content for drainage is temperature sensitive. The FSP is a better indicator of the hygroscopic region than the irreducible moisture content because the latter is determined from drainage experiments where the results are highly dependent on experimental conditions. The FSP enables direct distinction between the free water available for capillary transport and sorbed water unavailable for capillary transport.

In section 2.3 the significance of critical moisture content (X_c , denoting the transition from constant rate to falling rate drying) was discussed. The value of X_c , used by some researchers to identify the onset of hygroscopic region, is not a paper property but is also a sensitive function of drying conditions and drying rate. Kirk and Jones (1970) found that decreases in basis weight and beating would decrease the value of X_c . The extensive studies at McGill University by Polat (1989), Bond (1991), Chen (1994) and Hashemi (1996) all show that for a specific sheet the value of X_c increases significantly with drying rate. For example, Bond found that for a sheet with $X_{FSP} = 0.77$ kg/kg dry, the X_c for air impingement drying of paper varies between 0.2 and 1.5 (dry basis) depending on the drying intensity used. Also, in the range of industrial drying intensities there can be large moisture gradients across the sheet thickness, which is yet another reason why the hygroscopic region cannot be identified from drying rate data.

The conclusion is that the fiber saturation point, the best indicator of the onset of the hygroscopic region, will be used in the present study.

With the exception of the models of Harrmann and Schulz (1990), Lampinen and Ojala (1993), Coumans and Kruf (1994), most models of paper drying do not include

separate mass flux terms for free and sorbed water transport in the general heat and mass balance equations. The Bond and Douglas (1996) model, subsequently refined as reported by Sidwall et al. (1999a), describes transport of water as a diffusive process, without distinguishing free water from sorbed water but with an effective moisture diffusivity for all water transport as a function of moisture content. In the present study, by contrast, sorbed water transport is treated separately from capillary transport of free water. The modeling of sorbed water migration has received more attention for drying wood products where the process is dominated by sorbed water transport (Pang et al., 1994). The numerical values of the various mass fluxes, to be discussed in Chapter 5, will provide quantitative data for the relevant importance of the transport of sorbed water, free water and water vapor.

Sorbed water transport can be analyzed based on irreversible thermodynamics or a mechanistic approach. In the former, sorbed water transport is considered to be driven by the gradient in chemical potential. Siau (1984), Stanish et al. (1986), Nelson (1986), Gong and Plumb (1994) and Asensio (2000) all used the irreversible thermodynamics approach. Since the mechanistic approach is easier to use and will be shown in Chapter 4 to provide excellent results, the irreversible thermodynamics formulation is not further discussed here.

From a mechanistic perspective, transport of sorbed water in the sheet during drying has been modeled as either a capillary or a diffusive process. In the former, Darcy's law with the water vapor pressure gradient as driving force and a permeability for sorbed water migration have been used (Pei and Chen, 1989; Harrmann and Schulz, 1990):

$$n_s = -k_s \nabla P_v \quad (2-53)$$

Harrmann and Schulz (1990) define an effective permeability of paper to transport of sorbed water as:

$$k_s = (1 - S) 3.6 \times 10^{-5} \exp(8\phi) \quad (2-54)$$

determined from the experimental measurements of Ahlen (1970). The $(1 - S)$ factor was applied by Harrmann and Schulz because Ahlen's results were reported for vapor phase and should be modified to account for the effective surface available for sorbed water migration at moisture contents above the fiber saturation point. This indicates an internal contradiction in the Harrmann and Schulz work because above the fiber saturation point there can be no sorbed water transport because all the fibers are saturated.

Although it is possible, by using a form of permeability as introduced above, to describe sorbed water transport with Darcy's law, the movement of sorbed water is governed directly by gradients in sorbed water concentration rather than in pressure. Hence a better as well as more common approach is to model sorbed water transport as a diffusive process with an effective sorbed water diffusion coefficient. Several researchers have considered the sorbed water diffusion process to be driven by the gradient in sorbed water gradient and some have added a term to include a thermal diffusion effect (Perre and Degiovanni, 1990; Couture et al, 1995). Hence the mass flux of sorbed water can be expressed as (Lampinen and Ojala, 1993):

$$n_s = -(1 - \varepsilon)\rho_f D_s \nabla X_s \quad (2-55)$$

where $(1 - \varepsilon)$ represents the volume fraction of solid phase.

Either option within the mechanistic approach, i.e. as a capillary or diffusive transport, can be used in a paper drying model with equal ease. The diffusive process is chosen here because sorbed water concentration driven transport represents the physical reality rather than transport through capillary action when there is no sorbed water present in the capillary network within the sheet. In addition, choice of the diffusion process enables using the existing correlations for effective diffusivity of total moisture (sorbed and free water) which at low moisture content becomes the effective diffusivity of sorbed water. This subject is discussed further in Chapter 3. Thus Equation 2-55 is chosen as the element of the model to represent sorbed water transport.

2.6 Structural changes of moist paper

As a hygroscopic deformable material, paper undergoes structural changes during drying. For rigid, non-hygroscopic porous media, the pore structure and porosity remain constant during drying and all moisture is in the interparticle pores. For deformable porous media, as water is removed during drying the total pore volume varies with external influences such as mechanical loading and with internal effects, notably physical absorption and hydrogen bonding. For hygroscopic media removal of sorbed water causes shrinkage of the solid phase, thereby affecting porosity. During drying the paper structure first changes very little with removal of interfiber water (free water), then to a much greater extent due to the collapse of fibers resulting from removal of intrafiber absorbed water and finally with removal of adsorbed (bound) water. The impact on paper properties of web shrinkage during drying is a critical quality issue in high intensity drying technologies like impingement air drying and Condebelt drying which are being used increasingly.

An understanding of structural changes during drying requires consideration of how water molecules are attached to the fiber matrix. When dry, wood pulp fibers, consisting of about 100 lamellae connected by hydrogen bonds, are not porous (Harrmann and Schulz, 1990). During pulping, however, water molecules diffuse into fibers and dissolve the amorphous regions of cellulose and hemicellulose. The swelling pressure consequently increases. Hydrogen bonds between the lamellae are broken and the distance between the lamellae is increased, thereby enabling more water molecules to enter the fiber, building up a porous system within the fiber. This swelling from water sorption during pulping and the corresponding shrinkage which occurs from water desorption during drying causes changes in fiber thickness but not length. As the fiber orientation within a sheet is anisotropic, with a predominance of fibers in line with the sheet surface and with the machine direction, shrinkage during drying changes the sheet dimensions in the machine direction, cross-machine direction and thickness dimension in the proportion of about 1 to 2 to 50 (Hoyland, 1977). The shrinkage of fibers is not transmitted completely to sheet dimensions because some of the reduction in fiber thickness is reflected as increased sheet void volume and porosity. However for modeling purposes it is commonly assumed that fiber shrinkage is transmitted to sheet thickness

completely, thereby enabling a relationship between moisture content, porosity and thickness.

Several paper structure models have been proposed. The Harrmann and Schulz (1990) model takes into account various types of pores, i.e. those with and without dead ends and inclusions. A probability assessment technique allowed them to evaluate transport properties such as sheet permeability and thermal conductivity as a function of moisture content. Such theoretical models of paper structure for the prediction of transport properties are not used in the present study because well established experimental techniques are available to determine the transport properties directly. However the form of simple relations available in these models for the effect of moisture content on sheet thickness and porosity is useful for the present study.

Relations for the effect of moisture content on paper thickness have been proposed by Rhodius and Gottsching (1979) as well as by Asensio and Seyed-Yagoobi (1994), and used by Wilhelmsson (1995). The thickness is assumed to result from three components: a layer of fibers, a layer of air, a layer of water. Total thickness is simply the sum of the thickness of individual layers. Considering paper in equilibrium with dry air as the reference condition, sheet thickness is expressed as:

$$L = L_{\text{ref}} + \frac{BX}{\rho_1} \quad (2-56)$$

where L_{ref} is the sheet thickness corresponding to X_{ref} for paper of basis weight or grammage, B , air dry mass per unit area.

Based on the same assumption regarding the total thickness, a relation for the effect of moisture content on porosity, proposed by Asensio and Seyed-Yagoobi (1994), is:

$$\varepsilon = 1 - \frac{1 - \varepsilon_{\text{ref}}}{1 + \frac{XB}{\rho_1 L_{\text{ref}}}} \quad (2-57)$$

where the corresponding ε_{ref} is:

$$\varepsilon_{\text{ref}} = 1 - \frac{1}{\rho_f - \rho_a} \left(\frac{B(1 - X_{\text{ref}})}{L_{\text{ref}}} - \rho_a \right) \quad (2-58)$$

Equations 2-56 and 2-57 were used by Asensio and Seyed-Yagoobi in simulation of 300 g/m² linerboard drying from a moisture content of 1.5 to 0.06 kg/kg dry. For this grade they had the thickness of the wet sheet entering the dryer almost double the dry sheet thickness. Although they did not validate the thickness variation directly, the simulation of drying was reported to be successful. While Asensio and Seyed-Yagoobi ignored the distinction between the effect of sorbed water and free water on structural properties, Reardon (1994) used an expression similar to Equation 2-56 with the qualification that thickness change occurs only below the fiber saturation point, used as the identifier for the hygroscopic region, i.e. the relation using only for $X < X_{\text{FSP}}$. Reardon ignored any porosity variation during drying. Kruf et al. (1995) advocate a similar approach, allowing the web to shrink linearly with moisture removal once the moisture falls below the fiber saturation point.

What is needed in the present study is a set of equations for the sheet porosity and thickness changes during drying which reflects the hygroscopic behavior of paper. The approach adopted here to calculate web thickness and porosity as a function of moisture content is similar to that of Harrmann and Schulz (1990). Different equations are required for moisture contents above or within the hygroscopic region, taken here as starting at the fiber saturation point, which is a function of temperature. In the following, Equation 2-59 for sheet thickness is in principle similar to Equation 2-56, i.e. the basic idea is retained of total sheet thickness being equal to the sum of individual layer thickness. Bone dry paper (subscript bd) is, however, considered as the reference condition, eliminating the need for identifying the equilibrium moisture content. The basis weight term in Equation 2-56 is therefore replaced with equivalent expression based on the bone dry properties. For $X > X_{\text{FSP}}$ the web thickness and porosity are no longer a function of moisture content and therefore Equation 2-61 applies. These equations have not been validated directly but have been used in validating the present model (Chapter 4). Harrmann and Schulz also

used the same equations without independent validation in a drying simulation claimed to be successful.

$$X \leq X_{\text{FSP}}(T)$$

$$L(X, T) = L_{\text{bd}} \left[1 + \frac{X \rho_{\text{bd}}}{\rho_1 (1 - \varepsilon_{\text{bd}})} \right] \quad (2-59)$$

$$\varepsilon(X, T) = 1 - \frac{1 - \varepsilon_{\text{bd}}}{1 + \frac{X \rho_{\text{bd}}}{\rho_1 (1 - \varepsilon_{\text{bd}})}} \quad (2-60)$$

$$X \geq X_{\text{FSP}}(T)$$

$$L(T) = L_{\text{bd}} \left[1 + \frac{X_{\text{FSP}} \rho_{\text{bd}}}{\rho_1 (1 - \varepsilon_{\text{bd}})} \right] \quad (2-61)$$

$$\varepsilon(T) = 1 - \frac{1 - \varepsilon_{\text{bd}}}{1 + \frac{X_{\text{FSP}} \rho_{\text{bd}}}{\rho_1 (1 - \varepsilon_{\text{bd}})}} \quad (2-62)$$

In conclusion, once the basis weight, thickness and porosity of the dry sheet are known the thickness and porosity at any moisture content and temperature are calculated with Equations 2-59 and 2-60, or 2-61 and 2-62, depending on whether the sheet moisture content is above or within the hygroscopic region. As documented in Chapter 5 there are considerable gradients of moisture content and temperature in the thickness direction of the sheet. In the present model sheet porosity is calculated locally as a function of moisture content and temperature. Sheet thickness, however, is calculated based on the sheet average moisture content and temperature at any stage of the drying.

2.7 Summary

A comprehensive microscale model of paper drying was developed which includes all relevant species: fibers, free water, sorbed water, water vapor and air. This model does not suffer from the common shortcomings of the paper drying models discussed in Chapter 1 as the presence of none of the species has been ignored, all main transport mechanisms in all phases are included, and the sheet structural changes are treated. The fiber saturation point (FSP) is identified as the best indicator of the onset of hygroscopic region, i.e. the moisture content at which fibers are saturated with water but there is no water in the interfiber pores. Several effects of the hygroscopic nature of paper were included in the model. Two of these effects relate to the thermodynamic properties of moist paper, the reduction of vapor pressure for adsorbed water and increase in energy required to evaporate adsorbed water. Two other effects relate to the structural properties of moist paper, the sheet thickness and porosity. A continuum approach, along with considering the paper as a homogenous porous medium, was used to develop the general heat and mass balance equations. The resulting mass balance equations were reduced to two: Equation 2-7 for total moisture and Equation 2-10 for air. Equation 2-23 represents the general energy balance containing the contributions of convective fluxes, conduction and evaporation-condensation. Four mass flux terms are needed in the mass and energy balance equations thus developed. For each species, the mass flux was identified according to the relevant transport mechanism: capillary transport for free water, both convection and diffusion for humid air, diffusion for sorbed water. In all, about 50 basic equations including about 30 parameters are required in the most comprehensive model for drying paper yet developed.

CHAPTER 3

TRANSPORT AND THERMODYNAMIC PROPERTIES

In Chapter 2 macroscopic mass and energy balance equations were developed which, along with mass flux correlations and shrinkage/porosity estimation, provide a complete description of internal heat and mass transfer and the resulting moisture, temperature and air humidity profiles within the sheet during drying. The various model parameters, in this case the transport properties, capillary pressure and thermodynamic properties are presented in sections 3.1, 3.2 and 3.3 while the boundary conditions and numerical solution are given in the Appendix.

3.1 Transport properties in moist paper

Transport properties relate the flow, heat and mass transfer fluxes to the relevant gradients or differences of pressure, temperature and moisture content. With the mechanisms shown in Chapter 2 to control the internal transport phenomena during drying, five transport properties of moist paper are required: permeability (absolute and relative), thermal conductivity, water vapor diffusivity and sorbed water diffusivity. For each property, numerous correlations developed either theoretically or from experimental data are available. It will be seen that only for the case of absolute permeability is it clear what basis should be used for the model developed here. For the other transport properties the decision concerning which correlation to select will be based on the performance of the model when validated against operating data from dryer sections of many paper machines producing a wide range of grades, as detailed in Chapter 4.

3.1.1 Absolute permeability

Permeability represents the conductivity of porous media with respect to permeation by a Newtonian fluid (Dullien, 1992). The permeability in Equation 2-30, identified as K , is an absolute permeability which applies when the pores contain only a single fluid. Absolute permeability, which depends on the porosity and pore size distribution in the media, is proportional to the cross-sectional area of pores open to flow and inversely related to the average flow length. Darcy's law, as presented in Equation 2-

30, defines the permeability or fluid conductance in a porous media, in the same way that Fourier's law defines thermal conductivity:

$$\vec{v} = -\frac{K}{\mu}(\nabla P - \rho \vec{g}) \quad (2-30)$$

Only permeability in the sheet thickness dimension is discussed here because all transport in the present model, as discussed in Chapter 2, relates to that direction.

As permeability represents the bulk hydrodynamic behavior of the flow, description of the small scale pore structure is not pertinent. While no general relationship exists between effective porosity and permeability, several semi-empirical correlations have been developed. Dullien (1992) and Kaviany (1991) review the permeability models for flow in porous media. These models are generally based on conduit flow in which fluid flow in a porous medium occurs through a network of conduits.

The most common permeability model is the hydraulic radius theory of Kozeny-Carman (Kozeny, 1927; Carman, 1937, 1938). Here the porous media is modeled as an assembly of capillaries or conduits of a defined average hydraulic radius. Laminar flow within the channels is described with a Hagen-Poiseuille type equation while an average internal velocity reflects the porosity of the medium. Although Kozeny-Carman theory was developed for laminar flow, the hydraulic radius concept is used as an acceptable approximation under turbulent flow. Thus use of the hydraulic radius concept represents an assumption dependent on porous media flow experiments, not on hydraulics theory. The usual form of the Kozeny-Carman equation for permeability to single-phase flow (Dullien, 1992) is:

$$K = \frac{\varepsilon^3}{k_0 \left(\frac{L_e}{L}\right)^2 (1-\varepsilon)^2 S_0^2} \quad (3-1)$$

where S_0 is the specific area of the pores and k_0 is a shape factor. The specific surface of a porous body is defined as the interstitial surface area of the voids and pores, either per

unit mass or unit bulk volume. The $(L_e/L)^2$ term is a hydraulic “tortuosity factor”. Flow through the medium is affected by tortuosity, an indicator of the winding, twisted path a fluid must follow. Darcian flow is measured via a net flow velocity and a pressure drop across a material length, L , while the fluid actually travels a distance of L_e , the length of the tortuous path.

The Kozeny-Carman permeability equation as expressed by Ingmanson et al. (1959) is:

$$K = \frac{\epsilon^3 S_v^2}{k' (1 - \epsilon)^2 S_A^2} \quad (3-2)$$

where S_v is the specific volume of the medium, i.e. the reciprocal of its bulk density, and S_A is the specific surface area of the solid matrix while the composite factor $k' = k_0 (L_e/L)^2$ is termed the Kozeny constant. According to Carman, for most packed bed experimental data, the best value of this constant is 5. However Wyllie and coworkers (1952, 1953) sometimes obtained values for this Kozeny constant much greater than 5 (Dullien, 1992). Ramaswamy (1990) used Carroll’s correlation for the Kozeny constant (source not reported):

$$k' = 5.0 + \exp [14.0(\epsilon - 0.8)] \quad (3-3)$$

In order to calculate the absolute permeability of linerboard, Ramaswamy considered the specific surface and specific volume to be $920 \text{ m}^2/\text{kg}$ and $2.86 \times 10^{-3} \text{ m}^3/\text{kg}$.

Ingmanson (1952) concluded that Equation 3-2 was valid for water removal from pulp webs. Bliesner (1964) found that the Kozeny constant does not apply to thin mats because of the densification during pressing due to fiber collapse. Because Bliesner found the standard Kozeny-Carman equation based on capillary pores (Equation 3-1) to be inadequate for flow through paper, he proposed a modified hydraulic radius theory in which pore size distribution was included to account for flow tortuosity and multiple flow paths.

Reardon (1994) also rejected the application of Equation 3-1. A circular pore model with a pore size distribution determined experimentally was used for dry newsprint of specific volume $1.7 \times 10^{-3} \text{ m}^3/\text{kg}$ to calculate its specific area as $3100 \text{ m}^2/\text{kg}$. Application of the Kozeny-Carman equation then yielded a permeability twenty times that measured experimentally for air flow using a Parker Print-Surf tester at Australian Newsprint Mills Limited. Thus Reardon's study led to findings similar to those of Bliesner (1964).

Dullien (1992) as well as Murakami and Imamura (1984) have noted that the Kozeny-Carman equation, developed for spherical particles, may have limited validity for porous media of considerably different pore shape and structure. For deformable porous media the experimental permeability values often differ from those predicted by Kozeny-Carman equation. Kerekes and McDonald (1991) were however able to apply the Kozeny-Carman model to describe the dewatering of wet paper during pressing.

Measuring air flow, Nilsson (1996) compared the experimental permeability of paper to that from a theoretical model. His model was for creeping flow through a two-dimensional fiber mat subjected to a pressure gradient with the fibers modeled as cylindrical and band-shaped structures. Good agreement was obtained for specific fiber aspect ratios. Nilsson notes that the calculated permeabilities from a similar model by Wang (1996) reduce to expressions based on the Kozeny-Carman equation.

The alternative to relying on permeability models as discussed above is to use experimentally determined absolute permeabilities in the thickness direction. Laboratory techniques for measuring absolute permeability are typically steady-state displacement experiments. The procedure is based on Darcy's law where pressure drop across a sheet is related to the volumetric through flow rate of the fluid. The Gurley type permeability tester used in the paper industry measures gas absolute permeability following the TAPPI Technical Information Sheets TIS 460 om-96 (TAPPI, 1996b) or TIS 547 pm-88 (TAPPI, 1996c). Alternatively, displacement experiments have been conducted using water as the fluid (Lindsay and Brady, 1993a and 1993b).

The absolute permeability typically measured in the paper industry may be valid only for gas flow at low velocity due to the testing methods. For example, a standard Gurley tester supplies air at 1.22 kPa and measures the time for 50 to 300 cm^3 to pass

through the sheet. The resultant superficial velocities are less than 1 m/s whereas commercial through air dryers for tissue and towel grades, where drying capacity depends significantly on web permeability, operate with superficial velocity exceeding 4 m/s. This problem is not relevant to the present study as the convective gas phase velocity for the cylinder and Yankee dryers considered here does not exceed about 0.1 m/s.

Darcy's law is applied equally to gas and liquid flow through porous media. Thus if the sheet structure is the same, the absolute permeability would be the same for air or water flow through paper. As the fibers are saturated in determination of absolute permeability by water flow, then with air flow the same absolute permeability would be obtained only if the fibers are saturated, i.e. at the fiber saturation point. Another potential source of difference derives from gas compressibility and slippage at the gas-solid boundary. Gas compressibility causes the volumetric flow and velocity to vary in the direction of flow. Dullien (1992) derived a version of Darcy's law applicable to compressible gas flow. For gas flow at low pressure and in small capillaries where the mean free path of the gas molecules is on the order of the pore size, the gas velocity within the mean-free path from the wall is non-zero and becomes significant with respect to the average gas velocity in the channel. This velocity slip along the boundary constitutes the Knudsen diffusion discussed in section 2.5.4, which results in higher values of gas permeability (Kaviany, 1991). Due to Knudsen diffusion, the gas absolute permeability values measured under low pressure for materials of low permeability (small pores) are therefore larger than those measured for liquids. A slippage-correction method for determining the true gas permeability for the measured apparent gas permeability was developed by Klinkenberg (1941), who showed that gas permeability is linearly related to the reciprocal of mean pressure. The derived true gas permeability is then considered identical to liquid permeability. For reasons noted in Chapter 2, Knudsen diffusion is not included in the present study.

Asensio (2000) summarized all the experimentally determined values, as listed in Table 3-1. Although permeability for paper is typically given in m^2 , the more common unit of permeability is the darcy, d , based on its definition by Darcy's law. A porous medium has a permeability of one darcy if a pressure gradient of 1 atmosphere produces,

for a fluid with a viscosity of 1 centipoise (cP), a flow rate of 1 cm²/s through a 1 cm³ cube. Therefore the conversion factor is 1 d = 0.987×10⁻¹² m².

The Table 3-1 data cover most commercial paper grades although in all cases only limited number of sources are available for each grade. Polat et al. is the only source for tissue, with two measurements providing almost identical results. The average of the two is used in the present study. As Nilsson is the only source for LWC and fine paper, his determinations are used here. For newsprint three sources are available (Nilsson, Reardon and Asensio). In the absence of any reason for rejection or preference, the average value is used here. As for linerboard, again the average value of the two sources available (Nilsson and Asensio) is used in the present study.

Table 3-1 Experimental values of thickness direction absolute permeability

Reference	Medium	Method (fluid)	Value (m ²)
Nilsson (1996)	Linerboard	Gurley (air)	7-23 × 10 ⁻¹⁵
	Lightweight coated paper		1.7 × 10 ⁻¹⁵
	Newsprint		2-10 × 10 ⁻¹⁵
	Fine paper		13.5 × 10 ⁻¹⁵
	Pulp sheet (softwood)		460 × 10 ⁻¹⁵
	Pulp sheet (hardwood)		48 × 10 ⁻¹⁵
	Handsheets (softwood)		1-5 × 10 ⁻¹⁵
Reardon (1994)	Newsprint	Parker-Print (air)	5-12 × 10 ⁻¹⁵
Lindsay and Brady (1993)	Handsheets (softwood)	Displacement (water)	0.1-1 × 10 ⁻¹³
	Handsheets (hardwood)		0.5-6 × 10 ⁻¹⁵
Polat et al. (1993)	Handsheets (softwood)	Displacement (air)	2-3 × 10 ⁻¹⁴
	Handsheets (tissue weight)		9.43 × 10 ⁻¹⁴
Polat et al. (1993)	Handsheets (softwood)	Displacement (helium)	2.75 × 10 ⁻¹⁴
	Handsheets (tissue weight)		9.35 × 10 ⁻¹⁴
Asensio et al. (1994)	Newsprint	Gurley (air)	4 × 10 ⁻¹⁴
	Linerboard		8 × 10 ⁻¹⁶

3.1.2 Relative permeability

(a) Simultaneous flow of gas and liquid through porous media

For multi-phase flow in a porous media the permeability of the media to flow of each fluid is reduced due to the presence of the other phase. Relative permeability is the ratio of the effective permeability to the absolute permeability of the media to flow of a fluid when it is the only fluid present:

$$k_{ri} = k_i / K \quad (3-4)$$

Thus flow through a porous medium not fully saturated (i.e. pores not filled with one fluid) is analogous to flow through a medium of reduced permeability.

In the limiting case of very slow drying of paper, as illustrated in Figure 2-4, there would be negligible gradients of moisture content across the thickness direction of the sheet. However under industrial conditions of paper drying the moisture content difference across the sheet can be very significant with the paper surface being completely dry while at some interior position the moisture content remains high. Under such conditions, when free water is present it will flow by capillary force from high moisture content regions, where it occupies larger pores, to regions of lower moisture content where there is water only in smaller pores. Thus water is displaced by the nonwetting fluid (humid air) first from the larger pores, then progressively from smaller pores. The cross-sectional area available for water flow decreases during desaturation while its average flow path length increases because the remaining water must flow around air filled pores. For strongly wetted media such as paper, even before all of the water is removed from the pores, leaving only water saturated fibers, the water remaining in the smaller pores will be in isolated regions that are separated by regions of humid air. Therefore the relative permeability of water will approach zero while the moisture content is such that there is still significant amount of water in the pores, but it is isolated in non-communicating regions. Such water, being trapped, can no longer flow by capillary transport. Therefore as water is removed during drying, the effective permeability for water through wet paper decreases while that for humid air increases.

Relative permeability can be a function of both the pore structure and other system parameters such as the wetting angle, flow rates, fluid viscosity or density ratios. Relative permeability is usually reported as a function of saturation and capillary hysteresis. Capillary hysteresis causes fluid distribution within the pores to differ depending on whether the process is water imbibition or drainage (section 2.5.1). For application to drying, only permeability for water removal need be considered. Relative permeability data have been widely reported for the case of petroleum production. There are experimental methods (steady and unsteady state) as well as analytic techniques for relative permeability estimation (Rose, 1987). As the permeability of a medium to multi-phase flow is a strong function of its pore structure, the relative permeability is also a function of the underlying capillary pressure which dictates the amount of fluid flow. From a given capillary pressure-saturation relationship, mathematical models enable direct calculation of relative permeability for both the wetting and nonwetting phase.

Wyllie and Gardner (1958) developed a statistical model relating relative permeability to wetting phase saturation. Their model is based on separate Hagen-Poiseuille flows of the wetting and nonwetting fluids through segments of capillary tubes. The hypothetical pore structure is created by slicing perpendicularly through a bundle of capillary tubes of different size, rearranging the tube pieces within each slice, then re-layering the slices to generate a random connection of pores. Based on the structure thus developed, a pore size distribution is obtained. Saturation, the ratio of the volume of wetting phase fluid to total pore volume, is related directly to the pore size distribution. The permeability-saturation equations of Wyllie and Gardner may be developed using the Hagen-Poiseuille equation for flow through cylindrical pores (Dullien, 1992). Having been also developed earlier by Burdine (1953) using hydraulic radius theory, these equations are also termed the Burdine equations. Brooks and Corey (1966) generalized the equations by incorporating an empirical capillary pressure-saturation relation, developed based on consolidated rock desorption data. They thereby obtained a widely used empirical correlation for relative permeability.

(b) Relative permeability of water and air: Without furnish dependency

Although numerous relations for relative permeability have been proposed for lumber drying (Spolek and Plumb, 1980; Perre and Degiovanni, 1990; Perre et al., 1993; Couture et al., 1994) there has been less treatment for the case of paper. Insufficient data for the relative permeability of water and air limits the ability to predict drying rate and the internal distribution of moisture and temperature within paper.

The first of the three treatments presented here concerning relative permeability derives from the determination by Robertson (1963) of the relative permeability of a fiber mat (sulfite pulp) to water flow, for which Ahrens and Journeaux (1984) provided an empirical correlation for relative permeability of water, k_{rl} :

$$k_{rl} = \begin{cases} 4.51 \times 10^{-12} \exp(25.86 S) & 0.82 < S \leq 1 \\ 6.93 \times 10^{-6} \exp(8.54 S) & 0.36 < S \leq 0.82 \\ 1.0 \times 10^{-11} \exp(46.05 S) & 0.15 < S \leq 0.36 \\ 0 & S \leq 0.15 \end{cases} \quad (3-5)$$

where water saturation, S , is related to moisture content by Equation 2-1:

$$S = \frac{1 - \varepsilon \frac{\rho_f}{\rho_l} X}{\varepsilon \frac{\rho_f}{\rho_l}} \quad (2-1)$$

In the absence of experimental data for humid air relative permeability, k_{rg} , Ahrens and Journeaux postulated that the entire increase of k_{rg} from 0 to 1 occurs linearly with saturation as S goes from 1 to 0.5, i.e.:

$$k_{rg} = \begin{cases} 1 & S \leq 0.5 \\ 2 - 2S & 0.5 \leq S \leq 1 \end{cases} \quad (3-6)$$

In the second treatment of moist paper permeability, Lampinen (1979) developed analytic models of relative permeability and approximated liquid water relative permeability, k_{rl} , from the gas relative permeability, k_{rg} , by:

$$\frac{(1-S)^3}{k_{rg}/k_{rg,max}} + \frac{S^3}{k_{rl}/k_{rg,max}} = 1 \quad (3-7)$$

where the saturation term is defined as:

$$S = \frac{\rho_f}{\rho_l} \frac{X}{\varepsilon} \quad (3-8)$$

Based on this model Lampinen and Toivonen (1984) reported, without providing details, their experimental determination of air relative permeability for newsprint as:

$$k_{rg} = \frac{c_1}{T} \left[\exp(c_2 T X^{c_3}) - \exp(c_2 T X_0^{c_3}) \right] \quad (3-9)$$

$$k_{rg,max} = \frac{c_1}{T} \left[1 - \exp(c_2 T X_0^{c_3}) \right] \quad (3-10)$$

where the constants are: $c_1 = 7.988 \times 10^{-12} \text{ m}^2\text{K}$, $c_2 = -2.601 \times 10^{-3} \text{ K}^{-1}$, $c_3 = 1.378$ and $X_0 = 1.581 \text{ kg/kg dry}$.

In the third approach to paper permeability, one based on a purely theoretical paper structural model, Harrmann and Schulz (1990) provide the following correlations for relative permeability for air-water flow through paper:

$$k_{rl} = S^{c_3} \quad (3-11)$$

$$k_{rg} = \frac{\exp(c_1 S^{c_2}) - \exp(c_1)}{1 - \exp(c_1)} \quad (3-12)$$

where $c_1 = -6.68$, $c_2 = 3.11$, $c_3 = 5.13$ and the water saturation is defined as:

$$S = \frac{X - X_{\text{FSP}}}{X_{\text{max}} - X_{\text{FSP}}} \quad (3-13)$$

The fiber saturation point, X_{FSP} , was discussed in section 2.5.5. Harrmann and Schulz define X_{max} as the maximum moisture content for paper, but give no numerical values.

Harrmann and Schulz developed their correlations based purely on a model of paper structure, i.e. with no experimental measurements. They included three types of pores: those with a dead end, those open to capillary flow, and inclusions, i.e. pores completely separated from the network. By calculating the probability of a connection between each type of pore they could not only estimate sheet thickness and porosity during drying but also to provide correlations for transport properties such as permeability and thermal conductivity. Harrmann and Schulz used a definition of saturation different from that of Ahrens and Journeaux, i.e. a saturation derived from their paper structure model.

For relative permeability of both water and humid air in moist paper, Figures 3-1 and 3-2 show the substantial difference between the correlations of Ahrens and Journeaux for Robertson's data (Equations 3-5 and 3-6) and those of Harrmann and Schulz (Equations 3-11 and 3-12). Possible reasons for the observed differences are noted above.

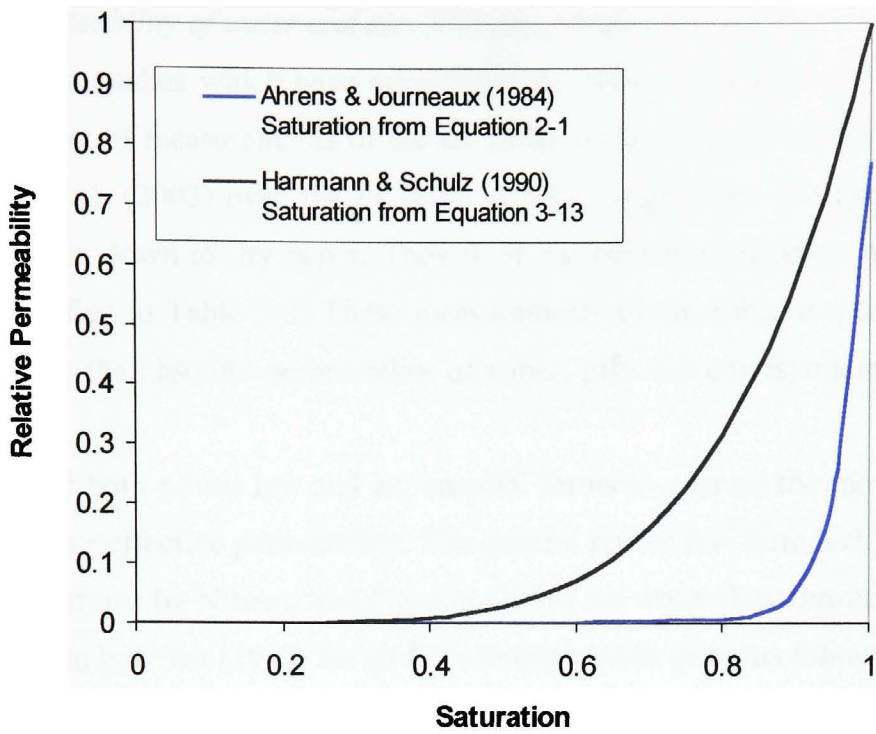


Figure 3-1 Correlations for water relative permeability of moist paper

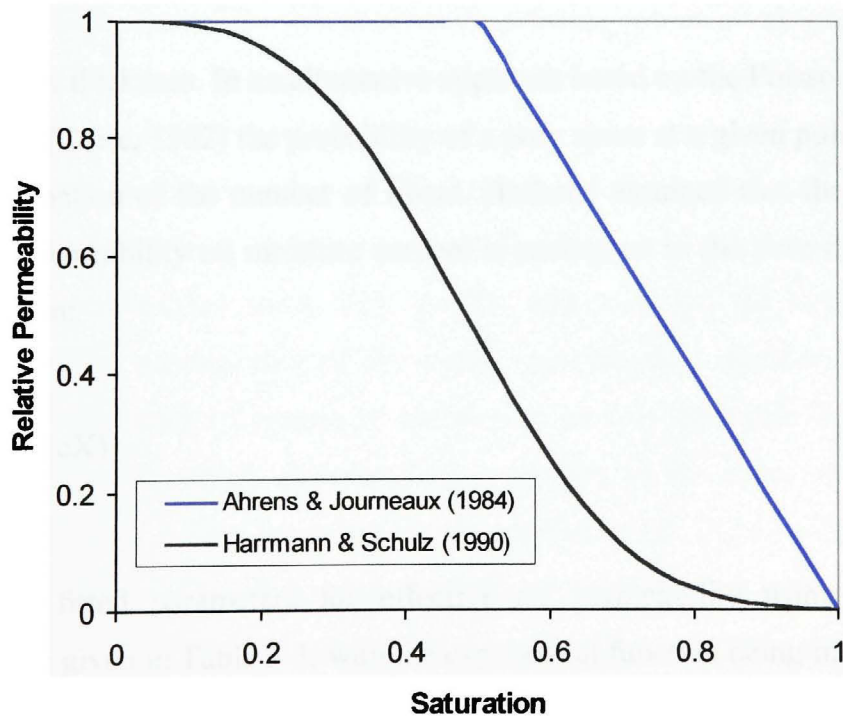


Figure 3-2 Correlations for air relative permeability of moist paper

(c) Relative permeability of water and air: With furnish dependency

Of the two studies which have considered the effect of furnish, the first was the comprehensive set of measurements of the air permeability of paper by Hashemi (1996) and Hashemi et al. (2002) over the moisture content range from that typical of paper entering the dryer down to dry paper. They used machine-formed paper made from 10 furnishes, identified in Table 3-2. These measurements of air effective permeability, k_i , when divided by the absolute permeability of paper, give the corresponding air relative permeability.

They used both power law and exponential forms to express the moisture content dependence for air effective permeability. The general power law form had been used for permeability relations by Nilsson and Larsson (1968) for water flow through paper webs in press nips, then by Polat (1989) for air flow through moist paper as follows:

$$\frac{L}{k_i} = A + B X^c \quad (3-14)$$

with L the sheet thickness. In an alternative approach based on the Poisson distribution of fibers in paper (Corte, 1982) the probability of a pore space at a given point is taken as an exponential function of the number of fibers. Hashemi assumed that the dependence of effective air permeability on moisture content is analogous to the pore diameter-number of fibers relation:

$$\frac{L}{k_i} = a + b \exp(cX) \quad (3-15)$$

The resulting fitted parameters for effective air permeability using both types of correlations are given in Table 3-3, with the exponential function being marginally better.

Table 3-2 Grades used for air relative permeability determination (Hashemi, 1996)

Type	Basis Weight g/m ²	Pulp Furnish of Paper Tested	% Fines Content
1	42.8	100% TMP	30.7
2	57.3	100% TMP	33.1
3	47.5	100% TMP	32.4
4	43.8	100% TMP	36.2
5	44	100% TMP	34.3
6	44.2	33% TMP, 59% GW, 8% SBK	36.5
7	44.5	48% TMP, 52% Flotation deinked	37.3
8	47.7	71.5% SGW, 28.5% Bleached kraft	44.2
9	68.5	100% Bleached filled kraft	28.3
10	81.7	100% Bleached filled kraft	28.8

Hashemi also studied the effect of wetting-drying cycles on air permeability. This characteristic is relevant because laboratory studies of paper permeability or drying generally start with a dry sheet which is then wetted. However for the application of such results only the characteristics of never-dried paper are of industrial relevance. The study by Polat (1989) of the effect of such a wetting-drying cycle showed that after a cycle of first drying the never-dried sheet, then wetting and re-drying the sheet, for the kraft handsheets used the permeability of dry paper approximately doubles. Both Polat and Hashemi found that major changes in the drying part of the cycle had no effect on permeability of the dry sheet, thus identifying wetting as the cause of the changes in permeability resulting from a complete wetting-drying cycle. Figure 3-3, from Hashemi (1996) and Hashemi et al. (2002), demonstrates a normalized air permeability, defined below, as a function of moisture content for machine-formed paper made from the 10 furnishes identified in Table 3-3 as well as for kraft handsheets. Figure 3-3 in addition provides their demonstration of the effect of 1,2 and 3 wetting-drying cycles on the normalized air permeability of type 1 paper. Also shown is the generalized permeability curve, a power law best fit for the 10 types of machine-formed paper tested, as follows:

Table 3-3 Parameters for effective air permeability-moisture content relations
for paper (Hashemi, 1996)

Paper Type	Exponential Model				Power Law Model			
	$a \times 10^{10}$	$b \times 10^{10}$	c	R^2	$A \times 10^{10}$	$B \times 10^{10}$	C	R^2
1	0.840	0.101	4.532	0.99	0.904	0.848	5.400	0.98
2	1.400	0.218	4.420	0.99	1.516	1.685	5.222	0.99
3	0.407	0.141	3.149	0.99	0.439	0.303	3.677	0.99
4	0.500	0.915	2.120	0.99	0.627	0.657	2.536	0.99
5	1.125	1.043	2.976	0.99	1.343	1.885	3.471	0.99
6	0.276	0.381	1.848	0.99	0.325	0.199	2.298	0.99
7	0.628	0.242	3.458	0.99	6.962	7.131	4.040	0.99
8	0.836	0.027	5.527	0.99	0.877	0.592	6.717	0.98
9	0.469	0.331	3.448	0.99	0.511	0.731	2.288	0.99
10	0.613	0.085	6.023	0.99	0.634	2.157	3.819	0.99

$$\frac{k_i/L}{(k_i/L)_0} = 1.0 - a X^b \quad (3-16)$$

where $(k_i/L)_0$ refers to the dry paper. A best fit of the parameters gave values of $a = 0.52$ and $b = 1.35$.

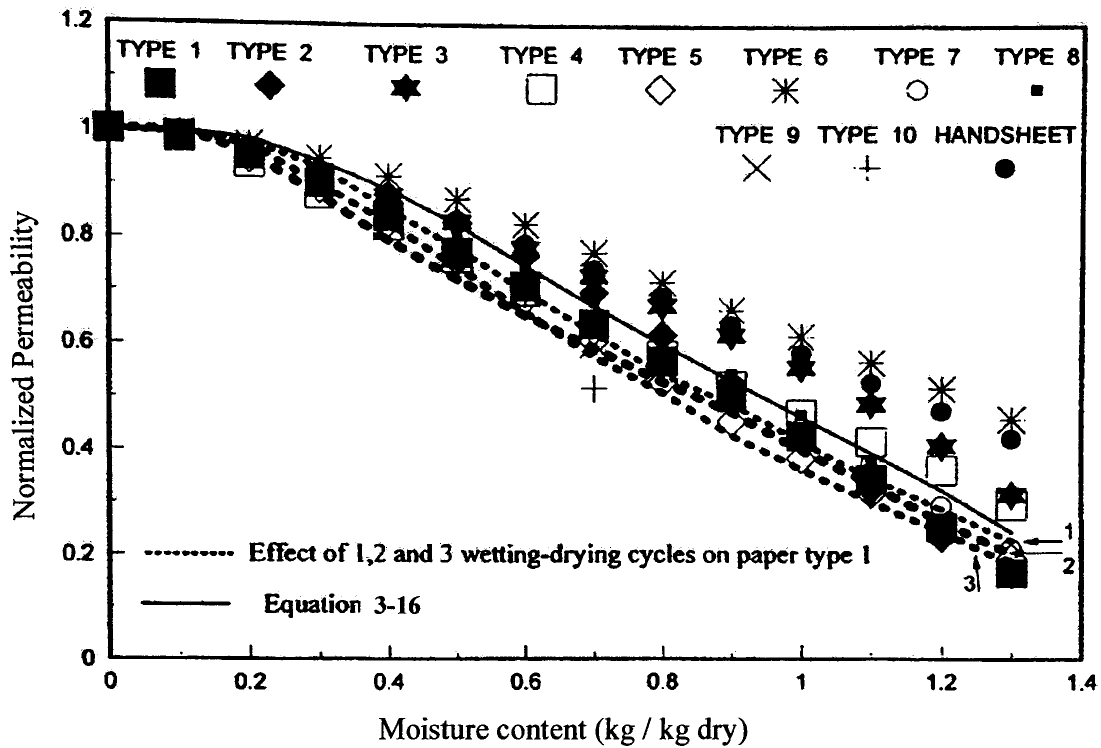


Figure 3-3 Effect of moisture content on normalized air permeability of paper (Hashemi, 1996; Hashemi et al., 2002)

The other study of moist paper permeability which incorporated the effect of the furnish was that by Asensio (2000). Using experimental measurement of the dependence of capillary pressure on saturation she applied the model of Wyllie and Gardner (1958), discussed in section 3.1.2 (a), to develop correlations for air and water relative permeability of paper. Although the original Wyllie-Gardner model was developed for rigid, non-hygroscopic porous media, Asensio presents a version modified to accommodate deformable hygroscopic material like paper.

After integrating the Wyllie-Gardner model equations Asensio correlated water relative permeability using the following two functional forms suggested by Lake (1989):

$$k_{ri} = a X_{fw}^b \exp(X_{fw}^c) \quad (3-17)$$

$$k_{ri} = a (X_{fw}/2)^b \exp[(X_{fw}/2)^c] \quad (3-18)$$

where X_{fw} represents the free water content:

$$X_{fw} = X - X_h \quad (3-19)$$

As discussed in Chapter 2, the fiber saturation point is considered in the present study as the onset of hygroscopic region, X_h , and the free water content is calculated accordingly. Asensio however used the irreducible moisture content, as defined in section 2.5.5, to identify the onset of hygroscopic region. The best fit values of the coefficients in Equations 3-17 and 3-18 as calculated by Asensio are tabulated in Table 3-4 for the furnishes she examined.

The air relative permeability data, obtained applying the Wyllie-Gardner equations to her capillary pressure-saturation measurements, were correlated by Asensio (2000) with the following function:

$$k_{rg} = a + \frac{b}{1 + \left(\frac{X_1}{c}\right)^d} \quad (3-20)$$

The best fit values of the coefficients in Equation 3-20 are summarized in Table 3-5.

Asensio examined the effect of free water saturation on water and air relative permeability. One such plot, Figure 3-4 for lightweight coated paper at 24°C, demonstrates the highly nonlinear dependence on saturation, S , by k_{rg} and, even more so, for k_{rl} . Asensio's data shows that for this furnish, 80% and 30% saturation correspond to moisture content of approximately 1.3 kg/kg dry (43% solids) and 0.8 kg/kg dry (56% solids). Figure 3-5 shows the water and air relative permeability of Asensio (2000) for the same furnish as a function of total moisture content (dry basis) instead of saturation.

Table 3-4 Water relative permeability in moist paper (Asensio, 2000)

Furnish	Temp. (°C)	X _b	Equation	a	b	c
LWC*	24	0.490	$k_{r1} = a (X_1)^b \exp [(X_1)^c]$	0.360	4.854	0.455
Newsprint	24	0.349	$k_{r1} = a (X_1)^b \exp [(X_1)^c]$	0.533	4.868	0.475
Linerboard	24	1.132	$k_{r1} = a (X_1/2)^b \exp [(X_1/2)^c]$	0.562	1.184	0.487
Eucalyptus A	24	0.536	$k_{r1} = a (X_1)^b \exp [(X_1)^c]$	0.021	4.164	0.578
Eucalyptus B	24	0.393	$k_{r1} = a (X_1/2)^b \exp [(X_1/2)^c]$	0.494	4.156	0.500
NSWK**	24	0.456	$k_{r1} = a (X_1)^b \exp [(X_1)^c]$	0.127	4.221	0.459
Linerboard	56	0.907	$k_{r1} = a (X_1/2)^b \exp [(X_1/2)^c]$	1.254	4.522	0.670
Eucalyptus A	56	0.504	$k_{r1} = a (X_1/2)^b \exp [(X_1/2)^c]$	1.447	4.528	0.704
Eucalyptus B	56	0.488	$k_{r1} = a (X_1/2)^b \exp [(X_1/2)^c]$	0.215	4.114	0.593
Linerboard	85	0.702	$k_{r1} = a (X_1/2)^b \exp [(X_1/2)^c]$	1.337	4.524	0.665

* LWC: Lightweight coated paper

** NSWK: Northern softwood kraft

Table 3-5 Humid air relative permeability in moist paper (Asensio, 2000)

Furnish	Temp. (°C)	Equation	a	b	c	d
LWC	24	$k_{rg} = a + b / [1 + (X_1/c)^d]$	-0.173	1.163	0.563	3.501
Newsprint	24	$k_{rg} = a + b / [1 + (X_1/c)^d]$	-0.123	1.109	0.510	3.778
Linerboard	24	$k_{rg} = a + b / [1 + (X_1/c)^d]$	-0.148	1.132	0.847	3.092
Eucalyptus A	24	$k_{rg} = a + b / [1 + (X_1/c)^d]$	-0.178	1.164	0.941	3.041
Eucalyptus B	24	$k_{rg} = a + b / [1 + (X_1/c)^d]$	-0.161	1.146	0.873	3.026
NSWK	24	$k_{rg} = a + b / [1 + (X_1/c)^d]$	-0.171	1.156	0.633	2.971
Linerboard	56	$k_{rg} = a + b / [1 + (X_1/c)^d]$	-0.141	1.127	0.788	3.598
Eucalyptus A	56	$k_{rg} = a + b / [1 + (X_1/c)^d]$	-0.172	1.161	0.780	3.476
Eucalyptus B	56	$k_{rg} = a + b / [1 + (X_1/c)^d]$	-0.182	1.168	1.050	3.028
Linerboard	85	$k_{rg} = a + b / [1 + (X_1/c)^d]$	-0.185	1.175	0.796	3.411

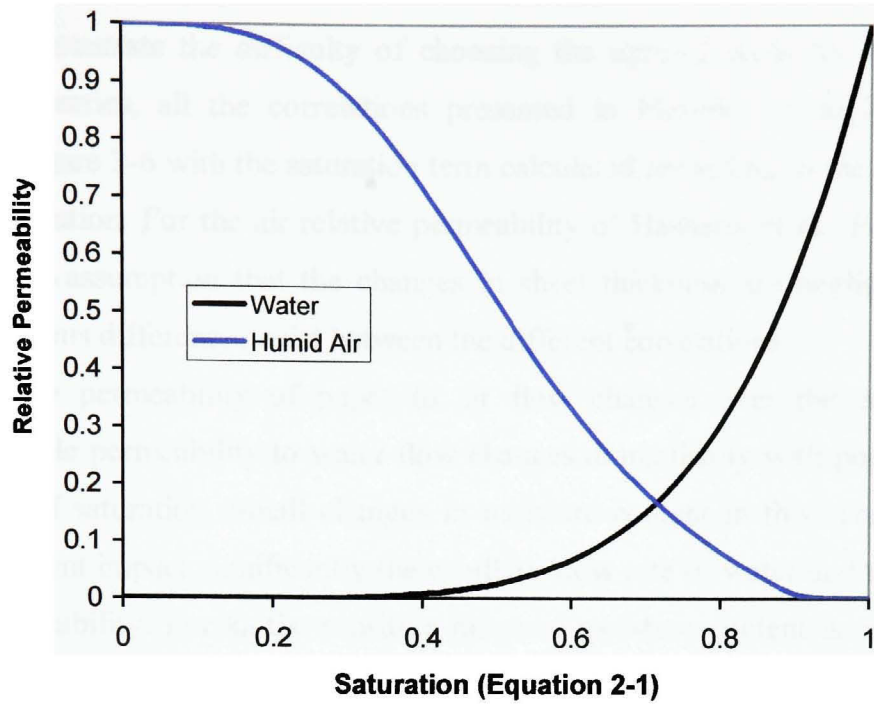


Figure 3-4 Water and air relative permeability for LWC paper at 24°C
(Asensio, 2000)

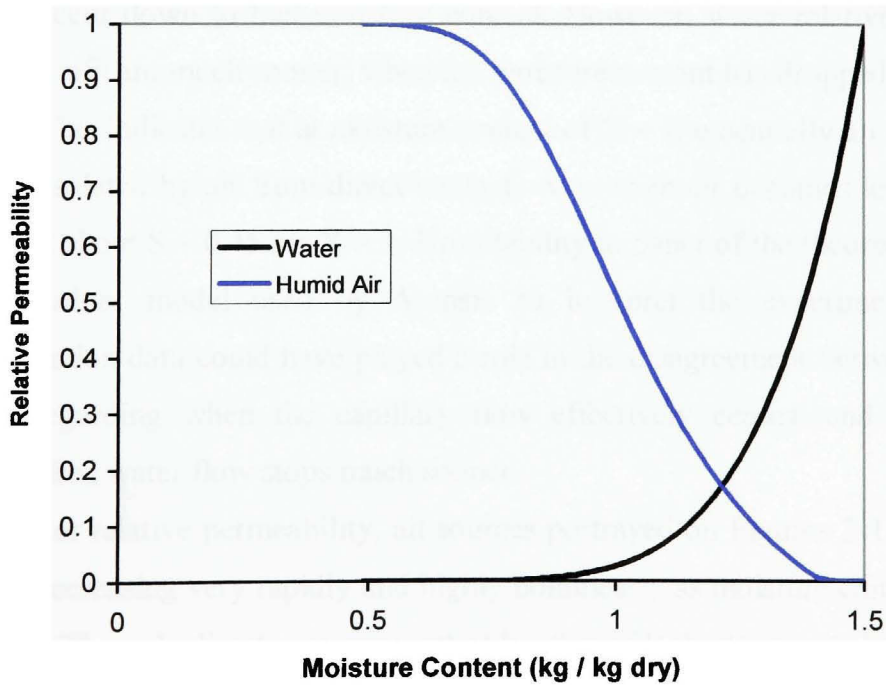


Figure 3-5 Water and air relative permeability for LWC paper at 24°C
(Asensio, 2000)

(d) Relative permeability of water and air: Conclusions

To demonstrate the difficulty of choosing the optimal basis for these important transport properties, all the correlations presented in Figures 3-1 to 3-5 are plotted together in Figure 3-6 with the saturation term calculated according to the definition used by each correlation. For the air relative permeability of Hashemi et al., Equation 3-16 is used with the assumption that the changes in sheet thickness are negligible. For both phases enormous differences exist between the different correlations.

Relative permeability of paper to air flow changes over the entire range of saturation while permeability to water flow changes dramatically with pore saturation at high values of saturation. Small changes in moisture content in this sensitive range of moisture content impact significantly the capillary flow rate of water and therefore water relative permeability. For k_{rl} the sensitive range of moisture content is seen to be over about $1 > S > 0.8$. Asensio's measurements with LWC paper, Figure 3-5, show that water relative permeability drops by over 95% for just a one-third reduction in moisture content from 1.5 to 1 kg/kg dry. Asensio considered that the hygroscopic region starts at $X = 0.49$ kg/kg dry for this furnish and therefore some capillary transfer of water might be expected to occur down to that moisture content. However, water relative permeability becomes insignificant much sooner, when the moisture content has dropped only to about 1 kg/kg dry. This indicates that at moisture content of $X = 1$, essentially all the free water is in regions isolated by air from direct contact, even when air occupies less of the pore volume, i.e. at about $S = 0.45$ for $X = 1$. Unsuitability to paper of the theoretical approach of Wyllie-Gardner model used by Asensio to interpret the experimental capillary pressure-saturation data could have played a role in the disagreement between Asensio's assumption regarding when the capillary flow effectively ceases, and the observed behavior that free water flow stops much sooner.

For water relative permeability, all sources portrayed on Figures 3-1, 3-4, 3-5 and 3-6 show k_{rl} decreasing very rapidly and highly nonlinearly as moisture content decreases during drying. The only direct measurement of k_{rl} , that of Robertson correlated by Ahrens and Journeaux, shows the sharpest drop to negligible water permeability, k_{rl} of about 0.05, when saturation has decreased only to 0.9. This identifies that the two effects discussed in section (a), i.e. increase in length of the actual capillary flow path and, even

more important, the trapping of isolated regions of water in pores, are extremely effective in making capillary transport of water negligible very early in the drying process.

For water permeability Asensio converted from experimentally determined capillary pressure to relative permeability using a theoretical relation of uncertain validity while Harrmann and Schulz used a purely theoretical model of questionable validity. Therefore the similarity between the results of Asensio and those of Harrmann and Schulz is considered fortuitous. For Robertson's experimental data for water relative permeability, which were for one furnish, a correlation by Ahrens and Journeaux is available. With the availability of two sets of results based on experimental measurements, the purely theoretical approach of Harrmann and Schulz was not retained for use here. For water relative permeability it is not possible at this stage to choose between the correlation of Asensio (for several furnishes) and that of Ahrens and Journeaux for Robertson's measurements (with one furnish), so both are included in the sensitivity analysis of chapter 4.

The divergence in air relative permeability displayed in Figure 3-6 is likewise great. As neither the relations of Ahrens and Journeaux or of Harrmann and Schulz are based on any measurements, these correlations are not retained for the sensitivity analysis of Chapter 4. The measurements of Hashemi et al., Figure 3-3, indicate that as moisture content decreases from the value for which S becomes zero, down to dry paper, k_{rg} continues to increase from 0.8 to the limit of 1. Such an increase is realistic because of the collapse of fibrils on to the main fibers over this range of moisture content decrease. The model used by Asensio does not allow for this increase in k_{rg} as moisture content decreases from the fiber saturation value. Therefore two bases for air relative permeability, the correlations of Hashemi et al. and Asensio, are included in the sensitivity analysis to find the optimal choice.

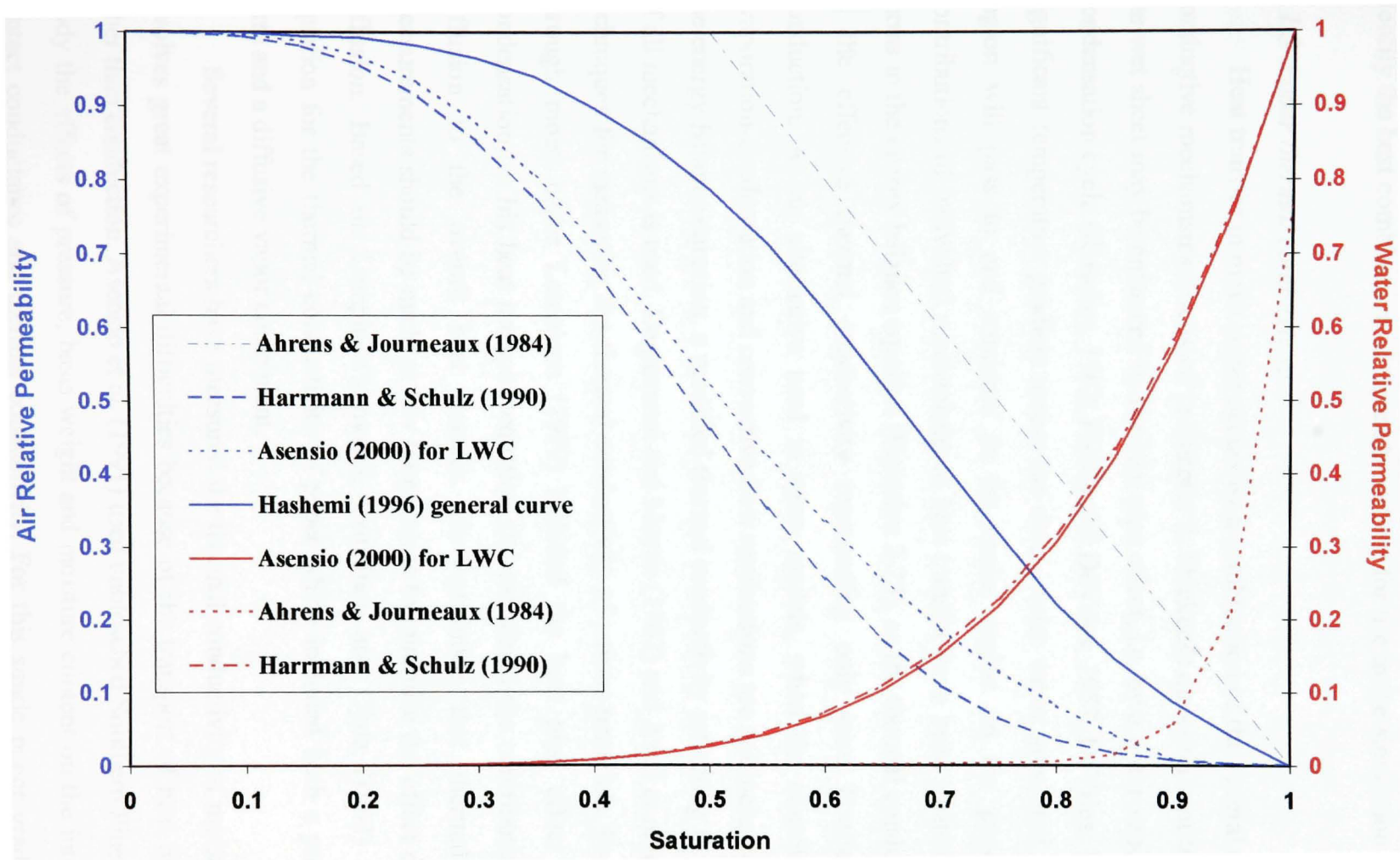


Figure 3-6 Comparison of different correlations for air and water relative permeability

In conclusion, four combinations of sources of air and water relative permeability are possible. In Chapter 4 a sensitivity analysis, based on the model performance, will identify the best combination of these alternatives for use in the simulation model.

3.1.3 Paper thermal conductivity

Heat transfer in moist paper occurs by a combination of the several convective and conductive mechanisms discussed in Chapter 2. Thickness direction heat transfer through the wet sheet may be enhanced by the heat pipe effect, i.e. by a water vapor evaporation-condensation cycle (Krischer, 1962; Phillip and DeVries, 1957; DeVries, 1958). Under a significant temperature gradient across the sheet, water vapor generated in the warmer region will pass to and condense in the cooler region. In the present study the contributions of individual mechanisms to heat transfer have been treated by individual terms in the energy balance equation (Equation 2-23), so the thermal conductivity needed is the effective thermal conductivity representing only pure Fourier's law heat conduction. As an alternative used in some models, when the contributions of the evaporation-condensation and convective flow mechanisms are not included separately in the energy balance equation, a modified thermal conductivity reflecting the contributions of all mechanisms is used. Degiovanni and Moyne (1987) and Azizi et al. (1988) present techniques for measuring the thermal conductivity of porous materials. For heat transfer through moist paper Lampinen (1979) included the heat pipe effect (evaporation-condensation) in his heat transport equation and calculated the contribution from vapor diffusion to the overall heat transfer. He concluded that thermal conductivity measurements should be made at low temperature to minimize the effect of water vapor diffusion. Based on Lampinen's model, Lampinen and Ojala (1993) developed an equation for the thermal conductivity of paper which included both a pure conduction term and a diffusive vapor component.

Several researchers have measured the thermal conductivity of moist paper, which involves great experimental difficulties because of the transport of heat by mechanisms other than conduction. Asensio et al. (1991) used unbleached Southern Pine handsheets to study the effects of pressure, basis weight and moisture content on the interface thermal contact conductance and thermal conductivity. For this single paper grade their results

show that k increases significantly with sheet density. However their moisture content range (between 0.27 and 0.4 kg/kg dry) was too small relative to that corresponding to typical paper drying (about 1.5 to 0.05 kg/kg dry).

To avoid the redistribution of moisture within the sheet from evaporation-condensation, Nederveen and Finken (1992) used a closed measuring cell submerged in a water bath of temperature varying sinusoidally. This cell consisted of a multi-ply sheet retained between brass plates with raised borders. Sheet temperature was measured at two thickness positions. From 40°C to 60°C, k was intermediate between that for dry paper and air. Around the maximum attainable temperature, 80°C, they found k to be higher than the thermal conductivity of water (0.67 W/mK at 80°C) for groundwood handsheets at $X > 0.8$ kg/kg dry and blotting paper at $X > 0.4$ kg/kg dry. They attempted to relate the experimental results to a theoretical parallel/series model but concluded that the amount and accuracy of their data, Figures 3-7 and 3-8, was insufficient for such an analysis. For 340 kg/m³ paper their measurements indicate that, for the typical moisture content decrease from the entry to the exit of a paper dryer, k may decrease by a ratio of about 6:1. For a density increase from 340 to 1030 kg/m³, k is seen to increase by a ratio in the range 2:1 to 3:1, while the data of Asensio et al. (1991) would indicate an increase of k by a factor of about 1.5 for this difference in sheet density. In addition to this uncertainty Nederveen and Finken did not determine the variation of k with the types of furnish used to make paper.

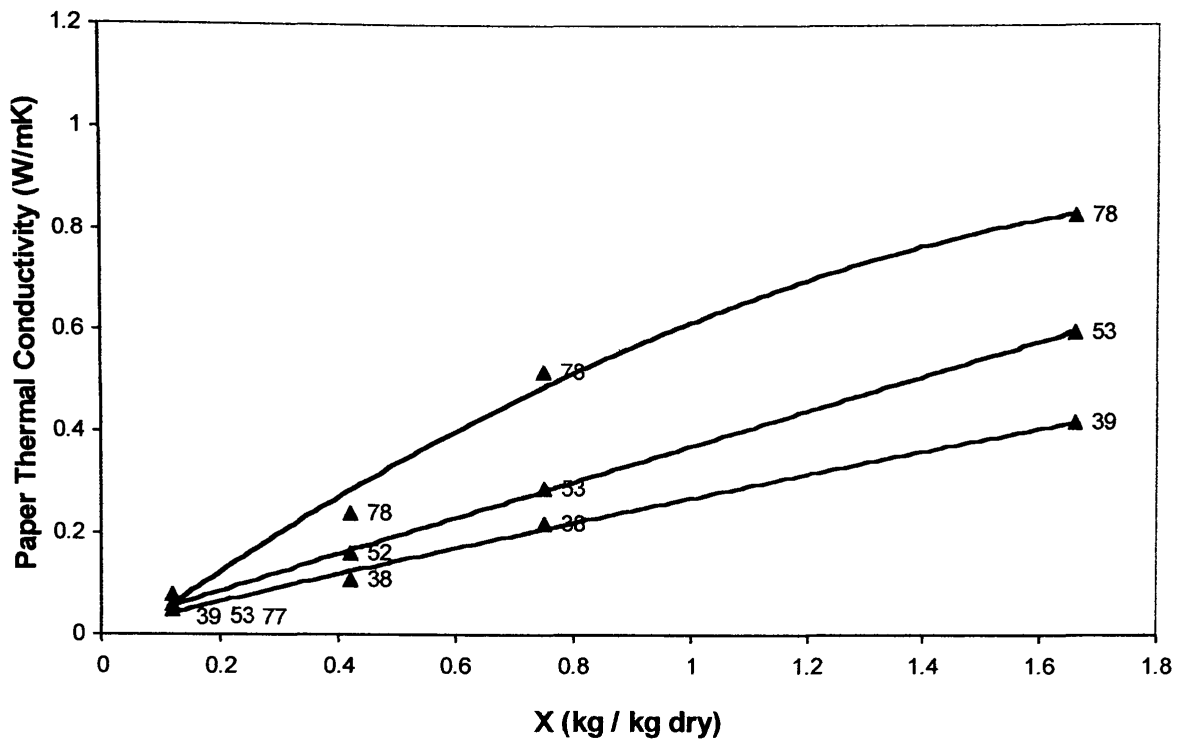


Figure 3-7 Effect of moisture content on thermal conductivity of groundwood handsheets, 340 kg/m^3 (numbers are temperature, $^{\circ}\text{C}$), Nederveen and Finken (1992)

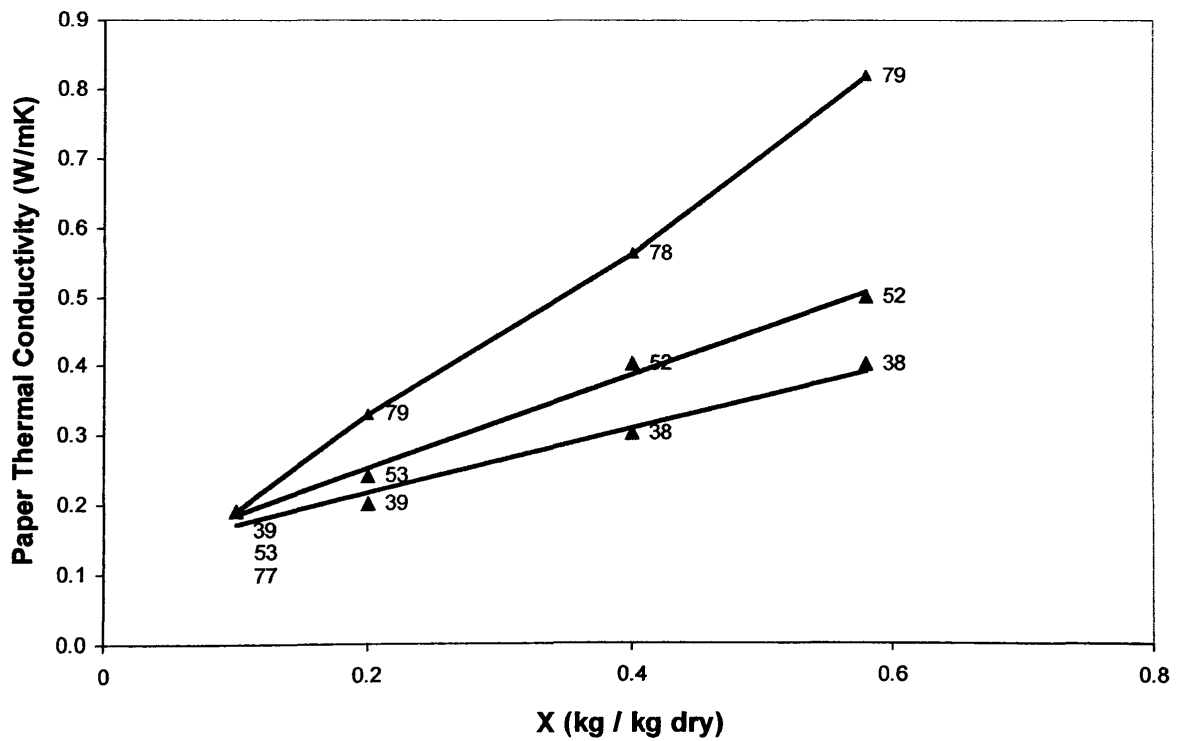


Figure 3-8 Effect of moisture content on thermal conductivity of densified blotting paper, 1030 kg/m^3 (numbers are temperature, $^{\circ}\text{C}$), Nederveen and Finken (1992)

The great difficulty in the experimental measurements and resultant uncertainty provide a strong incentive for the alternative of theoretical relations. Expressions for the effective thermal conductivity of moist paper can be developed from two geometric models for paper structure, i.e. by modeling the web as a bundle of conduits connected either in series or in parallel. A parallel flow model assumes heat conduction through humid air, water and solid phases in parallel, with cross-sectional areas proportional to each volume fraction and the length of each flow path equal to the web thickness. Considering the volume fraction of each phase, the effective thermal conductivity predicted by a parallel model becomes:

$$k_{\text{par}} = k_f(1 - \varepsilon) + k_l \varepsilon S + k_g \varepsilon(1 - S) \quad (3-21)$$

For the series model heat is conducted through a layer of humid air, of water and of fibers with the thickness of each layer proportional to the volume fraction of each phase. Thus the series model is:

$$k_{\text{ser}} = \frac{1}{\frac{1 - \varepsilon}{k_f} + \frac{\varepsilon S}{k_l} + \frac{\varepsilon(1 - S)}{k_g}} \quad (3-22)$$

While Harrmann and Schulz (1990) state that a parallel model yields a slightly lower thermal conductivity than a series model, Kartovaara et al. (1985) report just the opposite. Several researchers propose a combination series and parallel model (Kartovaara et al., 1985; Nederveen et al., 1991; Reardon, 1994) using a weighting factor, Λ , reflecting the relative influence of each arrangement:

$$k_{\text{eff}} = \frac{1}{\frac{1 - \Lambda}{k_{\text{par}}} + \frac{\Lambda}{k_{\text{ser}}}} \quad (3-23)$$

Kartovaara et al. (1985) found that the weighting factor should range from 0.4 to 0.7. To reflect the highly complex and irregular structure of paper, where heat conduction can alternate between series and parallel flow, a value of $\Lambda = 0.5$ was chosen by Reardon (1994) and used by Asensio (2000).

Harrmann and Schulz (1990) agreed that a combination model should be used but according to their paper structure model, discussed in section 3.1.2, fibers and sorbed water are assumed connected in series, with this resistance to heat transfer connected in parallel to the serially connected free water and moist air, as follows:

$$k_{\text{eff}} = \varepsilon_d S k_l + \varepsilon_d (1 - S) k_g + \frac{(1 - \varepsilon_d)^2}{(1 - \varepsilon) k_f^{-1} + (\varepsilon - \varepsilon_d) k_l^{-1}} \quad (3-24)$$

They used the same definition of saturation, S , for thermal conductivity as for permeability, Equation 3-13.

For effective thermal conductivity of moist paper Kobari et al. (1985) proposed:

$$k_{\text{eff}} = [k_f^{0.4} (1 - \varepsilon) + k_l^{0.4} \varepsilon S + k_g^{0.4} \varepsilon (1 - S)]^{2.5} \quad (3-25)$$

where k_f thermal conductivity of fibers, is taken as 0.35 W/mK. No physical reason for this functional form is provided. Kobari performed hot-surface drying experiments with sheets made of the insoluble portion of tobacco and used the measured drying rate and moisture content profiles to verify his model for contact drying of fibrous material. Presumably the exponents in Equation 3-25 are the best fit values chosen to optimize agreement with experimental data.

In Equation 3-23, the k_{par} and k_{ser} terms from Equations 3-21 and 3-22 include saturation, S , calculated from Equation 2-1 as a function of moisture content. Inclusion of saturation establishes the dependency of effective thermal conductivity on moisture content. The temperature dependency of conductivity derives from that of the three constituents. As thermal conductivity of water and humid air are well known, thermal conductivity of dry paper is the only parameter to be determined and as such has been the subject of many experimental studies. Table 3-6 shows experimentally determined

thermal conductivity values of various grades of dry paper. In most cases the corresponding values of paper porosity were not reported. The values cover a factor of four range, from 0.041 to 0.169 W/mK. For example thermal conductivity of newsprint with 8% moisture content is 0.041 W/mK according to Lau and Prattes (1969) and 0.127 W/mK according to Kerekes (1980). Estimation of the thermal conductivity of moist paper involves this level of uncertainty for thermal conductivity of dry paper along with the variation of paper thermal conductivity with moisture content by a ratio of about 6:1 as the sheet goes from wet to dry, noted in connection with Figures 3-7 and 3-8.

The values included in Table 3-6 provide only an incomplete picture of the variability of dry paper thermal conductivity. The furnish dependency of this transport property is not properly established and with the variation of results by a ratio of 4:1 it is not possible to reject or approve any particular value. Consequently an average value of thermal conductivity based on the available data is used in the present study, while noting that more work is needed to establish a better basis for the determination of dry paper thermal conductivity.

Most experimental determinations of paper thermal conductivity over-estimate its value because of contributions from mechanisms in addition to conduction, primarily from the evaporation-condensation (heat pipe) mechanism. Therefore the alternative to doubtful experimental measurements of paper conductivity is to determine the effective thermal conductivity for the 3-constituent system of solids, water and humid air from a theoretical correlation with the species connected in either serial, parallel or serial-parallel arrangements. To test this alternative, the experimentally determined values of thermal conductivity of Figures 3-7 and 3-8 as well as a theoretical expression for effective thermal conductivity are included in the sensitivity analysis of Chapter 4. Regarding the theoretical models there are conflicting opinions regarding the effect on thermal conductivity of pure parallel and pure series connection. In addition, for a medium of highly complex and irregular structure such as paper it is probable that some elements are organized in series, some in parallel structure. Therefore, as a combination series-parallel model, Equation 3-23, should be the more appropriate choice. Hence this structural arrangement is included in the sensitivity analysis. These two alternatives for k_{eff} (experimental and theoretical) are further analyzed in Chapter 4.

Table 3-6 Thermal conductivity of dry paper

Author(s)	Sheet Specifications	Thermal Conductivity W/mK
Kirk and Tatlicibasi (1972)	Bleached sulfite handsheets, 22-75 SR	0.084 to 0.117
Depoy (1972)	Unspecified – dry ($X < 0.04$) to 8% moisture	0.121 0.161
Lau and Prattes (1969)	Newsprint, 52 g/m ² , 8% moisture, $\rho = 0.64 \text{ g/cm}^3$	0.041
Powell and Strong (1974)	Dry newsprint	0.069
McAdams (1954)	Unspecified paper Lap of wood pulp	0.130 0.048
Kerekes (1980)	Newsprint, 8% moisture Uncalendered	0.127
	Calendered	0.169

3.1.4 Water vapor diffusivity

In section 2.5.4 the mass flux of water vapor was expressed as the sum of two components, convective and diffusive. To quantify the diffusive component requires an effective diffusivity for the air- water vapor system in Equation 2-51 where “effective” indicates that the diffusivity in a porous medium such as paper is much lower than the bulk phase diffusivity in air. The effective diffusivity allows for the influence exerted by the porous fiber structure of paper. The temperature dependence of D_{eff} has not been studied, all authors apparently assuming that D_{eff} and D_v have the same dependence. Incropera and Dewitt (1985) considered that the water vapor-air diffusivity would be reduced by a diffusibility factor, $0 < \delta < 1$, to account for two factors: the tortuous gas phase flow path within the paper web and the flow area reduction due to porosity less than unity.

Some of the correlations proposed for this effective water vapor diffusivity, D_{eff} , are summarized in Table 3-7 where D_v denotes the bulk phase water vapor-air diffusivity. Water saturation, S , is defined according to Equation 2-1. A shortcoming of these correlations is that the treatment for paper type and properties, such as density, porosity and tortuosity, is generally insufficient except by Han (1970) and Kobari et al. (1985). Han's correlation, developed from experimental measurements for air-water vapor diffusion in a nylon fiber mat (Han and Matters, 1966) is distinguished by inclusion of factors for pore shape, θ , and tortuosity, τ . Han suggested for his nylon fiber mat the use of $\theta = u = 1$ and that both τ and m be given values between 1 and 2. Ramaswamy (1990) used the basic equation of Han and Matters and assumed a linear decrease in $\frac{\tau}{\theta}$, thereby eliminating the pore shape factor parameters of Han and Matters from the final correlation.

Table 3-7 Correlations for effective air-water vapor diffusivity in paper

Author(s)	Correlation	Applicability
Han and Matters (1966) and Han (1970)	$\frac{D_{\text{eff}}}{D_v} = \frac{\theta}{\tau} \varepsilon^m (1-S)^u$	Not stated
Hartley and Richards (1974)	$D_{\text{eff}} = \varepsilon (1-S) D_v$	Not stated
Snow (1980)	$D_{\text{eff}} = \varepsilon D_v$	Not stated
Kobari et al. (1985)	$D_{\text{eff}} = \frac{\varepsilon (1-S)}{\tau} D_v$	Not stated
Ramaswamy (1990)	$\frac{D_{\text{eff}}}{D_v} = 0.4 \frac{\varepsilon^{1.23}}{\exp(1.574 S)}$ $\frac{D_{\text{eff}}}{D_v} = \frac{\varepsilon^{1.23} (1-S)^{1.08}}{4.33 - 3.33 S}$	$0 < S < 0.7$ $0.7 < S < 1$

With respect to the effect of moisture content on the water vapor effective diffusivity in paper it should be noted that as far as geometric factors are concerned the gas phase diffusivity and gas phase permeability are controlled by the same basic

parameters, the tortuosity of the gas flow path and the cross-sectional area for gas flow. As moisture content decreases for the range above the fiber saturation point, X_{FSP} , tortuosity decreases and cross-sectional flow area increases, both of which act to increase permeability and diffusivity of the gas phase. Thus for the region as X decreases towards X_{FSP} and $S \rightarrow 0$, D_{eff} must increase just as Figure 3-6 shows gas phase permeability increasing. During drying as X continues to decrease below X_{FSP} the extensive gas phase permeability data of Hashemi, Figure 3-3, show that gas phase permeability continues to increase all the way to the completely dry sheet. Sheet shrinkage would both decrease the cross-sectional area for gas flow and the length of gas flow path, but Hashemi's result indicate that the latter effect dominates. Thus it should be expected that as X decreases first to X_{FSP} , then to dryness, D_{eff} should continuously increase.

From measurements using steady-state sorption into 120 and 300 g/m² paper from 25°C air of various relative humidities, Lescanne et al. (1992) reported that vapor diffusivity increases as paper moisture content decreases, as do all the studies noted so far. From unsteady-state gravimetric experiments for paper subjected to a stepwise increase in vapor pressure, Lescanne et al. reported that Fick's diffusion law did not describe their results. Nilsson et al. (1993) determined air- water vapor effective diffusivity in paper and pulp pads for 10 furnishes, showing that with increasing paper density the corresponding decrease in porosity decreases vapor phase diffusivity greatly. In these measurements, like those of Lescanne et al., sheet moisture content did not exceed 0.15 kg/kg dry. The Nilsson et al. values of effective diffusivity in paper, from 2.1×10^{-8} to 5.4×10^{-6} m²/s, indicate that D_{eff} is reduced greatly, by ratios in the range 5:1 to 1400:1 relative to D_v . Nilsson et al. also reported that for relative humidity below 58%, the effective vapor diffusivity in paper does not depend on relative humidity, although Ahlen (1970) reported that this diffusivity in paper decreases with decreasing humidity until relative humidity falls to 30%. The Nilsson et al. finding is as expected while that of Ahlen is inconsistent with the fact that at the equilibrium paper moisture content for 58% relative permeability is about 7% (at 50°C) and the sheet microstructure is totally fixed by the time moisture content falls to this low value.

Figure 3-9 presents the measurements by Karlsson et al. (1992) of the D_{eff}/D_v ratio for newsprint (TMP + recycled fiber) and fine paper as a function of moisture content. Their finding that the D_{eff} in fine paper is only about 1/2 to 1/3 of that for newsprint reflects the substantial additional resistance to vapor phase transport coming from the small particles of the mineral filler component of fine paper, typically about 30%. However Figure 3-9 shows D_{eff} decreasing as X decreases. This finding is in contradiction with the fact that as moisture content decreases the effective water vapor diffusivity must increase as the effect of both factors inhibiting the diffusion, tortuous gas phase flow path and the reduction of flow area, would decrease. Thus it is not surprising that the Karlsson et al. results are in contradiction to those from all other investigations, theoretical and experimental. As there are evidently problems with the experimental work of Karlsson et al. these results are not considered further here.

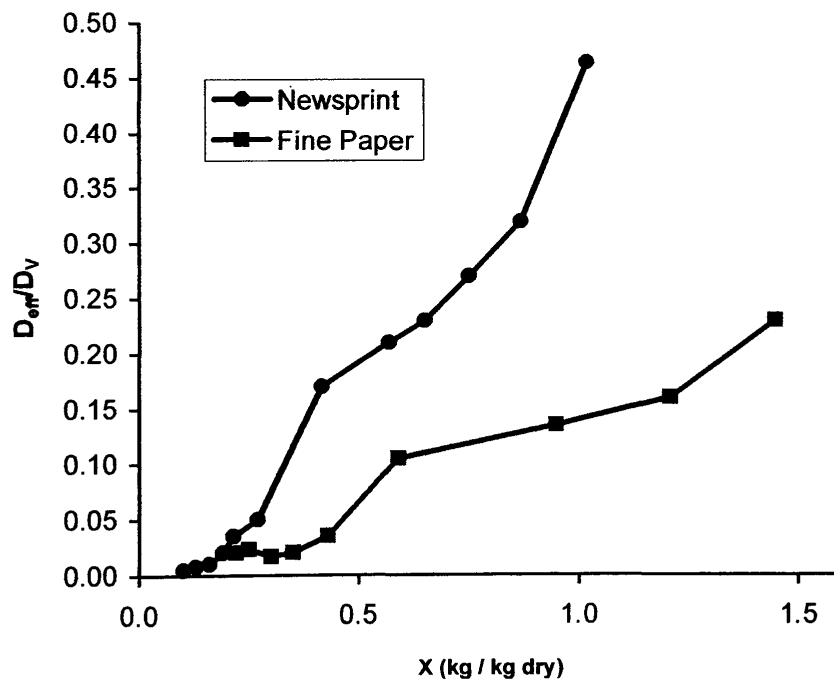


Figure 3-9 Effect of paper type and moisture content on D_{eff} , Karlsson et al. (1992)

As the experimental determinations of D_{eff} are either for too small a range of moisture content or are clearly in error, the air-water vapor diffusivity correlations of

Table 3-7 which have been retained for use are those considered reliable from the analysis above, and which allow for variation in pore structure within the porosity and density ranges occurring during drying to account for the increase in D_{eff} through the two basic effects, porosity and tortuosity. Thus two correlations are chosen for the sensitivity analysis of Chapter 4: Han (1970) because of the inclusion of paper pore geometry factors, and that of Ramaswamy (1990) which extends the Han equation by assuming a correlation for pore geometry factors and provides a more detailed description of the moisture content dependency of effective water vapor diffusivity.

3.1.5 Sorbed water diffusivity

In section 2.5.5 the mass flux of sorbed water was expressed as a diffusive process, Equation 2-56. Sorbed water diffusivity is the least known among the transport properties needed to simulate drying. The extensive data available for wood can be used as a basis of comparison of sorbed water diffusivity in paper. Siau and Babiak (1983) studied non-isothermal moisture migration in lumber and proposed an average value of $D_s = 1.8 \times 10^{-14}$ m²/s. In correlating sorbed water transport in paper as driven by moisture content gradient Lampinen and Ojala (1993) used a diffusivity correlation developed for wood but did not provide numerical values of the activation energy needed to quantify this diffusivity. The correlation by Siau (1971) for D_s in lumber was used by Asensio (2000) in her modeling study of lumber drying as:

$$D_s = \exp\left(-9.9 - \frac{4300}{T} + 9.8X_s\right) \quad (3-26)$$

Some researchers have used an effective moisture diffusivity to represent water transport by both mechanisms, capillary transport of the free water and diffusive transport of sorbed water in the fibers. Although this approach is not used here, such an effective moisture diffusivity must necessarily be the sorbed water diffusivity for moisture content sufficiently low that there is negligible contribution from capillary transport. Such a comparison has been made, at 100°C in Figure 3-10, between the values of Lin (1991) for the effective moisture diffusivity in the thickness direction in paper for $X < 0.15$ kg/kg

dry, and the correlation of Siau (1971), Equation 3-26, which according to Asensio (2000) is the optimal choice for sorbed water diffusivity in lumber. Lin's equation is retained for the present study because among the many correlations for effective moisture diffusivity, it is specifically proposed for the low moisture contents.

$$D_L = 2.616 \times 10^{-11} \exp(0.5X) \exp\left(\frac{16100}{R} \left(\frac{1}{298.15} - \frac{1}{T}\right)\right) \quad (3-27)$$

Sorbed water diffusivity of paper according to Lin is seen to be lower than that in wood according to Siau by a factor of as high as 100:1 for moisture content less than 0.15 kg/kg dry. The severe disruption in the orientation of the fiber matrix in wood which occurs in the production of paper would be expected to reduce greatly the diffusivity of water. As for other transport properties, the sensitivity of drying simulation results to the choice for sorbed water diffusivity will be examined in Chapter 4.

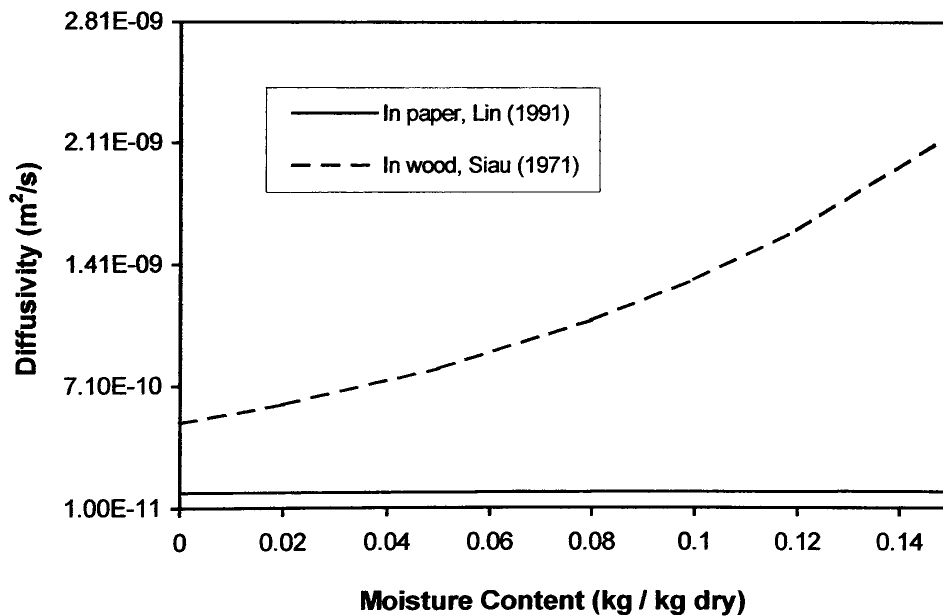


Figure 3-10 Comparison of correlations for sorbed water diffusivity at 100°C

3.1.6 Summary of transport properties in moist paper

Various sources of information concerning the transport properties needed in the drying model were reviewed in sections 3.1.2 to 3.1.5. Available correlations are based

either on experimental data or are developed for a particular theoretical model of paper structure. The conclusions reached for each property are summarized below:

- **Absolute permeability:** The Kozeny-Carman equation, the most common permeability model, is inadequate for paper primarily because it was developed for spherical particles and may have limited validity for porous media such as paper of greatly different pore shape and structure. The experimentally determined thickness direction values of absolute permeability in Table 3-1 are used here.
- **Relative permeabilities:** For water relative permeability, Ahrens and Journeaux (1984) correlation of Robertson's (1963) direct measurements for one furnish and Asensio's indirect determination from capillary pressure measurements for several furnishes were chosen for the sensitivity analysis of Chapter 4. With the availability of two sources of experimentally based determinations, the Harrmann and Schultz (1990) results based on a theoretical model of paper structure of uncertain validity were not used.

For air relative permeability, the measurement for 10 furnishes by Hashemi (1996), Hashemi et al. (2002) and those for 6 furnishes by Asensio (2000) are the best choices. The reservation noted above applies, i.e. Asensio did not measure relative permeability directly but interpreted her experimentally determined capillary pressure data using the Wyllie and Gardner (1958) theoretically based equations of uncertain validity for paper. With two sources based on measurements available, the Ahrens and Journeaux air relative permeability correlation not based on measurements was not used.

Hence two choices for both air relative permeability (Hashemi and Asensio) and for water relative permeability (Robertson and Asensio) are retained for Chapter 4 sensitivity analysis, thereby providing four alternative combinations.

- **Paper thermal conductivity:** Because the contributions of different mechanisms to heat transfer have in the present study been treated by separate terms in the energy balance, the thermal conductivity needed is that representing only pure Fourier's law conduction. Review of the experimental studies for moist paper thermal conductivity indicates that these values are probably all too high because of heat transfer by the evaporation-condensation mechanism as well as by conduction. As a combination

series-parallel geometrical model for paper structure is believed to provide a better description of this complex porous medium, Equation 3-23 was included in the sensitivity analysis. The other possibility, use of experimental measurements of moist paper thermal conductivity, Figures 3-7 and 3-8, was also included although it was expected that these results would be shown to be unsuitable because of being obtained under conditions for which conduction was not the only transport mechanism.

- **Water vapor diffusivity:** Water vapor diffusivity in paper is substantially less than the bulk diffusivity for the water vapor-air system. The experimental data unfortunately do not cover a sufficiently wide range of moisture content or are clearly in error. It is therefore necessary to use a theoretical relation which includes the saturation term, a function of moisture content, as well as pore geometry factors. Of these relations the two best, Han (1970) and Ramaswamy (1990), are included in the sensitivity analysis. In the absence of any information the temperature dependence of water vapor diffusivity in paper is assumed that for bulk phase diffusivity.
- **Sorbed water diffusivity:** This parameter is the least known and has the highest uncertainty among the transport properties needed to simulate paper drying. As the best relation in the thickness direction for paper is believed to be that of Lin (1991), this is the source retained. The extensive data available for wood are not relevant as the diffusivity in paper is lower by about a factor of 100:1. However, to demonstrate the extent to which transport of sorbed water affects drying rate, the correlation of Siau (1971) for sorbed water diffusivity in wood is also included in the sensitivity analysis.

In Chapter 4 the model is tested for different grades of paper using operating data from dryer sections of many paper machines using different drying techniques. By examining the results of the model with numerous combinations of transport properties, the best combination is selected.

3.2 Thermodynamic properties of moist paper

This section treats three key properties, capillary pressure, vapor pressure reduction and heat of sorption of moist paper.

3.2.1 Capillary pressure in moist paper

Experimental techniques for determining capillary pressure include the centrifuge method, the porous-plate technique, mercury intrusion porosimetry, and the lesser used method of water-vapor desorption at low saturation. These methods are discussed by Bass (1987) and Dullien (1992). When developing drainage capillary pressure curves for a medium the experiment starts with the sample 100% saturated with the wetting phase, water in case of moist paper. With gradual increases in the applied pressure, the nonwetting phase (humid air in paper) penetrates into the medium and displaces the wetting fluid which drains out. The air pressure and volume of fluid displaced are recorded.

Several researchers have obtained capillary pressure data specifically for pulp or wood. Spolek and Plumb (1981) used the centrifuge technique to obtain a capillary pressure correlation for wood:

$$P_c = 0.84 \times 10^4 S^{-0.63} \quad (3-28)$$

with S defined according to Equation 2-1. This correlation, determined for values of S from 1 to 0.05, was developed with consideration of both experimental data and a mechanistic model. Although developed for wood, Equation 3-28 was used by Asensio and Seyed-Yagoobi (1992, 1994) for paper drying applications and acceptable results were claimed.

Based on data presented in Cowan (1961) for kraft fiber mats, Ahrens and Journeaux (1984) expressed capillary pressure within moist paper as a function of saturation (from Equation 2-1) and temperature (through the surface tension term):

$$P_c = 5.8 \times 10^4 \left(\frac{\sigma}{\sigma_0} \right) \exp(-5S) \quad S \geq 0.24$$

$$P_c = 1.234 \times 10^6 \left(\frac{\sigma}{\sigma_0} \right) \exp(-17.74S) \quad S \leq 0.24$$
(3-29)

where S is from Equation 2-1 and σ is surface tension. Equation 3-29 has also been used by Ramaswamy (1990). Applicability of this equation to other furnishes has not been investigated.

Other researchers have also investigated capillary migration of liquid in paper. Snow (1980) measured capillary pressure data for two types of pulp using a liquid extrusion method. Lampinen and Toivonen (1984), Harrmann and Schulz (1990), Lampinen and Ojala (1993) and Reardon (1994) all used the basic capillary equation, Equation 2-28, discussed in Chapter 2:

$$P_c = \frac{2 \sigma \cos \theta}{r}$$
(2-28)

To use this equation the pore size of moist paper, r , is needed, which was determined via a pore size distribution, derived either based on a theoretical paper structural model (Harrmann and Schulz), determined experimentally for dry paper (Reardon, 1994) or, as follows, from sorption isotherms using the Kelvin equation (Lampinen and Ojala, 1993):

$$\ln(\Phi) = \frac{2 \sigma \cos \theta}{\rho_l r R' T}$$
(3-30)

where Φ is relative humidity and R' the gas constant of steam (0.462 kJ/kgK).

Since the pore size distribution of moist paper from different furnishes is rarely available, empirical correlations based on experimental determination of capillary pressure are required. Asensio (2000) provides such correlations for 6 types of paper so the furnish dependency of capillary pressure is also covered. The centrifuge method was

used for the measurements and a general capillary pressure-moisture content relation proposed:

$$P_c = c \left(\frac{b}{X-a} - 1 \right)^{1/d} \quad (3-31)$$

Best fit values of the parameters for Equation 3-31 are summarized in Table 3-8.

Table 3-8 Capillary pressure-moisture content relation (Asensio, 2000)

Furnish	Temp. (°C)	Equation	a	b	c	d
LWC	24	$P_c = c(b/(X-a) - 1)^{1/d}$	0.491	8.848	6.519	0.957
Newsprint	24	$P_c = c(b/(X-a) - 1)^{1/d}$	0.349	8.257	6.413	0.950
Linerboard	24	$P_c = c(b/(X-a) - 1)^{1/d}$	1.132	8.541	4.179	1.319
Eucalyptus A	24	$P_c = c(b/(X-a) - 1)^{1/d}$	0.536	6.670	5.117	1.302
Eucalyptus B	24	$P_c = c(b/(X-a) - 1)^{1/d}$	0.393	7.940	3.168	1.342
NSWK	24	$P_c = c(b/(X-a) - 1)^{1/d}$	0.456	7.327	2.649	1.344
Linerboard	56	$P_c = c(b/(X-a) - 1)^{1/d}$	0.907	8.298	2.982	0.995
Eucalyptus A	56	$P_c = (c/b)(b/(X-a) - 1)$	0.504	7.229	0.051	N/A
Eucalyptus B	56	$P_c = c(b/(X-a) - 1)^{1/d}$	0.488	6.809	4.143	1.315
Linerboard	85	$P_c = (c/b)(b/(X-a) - 1)$	0.702	8.417	0.304	N/A

These capillary pressure-moisture content relations at 24°C for all furnishes, Figure 3-11, show that all curves become asymptotic at moisture contents specific to each furnish. As discussed in Chapter 2, section 2.5.5, these values are termed the “irreducible moisture content”, identifying the moisture level reached during drying at which liquid water migration by capillary forces ceases. Asensio uses the irreducible moisture content

as the onset of hygroscopic region while, for reasons explained in section 2.5.5, the fiber saturation point is used in the present study to identify the condition when there is no more free water in the interfiber pores.

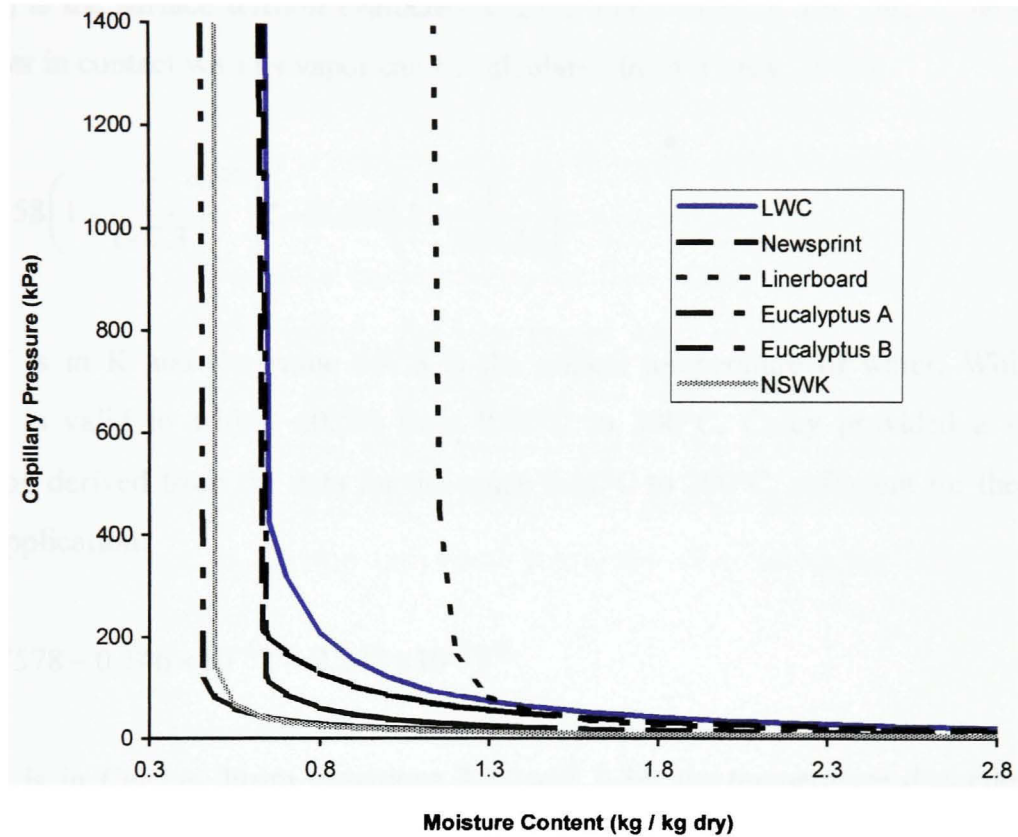


Figure 3-11 Capillary pressure-moisture content relation for various furnishes (24°C)
(Asensio, 2000)

Asensio measured the capillary pressure of linerboard at three temperatures (24°C, 56°C and 85°C). For other furnishes the temperature effect was not studied, except for Eucalyptus A and Eucalyptus B where measurements were made at 24°C and 56°C. Therefore the temperature dependence of capillary pressure requires further work. In general, the capillary pressure at any given moisture content decreases with increasing temperature due to the temperature dependence of surface tension, for which Ahrens and Journeaux (1984) proposed the following approximation:

$$\frac{\partial P_c}{\partial T} = \frac{\partial}{\partial T} \left(\frac{\sigma}{\sigma_0} \right) \quad (3-32)$$

where σ_0 is the surface tension evaluated at 27°C (71.7 mN/m). The surface tension of pure water in contact with its vapor can be calculated from (Carey, 1992):

$$\sigma = 0.2358 \left(1 - \frac{T}{647.3} \right)^{1.256} \left[1 - 0.625 \left(1 - \frac{T}{647.3} \right) \right] \quad (3-33)$$

where T is in K and the value 647.3 is the critical temperature of water. While this equation is valid to within $\pm 0.5\%$ from 0.01°C to 300°C, Carey provided a simpler expression derived from the data for the range 0.01°C to 200°C, sufficient for the paper drying application:

$$\sigma = 0.07578 - 0.146 \times 10^{-3} T - 2.242 \times 10^{-7} T^2 \quad (3-34)$$

where T is in Celsius. From Equations 3-32 and 3-34, the temperature dependence of capillary pressure becomes:

$$\frac{\partial P_c}{\partial T} = -0.00204 - 6.256 \times 10^{-6} T \quad (3-35)$$

The available correlations do not establish the furnish dependency of capillary pressure. The experimental results of Asensio (2000) are chosen here because she directly measured the capillary pressure for six types of paper, i.e. furnish dependency is established to an acceptable extent and no other information regarding the pore structure of moist paper is required.

3.2.2 Sorption characteristics of paper

The sorption characteristics of paper describe the degree of adsorption of water to the surface, i.e. the strength of bonding between sorbate, water, and the surface, paper. This bonding manifests itself in two ways, a reduction in water vapor pressure and an increase in the latent heat of vaporization for sorbed water. As discussed in Chapter 2, section 2.5.5, these characteristics have a two-fold effect on drying rate. The mechanism of drying by vapor transfer is retarded due to the vapor pressure reduction causing a decrease in the driving force either as the gradient which controls diffusion or the pressure difference which drives convective vapor flow. The second effect derives from the differential heat of sorption, the incremental heat of vaporization required to evaporate sorbed water from paper in addition to the latent heat of vaporization of free water. This incremental thermal requirement increases the heat required and thereby reduces the drying rate. During drying, both the vapor pressure reduction and differential heat of sorption start to develop only well below the fiber saturation point moisture content, as detailed below.

(a) Vapor pressure reduction

Within the hygroscopic region, sorption and desorption isotherms relate relative humidity to paper moisture content. For drying, only the desorption isotherm is relevant. Experimental sorption/desorption isotherm data and the resulting empirical correlations available in the literature for paper include those by Wink et al. (1985), Prah1 (1968), Karlsson and Soininen (1982), Lampinen and Toivonen (1984), Heikkila (1985), Harrmann and Schultz (1990), Karlsson and Paltakari (1992), Lampinen and Ojala (1993) and Reardon (1994). The desorption data of Prah1 (1968) is the most widely used due to the broad range of temperature and relative humidity in Prah1's experiments and an uncertainty of only 2% for his measurements of the isotherms. Prah1 measured sorption and desorption isotherms for a never-dried kraft pulp for five temperatures between 22°C and 80°C and for relative humidity between 1% and 99.6%. Through use of hardwood and softwood pulp produced by both the kraft and sulfite processes, for which he obtained essentially identical isotherms at 50°C, Prah1 concluded that the sorption isotherms of different papers are not significantly different.

The desorption data of Prah1 have been fitted by Karlsson and Soininen (1982) and by Reardon (1994) with the following relationship:

$$\Theta = \exp(\beta_1 T - \beta_2) \quad (3-36)$$

where Θ is the vapor pressure reduction factor (the ratio of sorbed water vapor pressure to that of free water), T is in Kelvin, and the coefficients β_1 and β_2 are functions of the dry basis moisture content. Karlsson and Soininen determined the coefficients for the Prah1 data to be:

$$\begin{aligned} \beta_1 &= \exp(-15.03 X - 1.37\sqrt{X} - 3.41) \\ \beta_2 &= \exp(-13.53 X - 2.90\sqrt{X} + 2.90) \end{aligned} \quad (3-37)$$

while Reardon presented:

$$\begin{aligned} \beta_1 &= \exp(-17.255 X + 0.121\sqrt{X} - 3.640) \\ \beta_2 &= \exp(-14.313 X - 2.167\sqrt{X} + 2.772) \end{aligned} \quad (3-38)$$

The following correlation, also based on Prah1's data but employing a different functional form, was used by Bond et al. (1996) in their paper drying model:

$$\Theta = \begin{cases} 51.29 X^{1.855} & X < 0.07 \\ 1 - \exp(0.544 - 14.5 X) & X \geq 0.07 \end{cases} \quad (3-39)$$

Figure 2-9 demonstrates the results of Equation 3-39 and shows that there is essentially no vapor pressure reduction until the moisture content is below 0.4 kg/kg dry, a value about half that of the fiber saturation point moisture content where there is no free water in the pores.

Equations 3-37 and 3-38 have the advantage of considering the effect of temperature on the vapor pressure reduction factor, included in Prahls study, while this effect is not included in Equation 3-39.

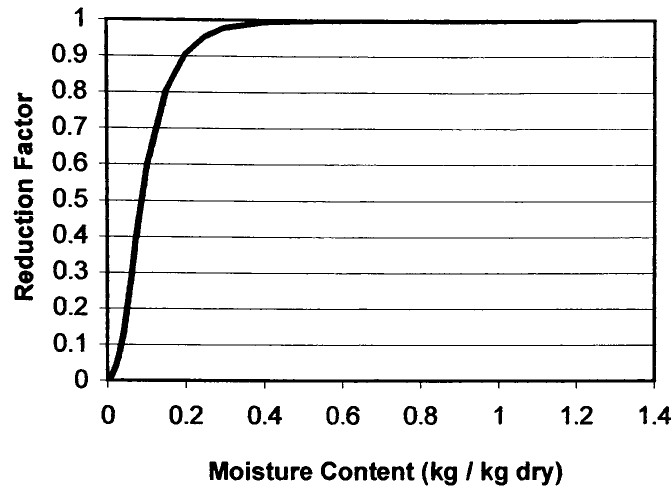


Figure 2-9 Vapor pressure reduction factor,
Bond et al. (1996) correlation of data of Prahls (1968)

The experimental measurements by Reardon (1994) for newsprint between 30°C and 65°C and at relative humidities between 30% and 90% closely match the shapes and magnitude of Prahls data although slightly larger differences were observed for temperatures above 50°C. As Prahls used chemical pulp, from which most of the lignin has been removed, while essentially all the lignin remains in the mechanical pulp used to make newsprint and related grades. It is significant for use of these results in a drying model for diverse grades of paper that the combination of Prahls and Reardon's measurements establish that the vapor pressure reduction factor is relatively insensitive to lignin content. The experimental results of Rhodius (1980) for softwood pulp between 23°C and 90°C, reported by Harrmann and Schultz (1990), differ from Prahls data at temperatures higher than 60°C.

Reardon (1994) notes that the shape of Prahls isotherms is consistent with the Type II classification of physical adsorption of Brunauer (1940). Isotherms of this type are observed only when there is a wide range of pore size. Such materials provide a

continuous progression rather than sharp breaks between monolayer adsorption, multilayer adsorption and capillary condensation. Monolayer adsorption describes a single layer of the sorbent (water) in contact with the sorbate (fiber). It is considered that this water forms a hydrate with the sorbate. At very low moisture content essentially all the water exists as a monomolecular layer on the fibers, so there is no free water to counteract the attraction between the sorbent and sorbate. The monolayer regime exists only at very low moisture content, below 2%. Multilayer adsorption occurs at moisture contents above about 2% when several layers of water are adsorbed on the sorbate, in which case van der Waals bonding, a weaker form of attachment, is predominant. The attraction of multilayer sorbed molecules to the sorbate is small compared to monolayer adsorption. Capillary condensation, the process occurring at higher moisture content, involves the liquid sorbent filling the larger intra-fiber pores of the sorbate. With such moisture in an interfiber pore being surrounded by the lignocellulosic substrate, this liquid is generally treated as sorbed moisture, i.e. indistinguishable from that within the substrate.

In integrating this theory with measurements for paper, the proportion of water held by each mechanism depends, as explained in Chapter 2, not only on moisture content but also on factors such as the type of pulp fibers, the extent of beating and the presence of fiber fines and inorganic filler. Kershaw (1980) reported that multilayer adsorption is the dominant model down to moisture content of about 0.01 to 0.02 kg/kg dry, with monolayer adsorption being the predominant form at moisture content below that level. According to Figure 2-9 at a moisture content of 0.02 kg/kg dry the vapor pressure is only about 4% that of free water, demonstrating the enormous effect of hydrogen bonding between water molecules and the lignocellulosic substrate when there is no free water present to provide competitive hydrogen bonding. However as most grades of paper are not dried to a moisture content of 2% or lower, the monolayer adsorption limit is generally not reached. Figure 2-9 shows that as drying progresses there is no bound water, i.e. no adsorption, until the moisture content drops below about 0.35 kg/kg dry, while even at 0.2 kg/kg dry there is only about 10% vapor pressure reduction from the multilayer effects occurring at this still relatively high moisture content.

The classic work of Prahl (1968) still represents the best choice for vapor pressure reduction factor. His data cover a wide range of temperature and relative humidity and are considered to have high reliability. Furthermore, as noted earlier, Prahl showed that the sorption isotherms of chemical pulp from both softwood and hardwood are essentially the same. In addition, experimental results of Reardon (1994) for newsprint, composed of 75% thermo-mechanical pulp, 20% eucalyptus pulp and 5% kraft pulp, closely match those of Prahl. As Prahl's data are then applicable to both mechanical and chemical pulps, his results were chosen for use in the present study. The Reardon (1994) correlation of Prahl's data, Equation 3-38, is used because it includes the effect of temperature that Prahl determined.

(b) Differential heat of sorption

Relative to free water, evaporation of adsorbed water requires more energy, the additional heat needed to break the sorptive bonds being the differential heat of sorption, H_s . To determine the differential heat of sorption, isotherm data are inserted into the Clausius-Clapeyron equation:

$$H_s = \frac{R T}{M_v P_v} \frac{\partial P_v}{\partial T} = \frac{R T^2}{M_v} \frac{\partial (\ln \Theta)}{\partial T} \quad (3-40)$$

Applying the data of Prahl (1968) to Equation 3-40, Reardon (1994) presented the following correlation for H_s , J/kg:

$$H_s = 1.364 \times 10^6 \exp\left(\frac{-19.45 X}{1 + X}\right) \quad (3-41)$$

This equation, provided on Figure 3-12, was developed by averaging the results over Prahl's five temperatures: 30°C, 35°C, 45°C, 65°C and 93°C. The effect of sorption on thermodynamic properties starts to be perceptible only when the moisture content has decreased to about 0.35 kg/kg dry, where Figure 2-9 indicates only a 2% reduction in

vapor pressure and Figure 3-12 shows that H_s is only about 1% of the latent heat for free water, about 2200 kJ/kg.

Based on experimental results of Stamm and Loughborough for kraft pulp (unpublished), Skaar (1988) provides the following correlation for H_s without identifying the applicable temperature range:

$$H_s = 1.172 \times 10^6 \exp\left(\frac{-14.0X}{1+X}\right) \quad (3-42)$$

Figure 3-12 shows that Skaar's correlation closely matches that of Equation 3-41.

Based on more recent sorption experiments for newsprint between 30°C and 80°C, the H_s expression developed by Lampinen and Ojala (1993) is:

$$H_s = 6.051 \times 10^7 \exp\left(-30.05 \frac{X}{X_0}\right) \left(\frac{T}{T_{cr}}\right) \left(1 - \frac{T}{T_{cr}}\right)^{5.06} \quad (3-43)$$

where $X_0 = 1.581$ and $T_{cr} = 647.25$ K.

Figure 3-12 shows that as paper dries below a moisture content of about 0.35 kg/kg dry, the additional heat required for vaporization of sorbed water increases exponentially. In the range of dryer section exit moisture content from 6% down to 1% moisture, the energy required per kg of sorbed water removed is, respectively, from about 20% to 50% larger than the latent heat of vaporization for free water, about 2200 kJ/kg at 100°C.

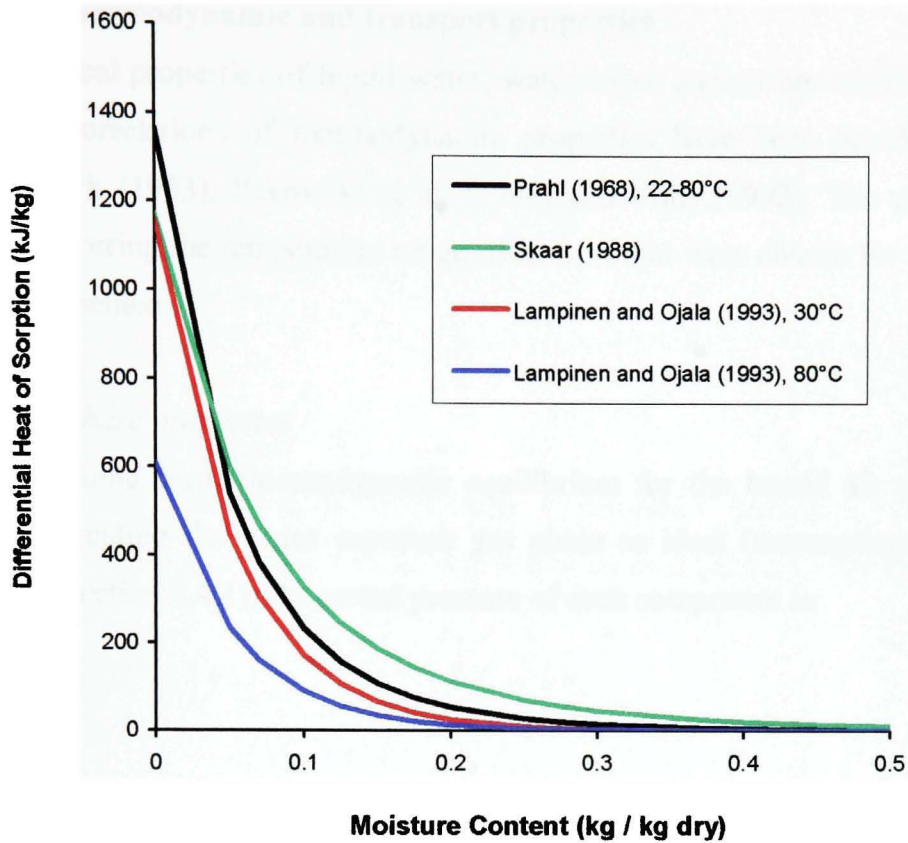


Figure 3-12 Differential heat of sorption in paper

Regarding the choice of correlation for use in the present model, the Figure 3-12 representation of the measurements for kraft pulp of Prah (1968) and Skaar (1988) indicate very close agreement. The Lampinen and Ojala (1993) correlation for newsprint at 30°C and 80°C shows a significant temperature effect, contradicting the Reardon (1994) results which, as noted in section 3.3.1, showed that sorption isotherms for a newsprint composed mainly of thermo-mechanical pulp do not differ significantly from those of kraft pulp. As noted earlier, Reardon's results are also in close agreement with those of Prah. Therefore the results of Lampinen and Ojala are not used here as they contradict two studies considered reliable. The furnish dependency of the vapor pressure reduction factor and consequently of differential heat of sorption requires more study. In section (a) Prah's data for the water vapor reduction factor were chosen for use in the present study, so to be consistent Reardon's correlation for differential heat of sorption, Equation 3-41, based on Prah's results is chosen here as the basis of H_s .

3.3 Fluid thermodynamic and transport properties

Physical properties of liquid water, water vapor and air are treated in this section. Empirical correlations of thermodynamic properties have been developed by Dewitt (1985), Wark (1983), Pakowski et al. (1991) and Mills (1992). The physical property relations covering the temperature range of interest that were chosen for use in the model are now presented.

3.3.1 Gas phase properties

Assuming local thermodynamic equilibrium for the humid air within the moist sheet and treating the water vapor-air gas phase as ideal (assumptions i and iv from Chapter 2, section 2.4.1), the partial pressure of each component is:

$$P_i = \frac{\rho_i R T}{M_i} \quad (3-44)$$

where $R = 8314 \text{ J/kmol.K}$, $M_a = 28.97$ and $M_v = 18.02 \text{ kg/kmol}$.

Partial pressure and density of water vapor and air by Dalton's law are:

$$P_g = P_v + P_a \quad (3-45)$$

$$\rho_g = \rho_v + \rho_a \quad (3-46)$$

Equation 3-46 can be derived from Equations 3-44 and 3-45 (Bird et al., 1960) for average molecular weight as:

$$M = \frac{\rho_v + \rho_a}{\rho_v/M_v + \rho_a/M_a} \quad (3-47)$$

Humid air viscosity as a linear function of mole fraction (Stanish et al., 1986) is:

$$\mu_g = \mu_v y_v + \mu_a y_a \quad (3-48)$$

for which

$$y_i = \frac{P_i}{P_g} \quad (3-49)$$

(a) Water vapor properties

With free water the vapor pressure is saturation pressure. At lower moisture contents the vapor pressure is related to moisture content through a sorption isotherm:

$$P_v = \Theta(X, T) P_{v, \text{sat}}(T) \quad (3-50)$$

where $\Theta(X, T)$ is the vapor pressure reduction factor discussed in section 3.3.

The saturated vapor pressure as expressed by Pakowski et al. (1991) is:

$$P_{v, \text{sat}}(T) = 0.133322 \exp\left(18.3036 - \frac{3816.44}{T - 46.13}\right) \quad (3-51)$$

with $P_{v, \text{sat}}$ in kPa, and T in K here and in all subsequent equations to 3-64. For $273 \text{ K} \leq T \leq 648 \text{ K}$, Equation 3-51 is accurate to 0.50% in the 0-100°C range and 1.64% over 100-350°C.

The water vapor specific heat expressed by Pakowski et al. (1991) is:

$$c_{pv} = -0.15522 + 0.02146T - 7.8421 \times 10^{-5} T^2 + 9.8102 \times 10^{-8} T^3 \quad (3-52)$$

with c_{pv} in kJ/kgK. For $273 \text{ K} \leq T \leq 450 \text{ K}$, Equation 3-52 is accurate to 0.07%.

The latent heat of vaporization as given by Pakowski et al. (1991) is:

$$\begin{aligned} \Delta H_v = & 2504.65 - 2.80701(T - 273.15) + 0.0121884(T - 273.15)^2 \\ & - 1.25205 \times 10^{-4} (T - 273.15)^3 + 4.50499 \times 10^{-7} (T - 273.15)^4 \\ & - 6.67186 \times 10^{-10} (T - 273.15)^5 \end{aligned} \quad (3-53)$$

with ΔH_v in kJ/kg. For $273 \text{ K} \leq T \leq 623 \text{ K}$, Equation 3-53 is accurate to 0.07% in the 0-100°C range and 0.21% over 100-350°C.

Water vapor dynamic viscosity was described by Pakowski et al. (1991) as:

$$\begin{aligned} \mu_v = & 7.76998 \times 10^{-6} + 7.27327 \times 10^{-8} (T - 273.15) - 8.1094 \times 10^{-10} (T - 273.15)^2 \\ & + 7.3741 \times 10^{-12} (T - 273.15)^3 - 2.83617 \times 10^{-14} (T - 273.15)^4 \\ & + 3.85826 \times 10^{-17} (T - 273.15)^5 \end{aligned} \quad (3-54)$$

with μ_v in kg/m.s. For $273 \text{ K} \leq T \leq 573 \text{ K}$, Equation 3-54 is accurate to 1.28% in the 0-100°C range and 0.59% over 100-350°C.

Thermal conductivity of water vapor was expressed by Incropera and Dewitt (1985) as:

$$k_v = 0.023376 - 7.9146 \times 10^{-5} T + 2.228 \times 10^{-7} T^2 \quad (3-55)$$

where k_v is in W/mK. For $273 \text{ K} \leq T \leq 450 \text{ K}$, Equation 3-55 is accurate to 0.52%.

Finally, the binary diffusion coefficient of the water vapor-air system was reported by Incropera and Dewitt (1985) as:

$$D_v = 0.26 \times 10^{-4} \left(\frac{T}{298} \right)^{1.5} \left(\frac{1.0133 \times 10^5}{P_g} \right) \quad (3-56)$$

for D_v in m^2/s , P_g in P.

(b) Air properties

Air density as expressed by Mills (1993) and Pakowski et al. (1991) is:

$$\rho_a = -0.003246 - \frac{268.979}{T^2} + \frac{355.45}{T} + 1.7114 \times 10^{-6} T \quad (3-57)$$

where ρ_v is kg/m³. For 150 K ≤ T ≤ 1000 K, Equation 3-57 is accurate to 0.10%.

Air specific heat reported by Pakowski et al. (1991) is:

$$c_{pa} = 1009.26 - 0.0404033 T + 6.17596 \times 10^{-4} T^2 - 4.09723 \times 10^{-7} T^3 \quad (3-58)$$

where c_{pa} is kJ/kgK. For 233 K ≤ T ≤ 1273 K, Equation 3-58 is accurate to 0.28% entire.

Air dynamic viscosity according to Pakowski et al. (1991) is:

$$\mu_a = 3.69045 \times 10^{-6} + 5.3547 \times 10^{-8} T - 1.6148 \times 10^{-11} T^2 \quad (3-59)$$

where μ_v is kg/ms. For 150 K ≤ T ≤ 1000 K, Equation 3-59 is accurate to 0.85%.

Thermal conductivity of air was given by Incropera and Dewitt (1985) as:

$$k_a = 0.00898 + 5.8947 \times 10^{-5} T \quad (3-60)$$

where k_a is W/mK. For 273 K ≤ T ≤ 625 K, Equation 3-60 is accurate to 0.10%.

3.3.2 Liquid water properties

Water density can be expressed by the relation of Pakowski et al. (1991) as:

$$\rho_1 = 1000. + 0.0153715(T - 273.15) - 5.8302 \times 10^{-3} (T - 273.15)^2 + 1.52108 \times 10^{-5} (T - 273.15)^3 \quad (3-61)$$

where ρ_l is kg/m^3 . For $273 \text{ K} \leq T \leq 623 \text{ K}$, Equation 3-61 is accurate to 0.02% in the 0-100°C range and 17.13% in the 100-350°C range (the error is 3% at 250°C).

The specific heat of water according to Pakowski et al. (1991) is:

$$c_{pl} = 5.4517 - 0.007965T + 1.24716 \times 10^{-5} T^2 \quad (3-62)$$

where c_{pl} is kJ/kgK . For $233 \text{ K} \leq T \leq 450 \text{ K}$, Equation 3-62 is accurate to 0.08%.

The temperature dependence of liquid water viscosity given by Pakowski et al. (1991) is:

$$\begin{aligned} \mu_l = & 0.4293361 - 0.005468T + 2.79145 \times 10^{-5} T^2 - 7.12313 \times 10^{-8} T^3 \\ & + 9.07413 \times 10^{-11} T^4 - 4.61279 \times 10^{-14} T^5 \end{aligned} \quad (3-63)$$

where μ_l is kg/ms . For $273 \text{ K} \leq T \leq 470 \text{ K}$, Equation 3-63 is accurate to 2.16%.

Finally, the thermal conductivity of water as given by Incropera and Dewitt (1985) is:

$$k_l = -0.46558 + 0.0059947T - 8.646 \times 10^{-6} T^2 + 2.1796 \times 10^{-9} T^3 \quad (3-64)$$

where k_l is W/mK . For $273 \text{ K} \leq T \leq 625 \text{ K}$, Equation 3-64 is accurate to 0.37%.

CHAPTER 4

PARAMETER SELECTION AND MODEL VALIDATION

The present chapter treats the two steps remaining to complete the development of the dryer simulator: selection of the optimal choice of transport properties for the model, then its validation against industrial dryer performance data. The model must be finalized before proceeding to its validation. However for finalizing the selection of physical properties the most objective criterion is to test the predictions of model against industrial data using, as parameters, the various sources available for these properties. Such tests of the model against industrial dryer performance data involve the same procedure as the model validation, but the final validation is performed only when every aspect of the model, including the choice of transport properties, has been fixed. The presentation begins with description in section 4.1 of the procedure for testing model performance, used in section 4.2 for the parameter selection and then again in section 4.3 for validation tests after all aspects of the model are final.

4.1 Testing model performance vs. industrial data

Dryer surveys, the periodic determination of paper machine dryer section operating conditions and performance, constitute the basis for testing a dryer model against industrial data. Although such results are not easy to obtain the drying research group at McGill University has been able to collect 32 dryer surveys from 12 paper machines producing a wide range of paper grades, detailed in section 4.3. The basic information customarily included in dryer surveys are the operating conditions such as machine layout and dimensions, condensing steam pressure and dryer pocket conditions. The type of test performed depends on the data available: exceptionally measurements such as sheet temperature or cylinder surface temperature are determined in a survey, enabling comparison of the corresponding model predictions. However any reliable dryer survey enables two types of test:

1. *Exit moisture content prediction:* Knowing the sheet moisture content into the dryer, machine speed and all dryer design specifications and operating conditions, the model

will predict directly the moisture content at the dryer section exit. This test is expressed as the predicted final moisture content relative to that measured.

2. *Machine speed prediction*: The alternate test mode is to predict the machine speed corresponding to the entering and exit sheet moisture contents reported in the dryer survey. This procedure is inherently iterative. Machine speed is assumed, then the exit moisture content is predicted and compared with the actual value, with the procedure repeated until an acceptable match is achieved. This iterative solution is carried out in an optimal way using a subroutine developed by Bond et al. (1996) for the first McGill dryer simulator.

Both types of test are performed for all 32 surveys. Although the average model error can be calculated from either test, it is the machine speed prediction that is more relevant to an industrial user because exit moisture content is a product specification which must be respected. Consequently machine speed prediction error is used here, along with the prediction of sheet temperature, when determined, as the measure of model error required both in the sensitivity analysis of section 4.2 and in the model validation of section 4.3.

4.2 Optimal choice of transport properties

4.2.1 Transport properties to be tested

As explained in Chapter 3, a sensitivity analysis is required to identify the optimal combination of the physical properties needed in the paper drying model. Sections 3.2 and 3.3 established that for the case of capillary pressure and thermodynamic properties of moist paper, no sensitivity analysis was required because the evidence was clear as to which literature source was most valid for these categories of model properties. As the transport properties in moist paper, analyzed in section 3.1, was the only category for which the choice was not clear, properties of this type are now treated.

There are 5 transport properties for which no clear choice could be made for the reference basis to use. As detailed in section 3.1 the alternative bases available for these 5 parameters of the model are as follows:

1. Effective water vapor diffusivity (D_{eff}): Two correlations from Table 3-7, those of Han (1970) or Ramaswamy (1990).

Han:
$$\frac{D_{\text{eff}}}{D_v} = \frac{\theta}{\tau} \varepsilon^m (1-S)^u \quad \text{with } \theta = u = 1 \text{ and } \tau = m = 1.5$$

Ramaswamy:
$$\frac{D_{\text{eff}}}{D_v} = 0.4 \frac{\varepsilon^{1.23}}{\exp(1.574 S)} \quad 0 < S < 0.7$$

$$\frac{D_{\text{eff}}}{D_v} = \frac{\varepsilon^{1.23} (1-S)^{1.08}}{4.33 - 3.33 S} \quad 0.7 < S < 1$$

2. Sorbed water diffusivity (D_s): Two correlations, those of Siau (1971), Equation 3-26, or Lin (1991), Equation 3-27.

Siau:
$$D_s = \exp\left(-9.9 - \frac{4300}{T} + 9.8X_s\right)$$

Lin:
$$D_s = 2.616 \times 10^{-11} \exp(0.5X) \exp\left(\frac{16100}{R} \left(\frac{1}{298.15} - \frac{1}{T}\right)\right)$$

3. Liquid water relative permeability (k_{rl}): Ahrens and Journeaux (1984) correlation of Robertson (1963) data, Equation 3-5, or Asensio (2000) experimental data, Table 3-4.

Robertson / Ahrens and Journeaux:

$$k_{rl} = \begin{cases} 4.51 \times 10^{-12} \exp(25.86 S) & 0.82 < S \leq 1 \\ 6.93 \times 10^{-6} \exp(8.54 S) & 0.36 < S \leq 0.82 \\ 1.0 \times 10^{-11} \exp(46.05 S) & 0.15 < S \leq 0.36 \\ 0 & S \leq 0.15 \end{cases}$$

Asensio: Parameters for effect of moisture content and paper type

Furnish	Temp. (°C)	X_b	Equation	a	b	c
LWC	24	0.490	$k_{rl} = a (X_l)^b \exp [(X_l)^c]$	0.360	4.854	0.455
Newsprint	24	0.349	$k_{rl} = a (X_l)^b \exp [(X_l)^c]$	0.533	4.868	0.475
Linerboard	24	1.132	$k_{rl} = a (X_l/2)^b \exp [(X_l/2)^c]$	0.562	1.184	0.487
Eucalyptus A	24	0.536	$k_{rl} = a (X_l)^b \exp [(X_l)^c]$	0.021	4.164	0.578
Eucalyptus B	24	0.393	$k_{rl} = a (X_l/2)^b \exp [(X_l/2)^c]$	0.494	4.156	0.500
NSWK	24	0.456	$k_{rl} = a (X_l)^b \exp [(X_l)^c]$	0.127	4.221	0.459
Linerboard	56	0.907	$k_{rl} = a (X_l/2)^b \exp [(X_l/2)^c]$	1.254	4.522	0.670
Eucalyptus A	56	0.504	$k_{rl} = a (X_l/2)^b \exp [(X_l/2)^c]$	1.447	4.528	0.704
Eucalyptus B	56	0.488	$k_{rl} = a (X_l/2)^b \exp [(X_l/2)^c]$	0.215	4.114	0.593
Linerboard	85	0.702	$k_{rl} = a (X_l/2)^b \exp [(X_l/2)^c]$	1.337	4.524	0.665

4. Humid air relative permeability (k_{rg}): Correlations of the measurements of Hashemi (1996) and Hashemi et al. (2002), or Asensio (2000).

Hashemi et al.: Parameters for effect of moisture content and paper type

Paper Type*	Exponential Model			
	$a \times 10^{10}$	$b \times 10^{10}$	c	R^2
1	0.840	0.101	4.532	0.99
2	1.400	0.218	4.420	0.99
3	0.407	0.141	3.149	0.99
4	0.500	0.915	2.120	0.99
5	1.125	1.043	2.976	0.99
6	0.276	0.381	1.848	0.99
7	0.628	0.242	3.458	0.99
8	0.836	0.027	5.527	0.99
9	0.469	0.331	3.448	0.99
10	0.613	0.085	6.023	0.99

* The specification of these 10 paper types is given in Table 3-2.

Exponential model:
$$\frac{L}{k_i} = a + b \exp(cX)$$

Asensio: Parameters for effect of moisture content and paper type

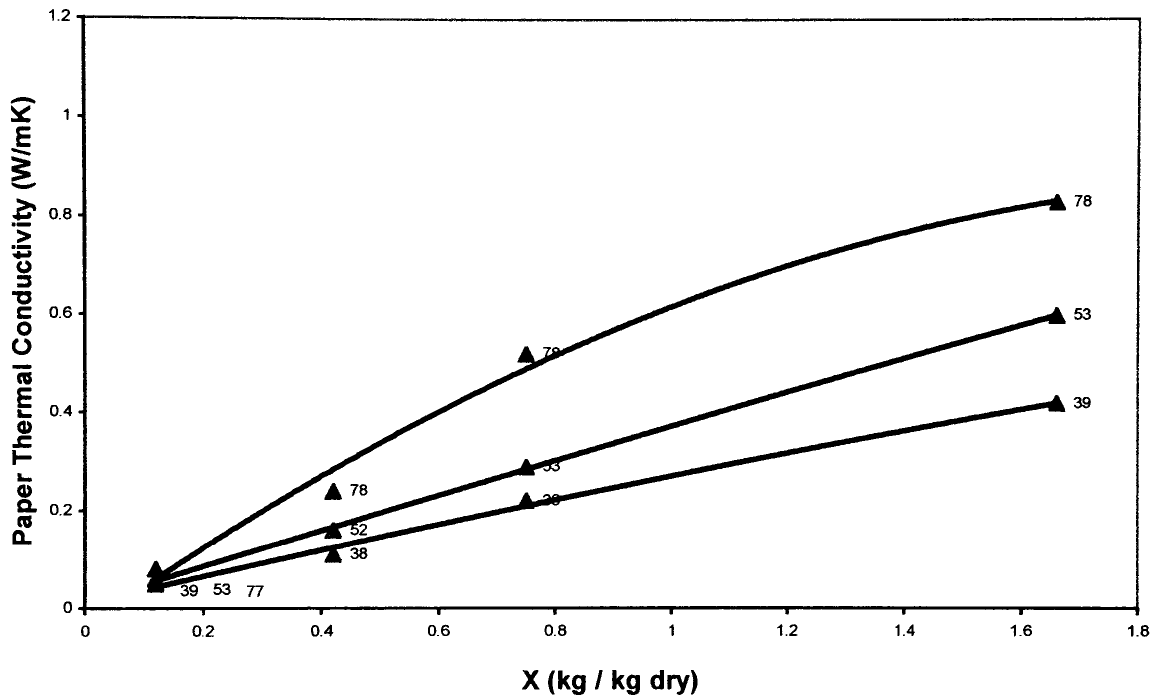
Furnish	Temp. (°C)	Equation	a	b	c	d
LWC	24	$k_{rg} = a + b / [1 + (X_1/c)^d]$	-0.173	1.163	0.563	3.501
Newsprint	24	$k_{rg} = a + b / [1 + (X_1/c)^d]$	-0.123	1.109	0.510	3.778
Linerboard	24	$k_{rg} = a + b / [1 + (X_1/c)^d]$	-0.148	1.132	0.847	3.092
Eucalyptus A	24	$k_{rg} = a + b / [1 + (X_1/c)^d]$	-0.178	1.164	0.941	3.041
Eucalyptus B	24	$k_{rg} = a + b / [1 + (X_1/c)^d]$	-0.161	1.146	0.873	3.026
NSWK	24	$k_{rg} = a + b / [1 + (X_1/c)^d]$	-0.171	1.156	0.633	2.971
Linerboard	56	$k_{rg} = a + b / [1 + (X_1/c)^d]$	-0.141	1.127	0.788	3.598
Eucalyptus A	56	$k_{rg} = a + b / [1 + (X_1/c)^d]$	-0.172	1.161	0.780	3.476
Eucalyptus B	56	$k_{rg} = a + b / [1 + (X_1/c)^d]$	-0.182	1.168	1.050	3.028
Linerboard	85	$k_{rg} = a + b / [1 + (X_1/c)^d]$	-0.185	1.175	0.796	3.411

5. Effective thermal conductivity (k_{eff}) of moist paper: Theoretical combination series-parallel model of Kartovaara (1985), Equation 3-23, or experimental results of Nederveen and Finken (1992), Figures 3-6 and 3-7.

Series-parallel model:

$$k_{\text{eff}} = \frac{1}{\frac{1-\Lambda}{k_{\text{par}}} + \frac{\Lambda}{k_{\text{ser}}}} \quad \text{with } \Lambda = 0.5, \text{ Reardon (1994)}$$

Nederveen and Finken: Relations for effect of moisture content and temperature



Effect of moisture content on thermal conductivity of groundwood handsheets, 340 kg/m³
(numbers are temperature, °C), Nederveen and Finken (1992)

of the procedure for obtaining the best model. For this purpose it is necessary to select, from many references in the literature, the physical properties judged to be the most relevant and reliable. Once this selection is made these choices of physical properties become an integral and permanent part of the paper drying model and are never subsequently changed including when, in use, the simulator is calibrated. Thus the objective of this sensitivity analysis is to find, without any error dependent alteration of the model, the best combination of parameters for use in the paper drying model.

As noted earlier, the measure of average error of machine speed prediction is used as the criterion for physical property parameter selection. There are two sources of error in the model predictions: dryer survey measurement error and model systematic error. The dryer surveys contain measurement errors which are random in nature because the surveys have been carried out on different paper machines, by different technical staff, using different instruments. The systematic error of the model, on the other hand, is not random because the same procedure is used for every simulation. As the model may systematically either over-predict or under-predict machine speed, this error could be either positive or negative. If the “average error” of machine speed prediction is calculated for all 32 dryer surveys, it could be reasonably assumed that the random errors of measurement approximately cancel out. Thus the average error for the 32 cases is the appropriate measure of model systematic error. As the goal of the sensitivity analysis is to find the optimal combination of transport properties, the average machine speed prediction error is therefore the choice as the criterion for parameter selection. Thus for each combination of transport properties, all 32 tests against industrial data are run and the resulting average error of machine speed prediction is compared to that using other transport property combinations.

The five parameters involved in the sensitivity analysis are D_{eff} , D_s , k_{rl} , k_{rg} and k_{eff} . With two alternatives for each of these, there are in total 32 combinations of transport properties. With 32 machine speed predictions required for each combination of properties treated, this indicates 32×32 or 1024 machine speed predictions. In order to reduce this enormous amount of calculation the following procedure was followed. Han's correlation for D_{eff} (water vapor diffusivity) and Lin's correlation for D_s (sorbed water diffusivity) were initially chosen, hence leaving the relative permeability of water and

humid air (k_{rl} and k_{rg}) and effective paper thermal conductivity, k_{eff} , as the three test variables. With the two possible bases for these three transport properties the number of combinations to be tested is reduced from 32 to 8, reducing the number of machine speed predictions from 1024 to 256. After finding the best choices for these three variables, the sensitivity of model to D_{eff} and D_s is then analyzed. This procedure is justified because, as shown shortly, the model has a much higher sensitivity to the two relative permeabilities and to thermal conductivity than to the two diffusivities.

Before proceeding to the numerical results it should be noted that there are in total 30 physical parameters in this comprehensive model, of which five are now tested against industrial data in sections 4.2.3, 4.2.4 and 4.2.5. It follows from the complexity of the model that changing just one parameter out of 30 would not be expected to cause a large change in the prediction of machine speed. However in order to obtain finally the best overall model, the best individual elements of the model should be chosen using exacting standards of accuracy. In addition, it will be shown that studying the effect of each transport property on the overall model performance provides insight into the relative importance of the corresponding transport mechanism at different stages of the drying, hence furthering the understanding of complex heat and mass transfer phenomena associated with the drying of paper.

4.2.3 Effect of relative permeability and thermal conductivity

As discussed earlier, with the use of Han's correlation for water vapor diffusivity and Lin's correlation for sorbed water diffusivity there remain two choices for each of the other three properties of paper - water relative permeability, effective thermal conductivity and humid air relative permeability. As noted earlier, testing these 8 combinations of parameters with the results for 32 dryer surveys involved performing $8 \times 32 = 256$ machine speed simulations. The sign for the average error is the predicted machine speed minus the actual speed. Table 4-1 provides the values of average error associated with each combination.

Table 4-1 Average error of machine speed prediction for
8 combinations of 3 transport properties, using D_{eff} of Han and D_s of Lin

	k_{rl} : Asensio k_{rg} : Hashemi	k_{rl} : Asensio k_{rg} : Asensio	k_{rl} : Robertson k_{rg} : Hashemi	k_{rl} : Robertson k_{rg} : Asensio
k_{eff} : Series - Parallel	+3.01%	+4.09%	+2.63%	+3.92%
k_{eff} : Experimental	+3.24%	+4.72%	+3.07%	+4.37%

The combination [k_{rl} : Robertson; k_{rg} : Hashemi et al.; k_{eff} : series-parallel model] is seen to provide the smallest error, 2.63%, the second best combination being: [k_{rl} : Asensio; k_{rg} : Hashemi et al.; k_{eff} : series-parallel model] with an error of 3.01%. Dependency of model results on transport properties is substantial, the best combination having an error of 2.63% while that of the worst combination is 4.72%. Recall that when changing just one parameter out of the total of 30, a large difference is not expected.

(a) Effect of water relative permeability

Comparison of the two best combinations, both using the k_{rg} of Hashemi et al., reveals that by switching from Asensio's k_{rl} to that of Robertson, the error reduces from 3% to 2.6%. This is surprising because Robertson's data, though experimentally determined, do not include furnish dependency of k_{rl} while Asensio made her measurements for six furnishes. However, as detailed in section 3.1.2 (c) of Chapter 3, Asensio did not directly measure the water relative permeability but rather converted the experimentally determined capillary pressure-saturation relation into permeability through use of the theoretically derived Wyllie-Gardner equations. The better performance of the Robertson data suggests that the Wyllie-Gardner theoretical approach is unsuitable for paper. This result also demonstrates the limited sensitivity of the model to liquid water relative permeability: although two very different correlations are used for k_{rl} , one including furnish dependency and the other not, the difference in overall model performance is small.

To provide a further basis for making the judgement concerning k_{rl} , another criterion is the error in prediction not of machine speed but of sheet temperature, using a dryer survey having this measurement. A survey of the Kruger Bromptonville Machine # 1 (April 1988) provided the sheet average temperature on all 46 cylinders (detailed in section 4.4). As the present model predicts the local values of temperature in the sheet thickness direction, the sheet temperature used for this purpose is that calculated by averaging all the local values. In Figure 4-1 the measured sheet temperature is compared to model predictions using two following combinations:

Combination 1: [k_{rl} of Asensio; k_{rg} of Hashemi et al.; k_{eff} of the series-parallel model]

Combination 2: [k_{rl} of Robertson; k_{rg} of Hashemi et al.; k_{eff} of the series-parallel model]

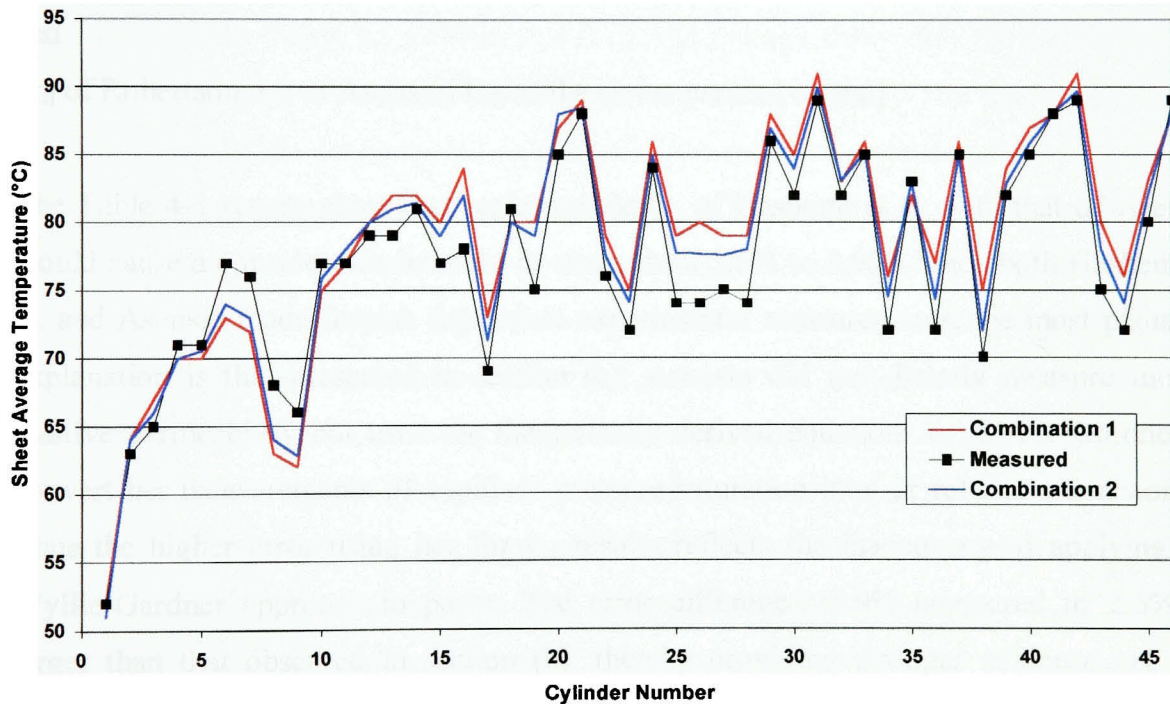


Figure 4-1 Sheet average temperature for different k_{rl} parameters, Kruger Bromptonville Machine # 1 (April 1988)

It is seen that again the combination with the Robertson k_{rl} provides a better sheet temperature prediction than that with the k_{rl} of Asensio. Consequently, despite the lack of

furnish dependency, k_{rl} from Robertson is chosen over that of Asensio because of better performance of model, both for machine speed prediction (Table 4-1) and for sheet temperature (Figure 4-1).

(b) Effect of air relative permeability

The two combinations with lowest error using Robertson's k_{rl} are now compared to assess the effect of air relative permeability. As the Table 4-1 results indicate that the average error in machine speed prediction is lower for the choice of the series-parallel model for thermal conductivity, k_{eff} , it is that pair of results which is used for assessing the effect of air relative permeability, k_{rg} . These combinations are:

[k_{rl} of Robertson; k_{rg} of Hashemi et al; k_{eff} of the series-parallel model]

and

[k_{rl} of Robertson; k_{rg} of Asensio; k_{eff} of the series-parallel model]

The Table 4-1 results show that replacing the k_{rg} of Hashemi et al. with that of Asensio would cause a considerable increase in error, from 2.6% to 3.9%. Since both Hashemi et al. and Asensio made furnish dependent experimental measurements, the most plausible explanation is that presented in section (a): Asensio did not directly measure the air relative permeability but used the theoretically derived equations of Wyllie-Gardner to convert her measurements of capillary pressure-saturation into air relative permeability. Thus the higher error using her for k_{rg} results reflects the inadequacy of applying the Wyllie-Gardner approach to paper. The error difference, 3.9% compared to 2.6%, is larger than that observed in section (b), thereby providing stronger evidence yet that Asensio's application of the Wyllie-Gardner equations to paper is inappropriate.

This result also shows that the model has a much higher sensitivity to air relative permeability than to liquid water relative permeability, underlining the fact that vapor phase convective transport plays a prominent role in the mechanism of paper drying. This finding is also consistent with the fact that dryer performance is determined much more towards the dry end, where drying rate is low and no liquid water is present, than near the

wet end where there is water in the pores and the drying rate is higher. This important aspect of the internal dynamics of paper drying is further discussed in Chapter 5.

In conclusion, as use of the experimental results of Hashemi et al. provides considerably better model prediction of machine speed, this basis for air relative permeability, k_{rg} , is chosen for the simulation model.

(c) Effect of thermal conductivity

Table 4-1 leaves no doubt about the inadequacy of the best available experimentally determined values, those of Nederveen and Finken, for effective thermal conductivity of moist paper for use in the drying model. For all combinations of transport properties the theoretical series-parallel model provides better results. For the best combination of the other parameters, i.e. water relative permeability, k_{rl} , of Robertson and air relative permeability, k_{rg} , of Hashemi et al., the average error using the experimentally determined conductivity, k_{eff} , of 3.1% drops to 2.6% with use of the theoretical series-parallel model. This confirms the hypothesis presented in section 3.1.3 of Chapter 3 which derives from the fact that the contribution of different mechanisms to heat transfer has been treated here by separate terms in the energy balance. The use of experimentally obtained thermal conductivity is hazardous because it is extremely difficult to exclude the contributions to measured heat transfer coming from other mechanisms when attempting to determine just pure conduction. Experimental determination of thermal conductivity typically produces higher values than true conductivity, as is confirmed by the results in Table 4-1 which shows that the use of such over-estimated thermal conductivity leads to the prediction of higher machine speed. Therefore the theoretical model of effective thermal conductivity, representing pure conduction, is the choice made for incorporation into the drying model.

The best combination found for the three most influential transport properties [k_{rl} of Robertson; k_{rg} of Hashemi et al.; k_{eff} of the series-parallel model] is now used to assess the sensitivity of model first to water vapor diffusivity, D_{eff} , then to sorbed water diffusivity, D_s .

4.2.4 Effect of water vapor diffusivity

As presented in section 4.2.1, analysis indicates that the two best choices of water vapor diffusivity, D_{eff} , are those of Han (1970) and Ramaswamy (1990). While using sorbed water diffusivity from Lin's correlation, the correlation of Han for D_{eff} was already used in section 4.2.3 to find the best combination of relative water and air permeabilities and effective thermal conductivity. Now that same combination for those three properties is treated, this time using Ramaswamy's correlation for D_{eff} for running all 32 sets of industrial test data again. The average error of machine speed prediction, given in Table 4-1 as 2.63% with Han's correlation for D_{eff} , was found to be 2.61% with that of Ramaswamy. Thus use of either Han's or Ramaswamy's D_{eff} makes no significant difference in predicting dryer performance. To put these results into perspective, water vapor diffusivity according to these two correlations is compared in Table 4-2 for two porosities and two saturations.

Table 4-2 Comparison of water vapor diffusivity according to correlations of Han and of Ramaswamy

Porosity	Saturation	$\frac{(D_{\text{eff}})_{\text{Han}}}{(D_{\text{eff}})_{\text{Ramaswamy}}}$
0.3	0.2	1.16
	0.9	0.68
0.7	0.2	1.46
	0.9	0.86

The values of D_{eff} from these two correlations are seen not only to differ by as much as 50% but these large differences are moreover in the opposite directions depending on the stage of the drying process. Early in drying, with 90% of the pores filled with free water ($S = 0.9$), the Ramaswamy correlation predicts a higher diffusivity than that of Han, but when the pores are 80% free from water ($S = 0.2$) it is the Han's correlation that predicts a much higher water vapor diffusivity. That the paper drying model shows practically no sensitivity to water vapor diffusivity confirms the hypothesis that the model sensitivity to the two permeabilities and thermal conductivity far exceeds that to gas phase diffusivity.

As use of the Han and Ramaswamy correlations provides effectively the same result, either basis could be used in the simulation model. However Han's correlation is chosen because he included the important paper pore geometry parameters, tortuosity and shape factor. In the future when these parameters become known, the correlation of Han has the potential to provide the better estimate of vapor diffusivity. Since these parameters are not known for the paper grades studied here, the generic suggested values discussed in Chapter 3 are used in the simulation model.

4.2.5 Effect of sorbed water diffusivity

Sections 4.2.3 and 4.2.4 establish that the best combination for the four transport properties [k_{rl} of Robertson; k_{rg} of Hashemi et al.; k_{eff} of the series-parallel model; D_{eff} of Han], has an error of 2.63% when the sorbed water diffusivity of Lin (1991) was used. All 32 sets of industrial test were run again, using the above combination for those four transport properties but with the alternative sorbed water diffusivity noted in section 3.1.5, that according to Siau (1971). As a result, the average error increased from 2.63% to 2.77%. As shown in Figure 3-9, the Siau correlation predicts diffusivity of liquid water up to 100 times that of Lin. That such enormous differences in water diffusivity generate only minor differences in drying rate, as indicated by the difference in machine speed prediction between 2.63% and 2.77%, suggests the almost negligible importance of sorbed water diffusivity in the drying mechanism, a hypothesis confirmed in Chapter 5. Although sorbed water diffusivity is the least important of the five transport properties tested, Lin's correlation for moisture diffusivity in paper, clearly the better choice, is used in the simulation model.

4.2.6 Summary of sensitivity analysis

320 tests of the model against industrial dryer performance data were performed to find the optimal combination of the five transport properties for which there was not a rational basis for choosing among alternatives available. This procedure involved 10 combinations of five transport properties, with each combination being tested using the same 32 sets of industrial data. The average error of machine speed prediction for these

32 dryer surveys was the criterion used for parameter selection. The findings were as follows:

- (1) In the case of the choice for liquid water relative permeability, k_{rl} , between studies of Robertson and Asensio, a further test using dryer survey measurements of sheet average temperature as the criterion confirmed that Robertson's correlation, despite its lack of furnish dependency, is the better choice.
- (2) For humid air relative permeability, k_{rg} , the experimental results of Hashemi et al. were found superior to the indirect determinations of Asensio, which suggests that the theoretical approach used by Asensio when converting measurements of capillary pressure-saturation into relative permeability is not appropriate for moist paper.
- (3) Regarding the choice for effective thermal conductivity, k_{eff} , the theoretical series-parallel model was selected as it provided better predictions than the experimental results of Nederveen and Finken. This confirms the hypothesis that use of experimental values of effective thermal conductivity, which include contributions to heat transfer of mechanisms in addition to conduction, would lead to errors.
- (4) Assessing the model sensitivity to water vapor diffusivity, D_{eff} revealed that the correlations of Han and of Ramaswamy provide essentially the same results and that the model is much less sensitive to vapor diffusivity than to the relative permeability of humid air and liquid water. Han's correlation for water vapor diffusivity was chosen because it includes description of pore geometry factors.
- (5) Evaluation of model sensitivity to sorbed water diffusivity, D_s , showed not only that the correlation of Lin should be chosen for the simulation model, but that the transport of sorbed water is of minimal importance in the mechanism of paper drying.

Based on this detailed sensitivity analysis, the final choice of transport properties for the paper drying model is summarized in Table 4-3:

Table 4-3 Transport properties chosen for the paper drying model

Water relative permeability, k_{rl}	Robertson (1963) data correlated by Ahrens and Journeaux (1984), Equation 3-5
Humid air relative permeability, k_{rg}	Hashemi (1996) and Hashemi et al. (2002), Equation 3-16
Thermal conductivity of moist paper, k_{eff}	Theoretical series-parallel model, Equation 3-23
Water vapor diffusivity, D_{eff}	Han (1970), Table 3-7
Sorbed water diffusivity, D_s	Lin (1991), Equation 3-27

4.3 Model validation

4.3.1 Basis for validation

Now that every element of the model has been finalized through the tests described in section 4.2, the model validation against experimental and industrial data can be carried out. Industrial paper drying involves a great complexity of conditions – reversing dozens of times the side of sheet in contact with heated surface, correspondingly frequent alteration between cylinder drying and convective drying between cylinders, the great number of changes in boundary conditions, choices of felting, condensate removal and dryer pocket ventilation. As these conditions cannot be duplicated, even in a complex pilot plant, the ultimate test of an industrial paper drying simulator is validation against paper machine data. Therefore the emphasis here is on industrial validation, although the model predictions are also compared to results of laboratory impingement drying as these can provide information concerning conditions inside the sheet which are unobtainable from a paper machine dryer.

Relative to developing a model, validation is as important, may be as complicated and even more time consuming. As noted in Chapter 1 paper drying models have generally suffered from lack of comprehensive validation, i.e. validation, without tuning or calibration, against industrial data covering a wide range of paper grades dried by different techniques. The notable exception was the previous dryer simulator developed at McGill, for which an extensive validation was presented by Sidwall et al. (1999a). The

step of thorough validation has been maintained with the drying model of the present investigation.

Following the new treatment of the transport phenomena within the sheet during drying, developed in Chapters 2 and 3 and finalized in section 4.2, several components are necessary for testing this model against industrial data. As noted in Chapter 1 the new model of transport phenomena within the sheet developed in the present study is combined with the treatment of the external systems (steam, cylinder, dryer pocket ventilation) of the Bond and Douglas model in order to constitute a complex dryer simulator for validation and testing in this section. The numerous boundary conditions required for the model equations are listed in Appendix. The last component is the input data, i.e. dryer design specifications and operating conditions, which are taken from the 32 sets of industrial dryer performance data. As noted in section 4.1 these surveys have been collected over the years by the drying research group at McGill University. Sidwall et al. (1999a) used the data from 31 surveys when validating the first McGill dryer simulator. The same input data plus the most recent case of the dryer section of a fine paper machine, section 4.3.2 (c), constitute the basis for validating the present model.

As reviewed in Chapter 1 most reported industrial validations of paper drying models involve calibration, i.e. one or more model parameters have been altered to provide a match with experimental and/or industrial data. Calibration, sometimes referred to as tuning, is a common practice when using a simulator for any complex process but should not be used during validation. Thus all validation results reported in the present study use the model without calibration. Once a simulator has been satisfactorily validated, then in subsequent use it is normal to calibrate it for a specific dryer when a set of direct measurements, i.e. a dryer survey, is available. For such calibration, the cylinder-paper contact heat transfer coefficient, condensate heat transfer coefficient or external heat and mass transfer coefficients have been used as the calibration variable. However as all validations here are without calibration, no parameter has been altered to provide a better match between model prediction and dryer survey measurements.

With 32 dryer surveys covering all major paper grades, from tissue to linerboard, being dried by a variety of drying techniques this is the most comprehensive validation reported for an industrial paper drying simulator. For each dryer survey both exit moisture

content prediction and machine speed prediction simulations, explained in section 4.1, are performed. In addition, model predictions are compared to values of parameters such as sheet temperature or cylinder surface temperature when, occasionally, these difficult measurements are reported. In a few cases where specifications in dryer surveys were incomplete, typical values corresponding to industrial operation were used (identified in bold type in the tables). All operating conditions and design specifications are presented in both SI and English units. The validations are presented first for cylinder dryer sections, grouped by grade of paper, then for air impingement drying of tissue and toweling, finally for hybrid drying with cylinder and impingement air drying combined.

4.3.2 Cylinder drying

For cylinder drying, the universally used method of producing printing and heavier grades of uncoated paper, the 26 dryer surveys presented here were obtained from eight paper mills which cover the production of newsprint, containerboard and fine paper.

(a) Newsprint machines

(a-1) Kruger Bromptonville paper machine #1

Three dryer surveys are available for this 46-cylinder machine with design specifications given in Table 4-4. The first 16 cylinders are felted on the top tier, the remaining being double felted (different felting arrangements are detailed in the Appendix). The operating conditions of the April 1988 dryer survey, listed in Table 4-5, are with steam turned off in cylinders 8,17,19,22,23,25,26,28,34,36,38,43,44. The sheet length in the dryer section and drying time, two useful values included in this and all subsequent sets of design specifications, are never reported in dryer surveys. Since the specifications of cylinder diameter, open draw between consecutive cylinders and the sheet wrap angle on all cylinders are known from surveys, the total sheet length in the dryer section is readily obtained. Total drying time is calculated from the total sheet length, thus obtained, and the machine speed from the dryer survey.

Table 4-4 Design specifications: Kruger paper machine #1 (April 1988)

Variable	S.I. Units	Alternate Units
Cylinder diameter	1.22 m	4 ft
Cylinder shell thickness	23.6 mm	0.93 in
Machine width	3.65 m	12 ft
Draw length (varies)	0.87 - 1.4 m	2.85 - 4.59 ft
Sheet length in dryer	159 m	523 ft
Felt thickness	1.8 mm	0.07 in
Top felted felt wrap angle	180°	
Double felted felt wrap angle	180°	
Paper wrap angle	230°	
Spoiler bars	none	

Table 4-5 Operating conditions: Kruger paper machine #1 (April 1988)

Variable	S.I. Units	Alternate Units
Machine speed	534 m/min	1751 fpm
Drying time	17.9 s	
Basis weight	48.8 g/m ²	10 lb/1000 ft ²
Inlet moisture content	1.27 kg/kg dry	44 % solids
Exit moisture content	0.084 kg/kg dry	92.25 % solids
Sheet inlet temperature	56°C	133°F
Fiber saturation point	0.7 kg/kg dry	58.8 % solids
Section 1	16 cylinders (1-16), top felting	
Condensing steam	84.8 kPag/118°C	12.3 psig/244°F
Section 2	14 cylinders (17-30), double felting	
Condensing steam	84.4 kPag/118°C	12.2 psig/244°F
Sections 3	16 cylinders (31-46), double felted	
Condensing steam	115.1 kPag/123°C	16.7 psig/253°F
Pocket conditions	varies-taken from dryer survey	

Results of the validation, Table 4-6, show that the model over-predicts drying by 6.6% relative to actual machine speed. Most cases of industrial validation discussed in this chapter have a smaller error of machine speed prediction.

Table 4-6 Uncalibrated validation: Kruger paper machine #1 (April 1988)

Exit moisture content	
Validation simulation	6.6 % d.b.
Measured	8.4 % d.b.
Machine speed	
Validation simulation	569 m/min
Measured	534 m/min
Difference	+6.6 %

This dryer survey also included sheet and cylinder surface temperature measurements which are compared here to the corresponding model predictions. As such temperatures are not easy to determine these measurements are subject to error and are infrequently found in dryer surveys. Figure 4-2 compares the measured and simulated sheet temperature. As can be seen the model is well able to follow the evolution of sheet temperature in the dryer. The average difference between the measured and simulated temperatures is indeed small, only +1°C. This is a remarkable result because, as discussed in more detail in section 4.4, the first McGill dryer simulator encountered large errors in predicting the sheet temperature (-7°C for this case) even though the performance regarding speed prediction was quite acceptable. Therefore the better description of transport phenomena within the sheet developed in the present study has provided good accuracy of the model for machine speed prediction while improving the predictions of sheet temperature.

A comparison is made in Figure 4-3 between the measured and predicted values of cylinder surface temperature. Although the model predictions follow the general trend of temperature variation, there are larger discrepancies than for the case of sheet temperature, Figure 4-2, particularly in the beginning of the drying. In addition to the difficulty of measuring cylinder surface temperature accurately, another possible explanation is the uncertainty of contact heat transfer coefficient between the cylinder surface and paper. This coefficient is expressed in the present model as a function of sheet moisture content (Appendix) but in reality several factors such as cylinder surface smoothness and cleanness, felt tension and felt wear can affect heat conduction between the hot cylinder surface and adjacent sheet. There is no basis for including the effect of these factors in the model.

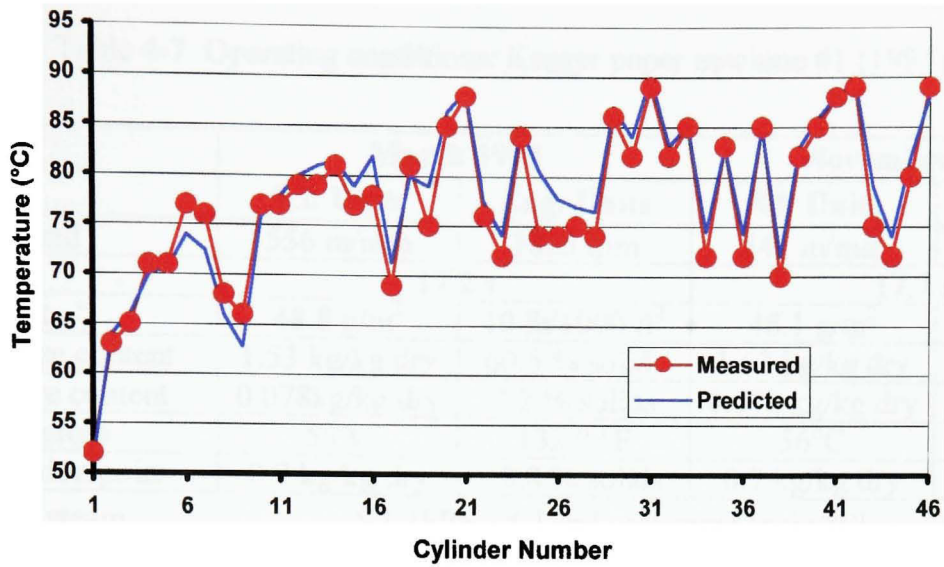


Figure 4-2 Sheet average temperature: Kruger paper machine #1 (April 1988)

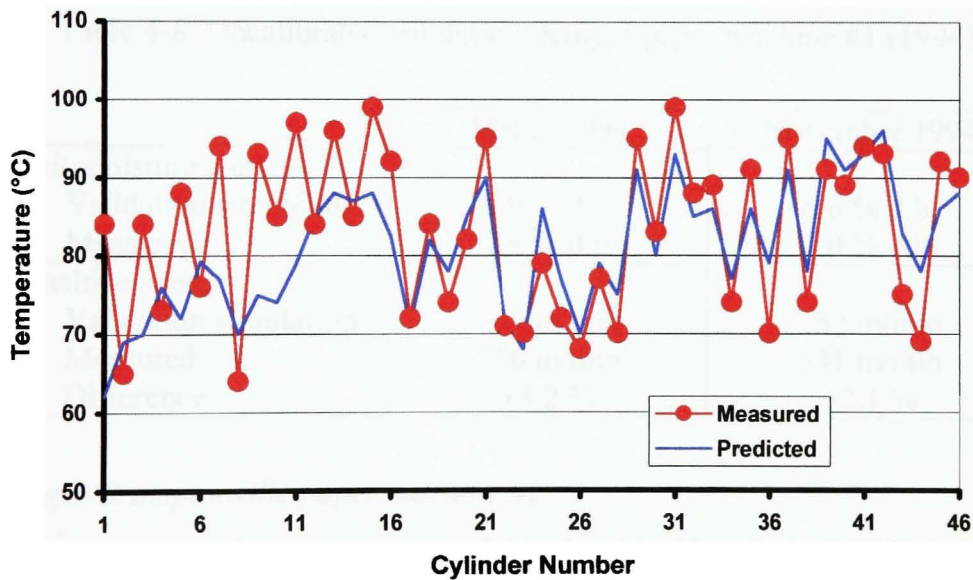


Figure 4-3 Cylinder surface temperature: Kruger paper machine #1 (April 1988)

Two 1994 dryer surveys are also available for this newsprint machine. Table 4-7 records the operating conditions and Table 4-8 demonstrates the highly successful validation of the model as the machine speed prediction errors are only +3.2% and +2.1%.

Table 4-7 Operating conditions: Kruger paper machine #1 (1994)

Variable	March 1994		November 1994	
	S.I. Units	Eng. Units	S.I. Units	Eng. Units
Machine speed	556 m/min	1825 fpm	541 m/min	1776 fpm
Drying time	17.2 s		17.7 s	
Basis weight	48.8 g/m ²	10 lb/1000 ft ²	48.1 g/m ²	10 lb/1000ft
Inlet moisture content	1.53 kg/kg dry	60.5 % solids	1.63 kg/kg dry	62 % solids
Exit moisture content	0.078kg/kg dry	7.2 % solids	0.076 kg/kg dry	7 % solids
Inlet temperature	56°C	132.8 °F	56°C	132.8 °F
Fiber saturation point	0.7 kg/kg dry	58.8 % solids	0.7 kg/kg dry	58.8 %
Condensing steam	S.I. [kPag/°C] and Alternate [psig/°F]			
Section 1 (1-16)	13.8/104°	2/219°	69/115°	10/239°
Section 2 (17-30)	62.1/114°	9/237°	124/124°	18/255°
Sections 3 (31-46)	121/124°	18/255°	166/130°	24/265°
Cylinders turned off	20, 22, 40 & 44		21, 22, 40 & 44	
Pocket conditions	varies-taken from dryer surveys			

Table 4-8 Uncalibrated validation: Kruger paper machine #1 (1994)

	March 1994	November 1994
Exit moisture content		
Validation simulation	6.9 % d.b.	6.6 % d.b.
Measured	7.8 % d.b.	7.0 % d.b.
Machine speed		
Validation simulation	574 m/min	552 m/min
Measured	556 m/min	541 m/min
Difference	+3.2 %	+2.1 %

(a-2) *Kruger Bromptonville paper machine #2*

There are seven dryer surveys available for this 42-cylinder machine with design specifications of Table 4-9. The first 16 cylinders are single felted (unirun), the rest double felted. Operating conditions for six surveys, performed internally by Kruger, are summarized in Table 4-10 and validation simulation results in Table 4-11. For these six validations the average error of machine speed prediction is only +0.8%.

Table 4-9 Design specifications: Kruger paper machine #2

Variable	S.I. Units	Alternate Units
Cylinder diameter	1.52 m	5 ft
Cylinder shell thickness	28.6 mm	1.12 in
Machine width	4 m	13.1 ft
Draw length	0.75 m	2.5 ft
Sheet length in dryer	162 m	531 ft
Felt thickness	1.8 mm	0.07 in
Unirun felted wrap angles	210°	
Double felted felt wrap angle	180°	
Paper wrap angle	240°	
Fiber saturation point	0.7 kg/kg dry	58.8 % solids
Spoiler bars	none	

Table 4-10 Operating conditions: Kruger paper machine #2

Dryer Survey	Condensing Steam [kPag/°C]			Machine Speed m/min	Drying Time s	Basis Weight g/m ²	Inlet Moisture Content kg/kg dry	Exit Moisture Content kg/kg dry
	Cyl. 1-5	Cyl. 6-32	Cyl. 33-42					
June 1992	90/ 119°	350/ 148°	350/ 148°	849	11.4	47.6	1.61	0.073
May 1995	82/ 118°	270/ 141°	275/ 141°	837	11.6	48.08	1.56	0.081
June 1995	84/ 118°	255/ 139°	255/ 139°	839	11.6	49.11	1.56	0.083
August 1 1995	78/ 117°	228/ 137°	282/ 142°	827	11.7	48.25	1.62	0.08
August 9 1995	81/ 117°	235/ 137°	260/ 140°	819	11.9	47.86	1.7	0.079
January 1996	90/ 119°	250/ 139°	250/ 139°	817	11.9	48.9	1.54	0.085

Table 4-11 Uncalibrated validation: Kruger paper machine #2

	June 1992	May 1995	June 1995	August 1 1995	August 9 1995	January 1996
Exit moisture content						
Validation simulation	7.2 %	7.6 %	9.4 %	7.8 %	9.5 %	8.3 %
Measured	7.3 %	8.1 %	8.3 %	8 %	7.9 %	8.5 %
Machine speed [m/min]						
Validation simulation	872	853	828	845	805	824
Measured	849	837	839	827	819	817
Difference	+2.7 %	+1.9 %	-1.3 %	+2.2 %	-1.7 %	+0.8 %

Another dryer survey, by JWI Inc., dates back to August 22, 1995 when the three dryer sections operated at steam pressures of 90, 255 and 275 kPag. The validation simulation results are presented in Table 4-12. This survey also includes measurements of sheet moisture content at several points which are compared with corresponding model predictions in Figure 4.4. As can be seen a change happens in the slope of simulated moisture curve after cylinder 16, i.e. transition from Unirun to double felted sections. In the unirun section the felt is sandwiched between the sheet and cylinder on every other cylinder while in the double felted sections only one side of the felt contacts the heated surface. This distinction between the unirun and double felted sections would affect the heat transfer contact coefficient between the cylinder and sheet, a fact not included in the treatment of felting in the external systems. The sharp change of slope of measured moisture content is related to a moisture control device after cylinder 31. Overall, the model is able to follow the moisture profile in the dryer section and to provide an accurate estimate of the machine speed.

Table 4-12 Uncalibrated validation: Kruger paper machine #2 (August 22, 1995)

	August 22 1995
Exit moisture content	
Validation simulation	8.5 % d.b.
Measured	9.2 % d.b.
Machine speed	
Validation simulation	871 m/min
Measured	861 m/min
Difference	+1.2 %

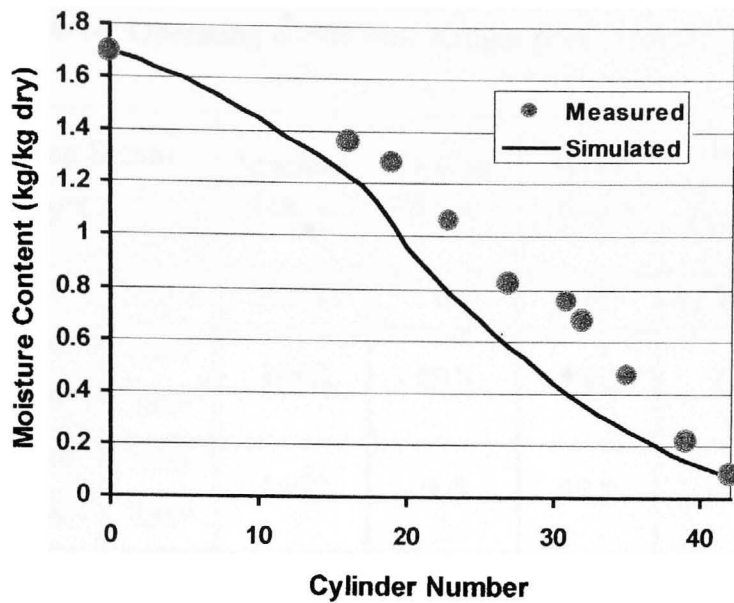


Figure 4-4 Sheet moisture content: Kruger paper machine #2 (August 22, 1995)

(a-3) Kruger Bromptonville paper machine #3

Design specifications for this 46-cylinder machine, with uniron felting on the first 29 cylinders and double felting thereafter, are included in Table 4-13 and operating conditions, according to five dryer surveys available, are given in Table 4-14. Validation simulation results are summarized in Table 4-15. The average error of machine speed prediction for these five surveys is only +0.54%.

Table 4-13 Design specifications: Kruger paper machine #3

Variable	S.I. Units	Alternate Units
Cylinder diameter	1.52 m	5 ft
Cylinder shell thickness	25.4 mm	1 in
Machine width	3.9 m	12.8 ft
Draw length	0.7 m	2.3 ft
Sheet length in dryer	186 m	610 ft
Felt thickness	1.8 mm	0.07 in
Uniron felted wrap angles	255°	
Double felted felt wrap angle	180°	
Paper wrap angle	250°	
Fiber saturation point	0.7 kg/kg dry	58.8 % solids
Spoiler bars-profiling	16, 18, 20, 22, 24, 26, 28, 29, 31, 33, 35, 37	
Spoiler bars-full-width	39, 41, 43	

Table 4-14 Operating conditions: Kruger paper machine #3

Dryer Survey	Condensing Steam [kPag/°C]			Machine Speed	Drying Time	Basis Weight	Inlet Moisture Content	Exit Moisture Content
	Sect.2	Sect.3	Sect.4	m/min	s	g/m ²	kg/kg dry	kg/kg dry
June 1992	270/ 141°	360/ 149°	320/ 145°	1080	10.3	48.2	1.33	0.085
Feb. 1995	230/ 137°	350/ 148°	390/ 151°	1160	9.6	48.2	1.173	0.105
April 1995	170/ 130°	260/ 140°	292/ 143°	1130	9.9	49	1.15	0.112
August 1995	200/ 134°	300/ 144°	251/ 139°	1130	9.9	49.2	1.2	0.099
Nov. 1995	190/ 133°	320/ 145°	251/ 139°	1133	9.9	48.4	1.227	0.10

Table 4-15 Uncalibrated validation: Kruger paper machine #3

	June 1992	February 1995	April 1995	August 1995	November 1995
Exit moisture content					
Validation simulation	9.2 %	8.4 %	10.5 %	11.2 %	10.5 %
Measured	8.5 %	10.5 %	11.2 %	9.9 %	10 %
Machine speed [m/min]					
Validation simulation	1059	1234	1154	1102	1117
Measured	1080	1160	1130	1130	1133
Difference	-1.9 %	+6.4 %	+2.1 %	-2.5 %	-1.4 %

A detailed study dated March 1995, when there was no steam to cylinders 1,3,5,7,9,11,13,15,17,19,30,32 and 34, includes the measurements of sheet and cylinder surface temperature for all cylinders which are compared to the corresponding model predictions in Figures 4-5 and 4-6. It is again observed that the model is able to predict the evolution of sheet and cylinder surface temperature reasonably closely, although compared to the case of Kruger paper machine #1, section a-1, larger differences are

observed. The average difference observed between the measured and simulated temperatures is -3°C , a considerable improvement over the difference of -12°C reported by the first McGill dryer simulator for this case. In both figures larger deviations are observed for cylinders with unironed felting, when the felt comes between the sheet and heated surface on every other cylinder. As explained in section a-2 this configuration will affect the heat transfer between the sheet and cylinder in a way that is not properly predicted by the current treatment of external systems.

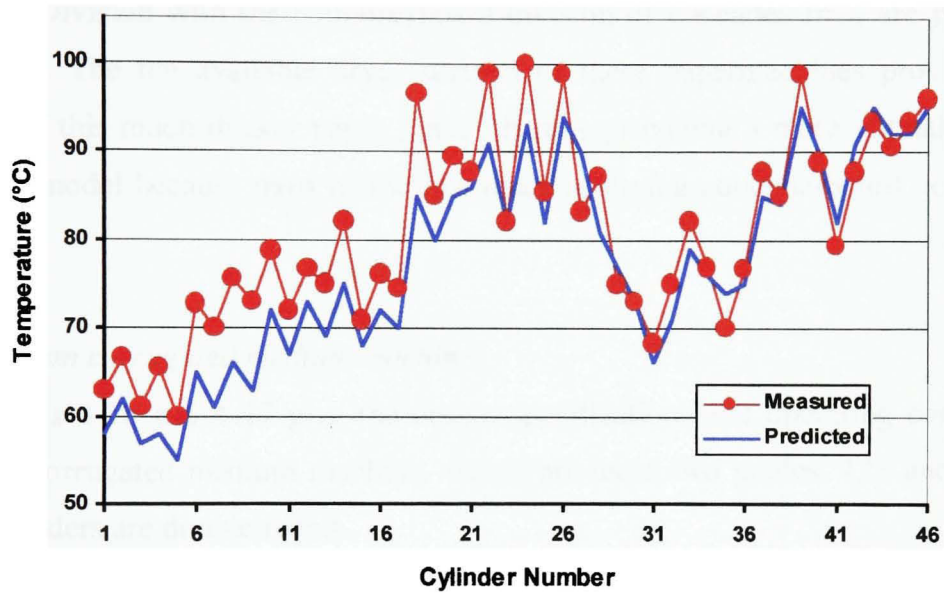


Figure 4-5 Sheet average temperature: Kruger paper machine #3 (March 1995)

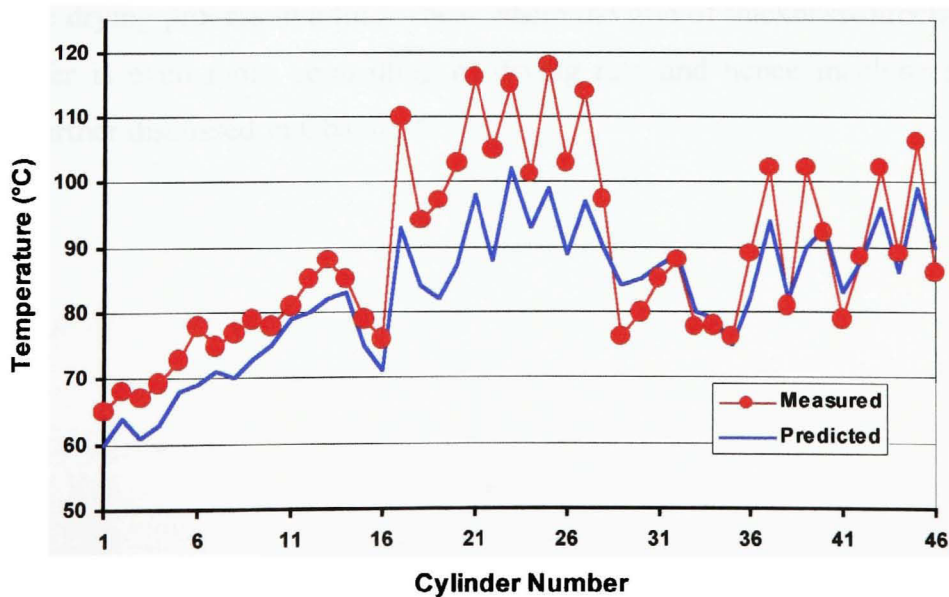


Figure 4-6 Cylinder surface temperature: Kruger paper machine #3 (March 1995)

The improvement in sheet temperature prediction is particularly important because in the latter stage of drying the sheet properties are being developed. The present model provides a close prediction while the first McGill dryer simulator showed considerable under-prediction of sheet temperature in this important region.

(b) Containerboard machines

Four paper machines of Norampac Inc., formed from the merger of Domtar Packaging Division with the containerboard division of Cascades Inc., are presented in this section. The ten available dryer surveys of these papermachines provide a good coverage of this much thicker paper grade, thereby providing a more critical test of the simulation model because most of the resistance to drying containerboard occurs within the sheet.

(b-1) Trenton corrugated medium machine

Tables 4-16 and 4-17 give the design specifications and operating conditions for this 3-ply corrugated medium machine, which produces two grades, 127 and 161 g/m². All 51 cylinders are double felted.

Simulation results are summarized in Table 4-18. The small values of machine speed prediction error demonstrate the capability of the present microscale model to simulate the drying process in a thick sheet where the role of thickness-direction heat and mass transfer is even more controlling of drying rate and hence machine speed. This subject is further discussed in Chapter 5.

Table 4-16 Design specifications: Trenton corrugated medium machine

Variables	S.I. Units	Alternate Units
Cylinder diameter	1.524 m	5 ft
Cylinder shell thickness	30.2 mm	1.2 inch
Machine trim	4.6 m	15.1 ft
Draw length	0.99 m	3.25 ft
Sheet wrap angle	230°	
Felt wrap angle	182°	
Felt thickness	2 mm	0.08 inch
Sheet length in dryer	211.5 m	693.9 ft
Spoiler bars (full-width)	Cylinders 1-51 (all)	

Table 4-17 Operating conditions: Trenton corrugated medium machine

Variable	127 g/m ²		161 g/m ²	
	S.I. Units	Alternate Units	S.I. Units	Alternate Units
Machine speed	686 m/min	2250 fpm	496 m/min	1627 fpm
Drying time	18.5 s		25.6 s	
Dry sheet caliper	250 microns		300 microns	
Sheet inlet moisture	1.44 kg/kg dry	41% solids	1.44 kg/kg dry	41% solids
Sheet exit moisture	0.08 kg/kg dry	92.6% solids	0.08 kg/kg dry	92.6% solids
Sheet inlet temp.	60°C	140°F	60°C	140°F
Fiber saturation point	0.8 kg/kg dry	55.6 % solids	0.8 kg/kg dry	55.6 % solids
Condensing Steam	S.I. [kPag/°C] and Alternate [psig/°F]			
Section 1 (1-6)	500/159°	72.5/318°	500/159°	72.5/318°
Section 2 (7-20)	550/162°	80/324°	550/162°	80/324°
Section 3 (21-34)	690/170°	100/338°	650/168°	94/334°
Section 4 (35-51)	800/175°	116/348°	700/170°	102/339°

Table 4-18 Uncalibrated validation: Trenton corrugated medium machine

	127 g/m ²	161 g/m ²
Exit moisture content		
Validation simulation	8.4 % d.b.	7.1 % d.b.
Measured	8.0 % d.b.	8.0 % d.b.
Machine speed		
Validation simulation	678 m/min	506 m/min
Measured	686 m/min	496 m/min
Difference	-1.1 %	+2.1 %

(b-2) *Mississauga linerboard machine*

The Mississauga 5-ply linerboard machine, Table 4-19, produces two grades, 183 and 205 g/m². Tables 4-20 and 4-21 give the operating conditions recorded in the dryer surveys. The first 11 cylinders are top felted, the remaining 44 cylinders being double felted.

Table 4-19 Design specifications: Mississauga linerboard machine

Variables	S.I. Units	Alternate Units
Cylinder diameter	1.524 m	5 ft
Cylinder shell thickness	30.2 mm	1.2 inch
Machine trim	4 m	13.1 ft
Draw length	0.9 m	2.95 ft
Sheet wrap angle	226°	
Felt wrap angle	182°	
Felt thickness	1.8 mm	0.07 inch
Sheet length in dryer	243.3 m	768.7 ft
Spoiler bars	none	

Table 4-20 Operating conditions: Mississauga linerboard machine

Variable	183 g/m ²		205 g/m ²	
	S.I. Units	Alternate Units	S.I. Units	Alternate Units
Machine speed	377 m/min	1237 fpm	391 m/min	1283 fpm
Drying time	38.2 s		37.3 s	
Dry sheet caliper	255 microns		290 microns	
Sheet inlet moisture	1.13 kg/kg dry	47% solids	1.13 kg/kg dry	47% solids
Sheet exit moisture	0.055 kg/kg dry	94.8% solids	0.055 kg/kg dry	94.8% solids
Sheet inlet temp.	40°C	104°F	40°C	104°F
Fiber saturation point	0.8 kg/kg dry	55.6 % solids	0.8 kg/kg dry	55.6 % solids
Condensing Steam	S.I. [kPag/°C] and Alternate [psig/°F]			
Section 1 (1-11)	335/147°	48.6/296°	573/163°	83.1/326°
Section 2 (12-27)	381/150°	55.2/303°	674/169°	97.8/336°
Section 3 (28-43)	405/152°	58.7/306°	496/159°	71.9/318°
Section 4 (44-55)	394/151°	57.1/305°	685/170°	99.4/337°

Table 4-21 Pocket conditions: Mississauga linerboard machine

Variable	Temperature		Humidity
	°C	°F	kg/kg dry air
Section 1	50.5	123	0.06
Section 2	53	127	0.07
Section 3	54.4	130	0.06
Section 4	53.3	128	0.06

The validation results presented in Table 4-22 again show machine speed prediction errors which are very small, demonstrating the excellent performance of the model.

Table 4-22 Uncalibrated validation: Mississauga linerboard machine

	183 g/m ²	205 g/m ²
Exit moisture content		
Validation simulation	5.3 % d.b.	5.3 % d.b.
Measured	5.5 % d.b.	5.5 % d.b.
Machine speed		
Validation simulation	382 m/min	394 m/min
Measured	377 m/min	391 m/min
Difference	+1.4 %	+0.8 %

(b-3) Red Rock linerboard machine #1

This 48-cylinder machine, Table 4-23, produces two linerboard grades with operating conditions according to Tables 4-24 and 4-25. Simulation results are listed in Table 4-26.

Table 4-23 Design specifications: Red Rock linerboard machine #1

Variables	S.I. Units	Alternate Units
Cylinder diameter	1.524 m	5 ft
Cylinder shell thickness (Cyl.1-12/13-48)	27/30 mm	1.1/1.2 inch
Machine trim	5.64 m	18.5 ft
Draw length	1.6 m	5.2 ft
Sheet wrap angle	220°	
Felt wrap angle	182°	
Felt thickness	1.8 mm	0.07 inch
Sheet length in dryer	217 m	712 ft
Spoiler bars	none	

Table 4-24 Operating conditions: Red Rock linerboard machine #1

Variable	127 g/m ²		161 g/m ²	
	S.I. Units	Alt. Units	S.I. Units	Alt. Units
Machine speed	497 m/min	1631 fpm	358 m/min	1175 fpm
Drying time	26.2 s		36.4 s	
Dry sheet caliper	215 microns		271 microns	
Sheet inlet moisture	1.94 kg/kg dry	34 % solids	1.94 kg/kg dry	34 % solids
Sheet exit moisture	0.07 kg/kg dry	93.5 % solids	0.07 kg/kg dry	93.5 % solids
Sheet inlet temperature	45°C	113°F	45°C	113°F
Fiber saturation point	0.8 kg/kg dry	55.6 % solids	0.8 kg/kg dry	55.6 % solids
Condensing Steam	S.I. [kPag/°C] and Alternate [psig/°F]			
Section 1 (1-4)	150/128°	22/262°	150/128°	22/262°
Section 2 (5-12)	200/134°	29/273°	200/134°	29/273°
Section 3 (13-36)	900/180°	131/356°	900/180°	131/356°
Section 4 (37-48)	1000/184°	145/363°	1000/184°	145/363°

Table 4-25 Pocket conditions: Red Rock linerboard machine #1

Variable	Temperature		Humidity
	°C	°F	kg/kg dry air
Cylinder 1	60	140	0.1
Cylinders 2-12	60	140	0.15
Cylinders 13-48	68	155	0.2

Table 4-26 Uncalibrated validation: Red Rock linerboard machine #1

	127 g/m ²	161 g/m ²
Exit moisture content		
Validation simulation	6.0 % d.b.	5.7 % d.b.
Measured	7.0 % d.b.	7.0 % d.b.
Machine speed		
Validation simulation	506 m/min	384 m/min
Measured	497 m/min	358 m/min
Difference	1.9 %	7.4 %

Another dryer survey available for this machine dates back to February 1997 when 118 g/m² sack paper was in production, Table 4-27. Simulation results are presented in Table 4-28.

Table 4-27 Operating conditions: Red Rock linerboard machine #1, Sack paper

Variable	118 g/m ²	
	S.I. Units	Alternate Units
Machine speed	365 m/min	1196 fpm
Drying time	35.6 s	
Dry sheet caliper	200 microns	
Sheet inlet moisture	1.85 kg/kg dry	35 % solids
Sheet exit moisture	0.072 kg/kg dry	93.3 % solids
Sheet inlet temperature	45°C	113°F
Fiber saturation point	0.8 kg/kg dry	55.6 % solids
Condensing Steam	S.I. [kPag/°C] and Alternate [psig/°F]	
Section 1	131/125°	19/257°
Section 2	172/130°	25/267°
Section 3	427/154°	62/309°
Section 4	400/152°	58/305°

Table 4-28 Uncalibrated validation: Red Rock linerboard machine #1, Sack paper

Exit moisture content	
Validation simulation	5.6 % d.b.
Measured	7.2 % d.b.
Machine speed	
Validation simulation	395 m/min
Measured	365 m/min
Difference	+8.1 %

The average error of machine speed prediction for the three dryer surveys of this linerboard machine is 5.8%, larger than those observed for previous cases but still acceptable considering the complexities of the drying process. For the case of 118 g/m² sack paper, at the time of survey the steam was shut off from three cylinders (1, 35 and 36) and a moisture profiler was used occasionally between cylinders 35 and 36. With the amount of profile water spray unknown, this addition of water to the sheet could not be allowed for in the simulation and would account for an unknown fraction of the over-prediction error of 8.1%.

(b-4) Red Rock linerboard machine #2

This very large 85-cylinder machine, Table 4-29, produces three grades of linerboard, 183, 205 and 337 g/m² as detailed in Tables 4-30 and 4-31. There are 36 unfelted cylinders present, a notable distinction for this paper machine.

Table 4-29 Design specifications: Red Rock linerboard machine #2

Variables	S.I. Units	Alternate Units
Cylinder diameter	1.524 m	5 ft
Cylinder shell thickness (Cyl.1-71)	27 mm	1.1 inch
Cylinder shell thickness (Cyl.72-85)	30 mm	1.2 inch
Machine trim	5.73 m	19 ft
Draw length	1.35 m	4.4 ft
Sheet wrap angle	220°	
Felt wrap angle	180°	
Felt thickness	1.8 mm	0.07 inch
Sheet length in dryer	343 m	1125 ft
Spoiler bars	none	

Table 4-30 Operating conditions: Red Rock linerboard machine #2

Variable	183 g/m ²		205 g/m ²		337 g/m ²	
	S.I. Units	Alternate	S.I. Units	Alternate	S.I. Units	Alternate
Machine speed	564 m/min	1850 fpm	558 m/min	1830 fpm	372 m/min	1220 fpm
Drying time	36.5 s		36.9 s		55.3 s	
Dry sheet caliper	258 microns		295 microns		475 microns	
Sheet inlet moisture	1.22 kg/kg dry	45 % solids	1.22 kg/kg dry	45 % solids	1.22 kg/kg dry	45 % solids
Sheet exit moisture	0.06 kg/kg dry	94.3 % solids	0.065 kg/kg dry	93.9 % solids	0.07 kg/kg dry	93.5 % solids
Sheet inlet temperature	45°C	113°F	45°C	113°F	45°C	113°F
Fiber satn. point	0.8 kg/kg dry	55.6 % solids	0.8 kg/kg dry	55.6 % solids	0.8 kg/kg dry	55.6 % solids
Condensing Steam S.I. [kPag/°C] and Alternate [psig/°F]						
Section 1	550/162°	80/324°	662/168°	96/335°	758/173°	110/344°
Section 2	650/168°	94/334°	738/172°	107/342°	758/173°	110/344°
Section 3	700/170°	101/339°	814/176°	118/349°	814/176°	118/349°
Section 4	725/172°	105/341°	750 /173°	109/343°	786/174°	114/345°
Section 5	800/175°	116/348°	800/175°	116/348°	800/175°	116/348°

Table 4-31 Pocket conditions: Red Rock linerboard machine #2

Variable	Temperature		Humidity	Relative Humidity	Wet Bulb Temperature
	°C	°F	kg/kg dry air	%	°C
Cylinders 1-18	55	130	0.11	97	54
Cylinders 19-85	38	100	0.04	92	37

Simulation results of Table 4-32 show an average machine speed prediction error of 9.7% with the two cases of 183 g/m² and 205 g/m² paper having the largest errors among all the 32 industrial validations. Since the simulation model was able to provide very acceptable results for other linerboard machines discussed in this section, including what would be the most difficult case to simulate, that for the 337 g/m² grade, it is possible that the large errors for the other two cases are more an anomaly resulting, especially for the 183 g/m² case, from measurement errors in the dryer surveys. Since this dryer section is almost twice as long as a typical 40-50 cylinder machine, one might expect to see higher simulation errors due to the accumulative nature of prediction error. That the error for the 337 g/m² paper was only 1.2% supports the possibility that the very large error for the 183 g/m² case is the result of dryer survey measurement error and not the systematic error of the model.

Table 4-32 Uncalibrated validation: Red Rock linerboard machine #2

	183 g/m ²	205 g/m ²	337 g/m ²
Exit moisture content			
Validation simulation	2.9 % d.b.	4.2 % d.b.	6.5 % d.b.
Measured	6.0 % d.b.	6.5 % d.b.	7.0 % d.b.
Machine speed			
Validation simulation	662 m/min	617 m/min	376 m/min
Measured	564 m/min	558 m/min	372 m/min
Difference	+17.3 %	+10.6 %	+1.2 %

(c) *Fine paper*

A 1999 dryer survey of the Weyerhaeuser Canada Ltd. fine paper machine in Prince Albert is the basis for this validation test. The main dryer section before the size press has an exit moisture content of only 1% so as to eliminate the moisture nonuniformity which

would have a negative effect on the cross-machine direction (CD) uniformity of sizing. The paper then passes through a size press where it picks up starch and moisture. There is a second dryer section after the size press but the present validation deals only with the main dryer section of 41 cylinders, all double felted, which provides the more critical validation test because of the exceptionally low exit moisture content. The design specifications and operating conditions are presented in Tables 4-33 and 4-34, respectively. Cylinders 1,2,3,4,6,8 were closed to steam at the time of survey.

Table 4-33 Design specifications: Weyerhaeuser fine paper machine

Variables	S.I. Units	Alternate Units
Cylinder diameter	1.83 m	6 ft
Cylinder shell thickness	25 mm	0.98 inch
Machine trim	0.8 m	2.65 ft
Draw length	varies-taken from dryer survey	
Sheet wrap angle	80° to 230°	
Felt wrap angle	100° to 190°	
Felt thickness	2 mm	0.08 inch
Sheet length in dryer	193m	633ft
Spoiler bars	none	

Table 4-34 Operating conditions: Weyerhaeuser fine paper

Variable	S.I. Units	Alternate Units
Machine speed	885 m/min	2902 fpm
Drying time	13.1s	
Basis weight	71.5 g/m ²	14.6 lb/1000 ft ²
Inlet moisture content	0.72 kg/kg dry	58 % solids
Exit moisture content	0.01 kg/kg dry	99 % solids
Sheet inlet temperature	45°C	113°F
Fiber saturation point	1.44 kg/kg dry	41 % solids
Section 1	9 cylinders (1-9)	
Condensing steam	-35.0 kPag/88.3°C	-5.1 psig/191°F
Section 2	6 cylinders (10-15)	
Condensing steam	148.0 kPag/127.2°C	21.5 psig/261°F
Sections 3	10 cylinders (16-25)	
Condensing steam	312.0 kPag/145°C	45.3 psig/293°F
Sections 4	16 cylinders (26-41)	
Condensing steam	362.0 kPag/149°C	52.5 psig/300°F
Pocket conditions	varies-taken from dryer survey	

The simulation results of Table 4-35 demonstrate an under-prediction of drying by 8.3%. This machine speed prediction error is significantly larger than the average error for the other cylinder dryer sections presented. However this case is distinguished by the extremely low exit moisture content. When the moisture content falls below the fiber saturation point there is no longer free water in the pores and, as moisture content decreases further, its vapor pressure correspondingly decreases from that of free water and the heat required for evaporation increases. These two effects reduce water vapor transport and reduce the evaporation rate, leading to extremely low drying rates as the moisture content approaches the very low level of 1%. If a model lacks the complete description of transport in gas phase (shown in Chapter 5 to be dominant at the later stages of drying) or the effect of hygroscopic region on drying dynamics, then prediction of water removal for a case such as this paper machine becomes problematic.

This difficulty was observed for the first McGill dryer simulator which, exceptionally, was unable to run a speed prediction simulation for the very low final moisture content case of Tables 4-33 and 4-34. As heat of sorption, vapor pressure reduction and paper thermal conductivity are all quite sensitive to moisture content in the range from 5% down to the 1% of the present case, these are the properties most involved in the speed prediction validation for the pre-size press section of this fine paper machine. Therefore a small error in the reported final moisture content would have a big effect on the speed prediction error. Considering the resolution of moisture sensors used in the industry, the reported 1% exit moisture content is subject to a potentially significant error. With these considerations, the acceptable speed prediction error of the model for this particularly difficult case is a further demonstration of the importance in a paper drying simulator of a comprehensive treatment of sheet internal transport phenomena. This finding also intensifies the need in future of more accurate determination of key transport properties in the very low moisture range when there can be a substantial effect on transport and thermodynamic properties from hydrogen bonding of water.

Table 4-35 Uncalibrated validation: Weyerhaeuser fine paper

Exit moisture content	
Validation simulation	3 % d.b.
Measured	1 % d.b.
Machine speed	
Validation simulation	812 m/min
Measured	885 m/min
Difference	-8.3 %

4.3.3 Air impingement drying

In production of the lightest grades of paper, tissue and toweling, air impingement drying, termed a “Yankee dryer”, is employed (Chapter 1). Now three dryer surveys taken from two tissue machines are used to validate the simulation model. In addition, model predictions are compared with experimental results of laboratory impingement drying of linerboard, consisting of internal thickness direction moisture content and temperature profiles during drying.

(a) Perkins tissue machine

A visit to Perkins Paper Ltd. provided the design specifications and 1989 operating conditions for a Yankee dryer producing tissue, Table 4-36. The simulation results, compared to the measured values in Table 4-37, demonstrate the excellent agreement with only 0.7% error in machine speed prediction. This validation shows that the present model is able to simulate the impingement drying under high intensity drying conditions of a very light grade, as well as the cylinder drying under far lower drying intensity of the much heavier grades of newsprint and containerboard documented in section 4.3.1.

Table 4-36 Design specifications and operating conditions: Perkins tissue machine

Variable	S.I. Units	Alternate Units
Machine width	3.33 m	10.9 ft
Cylinder diameter	3.66 m	12 ft
Cylinder shell thickness	24 mm	0.94 in
Nozzle diameter	7.9 mm	0.31 in
Nozzle to web distance	20 mm	0.78 in
Nozzle spacing/nozzle diameter	2.5	
Nozzle plate open area ratio	2 %	
Nozzle pattern	equilateral triangular	
Hood and paper wrap angle	260°	
Draw after Yankee	1.0 m	3.3 ft
Sheet length in dryer	9.3 m	30.5 ft
Machine speed	1038 m/min	3400 fpm
Drying time on cylinder	0.54 s	
Condensing steam	600 kPag/165°C	87 psig/329°F
Jet temperature	454°C	850°F
Jet velocity	112 m/s	22,000 fpm
Jet humidity	0.2 kg/kg dry air	
Basis weight	19 g/m ²	3.9 lb/1000 ft ²
Sheet inlet moisture	1.50 kg/kg dry	40 % solids
Sheet exit moisture	0.064 kg/kg dry	94 % solids
Sheet inlet temperature	40°C	104°F
Dry sheet caliper	50 microns	
Fiber saturation point	0.7 kg/kg dry	59 % solids

Table 4-37 Uncalibrated validation: Perkins tissue machine

Exit moisture content	
Validation simulation	6.3 % d.b.
Measured	6.4 % d.b.
Machine speed	
Validation simulation	1045 m/min
Measured	1038 m/min
Difference	+0.7 %

(b) Scott paper machine

A tissue-toweling machine of Scott Paper Co. consists of a Yankee dryer with the design specifications of Table 4-38. The operating conditions are included in Table 4-39 for two grades, 14 g/m² tissue and 21.1 g/m² toweling. All data are taken from a 1992

dryer survey. This dryer differs from that of Perkins, section (a), in having 20° of paper-cylinder wrap outside of the hood on both sides.

Table 4-38 Design specifications: Scott tissue machine

Variable	S.I. Units	Alternate Units
Machine width	3.68 m	12.1 ft
Cylinder diameter	3.66 m	12 ft
Cylinder shell thickness	24 mm	0.94 in
Nozzle diameter	9.5 mm	3/8 in
Nozzle to web distance	19 mm	3/4 in
Nozzle spacing/nozzle diameter	2.0	
Nozzle plate open area ratio	2.5 %	
Nozzle pattern	equilateral triangular	
Wrap angle before and after hood	20°	
Wrap angle inside hood	230°	
Draw after Yankee	1.0 m	3.3 ft
Sheet length in dryer	9.6 m	31.6 ft

Table 4-39 Operating conditions: Scott paper machine

Variable	21.1 g/m ²		14 g/m ²	
	S.I. Units	Alternate Units	S.I. Units	Alternate Units
Machine speed	924 m/min	3033 fpm	1218 m/min	4000 fpm
Drying time	0.62 s		0.47 s	
Condensing steam	613 kPag/166°C	88 psig/330°F	634 kPag/167°C	92 psig/332°F
Jet temperature	346°C	654°F	400°C	750°F
Jet velocity	125 m/s	24,600 fpm	91.5 m/s	18,000 fpm
Jet humidity	0.1 kg/kg dry air		0.1 kg/kg dry air	
Sheet inlet moisture	1.22 kg/kg dry	45 % solids	1.50 kg/kg dry	40 % solids
Sheet exit moisture	0.058 kg/kg dry	94.5 % solids	0.053 kg/kg dry	95 % solids
Sheet inlet temperature	90°C	194°F	90°C	194°F
Dry sheet caliper	60 microns		45 microns	
Fiber saturation point	0.7 kg/kg dry	58 % solids	0.7 kg/kg dry	58 % solids

The simulation results are summarized in Table 4-40, demonstrating again the very good performance of the model for the high intensity drying of light weight tissue, down

to 14 g/m², with drying time to less than 0.5 s in Yankee dryers. These conditions contrast greatly with the case tested previously of 337 g/m² linerboard dried in an enormous 85 cylinder dryer section for which the drying time was about 100 times longer, at 55 s.

Table 4-40 Uncalibrated validation: Scott paper machine

Basis Weight	21.1 g/m ²	14 g/m ²
Exit moisture content		
Validation simulation	5.5 % d.b.	5.8 % d.b.
Measured	5.8 % d.b.	5.3 % d.b.
Machine speed		
Validation simulation	945 m/min	1174 m/min
Measured	924 m/min	1218 m/min
Difference	+2.3 %	-3.6 %

The dryer survey for the 21.1 g/m² grade also included other measurements for testing the model predictions. The sheet average moisture content was determined not only at the entry and exit of the dryer section but also at the mid-point of the hood. The moisture content at the mid-point of the dryer, taken with a special sampling device, was determined gravimetrically to be 0.52 kg/kg dry. The model developed in this study predicts a moisture content of 51.2% d.b. at this location, which matches the measured value extremely well and confirms the model ability to predict the progress of drying. The average drying rates for the wet and dry halves of the hood, also reported, are compared with model predictions in Table 4-41. Again the model predictions are very close to the measured values. There is a significant change in relative importance of the various drying mechanisms between the wet end of the dryer, where there is a substantial amount of water in the pores, to the dry end where there is no water in the pores and the sorbed water present exerts a reduced vapor pressure and requires an additional differential heat of sorption to evaporate. It would be possible for a model to predict the overall drying rate satisfactorily through compensating errors in the model between these limiting conditions. Thus the good prediction independently for wet and dry halves of this dryer provides evidence that the model adequately allows for the elements which are dominant for wet paper as well as for the nearly dry sheet.

Table 4-41 Drying rates: Scott paper machine, 21.1 g/m²

Average Drying Rate	Wet End	Dry End
Measured	190 kg/m ² h	144 kg/m ² h
Simulated	190 kg/m ² h	143 kg/m ² h

(c) *Experimental results*

The experimental results used here were carried out by Bond and Douglas (1997) for air and superheated steam impingement drying of linerboard. A three-ply sheet with the basis weight of 430 g/m² was used and the complete drying history was studied by measuring temperatures continuously at the sheet surfaces and the two internal ply boundaries, as well as by gravimetric determination of the moisture content of each ply. The sheet was supported on an unheated base plate, corresponding to a Yankee dryer with zero condensing steam pressure. The design specifications and the experimental conditions for air impingement operation are given in Tables 4-42 and 4-43.

Table 4-42 Design specifications: Laboratory impingement dryer

Variable	S.I. Units	English Units
Nozzle diameter	6.35 mm	0.25 in
Nozzle to web distance	23 mm	0.9 in
Nozzle spacing/nozzle diameter	3.6	
Nozzle plate open area ratio	4.1 %	
Nozzle pattern	equilateral triangular	

Table 4-43 Experimental conditions: Laboratory impingement dryer

Variable	430 g/m ²	
	S.I. Units	Alternate
Jet temperature	400°C	750°F
Jet Reynolds number	2000	
Basis weight	430 g/m ²	88.3 lb/1000 ft ²
Sheet inlet moisture	1.5 kg/kg dry	40 % solids
Sheet inlet temperature	35°C	95°F
Dry sheet caliper	1260 microns	
Fiber saturation point	0.8 kg/kg dry	55.5 % solids

The evolution of moisture content and temperature are shown in Figures 4-7 and 4-8, respectively. The values of moisture content are local average, i.e. measured for each ply. The bottom ply on the graph is the one adjacent to the unheated plate. Temperatures, on the other hand, are local point values measured at the two external surfaces and at the two one-third positions within the sheet.

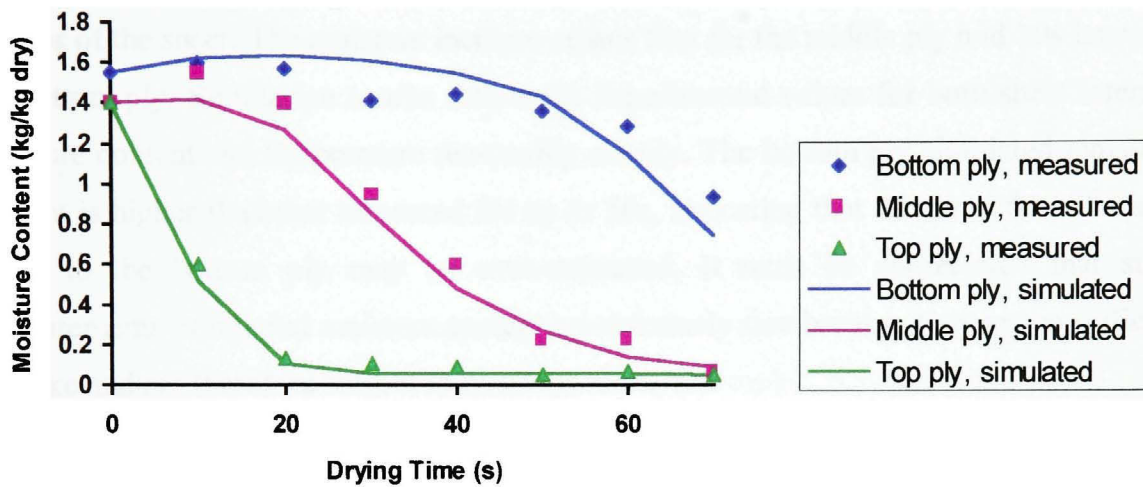


Figure 4-7 Evolution of moisture content for laboratory impingement dryer

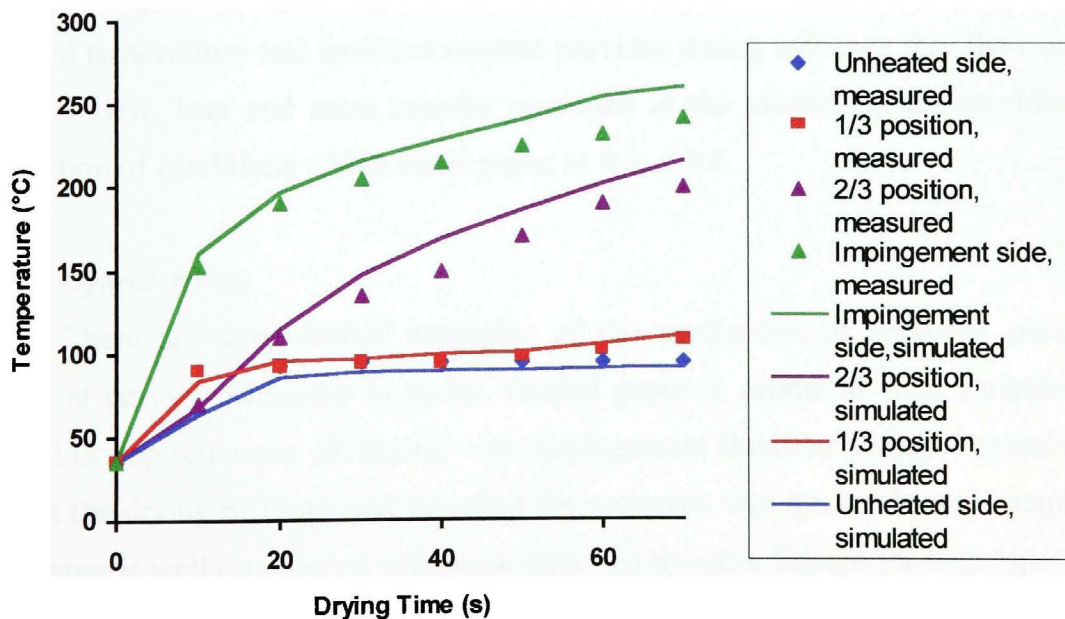


Figure 4-8 Evolution of temperature for laboratory impingement dryer

The experimental results show the temperature at the impingement side rising quickly, resulting in moisture content dropping in about 20s to its final value. The middle and bottom plies do not follow this trend as there is initially a slight increase in moisture content for both plies. As the temperature at these plies is much lower than that of the impingement side, the moisture increase in the cooler plies is due to condensation of the water vapor generated at the impingement side which has been transported back into the interior of the sheet. The moisture increase ceases first for the middle ply and 10s later for the bottom ply. Simulation results follow the experimental values for both sheet internal moisture content and temperature reasonably closely. The bottom ply simulated moisture content is higher than that measured for up to 50s, indicating that the mass flux of water vapor to the bottom ply may be over-estimated. It must be appreciated that such measurements of internal moisture content are extremely rare because they are so difficult to make and are therefore subject to measurement error.

These experiments provide unique measurements for the evolution of sheet moisture and temperature conditions as drying proceeds under high intensity air impingement conditions. Such internal sheet conditions are impossible to determine in an industrial dryer. The good agreement between measured and predicted values of sheet internal temperature and moisture content provides strong evidence that the treatment of internal flow, heat and mass transfer processes in the present model provides reliable prediction of conditions within moist paper as it is dried.

4.3.4 Hybrid drying

There are very limited examples of the production of uncoated papers using different drying techniques in series. Coated paper is produced with variations of the hybrid drying sequence: IR drying – air impingement flotation drying – cylinder drying, and in the drying of tissue and toweling the sequence through air drying – impingement air drying is well established with some paper companies. Except for these special cases, multiple technique or hybrid drying is rarely found in the major grades of largest tonnage production. Dryer surveys for two paper machines with hybrid dryer sections consisting of cylinder drying and air impingement drying in series are now used to test the capabilities of the present model for simulating this challenging category.

(a) Canadian International Paper

A 1961 dryer survey of paper machine #4 at the then Canadian International Paper Co. (now Bowater Inc.) is the basis for this validation test. Design specifications and operating conditions are given in Table 4-44. The dryer section consisted of 43 double-tier dryer cylinders, 10 with air impingement dryers. Three sectioned impingement air dryers (SIAD units) on the top tier cylinders were partitioned in the cross-machine direction (CD) for minimizing moisture profile nonuniformity in the CD direction while three unsectioned impingement air dryer (IAD) units were installed on five lower tier cylinders. As the felting arrangement was not fully described in the report a 180° wrap angle for both paper and felt was assumed.

The simulation results are summarized in Table 4-45. It is highly significant that there is only 1.2% difference between predicted and actual machine speed, demonstrating the model capability in simulation the operations of a complex, hybrid dryer section.

Table 4-44 Design specifications and operating conditions: Canadian International Paper

Variable		S.I. Units	Alternate Units
Machine speed		274 m/min	90 fpm
Drying time		34.2 s	
Basis weight		127 g/m ²	26 lb/100 ft ²
Inlet moisture content		1.941 kg/kg dry	34 % solids
Final moisture content		0.053 kg/kg dry	95 % solids
Fiber saturation point		0.8 kg/kg dry	55.5 % solids
Cylinder diameter		1.52 m	5 ft
Cylinder shell thickness		40 mm	1.6 in
Machine width		4.1 m	13.4 ft
Draw length		1 m	3.3 ft
Sheet length in dryer		156 m	512 ft
Felt thickness		3 mm	0.12 in
Felted and paper wrap angle		180°	
Condensing steam	Section 1 (Cyl. 1-11)	276 kPag/142°C	40 psig/287°F
	Section 2 (Cyl. 12-21)	290 kPag/143°C	42 psig/289°F
	Section 3 (Cyl. 22-37)	228 kPag/137°C	33 psig/278°F
	Section 4 (Cyl. 38-43)	386 kPag/151°C	56 psig/304°F
Nozzle exit jet velocity		69 m/s	13,600 fpm
Nozzle exit temperature	SIAD-1	288°C	550°F
	SIAD-2	278°C	533°F
	SIAD-3	238°C	461°F
	IAD-1	263°C	505°F
	IAD-2	257°C	495°C
	IAD-3	238°C	461°F
Nozzle diameter		9 mm	0.35 in
Nozzle to web distance		20 mm	0.8 in
Nozzle spacing/nozzle diameter		2.2	
Nozzle plate open area ratio		1.5%	
Nozzle pattern		equilateral triangle	

Table 4-45 Uncalibrated validation: Canadian International Paper

Exit moisture content	
Validation simulation	5.2 % d.b.
Measured	5.3 % d.b.
Machine speed	
Validation simulation	277 m/min
Measured	274 m/min
Difference	+1.2 %

(b) *Tembec Inc.*

This paper machine in Temiscaming, Quebec produces a high quality grade of linerboard used for printed products. The dryer section, Table 4-46, includes a Yankee dryer between cylinders 41 and 42, and thereby constitutes a hybrid dryer. There are five sections with the Yankee dryer located between the fourth and the fifth. Unirun felting is applied to the first two sections, double felting to the remainder. For the operating conditions according to two surveys given in Table 4-47, the validation results in Table 4-48 show excellent speed prediction with an average machine speed error of only -1%.

Table 4-46 Design specifications: Tembec Inc.

Variable	S.I. Units	Alternate Units
Regular cylinders diameter	1.524 m	5 ft
Yankee cylinder diameter	6.1 m	20 ft
Cylinder shell thickness (both)	25 mm	1 in
Machine width	4.572 m	15 ft
Draw length (average)	1.2 m	3.9 ft
Sheet length in dryer	306 m	1003 ft
Felt thickness	2.0 mm	0.08 in
Unirun felt & paper wrap angle	250°	
Double felted paper/felt wrap angle	230°/182°	
Paper wrap angle before and after hood	15°	
Paper wrap angle in Yankee hood	250°	
Nozzle exit temperature	110 °C	230 °F
Nozzle exit jet velocity	100 m/s	19,700 fpm
Nozzle diameter	7 mm	0.28 in
Nozzle to web spacing	20 mm	0.79 in
Nozzle spacing/nozzle diameter	2.9	
Nozzle pattern	equilateral triangle	
Nozzle plate open area ratio	1.5%	

Table 4-47 Operating conditions: Tembec Inc.

Variable	June 1996*		October 1997	
	S.I. Units	Alternate	S.I. Units	Alternate
Machine speed	344 m/min	1130 fpm	436 m/min	1430 fpm
Drying time	53.3 s		42.1 s	
Basis weight	202 g/m ²	41 lb/1000ft ²	152 g/m ²	31 lb/1000ft ²
Inlet moisture content	1.27 kg/kg dry	44 % solids	1.41 kg/kg dry	41.5 % solids
Exit moisture content	0.07 kg/kg dry	93.4 % solids	0.073 kg/kg dry	93.2 % solids
Inlet sheet temperature	40°C	104°F	40°C	104°F
Fiber saturation point	0.75 kg/kg dry	57.1 % solids	0.75 kg/kg dry	57.1 % solids
Condensing steam	S.I. Units [kPag/°C]		Alternate [psig/°F]	
Section 1	6 cylinders (1-6), uniron felting			
Cylinder #1	-5/99°	-0.7/209°	25/106°	3.6/223°
Cylinder #2	0/100°	0/212°	50/112°	7.3/233°
Cylinders #3-6	5/101°	0.7/214°	70/115°	10.2/240°
Section 2	11 cylinders (7-17), uniron felting			
Upper cylinders	100/120°	14.5/249°	100/120°	14.5/249°
Bottom cylinders	40/110°	5.8/229°	300/144°	43.5/291°
Sections 3 & 4	24 cylinders (18-41), double felted			
Upper cylinders	140/126°	20.3/259°	124/124°	18/255°
Bottom cylinders	140/126°	20.3/259°	180/131°	26.1/268°
Yankee Cylinder	233/137°	33.8/279°	300/144°	43.5/291°
Section 5	22 cylinders(42-63), double felted			
Upper cylinders	182/132°	26.4/269°	131/125°	19/257°
Bottom cylinders	182/132°	26.4/269°	181/131°	26.3/269°

* Cylinders 10,18,33 and 63 were closed to steam

Table 4-48 Uncalibrated validation: Tembec Inc.

	June 1996	October 1997
Exit moisture content		
Validation simulation	7.9 % d.b.	6.6 % d.b.
Measured	7.0 % d.b.	7.3 % d.b.
Machine speed		
Validation simulation	334 m/min	440 m/min
Measured	344 m/min	436 m/min
Difference	-2.8 %	+0.9 %

These dryer surveys are exceptional in that the sheet moisture content was determined not only at the dryer exit, as indicated in Table 4-48, but also at the entry and exit to the Yankee dryer following cylinder #41. These additional moisture contents are

compared with model predictions in Table 4-49. Cylinder 41 is followed in the dryer section by a Yankee dryer, providing an opportunity for evaluating the model performance for a hybrid dryer section. In a conventional cylinder machine, heat for drying comes only from the cylinder-contact side. In a Yankee dryer heat reaches the sheet both from the side in contact with the cylinder and from the opposite side which is subjected to high temperature impinging jets, the latter providing the dominant mechanism of heat transfer. Reasonable agreement between the model predictions and corresponding measurements shows that the model is able to follow satisfactorily the evolution of sheet moisture content as it goes through a sequence of very different drying techniques in such a hybrid dryer.

Table 4-49 Comparison of measured and predicted values of moisture content, Tembec Inc.

Survey	Cylinder	Moisture Content (kg/kg dry)	
		Prediction	Measurement
June 1996	#41	0.49	0.52
	Yankee	0.36	0.43
October 1997	#41	0.46	0.55
	Yankee	0.37	0.50

4.4 Summary

Development of the paper drying model was completed in this chapter through a rigorous sensitivity analysis using measurements on industrial dryers to establish the optimal choice of those transport properties for which the analysis in Chapter 3 could not clearly identify the best choice. This aspect is summarized in section 4.2.6. With the model thereby finalized, a comprehensive industrial validation was carried out to test the model reliability in predicting machine speed and other parameters reported in dryer surveys. Of the more than 30 paper drying models listed in Table 1-1 of Chapter 1, the first McGill dryer simulator, using the Bond and Douglas model described in 1996 and 1999, incorporates the most comprehensive description of the transport phenomena

involved. For that model Sidwall et al. (1999b) documented validation with 31 dryer surveys. Therefore that model is used here as the standard for comparison of the present model.

Table 4-50 demonstrates the thorough industrial validation performed on the model developed here. The 32 dryer surveys used cover all commercially important grades of paper dried not just by hot surface cylinder drying or air impingement drying but also in hybrid dryer sections where a combination of basic drying techniques, cylinder or air impingement, is used. In the course of the present study it was determined that the previous McGill model was unable to run a machine speed prediction simulation for the case listed in Table 4-50 for drying fine paper to a very low moisture content.

Table 4-50 Summary of dryer surveys used in industrial validation

Drying technique	Paper grade	No. of paper machines	No. of surveys
Air impingement drying	Tissue, 14-21 g/m ²	2	3
Cylinder drying	Newsprint, 48-49 g/m ²	3	15
	Corrugated medium, 127-161 g/m ²	1	2
	Linerboard, 118-337 g/m ²	3	8
	Fine paper, 72 g/m ²	1	1
Hybrid drying	Linerboard, 127 g/m ²	1	1
Cylinder + air impingement	Linerboard, 155-202 g/m ²	1	2
Totals:		12	32

It is important to note that, contrary to what has been done in some paper dryer modeling elsewhere, the validations of the model predictions against paper machine performance data was carried out with no calibration or tuning of any kind for the model. The results of machine speed prediction simulations for the 32 dryer surveys are summarized in Figure 4-8 as a comparison between the actual machine speed with that

predicted by the model. The machine speed prediction error is seen to be sometimes positive (over-prediction of drying rate by the model, hence prediction of too high a machine speed), sometimes negative, when machine speed is under-predicted. The average speed prediction error is +2.6%, demonstrating the model capability in simulating all the combinations of paper grades and drying techniques in the dryer surveys with an average over-prediction of machine speed by just 2.6%. For the relative difference between predicted and actual machine speed, the distribution of these differences for the 32 validations has a standard deviation of 4.6% around the mean value of +2.6% noted above. Thus the $\pm 2\sigma$ limits for these differences are from -6.6% to +11.8% from the actual machine speed.

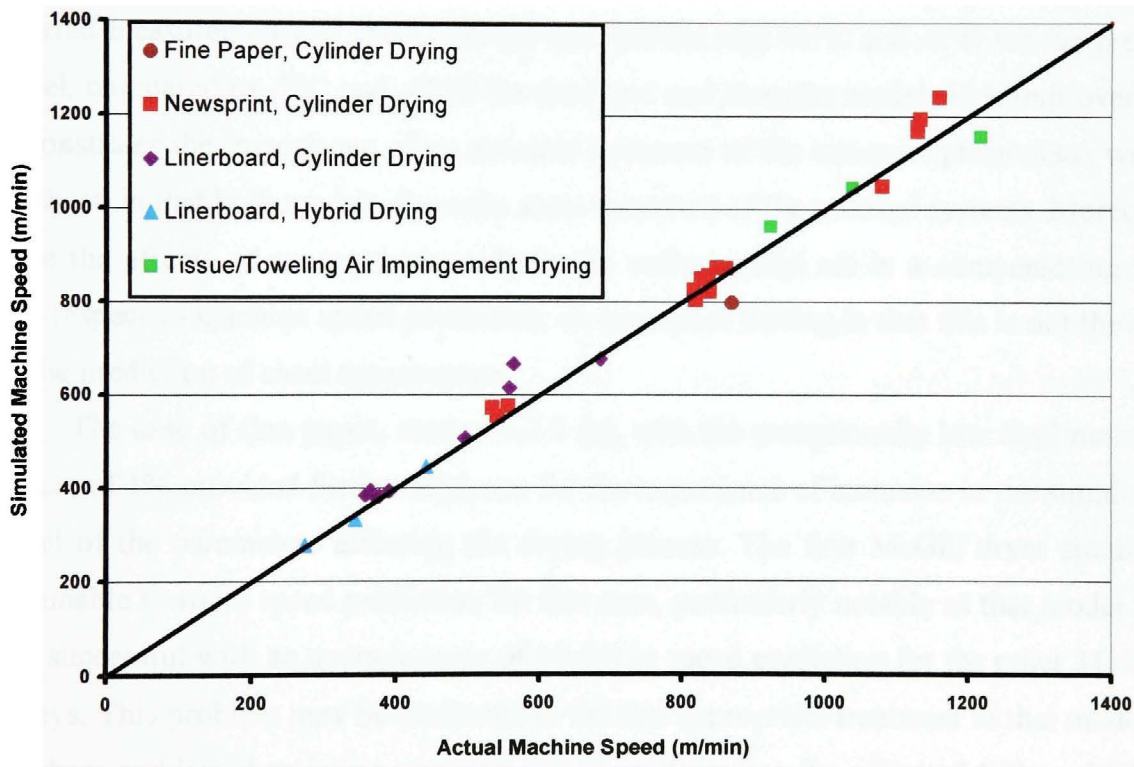


Figure 4-9 Comparison of actual machine speed to model predictions for 32 surveys

The difference between predicted and actual machine speed has two sources, errors in the model including in the values of model parameters, and errors in the measurements of dryer conditions as determined in dryer surveys. As the model used in all 32 validations is the same, the +2.6% average error found may be interpreted as the

systematic error of the model to over-predict drying rate by 2.6%. Because errors in measurement of dryer conditions, which are input to the model, may be assumed to be random over the 32 dryer surveys, the value of the standard deviation of 4.6% for the difference between predicted and measured machine speed may be interpreted as the effect of random error in dryer survey measurements.

In addition to machine speed, the model predictions were satisfactorily compared with other parameters as occasionally reported, such as sheet and cylinder surface temperature, and sheet moisture content at positions other than at the entrance and exit of the dryer. With respect to sheet temperature, a major improvement over its systematic under-estimation by the first McGill dryer simulator was observed. For two newsprint cases of sections 4.3.2 (a-1) and (a-3) the average difference between the predicted and reported measurements of sheet average temperature was +1°C and -3°C for the present model, compared to -7°C and -12°C for the Bond and Douglas model. This improvement demonstrates the importance of an accurate treatment of the transport phenomena within the sheet, in that both models share the same treatment of the external systems. Moreover, while the effects of assumptions made in the earlier model act in a compensating way with respect to machine speed prediction, an important finding is that this is not the case for the prediction of sheet temperature.

The case of fine paper, section 4.3.2 (c), with the exceptionally low final moisture content of 1% provided further evidence for the importance of inclusion in the simulation model of the parameters affecting the drying process. The first McGill dryer simulator was unable to run a speed prediction for this case, particularly notable as that model was very successful with an average error of +0.6% in speed prediction for the other 31 dryer surveys. This problem may be attributed to the less appropriate treatment in that model of gas phase and liquid moisture transport and to not including the effect of differential heat of sorption when the moisture content is below the fiber saturation point. Hence the more accurate treatment of transport phenomena within the sheet and the inclusion of all thermodynamic properties pertinent to drying has enabled the present model to handle a difficult case, improving the performance over that of the first McGill dryer simulator.

All of the above validation evidence relates to performance that can be determined in surveys of industrial dryers. However although the model is microscale, in treating

properties and the flow, heat and mass transfer characteristics within the sheet, no such measurements inside the sheet are possible for an industrial dryer. Exceptionally, such measurements were made by Bond and Douglas for laboratory air impingement drying of linerboard, with determination of both temperature and moisture content for each of the 3 plies as such sheets were dried. The good agreement between these measured values and those predicted now with the new model provide strong evidence that the internal moisture and temperature within the sheet predicted by this model are reliable, thereby providing unique validation of the modeling used for the internal transport phenomena during drying.

In conclusion, the present model proved successful in predicting the drying history of the full range of paper from tissue to linerboard in a variety of dryer sections, and for conditions within linerboard when dried by an air impingement laboratory dryer. Major improvements of this dryer simulator are that it provided the best predictions of sheet temperature and is able to treat the difficult case of fine paper being dried to an exceptionally low exit moisture content. No reported paper dryer simulator has as complete modeling of all major transport phenomena within the sheet, as critical an assessment of the transport and thermodynamic properties used by the model, or as extensive validation with use of no calibration or tuning of the model. This model will next be used to provide insight into the complex dynamics of transport phenomena within the sheet, the subject of the next chapter.

CHAPTER 5

DYNAMICS OF TRANSPORT PHENOMENA DURING DRYING

The sophisticated microscale model developed in Chapters 2 and 3 and validated in Chapter 4 provides a comprehensive and unique insight into the evolution of moisture content, temperature and pressure in the thickness direction of the sheet during drying and the associated flow, heat and mass transfer fluxes. The distribution of moisture content within the sheet, highly coupled with that of temperature and pressure, may have a significant effect on paper quality, for example being the direct source of undesirable properties such as curl. Therefore a reliable understanding of what happens inside the sheet would provide valuable help to papermakers in enabling optimization of the dryer section design and operation to achieve the best product quality as well as highest productivity. The analysis of the evolution of moisture content, temperature and pressure conditions within the sheet and the associated mass and heat transfer fluxes by the various mechanisms involved is now applied for a demonstration case of linerboard drying, selected because the differences in local conditions across a thick sheet are high.

5.1 Methodology

The results as thickness-direction profiles of three main parameters, moisture content, temperature and gas pressure, are presented first. The results are provided for five cylinders selected to cover a representative range of these thickness-direction profiles as the sheet goes from wet to dry.

The second part of the analysis provides thickness-direction profiles of the three mass fluxes in the gas, liquid and solid phases. These terms represent the contributions of different mechanisms to the drying process. These profiles are presented at a representative position between the wet and dry end of the dryer so as to display the behavior for moisture content both above and below the fiber saturation point, thereby illustrating how the hygroscopic behavior of paper affects the contributions of the various transport mechanisms within the sheet.

The last category of results provides quantitative evidence for the relative importance of the several contributions to mass transport and to heat transport within the

sheet, but now determined so as to provide an overall perspective for the importance of the various contributions over the entire drying process as the sheet goes from wet to dry. Together these results provide a comprehensive understanding of the transport phenomena involved in drying paper, and as well could be used to simplify the model equations by eliminating terms which do not constitute a significant effect.

The dynamics of the transport phenomena presented here derive from the model structure, assumptions and associated parameters. Therefore it would be informative to compare the present model predictions to those from the Bond and Douglas model, the most detailed and successful previous model, for which the characteristics were detailed by Sidwall et al. (1999a). As that model used a substantially different treatment of flow, heat and mass transfer within the sheet such a comparison will demonstrate the sensitivity of predictions of the profiles to the treatment of transport phenomena within the sheet. As both models share the same treatment of external systems, differences reported here relate only to the modeling of the complex internal phenomena within the sheet.

The type of analysis presented in this chapter for the dynamics of the drying process for different grades and for different phases of drying, including information within the sheet for moisture content, temperature and gas pressure, for mass fluxes in the three phases, for heat transport by the different mechanisms, enables rigorous scientific assessment of the effect of dryer section design and operating conditions.

5.2 Terminology

The profiles are defined at 10 positions in the thickness direction of the sheet. As alternate sides of the sheet contact the heated surface as the web travels from one cylinder to the next in a two-tier multi-cylinder dryer section, a consistent terminology is required for referring to the thickness-direction position. The convention adopted is that position 1 is always the “Vapor Transport Side” where water vapor leaves the sheet, while position 10 is the “Cylinder Contact Side”, the side contacting the heated surface when the sheet is on a cylinder.

In a multi-cylinder dryer section the drying process is divided into the four phases defined first by Nissan and Kaye (1955), as identified in Figure 1-2 given below:

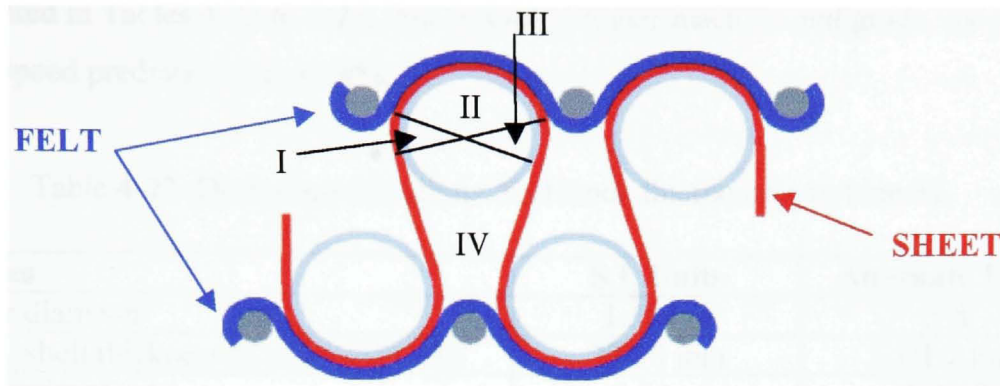


Figure 1-2 Four phases of cylinder drying, Nissan and Kaye (1955)

Phase I: One side of the sheet contacts the hot cylinder surface while the other side, not yet covered by the felt, is exposed to the dryer pocket.

Phase II: The vapor transport side of the sheet is now covered by the felt, so the sheet is sandwiched between the cylinder and the felt.

Phase III: The felt is removed from the sheet, making this stage identical to Phase I.

Phase IV: With its removal from the cylinder, both sides of the sheet are exposed to the dryer pocket.

The thickness-direction profiles of moisture content, temperature and gas pressure are presented in sections 5.3.1 to 5.3.6 for five drying cylinders (#3, 15, 27, 33 and 46) ranging from near the wet end to near the dry end of the dryer section. For an illustrative cylinder (#27) the treatment in section 5.3.4 is expanded to provide an analysis of the contributions of the various terms for the mass transport mechanisms. Section 5.3.7 provides a comprehensive comparison for the entire 48-cylinder drying process of the various mechanisms of both mass and heat transfer.

5.3 Drying dynamics for linerboard

5.3.1 Conditions for Norampac PM #1 in Red Rock

In section 4.3.2 (b-3) of Chapter 4, two dryer surveys for the Norampac linerboard paper machine #1 in Red Rock were used. Design specifications for this dryer section and

the operating conditions for the thicker grade of 161 g/m², requiring 36.4s drying time, are presented in Tables 4-23 to 4-25. For this 48-cylinder machine and grade, the error of machine speed prediction was +7.4%.

Table 4-23 Design specifications: Red Rock linerboard machine #1

Variables	S.I. Units	Alternate Units
Cylinder diameter	1.524 m	5 ft
Cylinder shell thickness (Cyl.1-12/13-48)	27/30 mm	1.1/1.2 inch
Machine trim	5.64 m	18.5 ft
Draw length	1.6 m	5.2 ft
Sheet wrap angle	220°	
Felt wrap angle	182°	
Felt thickness	1.8 mm	0.07 inch
Sheet length in dryer	217 m	712 ft
Spoiler bars	none	

Table 4-24 Operating conditions: Red Rock linerboard machine #1 (161 g/m²)

Variable	161 g/m ²	
	S.I. Units	Alt. Units
Machine speed	358 m/min	1175 fpm
Drying time	36.4 s	
Dry sheet caliper	271 microns	
Sheet inlet moisture	1.94 kg/kg dry	34 % solids
Sheet exit moisture	0.07 kg/kg dry	93.5 % solids
Sheet inlet temperature	45°C	113°F
Fiber saturation point	0.8 kg/kg dry	55.6 % solids
Condensing Steam	S.I. [kPag/°C] and Alternate [psig/°F]	
Section 1 (1-4)	150/128°	22/262°
Section 2 (5-12)	200/134°	29/273°
Section 3 (13-36)	900/180°	131/356°
Section 4 (37-48)	1000/184°	145/363°

Table 4-25 Pocket conditions: Red Rock linerboard machine #1

Variable	Temperature		Humidity
	°C	°F	kg/kg dry air
Cylinder 1	60	140	0.1
Cylinders 2-12	60	140	0.15
Cylinders 13-48	68	155	0.2

5.3.2 Cylinder #3

At this cylinder located early in the dryer section where the sheet is still warming up, the analysis shows that thickness-direction profiles across the sheet have already started to develop. The thickness-direction profiles of moisture content, temperature and pressure are shown in Figures 5-1 to 5-3. For reference, the sheet enters the dryer at 45°C and a moisture content of 1.94 kg/kg dry. The sheet average conditions entering and leaving cylinder #3 are for temperature 60°C and 71°C and for moisture content 1.89 kg/kg dry and 1.88 kg/kg dry. Each graph presents the profile at five stages: the conditions when the sheet enters the cylinder and the profiles at the end of each of the four phases of drying.

Figure 5-1 shows that for this early cylinder the moisture content variation in the thickness direction is still quite small because most of the heat received by the sheet is reflected in its increase in temperature with very little evaporation, as noted above. By contrast, with heat transfer into the sheet being reflected more in sensible heat than evaporation, the temperature difference across the sheet by the end of Phase II is substantial, about 13°C. The sheet enters cylinder #3 with both sides at a slightly lower moisture content than the interior of the sheet because of some evaporation from the edges of the sheet on the previous two cylinders. At cylinder #3 the reduction of moisture content by the end of phase I is negligible everywhere except positions 9 and 10. As recorded in Table 4-23 the felt wrap angle, which determines the extent of Phase II, is 182° while the wrap angle for Phases I and III is only 19° each. Thus changes on cylinder #3 are dominated by Phase II. Therefore it is as expected that the biggest drop of moisture content at the Cylinder Contact Side (CCS) occurs at the end of Phase II. Note that although the sheet moisture content does not change significantly at the Vapor Transport Side (VTS) it actually increases there due to capillary transport of liquid water driven by the gas pressure gradient from the interior towards the VTS surface. At cylinder #3 the moisture content is more than double that of the FSP and the percent saturation of the pores is $S = 0.65$. The ineffectiveness of Phase IV where both sides of the sheet are exposed in the dryer pocket demonstrates the poor pocket air ventilation for this paper machine.

Figure 5-2 shows that by cylinder #3 the sheet temperature has increased substantially from the level of 45°C at which it entered the dryer. From the dryer pocket of cylinder #2 the sheet enters cylinder #3 with an almost flat temperature profile between the limits of 57° and 61°C across the sheet. Although Phase I is of short duration, with a wrap angle of only 19° as noted above, the sensible heat effect is substantial as seen by the rapid heating at positions 8 to 10. This substantial sensible heat effect continues during Phase II with the temperature at the CCS surface increasing to 81°C by the end of Phase II. This effective internal heat transfer is apparent also in that the (81° - 68° =) 13°C difference across the sheet at the end of Phase II has decreased in the dryer pocket to about only 2°C by the end of Phase IV, just 0.31s later.

Figure 5-3 demonstrates the gas pressure build-up across the sheet thickness direction. Water evaporates inside the sheet primarily from positions 10 to 9, as shown by Figure 5-1, and thereby adding to the partial pressure of water vapor in the gas phase increasing the total pressure as shown on Figure 5-3. With the percent saturation of the pores at $S = 0.65$ as noted above, even at the high sheet moisture content level of about 1.9 kg/kg dry this increase of pressure at positions 9 and 10 is readily transmitted through the gas phase in the interfiber pores of the sheet. This pressure gradient provides the driving force for both vapor phase convective flow and liquid phase capillary transport towards the VTS surface. The exact location of the maximum pressure at the CCS surface, Figure 5-3, depends on several parameters, the cylinder surface and sheet temperature and the sheet moisture content. However this location will be near the end of Phase II, as is the case for this cylinder. Pressure equalization occurs during Phase IV when both sides of the sheet are exposed to atmospheric pressure. The pressure profile presented in Figure 5-3 for the sheet 10% through Phase IV (the open draw) shows that the pressure release is rapid but not instantaneous. This lag in pressure equalization is larger the bigger the pressure build-up on the cylinder. At the end of Phase IV the pressure gradient across the sheet thickness is essentially dissipated.

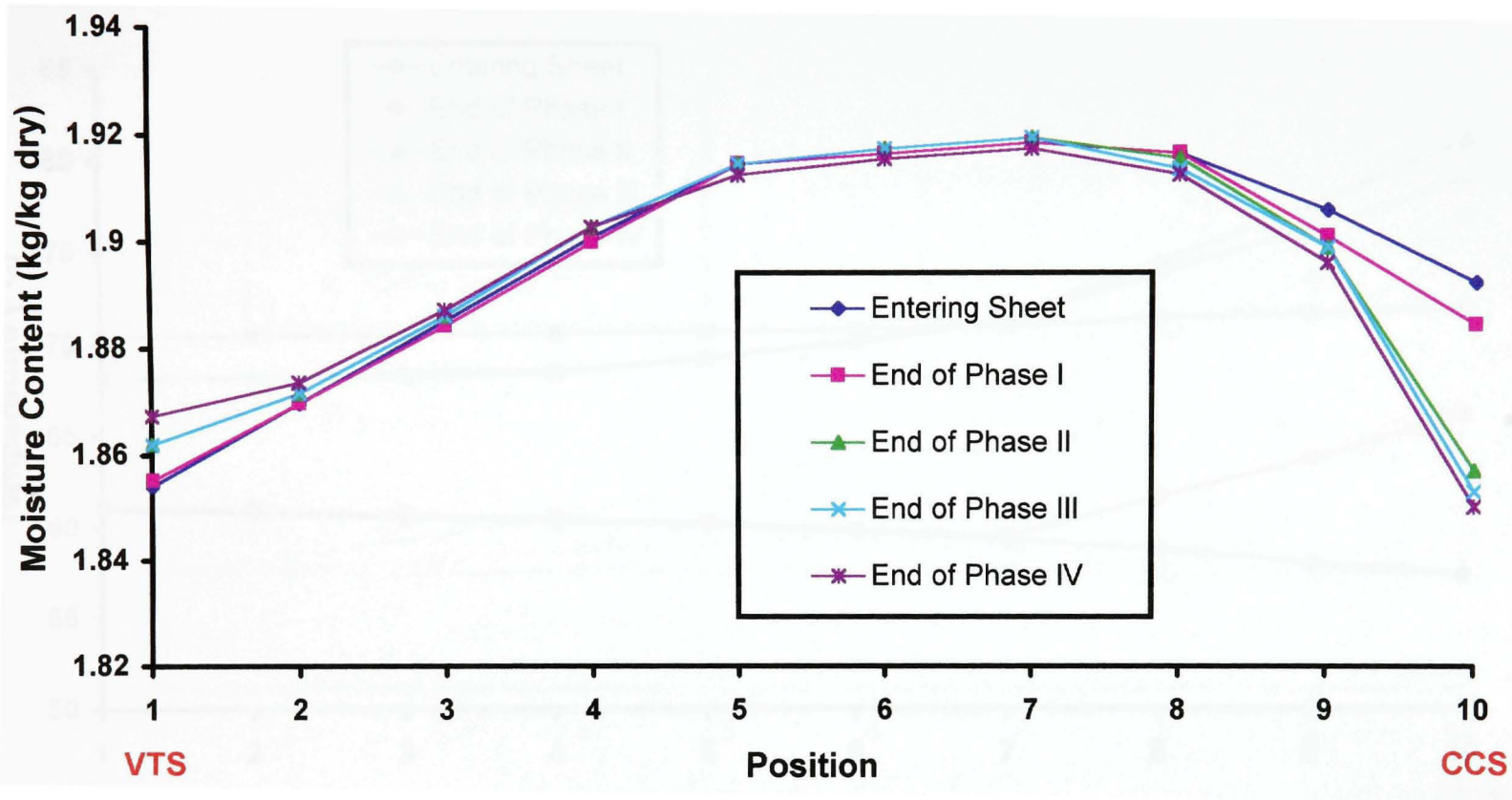


Figure 5-1 Thickness-direction profiles of moisture content
(Red Rock PM#1, 161 g/m², Cylinder #3)

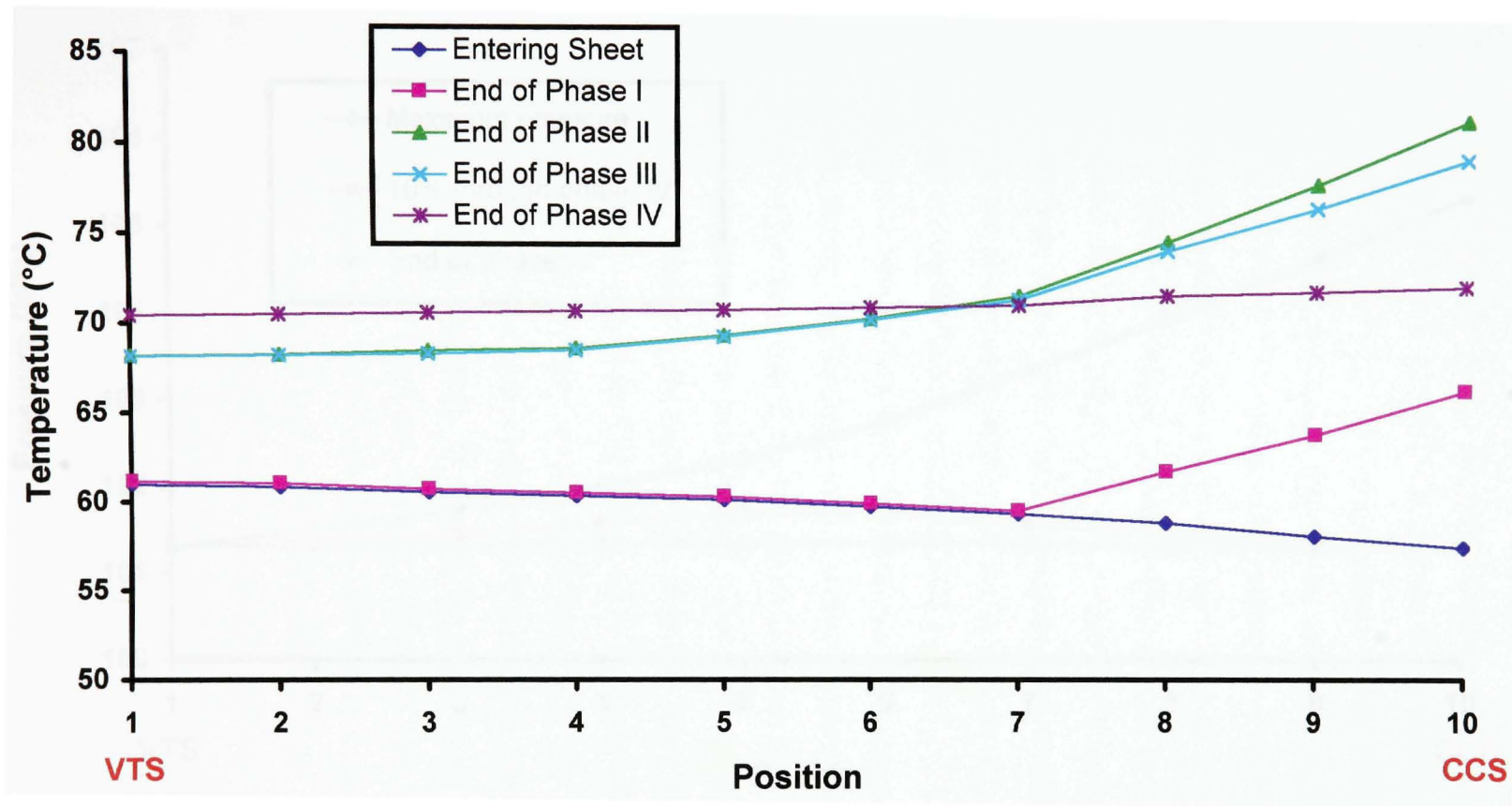


Figure 5-2 Thickness-direction profiles of temperature
(Red Rock PM#1, 161 g/m², Cylinder #3)

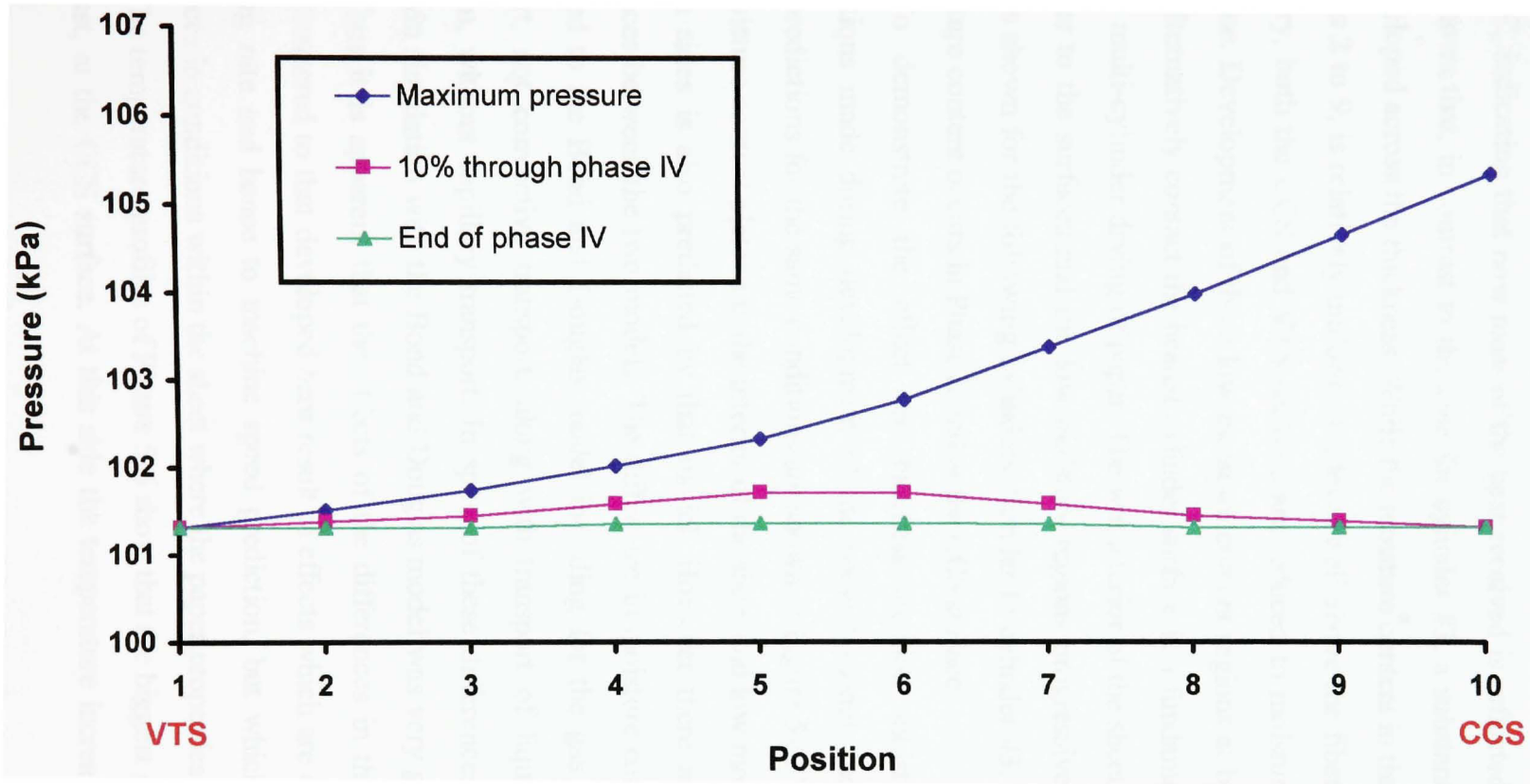


Figure 5-3 Thickness-direction profiles of pressure
 (Red Rock PM#1, 161 g/m², Cylinder #3)

5.3.3 Cylinder #15

The thickness-direction profiles of moisture content at the end of Phase II for this cylinder are presented in Figure 5-4. The sheet enters and leaves the cylinder at an average moisture content of 1.34 and 1.23 kg/kg dry, and at an average temperature of 84 and 85°C, indicating that now most of the heat received is reflected in evaporation. This graph shows that, in contrast to the case for cylinder #3, a substantial moisture gradient has developed across the thickness. While the moisture content in the interior of the sheet, positions 2 to 9, is relatively uniform at a level well above the fiber saturation point, 0.8 kg/kg dry, both the CCS and VTS surfaces are reduced to moisture contents below the FSP value. Development of these low moisture content regions at both sides of the sheet which alternatively contact the heated cylinder surface is a fundamental characteristic of two-tier multi-cylinder drying of paper. The wet interior of the sheet becomes a supply of the water to the surfaces and the low moisture regions progressively expand within the sheet, as shown for the following cylinders. Similar to cylinder #3, the biggest reduction of moisture content occurs in Phase II and at the CCS surface.

To demonstrate the effect on thickness-direction moisture profiles of the assumptions made during development of the present model, the Bond and Douglas model predictions for the same conditions are shown in Figure 5-5. The development of a high moisture content plateau in the interior of the sheet and low moisture content regions on both sides is also predicted by that model. However there are clearly significant differences between the two models. The difference in moisture content profile could be attributed to the Bond and Douglas model including for the gas phase only diffusive transport, not convective transport, along with transport of liquid moisture only by diffusion, without capillary transport. In spite of these differences, the machine speed prediction simulation with the Bond and Douglas model was very good, with an error of +6%. Thus it is apparent that the effects of the differences in the Bond and Douglas model compared to that developed here result in effects which are compensating relative to drying rate and hence to machine speed prediction, but which produce significant differences in conditions within the sheet where the paper properties are being developed.

The temperature profiles of Figure 5-6 show that the biggest gradient again occurs, as it must, at the CCS surface. At this side the temperature increases from the entering

level of 84°, up to 96°C at the end of Phase I after only 0.04s on the cylinder, with a further increase of 3°C by the end of Phase II. The temperature increase during the long Phase II is relatively small because at this high temperature level most of the heat received is reflected in evaporation, not sensible heat. The main temperature increase occurs at locations 8 to 10, about the same region where considerable evaporation and therefore moisture reduction is observed in Figure 5-4. The correlation between the moisture and temperature profiles demonstrates the highly coupled nature of heat and mass transfer during the drying. Temperature equalization occurs once again in Phase IV with the sheet leaving the cylinder with an essentially flat profile at 85°C. The decrease in the ΔT across the sheet from 10°C at the end of Phase III to less than 1°C at the end of Phase IV, 0.27s later, demonstrates again the high heat transfer characteristic of the moist paper.

Figure 5-7 illustrates the maximum gas pressure difference of 14 kPa, generated across the sheet for the water vapor convective flow, produces also the free water capillary transport towards the VTS surface. The ΔP across the sheet at the end of Phase II, which was only 4 kPa for cylinder #3, Figure 5-3, is seen to have increased to 14 kPa now that most of the heat transfer to the sheet is reflected not in sensible heat to increase sheet temperature, but in generation of water vapor which must flow to the VTS side of the sheet. This increase in ΔP across the sheet to 14 kPa reflects the greatly increased vapor phase convective flow through the sheet. The mass flux terms are detailed subsequently. In Phase IV when both sides of the sheet are at atmospheric pressure in the open draw there is still a slight ΔP of 2 kPa between the center and the edges of the sheet when the sheet is 10% through the open draw between the cylinders. The sheet leaves the open draw with the pressure build-up completely released. This lag in pressure equalization differs from the assumption of instantaneous pressure release made by Ramaswamy (1990).

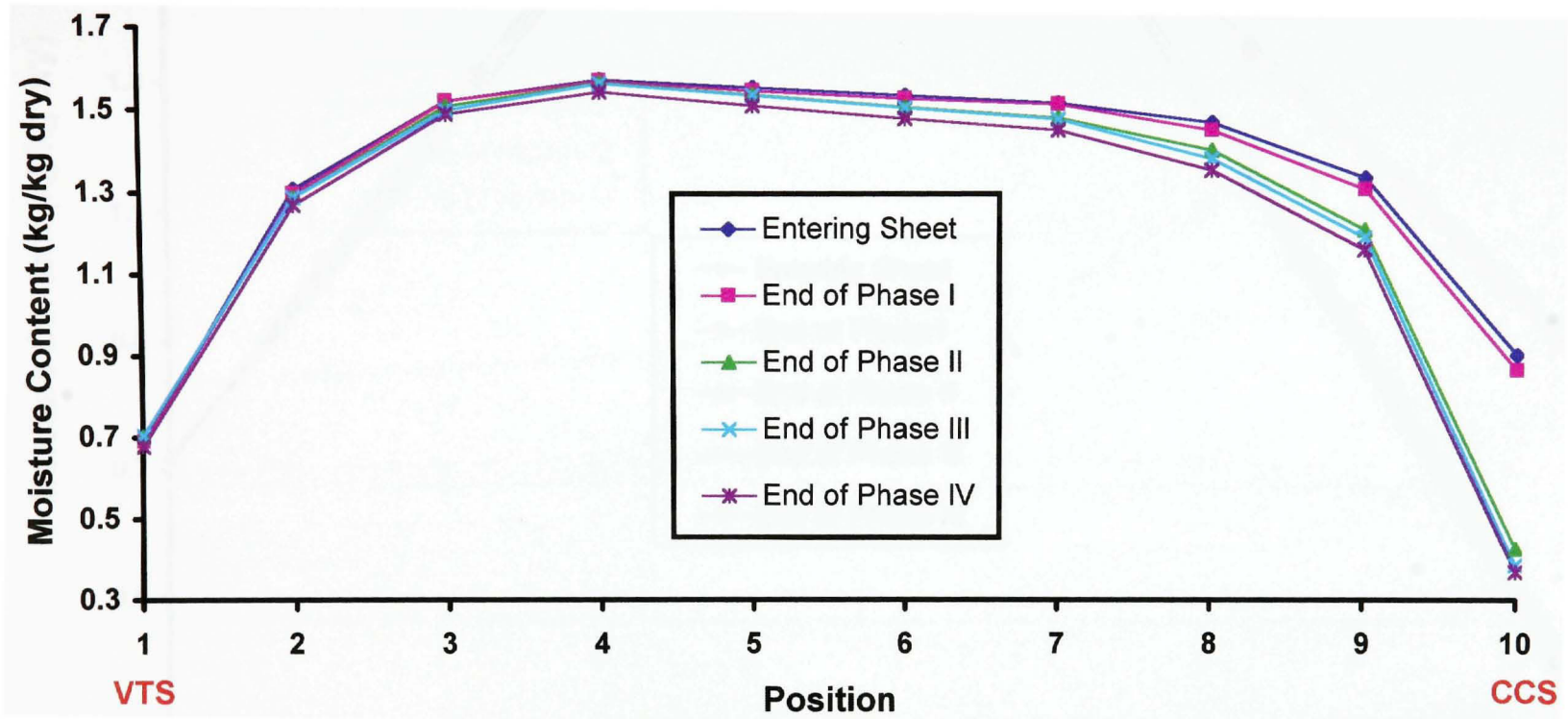


Figure 5-4 Thickness-direction profiles of moisture content
(Red Rock PM#1, 161 g/m², Cylinder #15)

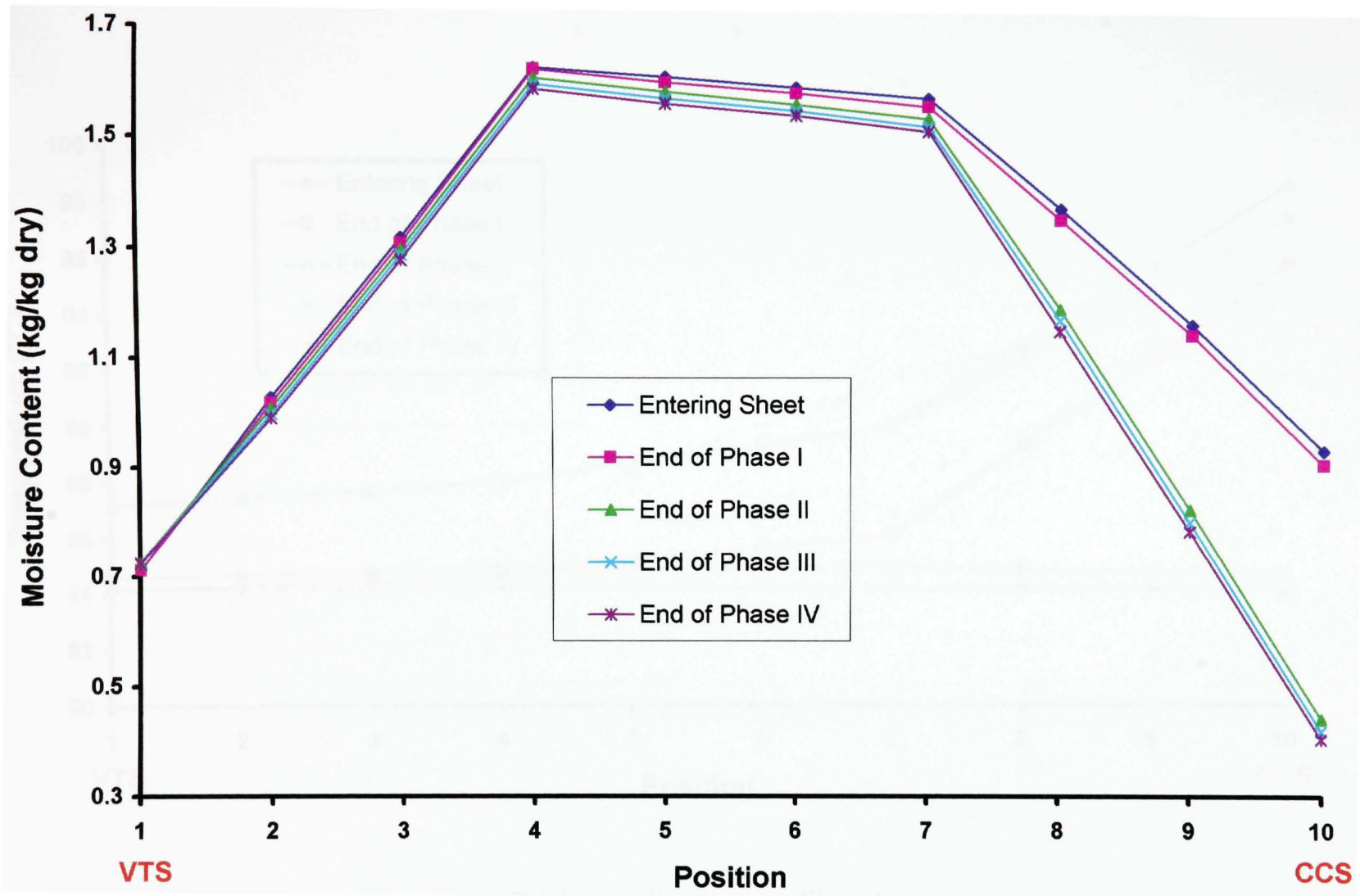


Figure 5-5 Thickness-direction profiles of moisture content, Bond and Douglas (Red Rock PM#1, 161 g/m², Cylinder #15)

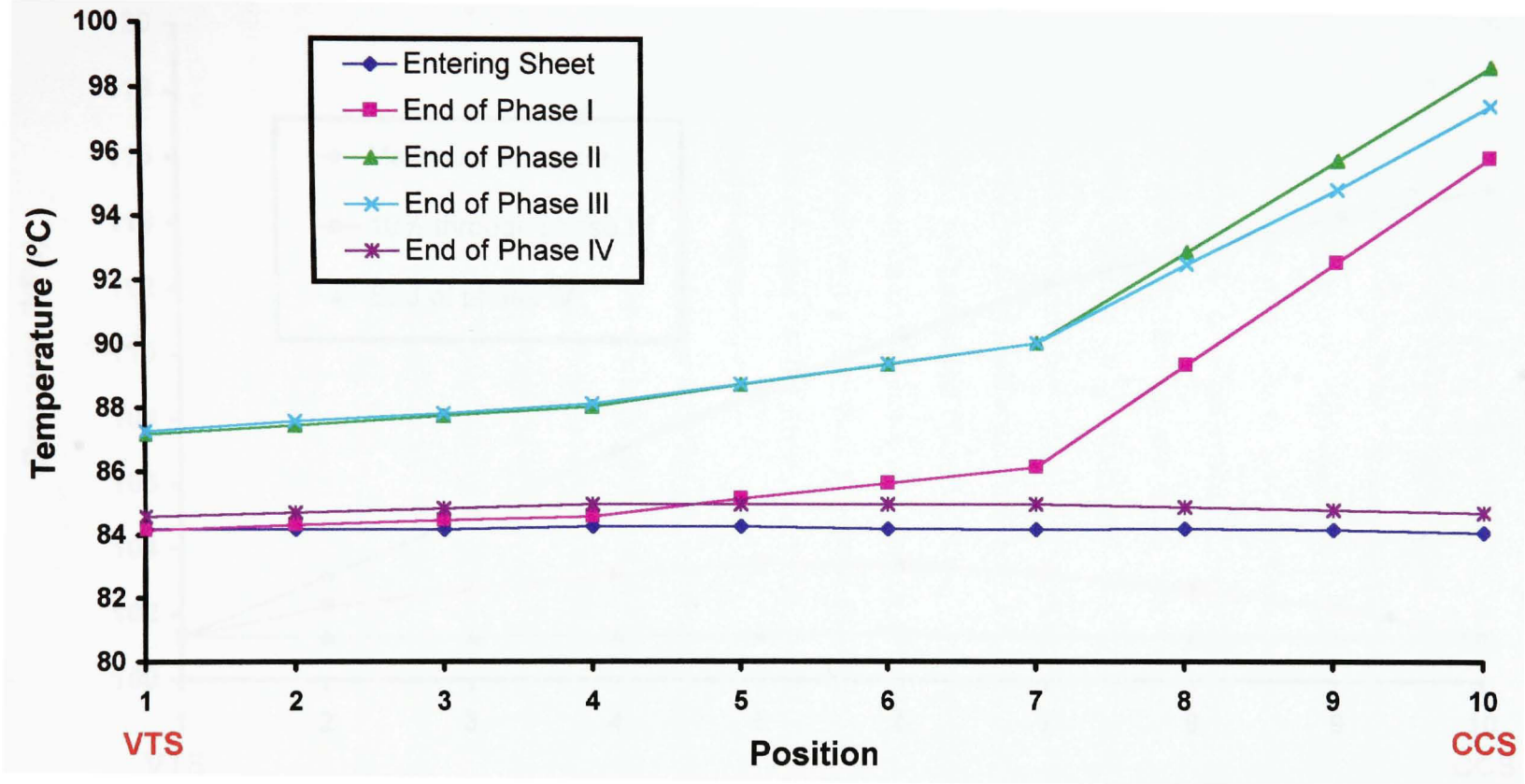


Figure 5-6 Thickness-direction profiles of temperature
(Red Rock PM#1, 161 g/m², Cylinder #15)

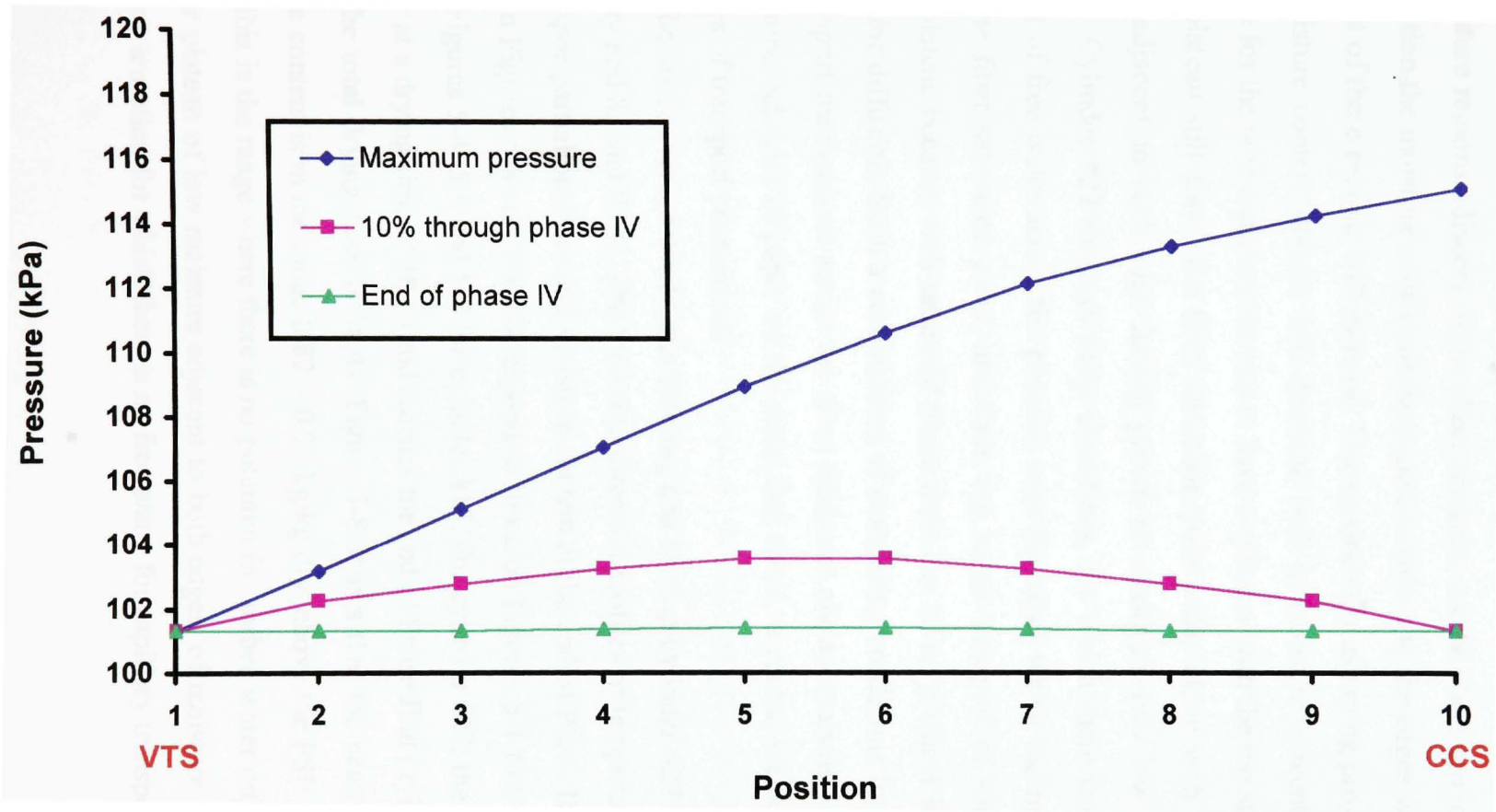


Figure 5-7 Thickness-direction profiles of pressure
 (Red Rock PM#1, 161 g/m², Cylinder #15)

5.3.4 Cylinder #27

(a) *Moisture content, temperature and pressure at the end of Phase II*

In the previous section it was observed that by cylinder #15 three moisture content regions are developing: a high moisture content plateau in the middle of the sheet and two low moisture regions adjacent to the sheet surfaces. As the sheet progresses through the dryer section the moisture content of the regions adjacent to the edges will decrease while the extent of these regions will increase. Correspondingly as drying progresses the central high moisture content plateau will decrease both in moisture content and extent. The objective for the next examination was to have a cylinder with the moisture content of the central plateau still above the fiber saturation point value along with the low moisture regions adjacent to each edge having grown to constitute two low moisture content plateaus. Cylinder #27 displays these conditions, for which there can be no capillary transport of free water across the plateaus near the edges where the moisture content is below the fiber saturation point, and there can be no transport of sorbed water in the central plateau because with saturated fibers there can be no gradient in sorbed moisture content for diffusion. Such a combination of contrasting conditions for moisture content and transport mechanisms across the sheet thickness allows analysis of the effect of the hygroscopic behavior of paper on the mass flux terms, a central element of the internal dynamics of transport phenomena.

The sheet average conditions entering and leaving cylinder #27 are 0.64 and 0.59 kg/kg dry and 83 and 85°C. The thickness direction profiles of temperature, gas pressure, water vapor partial pressure and moisture content at the end of Phase II for cylinder #27, shown in Figures 5-8 and 5-9, correspond to those on Figures 5-1 to 5-3 for cylinder #3, and on Figures 5-4, 5-6 and 5-7 for cylinder #15. For cylinder #27, the sheet contacts the cylinder at a drying time of 18.5s and reaches the end of Phase II at drying time of 18.95s, where the total drying time is 36.4s. Figure 5-8 shows that the central plateau of high moisture content is in the range 0.82 – 0.91 kg/kg dry, above the FSP value of 0.8 kg/kg dry, so this is the range where there is no potential for sorbed water diffusion. Also, there is a near plateau of low moisture adjacent to both edges, of moisture content 0.25 – 0.3 kg/kg dry, a section for which there is no free water for capillary transport.

From the open draw of cylinder #26 the sheet enters cylinder #27 with a nearly uniform temperature of 83°C and with internal pressure completely discharged. At the end of Phase II, Figure 5-8 shows that the temperature at the CCS edge has increased to 103°C, giving a ΔT across the sheet of 14°C, while the ΔP across the sheet has increased to 16 kPa between the two sides of the sheet. As always, the thickness direction temperature gradient is maximum near the heat source at the CCS edge, decreasing to negligible towards the VTS edge.

Figure 5-9 shows the profiles for water vapor pressure, P_v , and for the ratio P_v/P_g which is coupled with the water vapor mass flux, treated subsequently. Water vapor pressure is a function of temperature and the vapor pressure reduction factor, the latter being in turn a function of sheet moisture content as shown on Figure 2-9. Figure 5-8 shows that the lowest value of moisture content at the end of Phase II on cylinder #27 is 0.23 kg/kg dry, and Figure 2-9 shows that the vapor pressure reduction factor begins to drop sharply only below that moisture level. Thus for the moisture content range of Figure 5-8 the vapor pressure of water is controlled predominantly by temperature, as is apparent from the vapor pressure profile on Figure 5-9.

(b) Mass fluxes of moisture as sorbed water, free water and water vapor

Chapter 2 formulated the mass fluxes of three species relevant to drying process: water vapor, free water and sorbed water. These fluxes are functions of drying time and thickness-direction positions. As the end of Phase II marks the highest intensity of drying conditions, the results for all three fluxes were determined when the sheet reaches this point, 0.45s after the sheet arrives at Phase I, and for all 10 positions in the sheet thickness direction.

With the moisture content, temperature and pressure conditions within the sheet having been determined at this drying time, the thickness-direction profiles of the three mass fluxes are now presented and analyzed. For each of the 9 intervals between the 10 thickness-direction positions, the fluxes are calculated for the relevant driving force of moisture content or pressure, using all the properties required by the flux equations as the average between the two positions defining that interval. For example, the water vapor mass flux, n_v , for the interval between positions 9 and 8 is calculated based on the ΔP

between those two positions and using all required properties as the average of those at these two positions. All such fluxes appear on Figure 5-10 at the mid-point between two limiting positions. The boundary conditions at positions 1 and 10 make these locations special cases. At position 10 all fluxes are zero because that is the cylinder surface. At the vapor transport surface, position 1, any liquid water flux must be zero while the water vapor flux recorded at this position is the value corresponding to the calculated drying rate. The water vapor and free water fluxes, n_v and n_{fw} , are always in the direction from the cylinder contact to the vapor transport side while the sorbed water flux, n_s , can be in either direction. The n_s value is shown as positive for n_s in the direction towards the vapor transport side and negative when it is towards the cylinder side.

(c) *Water vapor mass flux, n_v*

As the water vapor flux, Figure 5-10, is coupled with the pressure gradient apparent from Figure 5-9, n_v is always positive and reflects the water evaporated within the sheet being carried towards the VTS surface and thereby out of the sheet. The total n_v flux is the sum of the convective and diffusive terms, each with a different driving force: difference of total gas pressure for the convective component and the gradient of water vapor concentration for molecular diffusion. For the conditions shown the transport in the gas phase is completely dominated by the convective mechanism.

The profile of water vapor flux must start from $n_v = 0$ at the impermeable boundary at position 10. Figure 5-10 shows n_v increasing rapidly in the first interval, from position 10 to 9, thereafter remains essentially constant across the sheet. Thus after about the first 10% of the sheet thickness little further evaporation occurs into the humid air convective flow. The agreement between the values of n_v at positions 1.5 and 1, calculated in completely different ways as noted in section (b) above, documents the internal consistency of the model.

Comparison of the water vapor flux with those of free water and sorbed water on Figure 5-9 demonstrates the dominant role of moisture transport in the gas phase. This aspect will be discussed further when the magnitude of the contributions of all the mechanisms has been treated.

(d) *Free water mass flux, n_{fw}*

This mass flux occurs only when the local moisture content is above the fiber saturation point, i.e. with free water present in the interfiber pores. Therefore the free water mass flux must be zero from positions 10 to 9 to 8 and again from just after position 3 to positions 2 and 1. The reference line at the moisture content of the fiber saturation point, 0.8 kg/kg dry as given in Table 4-24, appears on Figure 5-10 for convenience in indicating the regions with and without free water in the pores. Position 8 is slightly above the fiber saturation point with a moisture content of 0.91 kg/kg dry. A finer calculation mesh than 10 positions would reveal more precisely the location of the transition between the presence and absence of free water, but the results shown on Figure 5-10 are sufficient for the present analysis.

Over the central plateau of high moisture, all above the fiber saturation point, Figure 5-8 shows that both the moisture content and free water mass flux increase somewhat from positions 8 to 3 in the direction of free water flow. These concurrent increases are consistent because, as detailed in section 3.1.2 of Chapter 3, an increase in pore saturation causes the liquid relative permeability, k_{rl} , to increase. The driving force for this mass flux is the gradient of free water pressure, $P_{fw} = P_g - P_c$, Equation 2-37, which follows the gas pressure gradient of Figure 5-9. Thus capillary transport over this central region is acting against the concentration profile.

The free water mass flux is positive everywhere, reflecting that capillary transport is pushing the free water from the interior of the sheet always towards the VTS surface.

(e) *Sorbed water mass flux, n_s*

As the moisture content is above the fiber saturation point over the central region from position 8 to just beyond position 3, the mass flux of sorbed water must be zero over that entire region because the fibers are saturated, hence there is no gradient in sorbed water moisture content to drive this diffusion process. Adjacent to the vapor transport side this moisture gradient drives the sorbed water diffusion in the same direction as for n_v and n_{fw} , so in this region n_s is positive. By contrast, adjacent to the cylinder contact side this moisture gradient drives water diffusion in the opposite direction, so here n_s is negative. However the profiles of Figure 5-10 show that whether it is positive or negative, the n_s

flux is insignificant in magnitude compared to those of water vapor and free water. Note that the profile on Figure 5-10 is for $n_s \times 10$ in order that the small values of n_s become visible. These results then demonstrate definitively the negligible contribution of sorbed water transport to the paper drying process.

Although the negative flux of sorbed water towards the CCS surface is insignificant in magnitude compared to other fluxes, this n_s flux does provide an interesting demonstration of the evaporation-condensation cycle, the “heat pipe “ effect. In the thickness-direction region between positions 8 to 10, the vapor and liquid moisture transport fluxes n_v and n_s are moving in the opposite direction. Hence water is supplied by diffusion from the cooler, wetter interior of sheet to the warmer, drier region adjacent to the heat source, where it evaporates and then moves back in the opposite direction with the vapor flow n_v towards the interior of the sheet.

Between positions 2 and 3 near the vapor transport side a different kind of water vapor-liquid water interaction occurs. From position 4 to slightly beyond position 3, liquid water is carried by capillary transport in the direction towards the vapor transport side. This n_{fw} flux drops to zero when sheet moisture content drops to the fiber saturation point. However this liquid water being transported towards the vapor transport side may evaporate into the vapor phase convective flux in the same direction. In this case however, unlike that near the cylinder contact side noted above, there is no evaporation-condensation cycle, simply liquid water transported by pressure gradient from a warmer, wetter region, for possible evaporation into a co-current flow of water vapor being transported by the same pressure gradient towards a drier region.

A final observation can be made concerning the demonstration here that sorbed water transport plays a negligible role in the process of drying paper. These results are consistent with the findings from the sensitivity analysis of Chapter 4 that changes in the basis for determining sorbed water diffusivity had essentially no effect on the model performance. Thus the quantitative results for n_v , n_{fw} and n_s displayed on Figure 5-10 explain the lack of sensitivity to sorbed water diffusivity reported in Chapter 4.

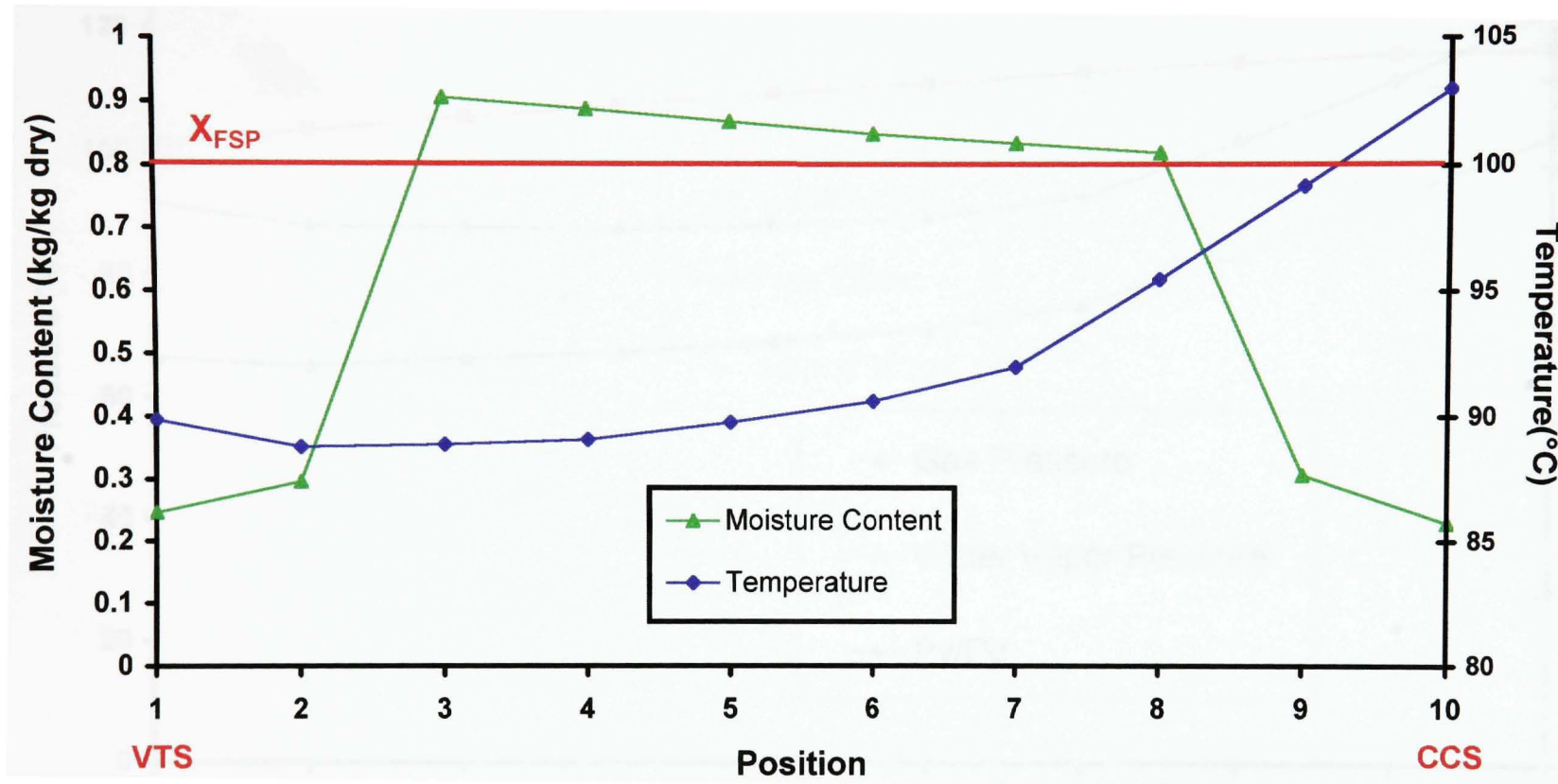


Figure 5-8 Thickness-direction profiles of moisture content and temperature (Red Rock PM#1, 161 g/m², Cylinder #27, End of Phase II)

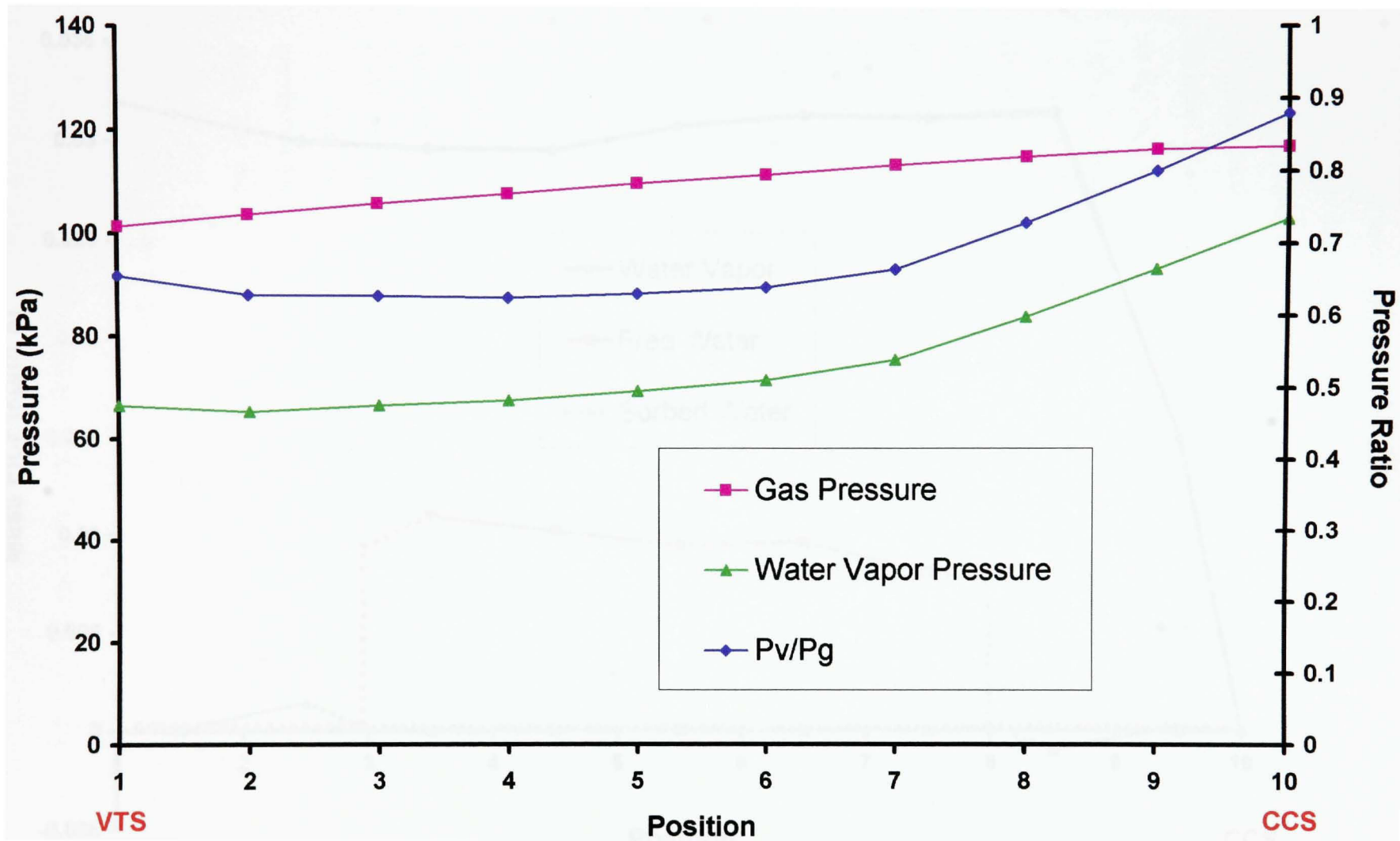


Figure 5-9 Thickness-direction profiles of pressure
 (Red Rock PM#1, 161 g/m², Cylinder #27, End of Phase II)

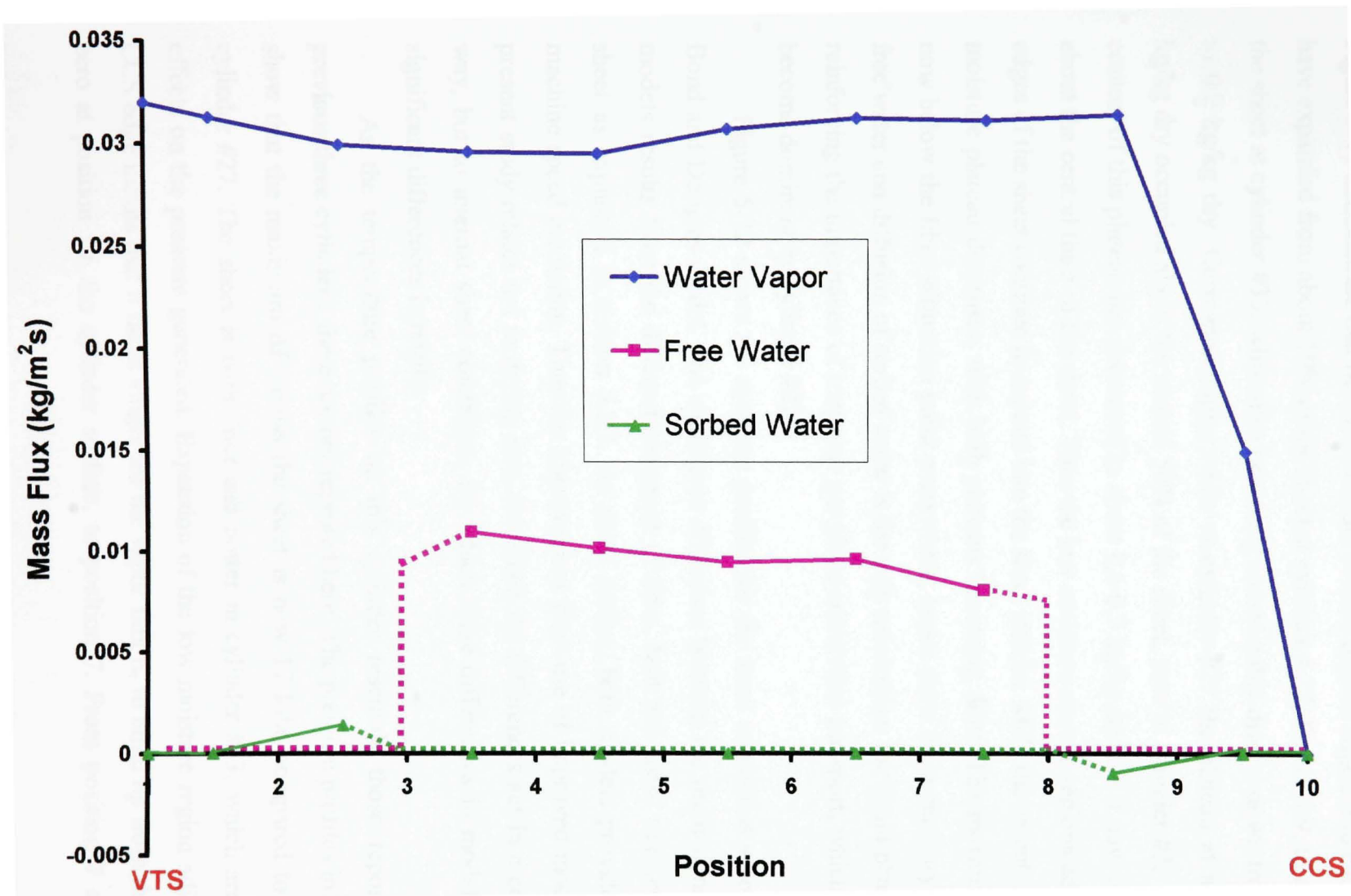


Figure 5-10 Thickness-direction profiles of three mass fluxes (Red Rock PM#1, 161 g/m^2 , Cylinder #27, End of Phase II)

5.3.5 Cylinder #33

The sheet enters and leaves this cylinder at average moisture contents of 0.38 and 0.32 kg/kg dry, and at sheet average temperatures of 85 and 87°C. Moisture profiles of Figure 5-11 demonstrate that the low moisture content regions adjacent to each sheet edge have expanded from about 10% of the sheet at cylinder # 27, Figure 5-9, to about 20% of the sheet at cylinder #33, while also becoming considerably drier – down from about 0.3 to 0.2 kg/kg dry. Correspondingly, while at cylinder #27 the plateau at about 0.8-0.9 kg/kg dry occupied about the central 50% of the sheet, now at cylinder #33 the moisture content of this plateau has decreased to about 0.6-0.7 kg/kg dry and it now occupies only about the central third of the sheet. Thus the low moisture content regions adjacent to the edges of the sheet continue to expand into the sheet interior while the extent of the middle moisture plateau decreases, with both plateaus becoming drier. The moisture content is now below the fiber saturation point everywhere, hence there is no capillary transport of free water and diffusion of sorbed water is the only mechanism for liquid phase transport, reinforcing the importance of transport gas phase convective transport, which has already become dominant by cylinder #27.

Figure 5-12 shows the moisture profiles for the same conditions according to the Bond and Douglas model. The significant difference between the predictions of the two models results from the different treatment of flow, heat and mass transfer within the sheet as explained in section 5.3.3. As noted earlier, both models provide successful machine speed prediction. Thus the improvement from use of improved modeling in the present study relates not to drying rate, for which the differences act in a compensating way, but to internal sheet conditions, for which these differences in modeling provide significant differences in results.

As the temperature profiles on this cylinder resemble those reported for the previous three cylinders, these are not repeated here. The pressure profiles in Figure 5-13 show that the maximum ΔP across the sheet is now 17 kPa, compared to 16 kPa for cylinder #27. The sheet is both drier and hotter in cylinder #33, which are competing effects on the pressure generated. Expansion of the low moisture region adjacent to the CCS edge means that it takes longer for the vapor flux n_v to build up from the a value of zero at position 10, the cylinder surface, to position 7. From position 7 to the vapor

transport edge of the sheet the pressure gradient is seen on Figure 5-13 to be essentially constant. From the analysis of the mass transfer flux profiles of cylinder #27 it is evident that for cylinder #33 the approximately constant pressure gradient from position 7 to the VTS edge corresponds to an approximately constant profile of water vapor flux over this region of the sheet. As the sorbed water fluxes will be even lower on cylinder #33 than was the case on cylinder #27, it is clear that the only effective mechanism for moisture transport is now the convective transport of water vapor.

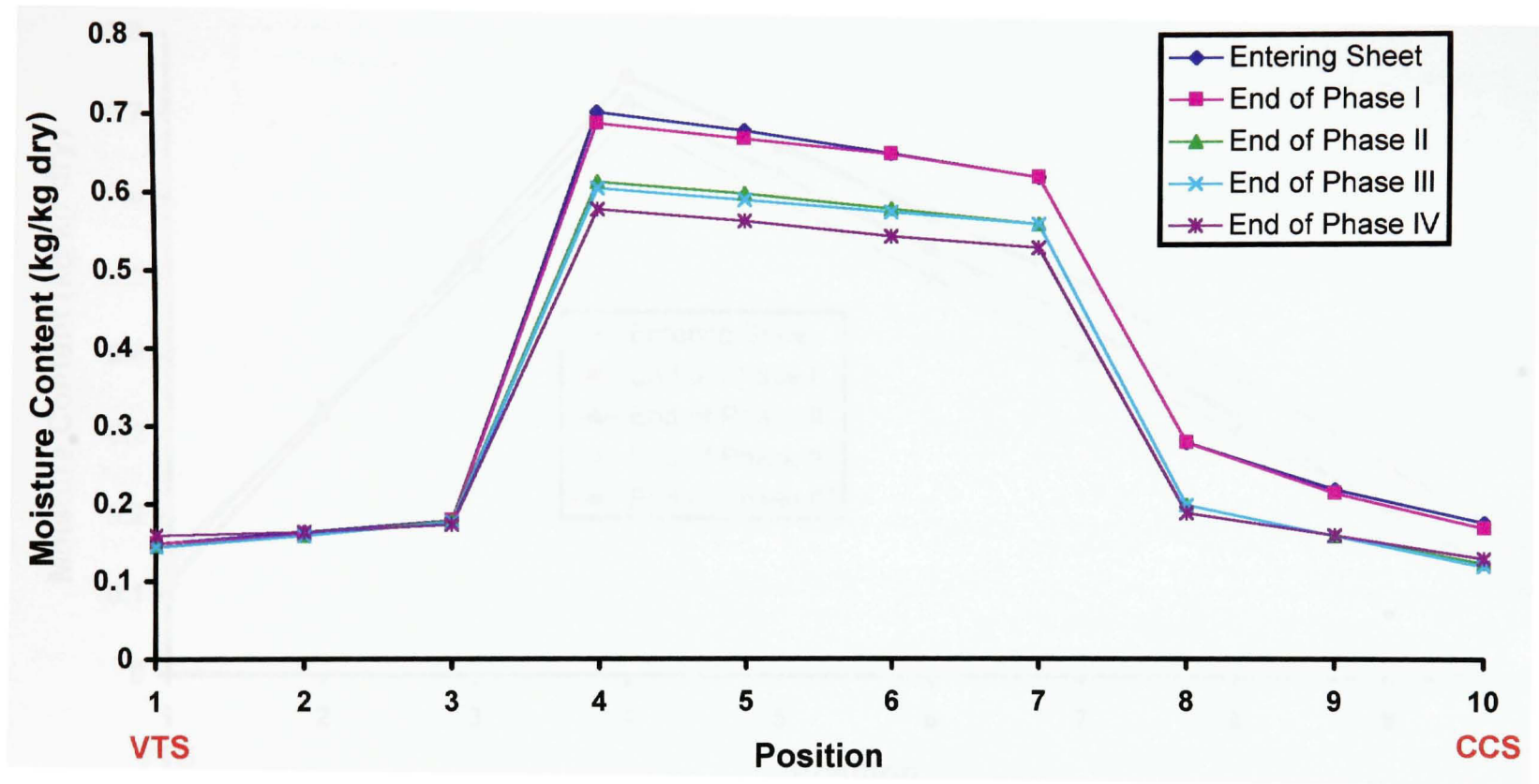


Figure 5-11 Thickness-direction profiles of moisture content
(Red Rock PM#1, 161 g/m², Cylinder #33)

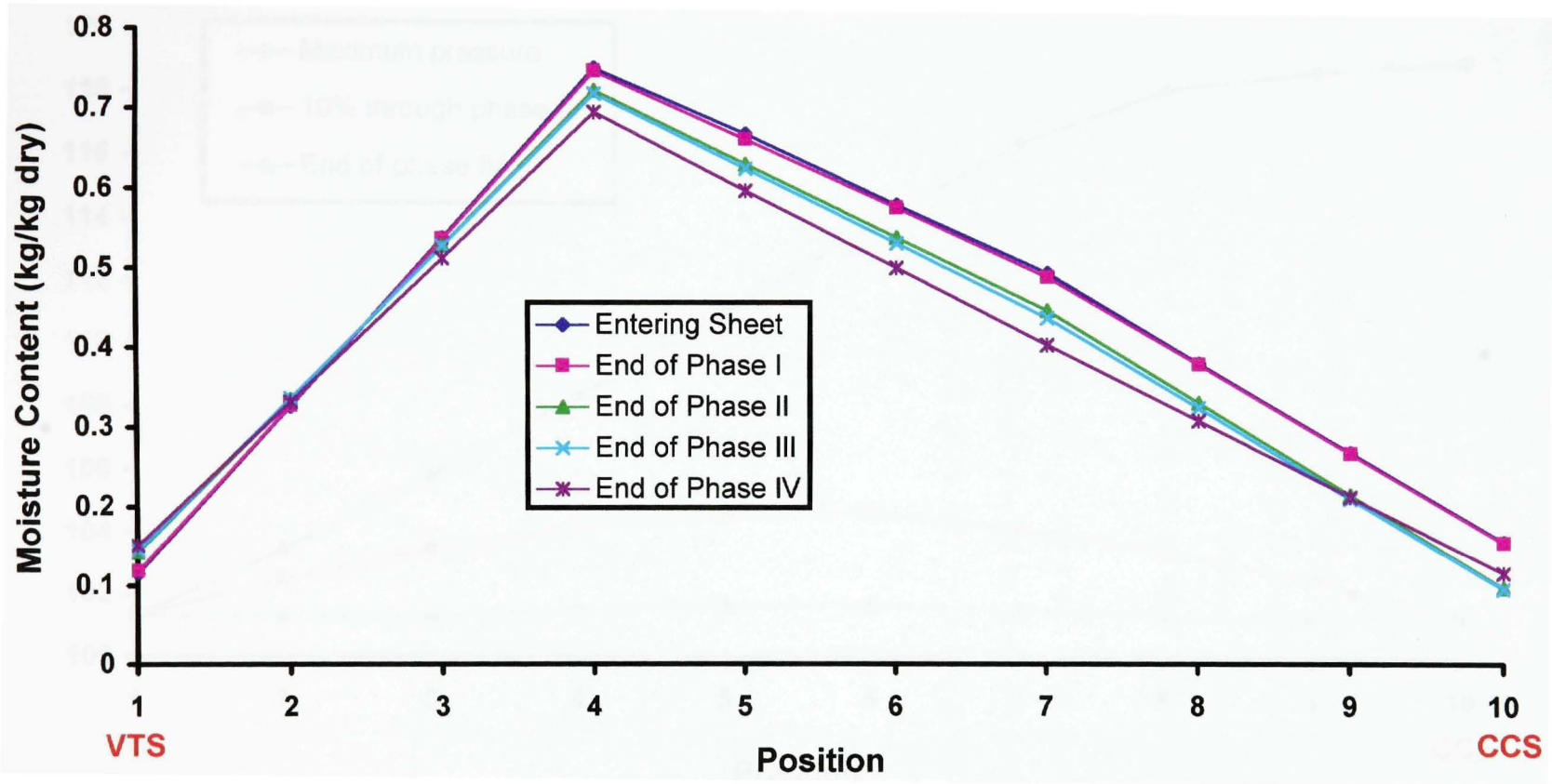


Figure 5-12 Thickness-direction profiles of moisture content, Bond and Douglas (Red Rock PM#1, 161 g/m², Cylinder #33)

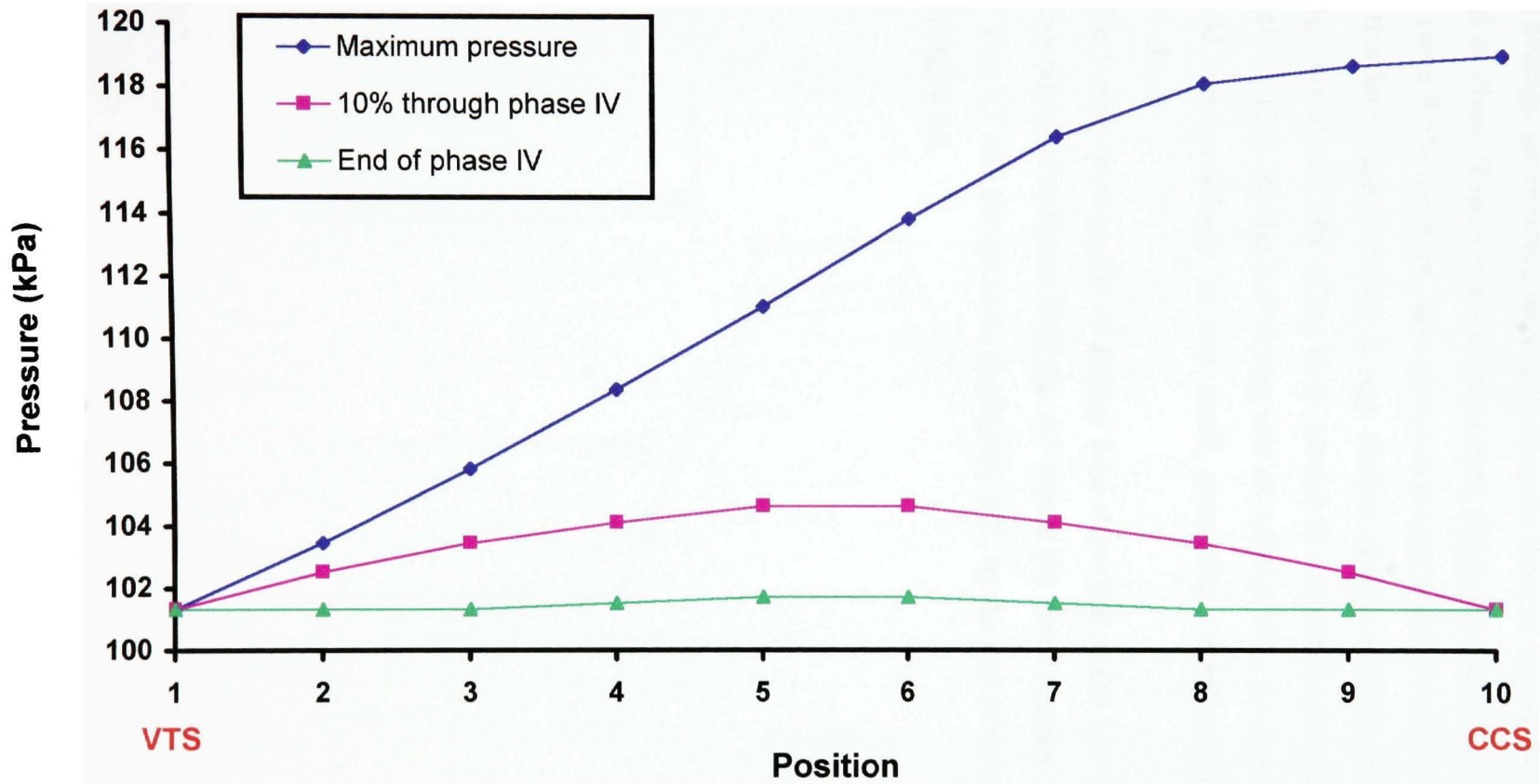


Figure 5-13 Thickness-direction profiles of pressure
 (Red Rock PM#1, 161 g/m², Cylinder #33)

5.3.6 Cylinder #46

The last cylinder to be analyzed, located almost at the end of the 48-cylinder dryer section, reduces the sheet average moisture content only from .095 to .091 kg/kg dry with the sheet average temperature increasing from 88 to 93°C. Figure 5-14 demonstrates that at the end of Phase II the low moisture content plateaus adjacent to the sheet edges, now down to about 8.5% moisture, have grown to occupy about 1/3 of the sheet at each edge. Even at this late stage of drying a very distinct central moisture plateau remains, now occupying only about 10% of the sheet around its centerline and reduced to a moisture level of about 12%. At the low drying rate of cylinder #46, the convective water vapor flux would correspondingly be very small, generating a correspondingly negligible ΔP across the sheet.

The temperature profile of Figure 5-14 show that at the low drying rate and high sheet temperature of cylinder #46, the ΔT across the sheet reaches 14°C at the end of Phase II. This ΔT still decays to be negligible, 3°C, by the end of the open draw of Phase IV of cylinder # 46.

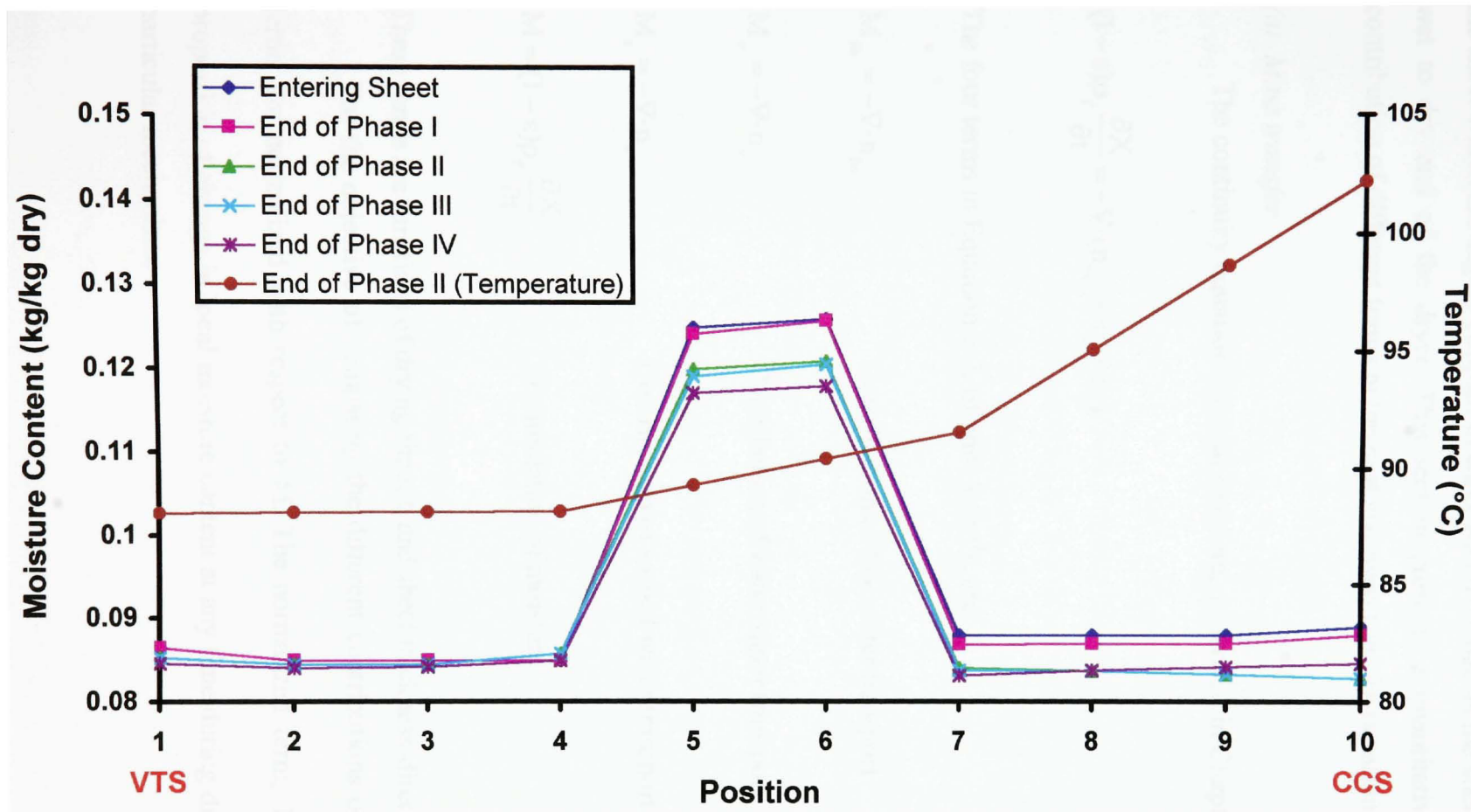


Figure 5-14 Thickness-direction profiles of moisture content and temperature (Red Rock PM#1, 161 g/m², Cylinder #46)

5.3.7 Contribution of different mechanisms to drying

Paper drying involves several mechanisms of flow, heat and mass transfer within the sheet which are highly coupled in ways which change as the sheet progresses from the wet to dry end of the dryer. This section presents a quantitative assessment of the contribution of different terms in the heat and mass transfer equations.

(a) Mass transfer

The continuity equation for total moisture, as derived in Chapter 2, is:

$$(1 - \varepsilon)\rho_f \frac{\partial X}{\partial t} = -\nabla \cdot (n_{fw} + n_v + n_s) \quad (2-7)$$

The four terms in Equation 2-7, of units $\text{kg/m}^3\text{s}$, are:

$$M_{fw} = -\nabla \cdot n_{fw} \quad \text{Contribution of free water transport}$$

$$M_v = -\nabla \cdot n_v \quad \text{Contribution of water vapor transport}$$

$$M_s = -\nabla \cdot n_s \quad \text{Contribution of sorbed water transport}$$

$$M = (1 - \varepsilon)\rho_f \frac{\partial X}{\partial t} \quad \text{Accumulation of moisture}$$

These terms are functions of drying time, t , and sheet thickness-direction position, z .

For the objective of comparing the different contributions of terms, the three M_i terms are normalized with respect to M . The normalized term, $M'_i = \frac{M_i}{M}$, shows the proportion of change in local moisture content at any time during drying resulting from a particular mechanism.

The normalized terms, also functions of drying time and thickness position, are averaged over the full computational domain to provide a comprehensive measure of importance of the relevant term for the entire drying process. A position-time array for each normalized term, M'_i , will have 10 columns for the 10 sheet thickness positions. The number of rows in this array depends on the total drying time and the computational time step used. For this 161 g/m² linerboard case, with drying time 36.4s for its 48 cylinders and a time step of 0.001s, the complete drying model is solved at 36,400 time steps, giving that number of rows for t in the array. Therefore there are available (36400 × 10) = 364,000 values for combinations of t and thickness positions for each of the three normalized terms. The calculation then averages the array for each term to make a direct comparison possible. The contribution of the three mechanisms, the transport of free water, water vapor and sorbed water, depends on whether the local moisture content is above or below the fiber saturation point. Therefore the M'_i terms for which X (z,t) was above the X_{FSP} were averaged together, as were the normalized terms related to the hygroscopic region. The averaging was then performed for each array. The results of these calculations are summarized in Table 5-1.

Table 5-1 Contribution of different mechanisms to mass transfer

Moisture Range	\overline{M}'_s	\overline{M}'_{fw}	\overline{M}'_v
Above X_{FSP}	0%	35%	65%
Below X_{FSP}	6%	0%	94%

The results in Table 5-1 demonstrate the overall importance of transport in the gas phase over the full range of conditions experienced by the sheet during drying. When the moisture content is above the X_{FSP} and the fibers are saturated, there can be no transport of sorbed water, hence the absence there of any contribution from this mechanism. Even for moisture content below X_{FSP} , the sorbed water diffusion mechanism makes a negligible contribution to moisture transport, only 6% over the entire drying process. Although the capillary transport of free water ceases once the moisture content is below the fiber saturation point, Table 5-1 shows that until that point is reached, free water transport contributes a substantial proportion, 35%, to moisture transport. Table 5-1

illustrates the dominance of water vapor transport, which contributes 65% of the moisture transport while the moisture content is above X_{FSP} and 94% for the region with moisture below X_{FSP} .

The results of this section, which provide an overall perspective for the entire dryer, are consistent with and complementary to the results of section 5.3.4 for the detailed analysis at the end of Phase II of drying on cylinder #27, i.e. at $t = 18.95s$ with the profiles of all three flux terms across the 10 thickness-direction positions.

(b) *Heat transfer*

The conservation of energy equation derived in Chapter 2 is:

$$\rho c_p \frac{\partial T}{\partial t} = - \left[(n_l + n_s) c_{pl} + n_v c_{pv} + n_a c_{pa} \right] \cdot \nabla T + \nabla \cdot \left[k_{eff} \cdot \nabla T - (\Delta H_v + H_s) n_v \right] + \nabla (\Delta H_v) \cdot n_v + \nabla H_s \cdot (n_v + n_s) \quad (2-23)$$

Six terms in Equation 2-23, of units J/m^3s , were selected as:

$q_1 = \nabla \cdot (k_{eff} \cdot \nabla T)$	Contribution of conduction
$q_2 = -\nabla \cdot [(\Delta H_v + H_s) n_v]$	Contribution of evaporation-condensation
$q_3 = - \left[(n_l + n_s) c_{pl} + n_v c_{pv} + n_a c_{pa} \right] \cdot \nabla T$	Contribution of convection
$q_4 = \nabla (\Delta H_v) \cdot n_v$	Contribution from convective effect of ΔH_v
$q_5 = \nabla H_s \cdot (n_v + n_s)$	Contribution from convective effect of H_s
$q = \rho c_p \frac{\partial T}{\partial t}$	Accumulation of energy

These terms are a function of drying time and thickness-direction position, exactly as for the analysis of mass transfer presented above. The calculation procedure is therefore identical to that in section (a). All terms are normalized, q'_i , with respect to the corresponding accumulation of energy term q , and the average contribution of each term, \bar{q}'_i , for the entire drying process, 36.4s, is calculated for the basic criterion of moisture content above or below that of X_{FSP} . The results are summarized in Table 5-2.

Table 5-2 Contribution of different mechanisms to heat transfer

Moisture Range	\bar{q}'_1	\bar{q}'_2	\bar{q}'_3	\bar{q}'_4	\bar{q}'_5
Above X_{FSP}	44%	45%	10%	1%	0
Below X_{FSP}	39%	50%	8%	2%	1%

The last two terms, q_4 and q_5 are negligible throughout the drying, demonstrating that the contribution due to the variation of latent heat of vaporization and differential heat of sorption is insignificant compared to the thermal effect of the evaporation-condensation term, q_2 . It is interesting to note that although convection was the dominant mechanism for mass transfer through water vapor transport, the convective contribution to heat transfer, q_3 , is a relatively unimportant mechanism for heat transfer in the sheet. The heat conduction, q_1 , and evaporation-condensation, q_2 , make about the same contribution to the heat transfer, with the heat conduction contribution becoming somewhat less important when the moisture content is below X_{FSP} . The results of Table 5-2 show that the thermal effect of the addition or deletion of the latent heat of vaporization for free water and differential heat of sorption for sorbed water is sufficiently large to overshadow all other terms except the conduction term.

(c) Summary

To complement the analysis of sections 5.3.1 to 5.3.6 which provide thickness-direction profiles of the properties and moisture transport fluxes across the sheet at various points in the evolution of drying from the wet to dry end, section 5.3.7 provides a comprehensive measure of the importance over the entire drying process of the contribution to the drying process from different terms in the heat and mass balance

equations. The computational domain includes the ten positions in the sheet thickness direction and the total drying time of 36.4s for drying 161 g/m² linerboard. This domain was segregated according to whether the local moisture content is above or below the fiber saturation point because the presence or absence of free water in the interfiber pores is fundamental to the transport mechanisms. For moisture transport the results demonstrate the insignificance of sorbed water transport, the substantial importance of free water capillary transport for the moisture region above the fiber saturation point, and the dominant contribution of water vapor convective transport. For heat transfer through the sheet two terms were found to be negligible while the convective mechanism contribution to heat transfer was found to be only minimal. The thermal effects associated with the evaporation or condensation of water were found to be dominant for the range of moisture content below the fiber saturation point while carrying equal weight as heat transfer by conduction for moisture content out of the hygroscopic region. Thus the analysis of section 5.3.7 shows that there are significant differences in the relative importance of various transport mechanisms between the case for moisture transport and heat transfer in the sheet.

CHAPTER 6

CONCLUSIONS

6.1 Contributions to knowledge

1. A comprehensive microscale model of transport phenomena within the sheet during paper drying was developed. Unlike other models presented to date, no simplifying assumptions were made regarding the main species contributing to the drying process or the key mechanisms of flow, heat and mass transfer relevant to drying. The model includes five species (free water, sorbed water, water vapor, air and fibers) in three phases (liquid, gas and solid). Capillary transport of free water, diffusion of sorbed water and convective-diffusive transport of water vapor were included.
2. The distribution of water at different stages of the drying process was clearly defined, based not only on thermodynamic properties but also on principles of transport phenomena. The hygroscopic behavior of paper, seldom fully treated in drying models, was fully incorporated into the model by inclusion of the terms related to the vapor pressure reduction, the differential heat of sorption and the structural changes of paper associated with sorbed water removal.
3. This microscale model treating the transport phenomena in the sheet thickness direction is applicable to all paper grades, from tissue to heavy linerboard. The model is also able to use all the boundary conditions related to industrial hot surface cylinder drying, air impingement drying, or hybrid drying (combinations of cylinder and impingement drying,).
4. The great uncertainty associated with the five key transport properties required by the model (liquid and gas relative permeability, paper thermal conductivity, water vapor diffusivity and sorbed water diffusivity) was investigated. All the theoretical and experimental sources for these five properties were analyzed and the two best bases for each property were identified. A rigorous sensitivity analysis including 320 simulations using 32 industrial dryer surveys enabled the optimal choice of these five transport properties. Such a complete and rigorous determination of the effect of transport properties on a paper drying model has not previously been reported.

5. The most comprehensive industrial validation of a paper drying model with this level of complexity was performed. The 32 dryer surveys used cover all the commercially important grades, from tissue and toweling to fine paper to linerboard, being dried by a variety of drying techniques. Two types of simulations, machine speed prediction and exit moisture prediction, were carried out. The average machine speed prediction error for the 32 uncalibrated validations was only +2.6%. Model predictions were also satisfactorily compared to other occasionally available parameters such as sheet and cylinder surface temperature or sheet average moisture content at locations other than the entrance and exit of the dryer section. For the prediction of moisture content and temperature within the sheet, measurements which are impossible to make for an industrial dryer, good agreement was obtained with such determinations made earlier for the laboratory drying of 3-ply linerboard in a high intensity air impingement dryer.
6. The present model made major improvements over the performance of the first McGill dryer simulator. Systematic under-estimation of sheet temperature by the previous simulator is eliminated. Also, an industrial case with exceptionally low moisture content was successfully analyzed using the present model while the first simulator was unable to run a speed prediction simulation for this case. This improvement is attributed to the better treatment in the present model of transport phenomena and the hygroscopic behavior of paper.
7. Thickness-direction profiles of moisture content, temperature and gas pressure were demonstrated for all phases of an industrial case of linerboard drying. Development of a central high moisture plateau and two low moisture plateaus close to the edges of the sheet was demonstrated to be a fundamental characteristic of two-tier cylinder drying.
8. Thickness-direction profiles of mass fluxes for free water, water vapor and sorbed water were determined for a representative dryer cylinder chosen to have the moisture content in the central plateau above the fiber saturation point while the edge regions of the sheet were in the hygroscopic region. The interaction of three mechanisms of moisture transport within the sheet at various stages of drying were thereby analyzed for the first time. The convective transport of water vapor was found to be the

dominant mechanism for moisture transport while the contribution of sorbed water diffusion was shown to be negligible. Capillary transport of free water through the interfiber pores plays a significant role while the local moisture content is above that which defines the hygroscopic region.

9. To assess the relative contribution of the various mechanisms to flow, heat and mass transfer during drying, the numerical values of 4 terms in the moisture conservation equation and 5 terms in the energy balance equation were calculated for the entire computational domain for a linerboard dryer. The results were segregated for local regions with and without free water in the interfiber pores. By averaging the normalized terms it was possible to quantify for the entire dryer the relative importance in local change of moisture content or temperature which derives from particular mass or heat transfer mechanisms. For mass transfer, water vapor convective transport in the gas phase was found to be dominant when the moisture content is below the fiber saturation point and to make a larger contribution to mass transfer than free water capillary transport at moisture contents above the hygroscopic region. As for heat transfer, the thermal effects associated with evaporation or condensation of free water and sorbed water, as well as the contribution of conduction were found to overshadow all other terms. This analysis, not previously reported, provides unique insight into the complex dynamics of transport phenomena during the drying of paper.

6.2 Suggestions for future work

1. Addition of the ability to treat drying technologies other than cylinder drying and air impingement drying is a logical next step. The present treatment of transport phenomena within the sheet is able, or would be able with modifications, to treat technologies such as IR drying or through drying.
2. Better experimental and/or theoretical work is needed to address the enormous uncertainty of the transport properties. Furnish dependency of most properties is not well established.

3. The treatment of external systems could be improved. Parameters such as the effect of the felt on heat and mass transfer coefficients are not fully investigated. The cylinder-sheet contact coefficient is expressed as a function only of moisture content in the present model while other parameters such as felt tension and sheet temperature could affect the contact coefficient.
4. Thermodynamic properties of moist paper in the hygroscopic region play an important role when the final moisture content is extremely low, as happens often when a size press or coater is installed after the main dryer section. Better determination of these properties would improve the accuracy of the model predictions for these industrially important cases.
5. The treatment of structural changes of paper during drying could be improved. While the current treatment served its purpose, different grades of paper would have different behaviors in terms of the variation of sheet thickness and porosity during drying. Experimental work could establish the furnish dependency of the structural parameters.
6. Establishing a quantitative link to paper quality and properties from the thickness-direction profiles of moisture content and temperature developed in this work could have great potential through enabling papermakers to optimize the drying operation to achieve both high productivity and the best product quality.

REFERENCES

- Abbott, R.D., Edwards, L.L., Fischer, F.B. and Dimond, P.M., 1984, Linerboard Drying: Model Development and Heat Transfer Coefficient Determination, Proc. Tappi Engineering Conference, pp.241-252
- Ahlen, A.T., 1970, Diffusion of Sorbed Water Vapor Through Paper and Cellulose Fiber, Tappi Journal, Vol. 53, No. 7, pp. 1320-1326
- Ahrens, F. and Journeaux, I., 1984, An Experimental and Analytical Investigation of a Thermally Induced Vacuum Drying Process for Permeable Mats, Drying '84, Proceedings of 4th International Drying Symposium, Kyoto, Japan, A.S. Mujumdar. Ed., Hemisphere Publishing Corp., Washington, DC, pp. 281-291
- Asensio, M.C., 2000, Transport Phenomena During Drying of Deformable Hygroscopic Porous Media: Fundamentals and Application, Ph.D. Thesis, Texas A&M University, College Station, TX
- Asensio, M.C., Seyed-Yagoobi, J., Ng, K.H. AND Fletcher, L.S., 1991, Thermal Contact Conductance of a Paper Handsheet/Metal Interface, ME-CHTL-90-6698, Texas A&M University, College Station, TX
- Asensio, M.C. and Seyed-Yagoobi, J., 1992, Further Analysis of Heat and Mass Transfer in a Paper Sheet During Drying, HTD, Vol. 193, ASME National Heat Transfer Conference, San Diego
- Asensio, M.C. and Seyed-Yagoobi, J., 1992, Theoretical Drying Study of Single-tier vs. Two-tiered Dryer Configurations, Tappi Journal 75(10), pp.203-211
- Asensio, M.C. and Seyed-Yagoobi, J., 1994, Simulation of Paper Drying Systems with Incorporation of an Experimental Drum/Paper Thermal Contact Conductance Relationship, Transactions of ASME – Journal of Energy Resources, Vol. 115, No. 4, pp. 291-300
- Asensio, M.C., Seyed-Yagoobi, J., Lehtinen, J.A., Karlsson, M.A., Timofeev, O.N. and Kuppi, K., 1994, Comparison of Several Multi-Cylinder Paper Drying Simulation Models, Drying '94, Hemisphere Publishing Corporation, pp. 1171-1178
- Azizi, S., Moyne, C. and Degiovanni, A., 1988, Approach experimentale et theorique de la conductivite thermique des millieux poruex humides – I. Experimentation, International Journal of Heat and Mass Transfer, Vol. 31, No. 11, pp. 2305-2317
- Bass, D.M., 1987, Properties of Reservoir Rocks, Petroleum Engineering Handbook, H.B. Bradley, ed., Society of Petroleum Engineers, Richardson, TX, pp. 693-749

- Bear, J., 1972, *Dynamics of Fluids in Porous Media*, American Elsevier, New York
- Bell, D.O., Seyed-Yagoobi, J. and Fletcher, L.S., 1990, *Recent Developments in Paper Drying*, *Advances in Drying Vol.5*, Hemisphere Publishing Corporation, pp. 203-261
- Bird, R.B., Stewart, W.E. and Lightfoot, E.N., 2002, *Transport Phenomena*, John Wiley and Sons, New York, 780 pp.
- Bliesner, W.C., 1964, *A Study of Porous Structures of Fibrous Sheets Using Permeability Techniques*, *Tappi Journal*, Vol. 47, No. 7, pp. 392-400
- Bond, J.F., 1991, *Drying Paper by Impinging Jets of Superheated Steam: Drying Rates and Thermodynamic Cycles*, Ph.D. Thesis, McGill University, Montreal, 175pp.
- Bond, J.F., Crotigino, M.H. and Douglas, W.J.M., 1992, *An Experimental Study of the Falling Rate Period of Super Heated Steam Impingement Drying of Paper*, *Drying Technology* 10(4), pp. 961-977
- Bond, J.F., Gomes, V.G. and Douglas, W.J.M., 1996, *Computer Simulation of Drying Paper by Multiple Techniques*, *Pulp & Paper Canada* 97(12), pp. 110-112
- Bond, J.F., and Douglas, W.J.M., 1997, *Drying of Heavy Paper Products by Impinging Jets of Air or Superheated Steam, Part I: Experimental Results*
- Brooks, R.H. and Corey, A.T., 1966, *Properties of Porous Media Affecting Fluid Flow*, *Journal of the Irrigation and Drainage Divisions, ASCE*, Vol. 92, No. IR 2, pp. 61-88
- Brunauer, S., *Journal of the American Chemistry Society*, Vol. 62, p. 1723
- Burdine, N.T., 1953, *Relative Permeability Calculations from Pore-Size Distribution Data*, *Transactions of AIME*, Vol. 198, pp. 71-77
- Carey, V.P., 1992, *Liquid-Vapor Phase Change Phenomena*, Hemisphere Publishing Corp., Washington, DC, 645 PP.
- Carman, P.C., 1937, *Transactions of the Institution of Chemical Engineers (London)*, Vol. 15, pp. 150-166
- Chiogioji, M.H., 1979, *Industrial Energy Conservation*, Marcel Dekker, New York
- Corte, H., 1982, *Handbook of Paper Science, Volume 2: The structure and Physical Properties of Paper – Chapter 6: The Porosity of Paper*, edited by H.F. Rance, Elsevier Scientific Publishing Company, pp. 1-70

Coumans, W.J. and Kruf, W.M.A., 1995, Mechanistic and Lump Approach of Internal Transport Phenomena During Drying of Paper Sheets, *Drying Technology*, Vol. 13, No. 4, pp. 985-998

Cunningham, R.E. and Williams, R.J.J., 1980, *Diffusion in Gases and Porous media*, Plenum Press, New York, 275 pp.

Darcy, H., 1856, *Les Fontaines Publiques de la Ville de Dijon*, Victor Dalmont, Paris, 647 pp.

Degiovanni, A. and Moyne, C., 1987, Conductivite thermique des materiaux poreux humides: evaluation theorique et possibilite de mesure, *International Journal of Heat and Mass Transfer*, Vol. 30, No. 11, pp. 2225-2245

Depoy, J.A., 1972, Analog Computer Simulation of Paper Drying: A Workable Model, *Pulp and Paper Magazine of Canada* 73(5), pp. 67-74

DeVries, D.A., 1958, Simultaneous Transfer of Heat and Moisture in Porous Media, *Transactions of the American Geophysical Union*, Vol. 39, pp. 909-916

Deshpande, R.D. and Pulkowski, J.H., 1992, Effects of Operating Parameters on Dryer Performance, *Proceedings of Tappi Engineering Conference*, Book 2, pp. 639-654

Dreshfield, A.C., 1956, The Drying of Paper, *Tappi Journal*, Vol. 39, No. 7, pp. 449-455

Donner, B.C. and Renk, F.J., 1982, Evaluation and Improvement of Individual Dryer Performance, *Proc. Tappi Papermakers Conference*, pp. 227-236

Dullien, F.A., 1992, *Porous Media: Fluid Transport and Pore Structure*, Academic Press, San Diego, 574 pp.

Eskelinen, P.J., 1985, How to Improve the Paper Machine Performance by Combining Dryer Section Survey and Computer Simulation, *Drying Technology* 3(2), pp.255-269

Farell, M., Dragu, J., Pannersleven, M., Bond, J.F., Douglas, W.J.M. and Kerr, R.B., Accepted for publication in CPPA January, 1999, *Integrated Pressing and Drying Simulation of PM7*, Domtar, Windsor

Fralic, G., Guertin, D. and Glendenning, S., *Computer-Aided Optimization of Company-Wide Drying Operations*, Pulp and Paper Design Project, McGill University, April 1996

Fralic, G., Glendenning, S., Guertin, D., Kerr, R.B., Bond, J.F. and Douglas, W.J.M., 1997, *Computer Aided Engineering of Paper Machine Dryer Sections at Kruger's Bromptonville Mill*, TAPPI Conference

Geankoplis, C.J., 1993, *Transport Processes and Unit Operations*, 3rd ed., Prentice Hall, Englewood Cliffs, NJ, 921 pp.

- Gong, L. and Plumb, O.A., 1994, The Effects of Heterogeneity on Wood Drying, Part I: Model Development and Predictions, *Drying Technology*, Vol. 12, No. 8, pp. 1983-2001
- Han, S.T., 1970, Drying of Paper, *Tappi Journal*, Vol. 53, No. 6, pp. 1034-1046
- Han, S.T. and Matters, J.F., 1966, Vapor Transport in Fiber Mats During Drying
- Harrmann, M. and Schulz, S., 1990, Convective Drying of Paper Calculated with a New Model of the Paper Structure, *Drying Technology*, Vol. 8, No. 4, pp. 667-703
- Hartley, F.T. and Richards, R.J., 1974, Hot Surface Drying of Paper - The Development of a Diffusion Model, *Tappi* 57(3), pp. 157-160
- Hashemi, S.J., 1996, Through drying of machine formed paper and drying nonuniformity, Ph.D. Thesis, McGill University, Montreal
- Hashemi, S.J., Gomes, V.G. and Douglas, W.J.M., 2002, Air permeability and pressure drop for moist machine formed paper, *Progress in Paper Physics Seminar*, Syracuse, 12 pp.
- Heikkilä, P. and Karlsson, M., 1988, Experience Gained from Dryer Section Surveys, *Paperi ja Puu* 70(8), pp. 684-687
- Hinds, J.A. and Neogi, A.N., 1983, The Dynamic Computer Simulation of a Paper Machine Dryer, *Tappi Journal* 66(6), pp. 79-82
- Hubbert, M.K., 1956, Darcy's Law and the Field Equations of the Flow of Underground Fluids, *Transactions of AIME*, Vol. 207, TP 4352, pp. 222-239
- Iida, K., 1985, The Computer Simulation of Web Drying in a Paper Machine Dryer Section, *Preprints Japanese Tappi/CPA Pulp and Paper Technology Conference*, Tokyo, pp. 115-127
- Incropera, F.P. and Dewitt, D.P., 1985, *Fundamentals of Heat and Mass Transfer*, 2nd ed., John Wiley and Sons, New York
- Ingmanson, W.L., Andrews, B.D. and Johnson, R.C., 1959, Internal Pressure Distributions in Compressible Mats Under Fluid Stress, *Tappi Journal*, Vol. 42, No. 10, pp. 840-849
- Karlsson, K. and Soininen, M., 1982, The Influence of the Hygroscopic Properties of Paper on the Transient Phenomena During Contact Drying of Paper Webs, *Proc. 3rd International Drying Symposium*, Vol.1, pp.494-503
- Karlsson, K. and Paltakari, J., 1992, A Simulation Model for Paper Machine Dryer Section, *Drying '92*, Elsevier Science Publishers, pp.913-923

- Karlsson, M.A. and Timofeev, O.N., 1994, The Computer Simulation of a Multi-Cylinder Dryer with Single-Tier Configuration, Proceedings of Fifth International Symposium on Process Systems Engineering, Kyongju, Korea, June, pp. 332-340
- Karlsson, M.A., Soininen, M., Paltakari, J. and Paulapuro, H., 1992, A Simulation Model for Board and Paper Machine Dryer Section, Heat and Mass Transfer in Pulp and Paper Processing, American Society of Mechanical Engineers Winter Annual Meeting, HTD-Vol. 238, pp. 9-16
- Kartovaara, I., Rajala, R., Luukkala, M. and Sipi, K., 1985, Conduction of Heat in Paper, Papermaking Raw Materials: Transactions of the Eighth Fundamental Research Symposium, Vol. 1, Oxford, September, pp. 381-412
- Kaviany, M., 1991, Principles of Heat Transfer in Porous Media, Springer-Verlag, New York, 625 pp.
- Kerekes, R.J., 1980, A Simple Method for Determining the Thermal Conductivity and Contact Resistance of Paper, Tappi Journal, Vol. 63, No. 9, pp. 137-140
- Kerekes, R.J. and McDonald, J.D., 1991, A Decreasing Permeability Model of Wet Pressing: Theory, Tappi Journal, Vol. 74, No. 12, pp. 105-156
- Kiiskinen, H. and Retulainen, E., 1995, Simulation of Papermaking Processes, Technical Research Centre of Finland
- Kirk, L.A., 1980, Digital Simulation of the Effect of Operating and Design Variables on the Dryer Section of a Paper Machine, Paper Technology and Industry 21(2), pp.61-71
- Kirk, L.A., 1984, A Literature Review of Computer Simulation of Paper Drying, Advances in Drying Vol.3, Hemisphere Publishing Corporation, New York, pp.1-37
- Kirk, L.A. and Tatlicibasi, C., 1972, Measurements of Thermal Conductivity of Paper by a Heat Pulse Method, Tappi Journal, Vol. 55, No. 12, pp. 1697-1972
- Klinkenberg, L.J., 1941, The Permeability of Porous Media to Liquids and Gases, API Drill Production Practice, pp. 200-213
- Knight, R.L.C and Kirk, L.A., 1975, Simulation of the Papermachine Drying Section, Proc. International Water Removal Symposium, London, pp. 276-278
- Krischer, O., 1962, Die wissenschaftlichen Grundlagen der Trocknungstechnik, 2nd ed., Sringer-Verlog, New York
- Kobari, M., Shimizu, Y., Endo, M. and Inazumi, H., 1985, Contact Drying of Fibrous Sheet Material, Ind. Eng. Chem. Process Des. Dev., Vol. 24, No. 1, pp. 188-194
- Kozeny, J., 1927, Akad. Wiss. Wien., Math-Nat. KL. 36 (Abt IIa), pp. 271-206

Kuhasalo, A., 1995, Challenges Set by High Speed On Dryer Section, PaperAge, December, pp.16-19

Lampinen, M.J., 1979, Mechanisms and Thermodynamics of Drying, Acta Polytechnica Scandinavica, Mechanical Engineering Series No. 77 (technical publication from Helsinki University of Technology), Helsinki, Finland

Lampinen, M.J. and Toivonen, K., 1984, Application of a Thermodynamic Theory to Determine Capillary Pressure and other Fundamental Material Properties Affecting the Drying Process, Drying '84, Hemisphere Publishing Corporation, pp. 228-244

Lampinen, M.J. and Ojala, K.T., 1993, Mathematical Modeling of Web Drying, Advances in Transport Processes, Elsevier Publishers, New York, pp. 1-77

Lau, Y.L. and Prattes, B.D., 1969, Measurements of Thermal Conductivity of Wet Paper, NRC, Divisions of Mechanical Engineering, Report No. LTR-HY-8

Lee, P.F. and Hinds, J.A., 1980, Measurement of Heat and Mass Transport within a Sheet of Papermaking Fibers During Drying, Drying '80, Hemisphere Publishing Corporation, pp. 523-528

Lee, P.F. and Hinds, J.A., 1981, Modeling Heat and Mass Transfer Within a Moist Sheet of Paper or Board, Tappi 64(12), pp.39-44

Lehtikoski, O.I., 1970, A Mathematical Model of the Dryer Section, Paperi ja Puu 52(2), pp.63-72

Lehtinen, J.A., 1982, Some Theoretical aspects Regarding the Basic Process and the Energy Economics of the Convac Drying Process for Paper and Board, Proceedings of 3rd International Drying Symposium, Birmingham, England, A.S. Mujumdar, ed., McGraw-Hill, NEW York, Vol. 2, pp. 382-394

Lehtinen, J.A., 1986, Some Structural Effects on the Diffusional and Fluid Flow Frictional Resistance of Paper Webs Undergoing Hot-Surface Drying, Drying 86, proceedings of the 5th International Drying Symposium, Cambridge, England, A.S. Mujumdar, ed., Hemisphere Publishing Corp., Washington, D.C., Vol. 1, pp. 332-340

Lehtinen, J.A., 1989, On the Theory of Intraweb Heat Transfer and Vapor Exhaust Flow in Hot Surface Paper Drying, Proceedings of the 1989 Tappi Engineering Conference, pp. 341-355

Lehtinen, J.A., 1990a, Paper Machine Drying: A Continuing Demand for Improvements in Web Properties, Runnability, and Energy Usage Causes Efforts for Basic Studies. Simulation and Experiments, Keynote Address, 2nd International Pira Conference, Modern Technologies in Pressing and Drying, Bournemouth, UK

Lehtinen, J.A., 1990b, On the Theory of Thermocapillary, or Marangoni, Convection in the Capillary Water on Paper Fibers, Tappi Journal, Vol. 73, No. 4m pp. 210-213

Lemaitre, A., Veyre, J., Lebeau, B. and Foulard, C., 1980, Case Study: Method for Systemic Analysis of Paper Machine Multi-cylinder Drying Section, Preprints 4th IFAC Instrumentation and Automation Conference, Ghent, Belgium, pp.261-270

Lin, S.H., 1991, Moisture Adsorption in Cellulosic Materials, Ind. Eng. Chem. Res, 30, pp.1833-1836

Lindsay, J.D. and Brady, P.H., 1993a, Studies of Anisotropic Permeability with Application to Water Removal in Fibrous Webs, Part 1: Experimental Methods, Sheet Anisotropy and Relationships to Freeness, Tappi Journal, Vol. 76, No. 9, pp. 119-127

Lindsay, J.D. and Brady, P.H., 1993a, Studies of Anisotropic Permeability with Application to Water Removal in Fibrous Webs, Part 2: Water Removal and Other Factors Affecting Permeability, Tappi Journal, Vol. 76, No. 11, pp. 167-174

Marle, C.M., 1981, Multiphase Flow in Porous Media, Gulf Publishing Company, Houston, TX, 257 pp.

Martin, H., 1977, Heat and Mass Transfer Between Impinging Gas Jets and Surfaces, Adv. Heat Transfer, vol. 13, Academic Press, pp.1-80

Mills, A.F., 1992, Heat Transfer, Richard D. Irwin, Inc., New York

Nault, G. and Maltais, D., 1997, Application of an on-line expert system to optimize dryers and press sections at Domtar Windsor, Pulp and Paper Canada , pp.111-113

Navarri, S., 1992, Mechanisms of Moisture Diffusion in Porous Media, Journal of Colloid and Interface Science, 154(2), pp.305-315

Nederveen, C.J., Van Schaik, A.L. and Dijkstra, J.J.F.M., 1991, Present Theories on Multi-Cylinder Paper Drying, proceedings of Helsinki Symposium on Alternate Methods of Pulp and Paper Drying, Helsinki, Finland, pp. 23-41

Nederveen, C.J. and Finken, J.G.M., 1992, Thermal Conductivity Measurements on Wet Paper Samples at High Temperature, Drying Technology, Vol. 11, No. 1, pp. 189-198

Nelson, R.M., 1986, Diffusion of Bound Water in Wood, Part 3; A Model for Non-isothermal Diffusion, Wood Science and Technology, Vol. 20, pp. 309-328

Niemenmaa, A., Lappalainen, J., Juslin, K. and Laukkanen, I., 1996, Dynamic Modeling and Simulation of Paper Machine Drying Section, Drying '96 Vol. B, Hemisphere Publishing Corporation, pp.1157-1164

- Nilsson, L., 1996, Some Studies of the Transport Coefficients of Pulp and Paper, Ph.D. Thesis, University of Lund, Lund, Sweden
- Nilsson, L., Wilhelmsson, B. and Stenström, S., 1993, The Diffusion of Water Vapor Through Pulp and Paper, *Drying Technology*, Vol. 11, No. 6, pp. 1205-1225
- Nissan, A.H. and Kaye, W.G., 1955, An Analytical Approach to the Problem of Drying of Thin Fibrous Sheets on Multi-cylinder Machines, *Tappi* 38(7), pp. 385-398
- Nissan, A.H. and Hansen, D., 1960, Heat and Mass Transfer Transients in Cylinder Drying: Part I. Unfelted Cylinders, *AIChE Journal* 6(4), pp.606-611
- Nissan, A.H. and George, H.H., 1961, Heat and Mass Transfer Transients in Cylinder Drying: Part II. Felted Cylinders, *AIChE Journal* 7(4), pp.635-641
- Pakowski, Z., Bartczak, Z., Strumillo, C. and Stenström, S., 1991, Evaluation of equations Approximating Thermodynamic and Transport Properties of Water, Steam and Air for Use in CAD of Drying Processes, *Drying Technology*, Vol. 9, No. 3, pp. 753-773
- Pang, S., Langrish, T.A.G. and Keey, R.B., 1994, Moisture Movement in Softwood Timber at Elevated Temperature, *Drying Technology*, Vol. 12, No. 8, pp. 1897-1914
- Pearson, D.R., 1986, Modeling Paper Machine Drying on a Microcomputer, *Tappi Journal* 69(9), pp.194-495
- Pei, D. and Chen, P., 1989, A Mathematical Model of the Drying Process, *International Journal of Heat and Mass Transfer*, Vol. 32, No. 2, pp. 297-310
- Peel, J.D., 1999, Paper Science and Paper Manufacture, Angus Wilde Publications Inc., Vancouver, Canada
- Perre, P. and Turner, I., 1997, The Use of Macroscopic Equations to Simulate Heat and Mass Transfer in Porous Media, *Mathematical Modeling and Numerical Techniques in Drying Technology*, I. Turner and A.S. Mujumdar, eds., Marcel Dekker, New York, pp. 1-82
- Persson, H. and Stenström, S., 1996, Possibilities for Capacity Increase in Dryer Limited Paperboard Machines, *International Dryer Symposium 1996*, Krakow. Poland
- Phillip, J.R. and DeVries, D.A., 1957, Moisture Movement in Porous Materials Under Temperature Gradients, *Trans. Am. Geophys. Union*, Vol. 38, No. 2, pp. 222-232
- Polat, O. and Mujumdar, A.S., 1987, Drying of Pulp and Paper, *Handbook of Industrial Drying*, A. Mujumdar, ed., Marcel Dekker, New York, pp. 643-682

- Polat, O., Crotagino, R.H., van Heiningen, A.R. and Douglas, W.J.M., 1993, Permeability and Specific Surface of Paper, *Journal of Pulp and Paper Science*, Vol. 19, No. 4, pp. J137-J142
- Powell, T. and Strong, A.B., 1974, An analysis of Drying on Conventional Paper Machines, *Pulp and Paper Magazine of Canada* 75(3), pp.71-78
- Prahl, J.M., 1968, Paper Fiber and Water Mixtures, Ph.D. Thesis, Harvard University, Cambridge, MA
- Ramaswamy, S., 1990, Analysis of Heat and Mass Transfer During Drying of Paper/Board Under Conventional and High-intensity Conditions, Ph.D. Thesis, State University of New York, Syracuse, pp. 201
- Reardon, S.A., 1994, A Mathematical Model for the Simulation of Paper Drying Energy Consumption, Ph.D. Thesis, University of Tasmania, Tasmania, Australia
- Reese, R., 1988, Revised TAPPI Drying-Rate Curves, *Tappi Dec. 1988*, pp. 231-233
- Rhodus, D. and Göttsching, L., 1979, Der Trocknungsverlauf von Papier und Pappe in Abhängigkeit von trocknungstechnischen und papiertechnologischen Parametern. Teil IV: Trocknung in der Mehrzylinder-Trockenpartie, *Das Papier* 33(1), pp. 1-9
- Robertson, A.A., 1963, The Physical Properties of Wet Webs, *Svensk Papperstidning*, Vol. 66, No. 12, pp. 477-497
- Robinson, G.W.F., and Baker, C.D., 1989, Understanding and Troubleshooting Papermachine Dryer Sections, CPPA Publication, pp.1.13-1.24
- Salama, S.Y., Minsker, B.S. and Olsen, K.G., 1987, Competitive Positions of Natural Gas: Industrial Solids Drying, Energy and Environmental Analysis, Inc., Arlington, VA
- Siau, J.F., 1971, *Flow in Wood*, Syracuse University Press, New York
- Siau, J.F., 1984, *Transport Processes in Wood*, Springer-Verlag, New York
- Siau, J.F. and Babiak, M., 1983, Experiments on Non-isothermal Moisture Movement in Wood, *Wood Fiber Science*, Vol. 15, No. 1, pp. 40-46
- Sidwall, S., Sadeghi, M. and Douglas, W.J.M., 1999a, Comparative Structures for Simulation of Paper Drying. *Proceedings, 1999 Tappi Engineering Conference, Anaheim*: pp. 239-270
- Sidwall, S., Bond, J.F. and Douglas, W.J.M., 1999b, Industrial Validation of a Multiple Technique Paper Drying Simulator, *Proceedings, 1999 Tappi Engineering Conference, Anaheim*: pp. 271-301

- Skaar, C., 1988, Wood-Water Relations, Springer-Verlag, New York
- Slattery, J.C., 1972, Momentum, Energy and Mass Transfer in Continua, McGraw-Hill, New York
- Snow, R.H., 1980, Computer Modeling of Drying in Paperboard Machines, Proceedings of the Tappi Annual Meeting, Atlanta, pp.243-258
- Spolek, G.A. and Plumb, O.A., 1980, A Numerical Model of Heat and Mass Transport in Wood During Drying, Proceedings of 2nd International Drying Symposium, Montreal, Canada, A.S. Mujumdar, ed., Vol. II, pp. 84-92
- Stanish, M.A., Schajer, G.S. and Kayihan, F., 1986, A Mathematical Model of Drying for Hygroscopic Porous Media, AIChE Journal, Vol. 32, No. 8, pp. 1301-1311
- Stenström, S., 1997, Mathematical Modeling and Numerical Techniques for Multi-Cylinder Paper Dryers, Mathematical Modeling and Numerical Techniques in Drying Technology, Marcel Dekker Inc., pp.613-661
- Stenström, S., Wilhelmsson, B., Nilsson, L., Krook, R. and Wimmerstedt, R., 1994, Measurement of Reference Experimental Data for the Multi-Cylinder Paper Dryer, Drying '94, Hemisphere Publishing Corporation, pp. 1179-1186
- Storat, R.E., 1993, The U.S. Pulp and Paper and Paperboard Industry: A Profile, Tappi JOURNAL. Vol. 76, No. 3, pp. 53-57
- Wark, E., 1983, Thermodynamics, 4th ed., McGraw-Hill, New York
- Whitaker, S., 1967, Diffusion and Dispersion in Porous Media, AIChE Journal, Vol. 13, pp. 1066-1085
- Whitaker, S., 1969, Advances in the Theory of Fluid Motion in Porous Media, Ind. Eng. Chem., Vol. 61, pp. 14-28
- Whitaker, S., 1977a, Simultaneous Heat, Mass and Momentum Transfer in Porous Media: A Theory of Drying, Advances in Heat Transfer, J.P. Hartnet and T.F. Irvine, eds., Academic Press, New York, Vol. 13, pp. 119-203
- Whitaker, S., 1977b, Drying in Porous Media, Second Australian Conference on Heat and Mass Transfer, University of Sydney, Australia, pp. 409-420
- Wilhelmsson, B., Nilsson, L., Stenström, S. and Wimmerstedt, R., 1993, Simulation Models of Multi-Cylinder Paper Drying, Drying Technology 11(6), pp.1177-1203
- Wilhelmsson, B., 1995, An Experimental and Theoretical Study of Multi-Cylinder Paper Drying, Ph.D. Thesis, Lund University, Lund, Sweden

Wilhelmsson, B., Stenström, S., Nilsson, L., Krook, R., Persson, H. and Wimmerstedt, R., 1996, Modeling Multi-cylinder Paper Drying-Validation of a New Simulation Program, Tappi Journal 79(4), pp. 157-167

Wink, W.A., Bobb, F.C. and van Den Akkar, J.A., 1958, Equilibrium Moisture Content Determination at High Temperature, Tappi Journal, Vol. 41, No. 11, pp. 643-646

Wyllie, M.R.J. and Spangler, M.B., 1952, Application of Electrical Resistivity Measurements to Problem of Fluid Flow in Porous Media, Bulletin of the American Association of Petroleum Geol., Vol. 36, pp. 359-403

Wyllie, M.R.J. and Gregory A.R., 1953, Formation Factors of Unconsolidated Porous Media: Influence of Particle Shape and Effect of Cementation, Transactions of AIME, Vol. 198, pp. 103-110

Wyllie, M.R.J. and Gardner, G.H.F., 1958, The Generalized Kozeny-Carmen equation, Part II, World Oil, pp. 210-228

NET1-1994, Paper Drying Expert System,
http://ai.iit.nrc.ca/IR_public/pma/pdes_desc.html

NET2-1997, APROS/APMS-Advanced PROcess Simulator/Advanced Paper Mill Simulator, VTT, <http://www.vtt.fi/aut/tau/ala/apros.htm>

NET3-1997, APMS-A Multi-Purpose Tool for Dynamic Simulation of Paper and Board Mills, VTT Automation, <http://www.vtt.fi/aut/tau/ala/apms.htm>

APPENDIX

BOUNDARY CONDITIONS AND NUMERICAL SOLUTION

A.1 Boundary conditions

Drying of paper involves a variety of systems external to the sheet that an industrial simulator must treat. These external systems include heat transfer from the cylinder to the sheet, effect of felting on external heat and mass transfer coefficients, alternation of boundary conditions in a multi-cylinder dryer section, and the treatment of air impingement drying. The boundary conditions are first developed for a base case, when the sheet is in contact with the cylinder surface on one side and open directly to the ambient air on the other. That set of equations is then modified for other aspects of the external systems.

As explained in Chapters 4 and 5, the present model uses the description of external systems developed by Bond and Douglas (1996). This treatment, which includes determination of external heat and mass transfer coefficients, effect of felting, etc. is not repeated here.

A.1.1 Base case, cylinder contact side

At the impermeable cylinder contact side (CCS) all mass fluxes of the sheet are zero. These include the mass flux of free water, n_{fw} ; sorbed water, n_s ; air, n_a ; and both the convective and diffusive components of the water vapor flux, n_v .

$$n_{fw} \Big|_{ccs} = 0 \quad (A-1)$$

$$n_s \Big|_{ccs} = 0 \quad (A-2)$$

$$n_{v,conv} \Big|_{ccs} = 0 \quad (A-3)$$

$$n_{v,diff} \Big|_{ccs} = 0 \quad (A-4)$$

The heat flux at this surface of the sheet is:

$$-k_{\text{eff}} \left. \frac{\partial T}{\partial z} \right|_{\text{ccs}} = h_{\text{cont.}} (T_{\text{cyl.}} - T_{\text{ccs}}) \quad (\text{A-5})$$

The contact heat transfer coefficient, $h_{\text{cont.}}$, in $\text{W/m}^2\text{K}$ is expressed as a function of sheet moisture content using the Rhodius and Göttsching (1979) correlation:

$$h_{\text{cont.}} = 1556.6 X_{\text{ccs}} + 52.87 \quad (\text{A-6})$$

A.1.2 Base case, vapor transport side

The boundary conditions at this surface, designated VTS, include the external coefficients of heat and mass transfer between the sheet and the ambient condition. Designating the water vapor mole fraction as y_v , the boundary conditions are:

$$-D_v \left. \frac{\partial y_v}{\partial z} \right|_{\text{vts}} = h_{\text{em}} (y_{v,\text{vts}} - y_{v,\text{amb.}}) \quad (\text{A-7})$$

$$-k_{\text{eff}} \left. \frac{\partial T}{\partial z} \right|_{\text{vts}} = h_{\text{eh}} (T_{\text{vts}} - T_{\text{amb.}}) \quad (\text{A-8})$$

$$P_g \Big|_{\text{vts}} = P_{\text{amb.}} \quad (\text{A-9})$$

where h_{eh} and h_{em} represent the external heat and mass transfer coefficients, respectively.

A.1.3 Multi-cylinder dryer section

A multi-cylinder dryer section can have single-tier or double-tier arrangements of the drying cylinders (Chapter 1). Several configurations of felting are demonstrated in Figure A-1. For the single felted (Unirun) configuration, on one tier the felt is sandwiched between the sheet and cylinder. Because of the associated low heat transfer rate to the

sheet this tier may be small diameter cylinders operated without condensing steam. For other configurations, definition of the four phases of drying by Nissan and Kaye (Chapters 1 and 5) applies.

The base case boundary conditions developed earlier could be used with some modifications for all the arrangements in Figure A-1. When the sheet contacts the cylinder the base case equations for the CCS surface, section A.1.1, is used. For the VTS surface the sheet is either covered by the felt during Phase II of drying, or directly exposed to ambient air during Phases I and III of drying or to the dryer pocket air during Phase IV, shown in Figure A-2. Without the presence of the felt, boundary conditions of section A.1.2 are applicable. Presence of the felt will reduce the external heat and mass transfer coefficients to an extent that depends on felt type and conditions. For the Unirun configuration, when the felt is sandwiched between the sheet and cylinder, the heat transfer from the hot cylinder surface to the sheet is reduced. Felting is treated by relating heat transfer to the thermal conductivity and thickness of the felt, then using the heat-mass transfer analogy

For the open draw between cylinders, both sides of the sheet act as a VTS surface, hence the equations of section A.1.2 are applicable with the consideration that external coefficients will be different from those determined for when the sheet is on the cylinder. The heat and mass transfer rates on the two sides may be different because the temperature and humidity of the dryer pocket air may be different from one pocket to the next.

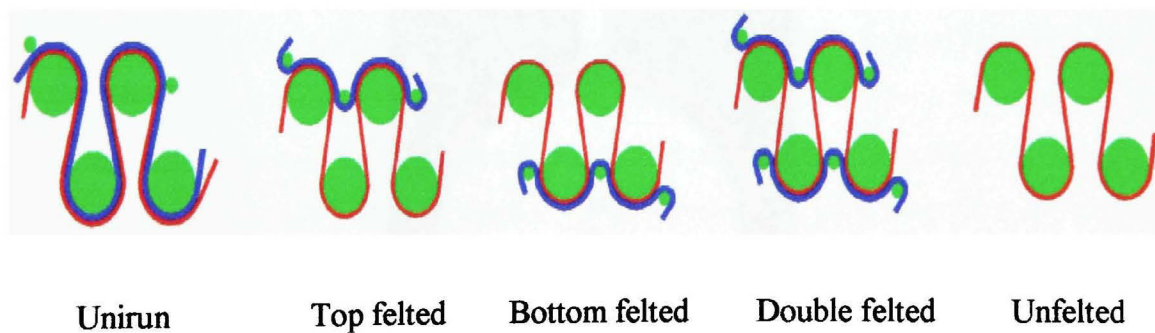


Figure A-1 Felting arrangements

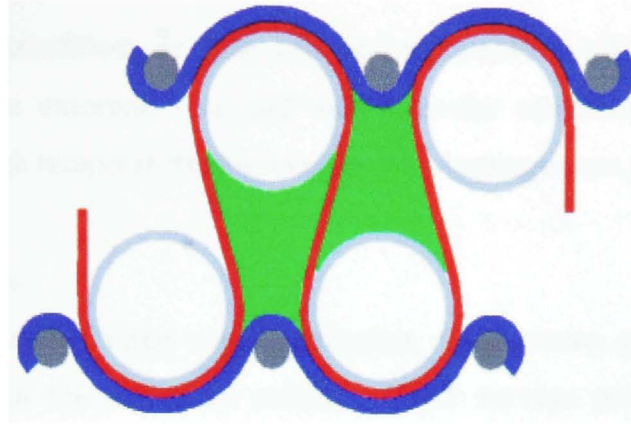


Figure A-2 Cylinder pockets

A.1.4 Air impingement drying

Tissue is dried on a Yankee dryer (Chapter 1) which is divided into three phases as shown in Figure A-3. Phases I and III are as described above for cylinder drying.

Phase I: Before entering the impingement hood one side of the sheet contacts the cylinder surface while water vapor leaves from the other side, the unheated vapor transport side.

Phase II: With the sheet inside the impingement hood the vapor transport side of the sheet is subjected to an array of high temperature, high velocity impinging jets while the CCS side is heated by contact with the cylinder surface.

Phase III: The sheet has left the hood but still contacts the cylinder. Identical to Phase I.

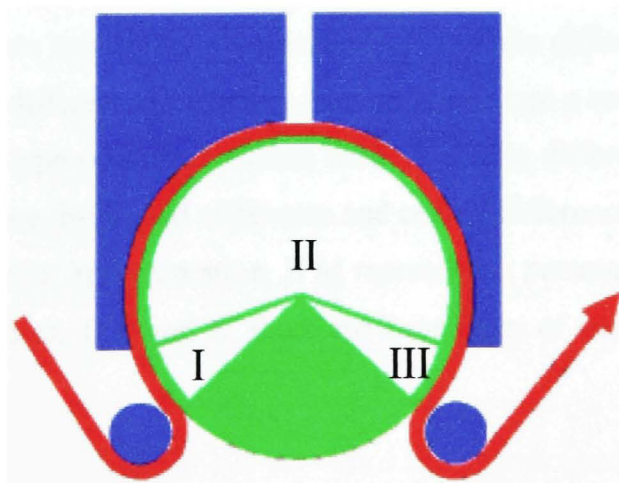


Figure A-3 Three phases of drying for a Yankee dryer

The boundary conditions of base case are applicable to all three phases with the consideration that the external heat and mass transfer coefficients for Phase II are determined for the high temperature, high velocity air impingement jets.

A.2 Initial conditions

The initial values of three main parameters, temperature, pressure and moisture content are needed for the numerical solution. Dryer surveys provide the sheet initial moisture content and temperature which are assigned to all positions across the sheet. Pressure is considered atmospheric when the sheet enters the dryer section.

$$X|_{t=0} = X_0 \quad (\text{A-10})$$

$$T|_{t=0} = T_0 \quad (\text{A-11})$$

$$P|_{t=0} = P_0 \quad (\text{A-12})$$

A.3 Numerical solution

The macroscopic heat and mass balance equations were developed in Chapter 2 by following a sheet “body” as it moves along the drying section (Lagrangian approach). In the absence of an analytical solution to the partial differential equations thus obtained, numerical approximate solutions are necessary. In the finite difference method used here the system of partial differential equations is transformed into a set of algebraic equations.

Based on the type of approximation used, the finite difference method is divided into forward difference, backward difference and central difference formulation, the latter being in general a better approximation. If M represents a parameter that could be any of the three main variables, T, P and X, there are three types of derivatives that need to be approximated:

1. Time derivative, approximated by the forward difference technique:

$$\frac{\partial M}{\partial t} = \frac{M(z, t + \Delta t) - M(z, t)}{\Delta t}$$

2. First order spatial derivative, approximated by the central difference technique:

$$\frac{\partial M}{\partial z} = \frac{M(z + \Delta z, t) - M(z - \Delta z, t)}{2 \Delta z}$$

3. Second order spatial derivative, approximated by the central difference technique:

$$\frac{\partial^2 M}{\partial z^2} = \frac{M(z + \Delta z, t) - 2M(z, t) + M(z - \Delta z, t)}{\Delta z^2}$$

Although it is possible to establish simple stability and convergence criteria for an equation such as $\frac{\partial M}{\partial t} = \frac{\partial^2 M}{\partial z^2}$, those criteria do not apply to the significantly more complex system of non-linear equations to be solved here. The optimal choice of Δz and Δt is determined by trial. For the time step, 0.001s was found to be adequate for most cases of industrial drying in Chapter 4, although it was necessary to use the smaller time step of 0.0001s for a few cases to obtain a stable solution. The determination of satisfactory grid spacing is described below.

While it is desirable to use the minimum number of sheet slices to avoid excessive computation time, that aspect is secondary to finding a reliable, convergent and stable solution for machine speed prediction and for thickness-direction profiles of moisture content, temperature and pressure. To assess the effect of Δz on the solution, comparisons were made of discretization for 10 and 20 positions in the sheet thickness direction. Using dryer survey results for the performance of industrial dryers, this test was carried out twice, for one tissue case and one linerboard case. For both cases the reduction from 20 to 10 point discretization resulted in the machine speed prediction error changing insignificantly. For a yet more critical convergence test, the experimentally determined profiles of moisture content and temperature within a linerboard sheet, Chapter 4, section

4.3.3 (c), were simulated using both 20 and 10 point discretization. Using 10 nodes in the thickness direction, the average error of moisture prediction for the 3 thickness-direction positions determined experimentally was +6% and that of average temperature prediction for the 4 thickness-direction positions for which sheet temperature was measured was +2%. Increasing the number of nodes from 10 to 20 made only an insignificant change to both the temperature prediction and moisture prediction error. The moisture prediction error was reduced from +6.01% to just +5.96%, while the temperature prediction error changed even less. These several tests establish that a Δz resulting from 10 positions in the thickness direction provides fully satisfactory convergence and consistency of numerical solution.

The computational time on a personal computer running at 200Mhz depended on the type of the simulation performed and the total drying time. While the exit moisture content prediction required only a couple of minutes at most, the iterative procedure of machine speed prediction needed up to an hour for more difficult cases. A more powerful computer would certainly require less computation time.

